PB-230 896

LOW EMISSION COMBUSTOR/VAPOR GENERATOR FOR AUTOMOBILE RANKINE CYCLE ENGINES

T. E. Duffy, et al

Solar

Prepared for:

Environmental Protection Agency

October 1973

DISTRIBUTED BY:

NTIS

National Technical Information Service
U. S. DEPARTMENT OF COMMERCE
5285 Port Royal Road, Springfield Va. 22151

BIBLIOGRAPHIC DATA SHEET

1. Report No. EPA-450/3-004

2.

PB 230 896

4. Title and Subtitle

Low Emission Combustor/Vapor Generator for Automobile Rankine Cycle Engines

5. Report Date October 1973

6.

7. Author(s) T. E. Duffy, J. R. Shekelton, R. B. Addoms, and W. A. Compton

8. Performing Organization Rept. No.

9. Performing Organization Name and Address

Solar Division International Harvestor Company
2200 Pacific Highway
San Diego, California 92138

10. Project/Task/Work Unit No.

11. Contract/Grant No. 68-04-0036

12. Sponsoring Organization Name and Address

U.S. ENVIRONMENTAL PROTECTION AGENCY - OAWP
Office of Mobile Source Air Pollution Control
Alternative Automobile Power Systems Division
Ann Arbor, Michigan 48105

13. Type of Report & Period Covered

14.

15. Supplementary Notes

16. Abstracts

This is a final report on a program to demonstrate a low emission vapor generator for automotive Rankine cycle power plant. Program goals are presented together with system requirements. It evaluates the combustor rig tests and the integrated combustor performance. A steam generator with an output of 1200 pounds per hour at 1000°F and 1000 psia was demonstrated by tests to have a weighed emissions below the 1976 emission standard over a simulated driving cycle. Parasitic power limitations were the major factors in determining the overall configuration. Low emissions required the maximum possible mixing velocities at the low flow. To achieve this, a unique variable flow combustor design was used. This was a modified version of one developed and reported in an earlier demonstration contract. The emission test results are summarized. Two organic fluid vapor generators were designed as backup for EPA system contractors. They were designed to interface with the same type combustor tested with the steam generators described above. The system requirements, configuration analysis, and design constrains are described. The control system description, components, electronic control and test results are included. The results indicates that a low emission compact vapor generator could be developed for automotive vehicles. The emission levels are borderline and require future development work.

17. Key Words and Document Analysis. 17a. Descriptors

Air pollution
Reaction kinetics
Design
Nitrogen dioxide
Hydrocarbons
Carbon monoxide
Rankine cycle
Exhaust emissions
Performance tests
Organic compounds
Test stand

17b. Identifiers/Open-Ended Terms

Vapor generator
Combustor
Control system
Finned tube steam generator
Monotube steam generator

17c. COSATI Field/Group 13B, 13F

18. Availability Statement

19. Security Class (This Report) UNCLASSIFIED

20. Security Class (This Page) UNCLASSIFIED

21. No. of Pages 330

22. Price 19.50/1.45

ORM NTIS-35 (10-70)

1a

USCOMM-DC 40329-P71

EPA-460/3-73-004

LOW EMISSION COMBUSTOR/VAPOR GENERATOR FOR AUTOMOBILE RANKINE CYCLE ENGINES

Prepared by

T. E. Duffy, J. R. Shekleton,
R. B. Addoms, and W. A. Compton

Solar Division International Harvestor Company
2200 Pacific Highway
San Diego, California 92138

Contract No. 68-04-0036

EPA Project Officers:

F. P. Hutchins, S. Luchter, and E. Beyma

Prepared for

U. S. ENVIRONMENTAL PROTECTION AGENCY
Office of Air and Water Programs
Office of Mobile Source Air Pollution Control
Alternative Automotive Power Systems Division
Ann Arbor, Michigan 48105

October 1973

This report is issued by the Office of Mobile Source Air Pollution Control, Office of Air and Water Programs, Environmental Protection Agency, to report technical data of interest to a limited number of readers. Copies of this report are available free of charge to Federal employees, current contractors and grantees, and non-profit organizations - as supplies permit - from the Air Pollution Technical Information Center, Environmental Protection Agency, Research Triangle Park, North Carolina 27711 or may be obtained, for a nominal cost, from the National Technical Information Service, 5285 Port Royal Road, Springfield, Virginia 22151.

This report was furnished to the U.S. Environmental Protection Agency by Solar Division International Harvestor Company in fulfillment of Contract No. 68-04-0036 and has been reviewed and approved for publication by the Environmental Protection Agency. Approval does not signify that the contents necessarily reflect the views and policies of the agency. The material presented in this report may be based on an extrapolation of the "State-of-the-art". Each assumption must be carefully analyzed by the reader to assure that it is acceptable for his purpose. Results and conclusions should be viewed correspondingly. Mention of trade names or commercial products does not constitute endorsement or recommendation for use.

Publication No. EPA-460/3-73-004

FOREWORD

This is a final technical report on the work performed under contract 68-04-0036. The opinions, findings, and conclusions expressed are those of the author and not necessarily those of the Environmental Protection Agency.

Contract 68-04-0036 with Solar Division of International Harvester Company, San Diego, California, was sponsored by the Environmental Protection Agency, Division of Advanced Automotive Power Systems Development, Ann Arbor, Michigan. It was administered initially under the direction of Mr. F. P. Hutchins, and subsequently by Mr. S. Luchter and Mr. E. Beyma, EPA Project Officers.

The program was conducted at Solar Division of International Harvester Research Laboratories with Mr. W. A. Compton, Assistant Director of Research and Technical Director and Mr. T. E. Duffy, Research Staff Engineer, the Project Manager. Others contributing to the program are: Mr. J. R. Shekleton, Dr. R. B. Addoms and Mr. J. C. Napier. Geoscience Ltd. provided analysis used in Appendix VII and VIII.

Solar's internal report number is RDR-1708-6.

CONTENTS

Section		Page
1	SUMMARY	1
2	INTRODUCTION	7
3	SYSTEM REQUIREMENTS	9
	3.1 Test Bed Combustor/Steam Generator	9
	3.1.1 Combustor Requirements	9
	3.1.2 Parallel Flow-Bare Tube Steam Generator Goals	10
	3.1.3 Controls	11
	3.2 High Efficiency Finned Tube Steam Generator	11
	3.2.1 Combustor	11
	3.2.2 Steam Generator	11
	3.2.3 Controls	11
	3.3 Units Designed for EPA System Contractors	12
	3.3.1 Fluorinol-85 System	12
	3.3.2 AEF-78 Vapor Generator	13
	3.3.3 SES Steam Generator	14
4	SYSTEM CONFIGURATION ANALYSIS	15
	4.1 General Constraints and Selection of a Rotating Cup System	15
	4.2 Configuration Analysis	18
5	COMBUSTOR	21
	5.1 Overview of Combustor Section	21
	5.2 Combustor Rig Tests	22
	5.2.1 Description of Combustor Rig	22
	5.2.2 Control of NO_x in Combustor	26
	5.2.3 Combustor Rig Test Results	27
	5.3 Integrated Combustor Performance	34
	5.3.1 Design	34
	5.3.2 Air Supply System	39
	5.3.3 Flame Performance	51
	5.3.4 Integrated System Emissions Evaluation	57
	5.3.5 Temperature Pattern	77

Preceding page blank

CONTENTS (Contd)

Section Page

6 PARALLEL FLOW STEAM GENERATOR (TEST BED UNIT) 81

6.1 Steam Generator Core Matrix 81
6.2 Construction 82
6.3 Performance Tests 87
6.3.1 Mechanical Integrity 90
6.3.2 Flow Stability 91

7 HIGH EFFICIENCY SINGLE FLOW PATH STEAM GENERATOR 99

7.1 Construction 102
7.2 Steady State Performance 105

8 CONTROL SYSTEM 109

8.1 System Description 110
8.2 System Components 112
8.2.1 System Flow Arrangement 112
8.2.2 Air Valve and Triple Valve Mechanization 112
8.2.3 Air Valve 115
8.2.4 Fuel Valve 115
8.2.5 Water Metering System 120
8.3 Electronic Control 124
8.4 Test Results With Parallel Flow Steam Generator 125
8.4.1 Explanation of Test Results 125
8.4.2 Cycling and Step Transient Performance 136
8.5 High Efficiency Monotube Steam Generator Performance 141

9 ORGANIC SYSTEMS 153

9.1 Fluorinol-85 System Design 153
9.1.1 Design Constraints 154
9.1.2 Core 154
9.1.3 Manifolds 155
9.1.4 Combustor and Air Valve Design 156
9.2 AEF-78 System Design 162
9.3 Internally Finned Tubing 165

CONTENTS (Contd)

Section		Page
10	SYSTEM NOISE	169
	APPENDIX I	181
	APPENDIX II	199
	APPENDIX III	203
	APPENDIX IV	235
	APPENDIX V	241
	APPENDIX VI	245
	APPENDIX VII	249
	APPENDIX VIII	269
	NOMENCLATURE	337
	REFERENCES	343

ILLUSTRATIONS

Figure		Page
1	Final Combustor/Steam Generator Configuration	2
2	Emission Measurements Versus Air Valve Position (Power Level)	4
3A	20 Percent to 40 Percent Low Frequency Cycling of Steam Flow	4
3B	Step Changes in Steam Flow From High Power	5
3C	Maximum Amplitude and Frequency Cycling	5
4	Preliminary Combustor Test Rig	23
5	Schematic of Gas Temperature Sensor and Mechanical Support	24
6	Combustor Side of Vapor Generator Simulator Showing Location of Thermocouples	25
7	Emission Probe	25
8	Test Combustor Installed in Rig	26
9	Emission of Nitric Oxide as a Function of Air-Fuel Ratio and Time	28
10	Rig Test Combustor	29
11	Upstream Side of Combustor	29
12	Combustor Ready for Installation on Rig	30
13	NO_2 Emissions Versus Fuel Flow	32
14	CO Emissions Versus Fuel Flow	33

ILLUSTRATIONS (Contd)

Figure		Page
15	Hydrocarbon Emissions Versus Fuel Flow	33
16	Combustor Exit Plane Radial Temperature Distribution at Maximum Flow	34
17	Initial Integrated System Test Configuration With Conical Cup	35
18	Combustor/Air Supply System (Drive Motor Side)	35
19	Top View of Combustor Air Inlet to Fan	36
20	Fan Mounted to Control Valve Backup Plate	37
21	Rotary Shear Plate	37
22	Combustor/Air Supply System (Vapor Generator Side)	38
23	Conical Fuel Cup	38
24	Air Supply Fan	40
25	Calculated Characteristics of Fan	41
26	Total Pressure Rise Calculated Compared to Test Points	42
27	Actual Static Pressure Rise Compared to Calculated Total Pressure	43
28	Primary and Secondary Air Metering Port Configuration Shown in 50 Percent Power Position	44
29A	Air Valve in 2 Percent Position	45
29B	Air Valve in 50 Percent Position	45
29C	Air Valve in 100 Percent Position	46
30	Air Valve Backup Plate	46
31A	Fan-Air Valve Flow Test Rig	47

ILLUSTRATIONS (Contd)

Figure		Page
31B	Fan Test Rig Diffuser Air Valve Section	47
32	Cd Versus Fan Flow for Several Metering Plate Orifice Areas	49
33	Fan Drive Motor	50
34	Fan Drive Motor Characteristics	51
35	Combustor/Air Supply System Test Arrangement	52
36	Flame at 1.5 PPH	53
37	Flame at 60 PPH Fuel Flow	53
38	Flame at 80 PPH Fuel Flow	54
39	Flame at 100 PPH Fuel Flow	54
40	Flame at 130 PPH Fuel Flow	55
41	Emission Probe Location and Configuration	58
42	Cylindrical Cup Configuration for Emission Tests	60
43	Cylindrical Cup With Double Heat Shield	61
44	Auxiliary Air Swirler Ports	62
45	Tangential Slots at Base of Auxiliary Air Swirler	62
46	Recirculation Fan on Conical Cup	63
47	Conical Cup Emissions With Recirculation Fan (CO_2 Adjusted to Maintain NO_x at 1.38 GM/KGM)	63
48	Emissions With JP-4 and "A" = 0.125 and 2 Heat Shields	65
49	Emissions With JP-4 and "A" = 0.125 With Auxiliary Air Swirler	66
50	NO_2 Emissions With A = 0.192, 2 Heat Shields and Auxiliary Air Swirler	67

ILLUSTRATIONS (Contd)

Figure		Page
51	CO Emissions With A = 0.192, 2 Heat Shields and Auxiliary Air Swirler	67
52	HC Emissions With A - 0.192, 2 Heat Shields and Auxiliary Air Swirler	68
53	Combustor Post Tests Recorded in Figures 50, 51 and 52	68
54	Emissions With Gasoline, A = 0.192 and 2 Heat Shields	69
55	Emissions With Gasoline, A = 0.03, Auxiliary Air Swirler and Recirculation Fan	70
56	Auxiliary Air Swirler Configuration Variations	73
57	Combustor After 70 Hours of Operation on EPA Reference Gasoline	75
58	Auxiliary Air Swirler After 70 Hours of Operation With EPA Reference Gasoline	75
59	Combustor and Steam Generator Outlet Gas Temperature	78
60	Test Bed Vapor Generator - Water Working Fluid	82
61	Vapor Generator Coil Connectors	83
62	Vaporization Coils (6 Per Row)	83
63	Special Box Connection After Burst Pressure Test	84
64	Vapor Generator Flow and Instrumentation	85
65	Assembly of Two Preheater Coils With Special Connector Welded at Inside of Coils	86
66	Superheater Outlet Row Showing the Six Thermocouples	87
67	Test Cell Flow Schematic	88
68	Test Cell Steam Generator Control Panel	89

ILLUSTRATIONS (Contd)

Figure		Page
69	Steam Generator After 500 Hours of Emission and Control Systems Tests	91
70	Vaporizer Spacers After 500 Hours of Operation	92
71	Superheater Outlet Tube Wall Temperature (Six Flow Paths)	94
72	Test Bed Vaporizer Steady State Performance	97
73	Test Bed Vaporizer. Tube Wall Temperature at Superheater Outlet	98
74	Preheater Coils With Copper Fins	103
75	One of the Two Dryer Coils	103
76	Assembled Steam Generator	104
77	Steam Generator U Connections	104
78	High Efficiency Finned Tube Steam Generator Steady State Efficiency Measurements	106
79	Top Coil (Vaporizer) After 70 Hours of Operation	107
80	Bottom Coil (First Row Preheater) After 70 Hours of Operation	107
81	Combustor/Vapor Generator Control System	111
82	Controls System Flow Schematic	113
83	Triple Valve Actuator Showing Air Valve Actuation Tab	114
84	Triple Valve Actuator With Fuel and Water Valves Installed	114
85	Exploded View of Fuel Valve	116
86	Fuel Valve Components	116

ILLUSTRATIONS (Contd)

Figure		Page
87	Metering Slot	117
88	Assembled Fuel Valve	117
89	Reynolds Number Vs. Percent Fuel Flow for JP-4 and Gasoline	118
90	Fuel Valve Calibration	119
91	Fuel Valve Calibration 1 to 10 ppm Range	120
92	Water Metering Valve Orifice	121
93	Component Parts of the Water Metering Valve	121
94	Assembled Water Metering Valve	122
95	Water Metering Vavle Calibration at 50 psi Differential	123
96	Differential Pressure Control Valve Components	123
97	Differential Pressure Control Valve Assembled With Electric Actuator	124
98	Electronic Components Required to Perform Control Functions	125
99	Steam Generator Control Transients, Step Changes Prior to Installation with 44 lb/in. Spring in ΔP Valve	127
100	Low Frequency 10 to 30 Percent Ramp Cycles After Installation of High Gain ΔP Valve	129
101	Full Power Steady State Performance With Step Transients in Steam Flow	131
102	High Amplitude and Maximum Frequency Steam Flow Cycling System Response	133
103	Transient Emissions During Peak Steam Generator Cycling	140

ILLUSTRATIONS (Contd)

Figure		Page
104	Open Loop Characteristics to Step Inputs in Water Rate	143
105	Open Loop Sinusoidal Frequency Response	145
106	Closed Loop Transient Response With and Without Derivative Compensation	147
107	High Frequency Cycling	149
108	Response to Step Changes in Steam Flow	151
109	Fluorinol-85 Combustor/Vapor Generator (Front View)	157
110	Fluorinol-85 Combustor/Vapor Generator (Top View)	157
111	Fluorinol-85 Combustor/Vapor Generator (Side View)	158
112	Fluorinol-85 System Air Metering Valve Shown in 56.7 Percent Position	161
113	AEF-78 Combustor/Vapor Generator (Front View)	163
114	AEF-78 Combustor/Vapor Generator (Top View)	163
115	AEF-78 Combustor/Vapor Generator (Side View)	164
116	Tube Cross Section	165
117	Photomicrographs of Tube-Fin Wall	166-7
118	Noise Emission Microphone Location in Test Cell	171
119	Sound Level, dB(A), Versus 1/10 Octave Frequency, Water Pump Only - 600 psi Outlet Pressure - 88 dB(A) Overall	172
120	Sound Level, dB(A), Versus 1/10 Octave Frequency, Fan Only, 5700 rpm - 30 Percent, 92 dB(A) Overall	173
121	Sound Level, dB(A), Versus 1/10 Octave Band Frequency. Full System, 20 Percent Fan, 380 lb/hr Steam, 96 dB(A) Overall (Background Included)	174

ILLUSTRATIONS (Contd)

Figure		Page
122	Sound Level, dB(A), Versus 1/10 Octave Frequency. Full System, 20 Percent Fan, Boiler Flooded, 94 dB(A) Overall (Background Included)	175
123	Sound Level, dB(A), Versus 1/10 Octave Frequency. Full System, 50 Percent Air Valve, 780 lb/hr Steam, 101 dB(A) Overall (Background Included)	176
124	Sound Level, dB(A) Versus 1/10 Octave Frequency. Full System, 50 Percent Fan, Boiler Flooded, 96 dB(A) Overall (Background Included)	177
125	Sound Level, dB(A), Versus 1/10 Octave Frequency. Full System, 77 Percent Fan, 1200 lb/hr Steam, 108 dB(A) Overall (Background Included)	178

TABLES

Table		Page
I	Measured Levels at Simulated Driving Cycle Steady State Points	3
II	Emission Level Goals	10
III	Fan Test Results With No Bypass - Fan Speed 5700 RPM	48
IV	Initial Combustor Plus Fan Air Supply Test Results	56
V	Fan Power With High Ratio Pulley	56
VI	Residue Removed From First Row of Steam Generator	92
VII	Fluid Conditions	100
VIII	Summary of Performance Parameters	101
IX	Overall "A" Scale Weighed Sound Level for Steam Generator System and Components	170

1

SUMMARY

This is the final report on a program to demonstrate a low emission vapor generator for automotive Rankine cycle power plants. Program goals were to design and test a low emission system that required low parasitic power, had compact packaging, high steam generator efficiency and suitable controls for fuel, air and water for the regulation of steam pressure and temperature. A steam generator with an output of 1200 pounds per hour at 1000°F and 1000 psia was demonstrated by tests to have weighed emissions below the 1976 emission standards over a simulated driving cycle. Figure 1 is a cross section of the unit tested.

Parasitic power limitations were the major factor in determining the overall configuration. Maximum available electrical power requirements established a maximum ideal input to the system of 1.2 HP. To flow the necessary air through the system, a large frontal area steam generator was integrated with a low pressure drop combustor (5 inches of water). Low emissions required the maximum possible mixing velocities at the low flows. To achieve this a unique variable flow combustor design was used in which an air valve splits the flow between primary and secondary air injection as a function of power level required. In this manner the pressure drop, and thus velocity was maintained relatively high at low firing rates.

Major design features include: rotating cup fuel atomization and injection, fully modulated controls for air, fuel and water, symmetrical air distribution with no exhaust recirculation, flat spiral steam generator tube matrix with extensive use of finned tubing and a straight-through combustion gas flow path. A high degree of component integration was used to allow co-axial mounting of the fan and fuel cup with a single belt drive from a DC side mounted electric motor. Performance tests on this unit showed that it met major performance goals of the program.

Table I summarizes the results of emission tests. All tests were performed with the configuration shown in Figure 1, while operating the steam generator at 1000°F and 1000 psia. Emissions were measured by an averaging probe located two inches downstream of the vapor generator in the exhaust duct. The characteristics of the emissions as a function of flow are shown in Figure 2.

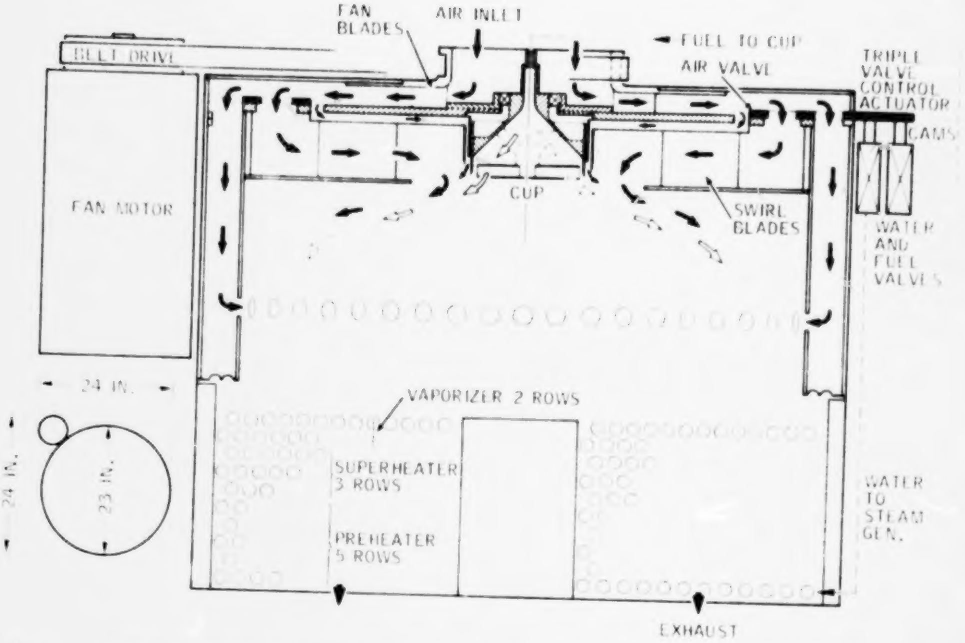
FAN BLADES
AIR INLET
FUEL TO CUP
AIR VALVE
TRIPLE VALVE CONTROL ACTUATOR
CAMS
BELT DRIVE
FAN MOTOR
CUP
SWIRL BLADES
WATER AND FUEL VALVES
24 IN.
VAPORIZER 2 ROWS
24 IN.
23 IN.
SUPERHEATER 3 ROWS
PREHEATER 5 ROWS
WATER TO STEAM GEN.
EXHAUST

FIGURE 1. FINAL COMBUSTOR/STEAM GENERATOR CONFIGURATION

Two different types of steam generator tube matrices were fabricated and tested. One unit was a test bed for initial combustor development and was used to investigate the feasibility of parallel flow passages for compact forced circulation steam generators. Parallel flow development tests were to provide background for future organic system designs normally requiring multiple flow passages. Parallel flow instability was observed and analyzed in the first unit but could be controlled by correct scheduling of the startup procedure. At near design conditions, serious instabilities disappeared. A steady state flow imbalance between passages caused outlet temperature differences between each of the six parallel flow paths, but did not present a serious operational problem. A second unit made extensive use of extended surfaces and had a measured efficiency of 86 percent LHV at full steam flow and 93 percent LHV at 25 percent steam flow.

Both the parallel flow unit and the single flow path high efficiency steam generator were integrated and tested with fully modulated electronic control system tailored for each unit.

Steady state control system performance was within ±50 psi and ±50°F of the setpoints. Transient response to the steam flow demand changes resulting from rapid opening and closing of a throttle valve are shown in Figure 3. Pressure and temperature outlet errors were maintained at values

TABLE I

MEASURED LEVELS AT SIMULATED DRIVING CYCLE STEADY STATE POINTS

Fuel Flow	Time (%)	NO_2 (gm/kgm)	HC	CO
9 pph	3	1.31	1.0	9.8
12	76	1.32	0.8	9.5
15	20	1.35	0.9	9.0
25	1	1.25	0.5	6.2

TIME INTEGRATED LEVELS FOR DRIVING CYCLE (10 MPG)

	Actual	Limit	ER*
NO_2	0.38 gm/mile	0.40 gm/mile	0.95
HC	0.24 gm/mile	0.41 gm/mile	0.59
CO	2.75 gm/mile	3.4 gm/mile	0.81

$*ER = \text{Emissions Ratio} = \frac{\text{Actual}}{\text{Limit}}$

of less than ±50 psia and ±50°F during "normal" driving steam flow demands shown in Figure 3A. Under severe steam flow demands (Figs. 3B and 3C) steam conditions were maintained within a ±150 psia and ±100°F control band. An open loop schedule of fuel-air-and-water valve position as a function of steam flow was the primary control mode. A closed loop electronic control of firing rate provided a trim regulation of pressure. Temperature trim was also done electronically with a thermocouple in the superheater outlet providing a signal to regulate feedwater rate.

Sound level measurements were made on the system and showed levels that can be made acceptable in a closed engine compartment given noise suppression treatment.

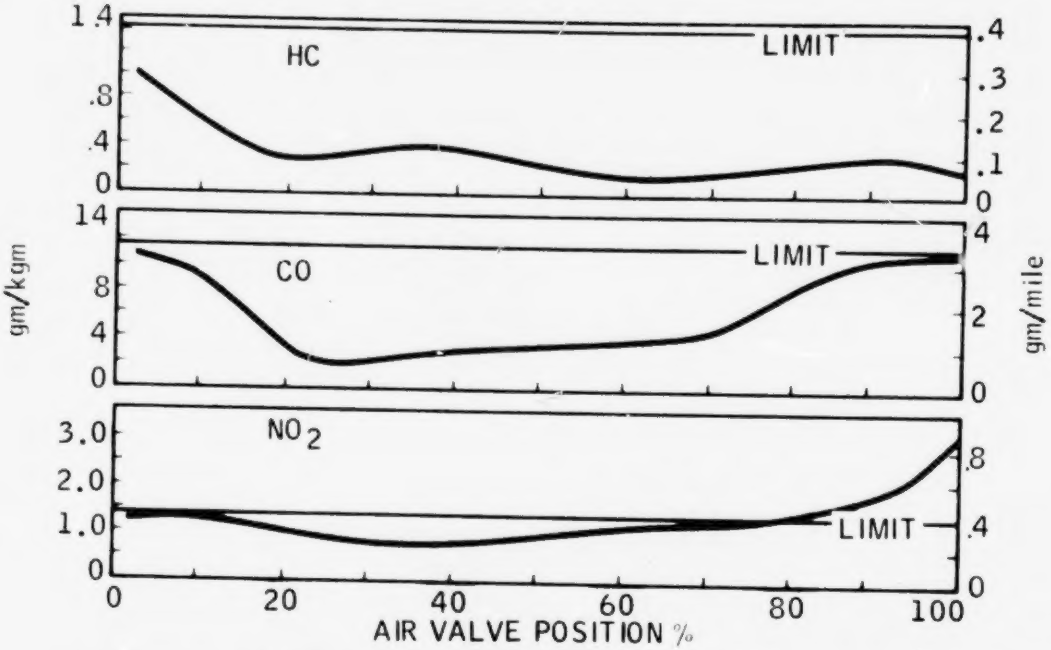

FIGURE 2. EMISSION MEASUREMENTS VERSUS AIR VALVE POSITION (POWER LEVEL)

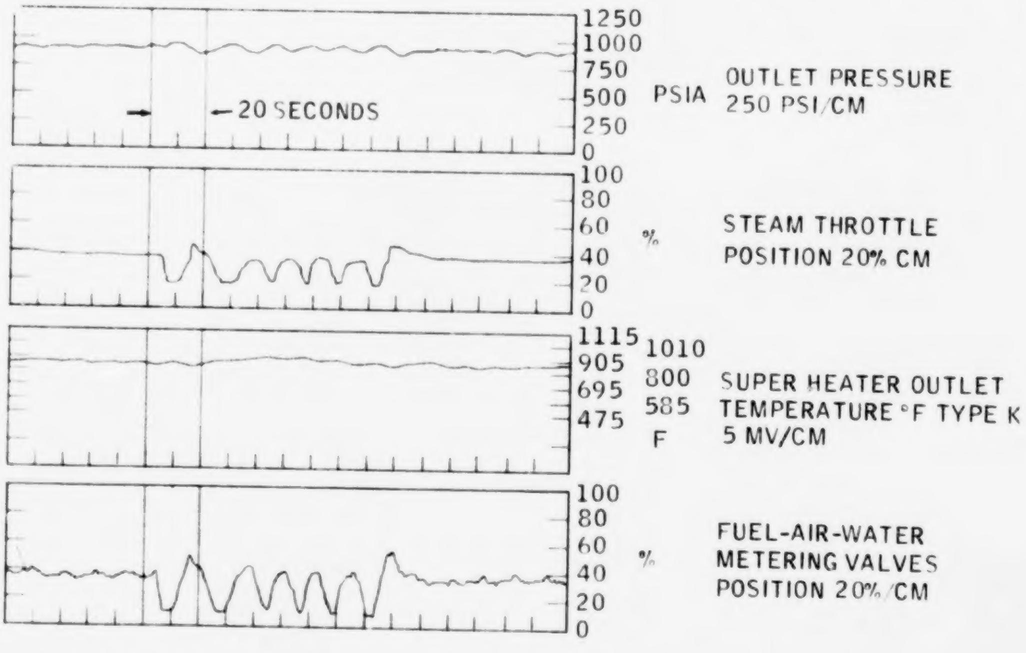

FIGURE 3A. 20 PERCENT TO 40 PERCENT LOW FREQUENCY CYCLING OF STEAM FLOW

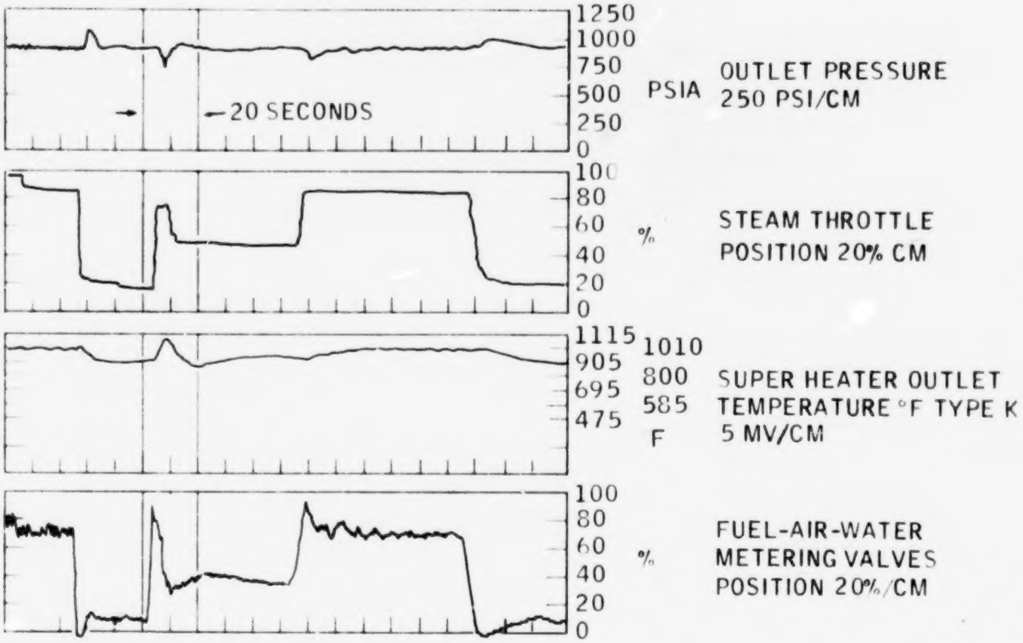

FIGURE 3B. STEP CHANGES IN STEAM FLOW FROM HIGH POWER

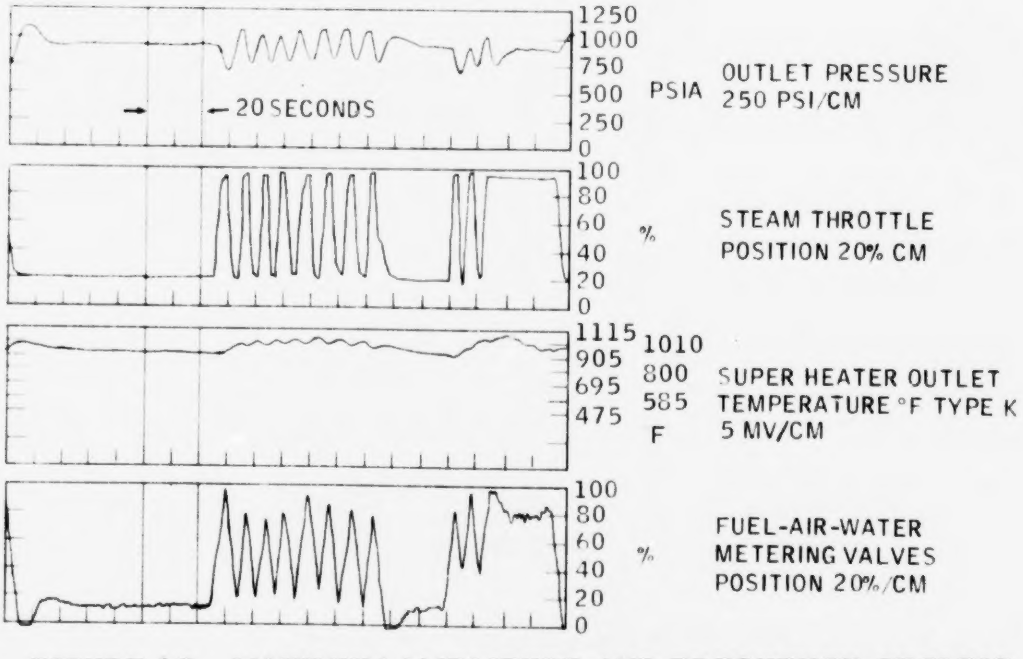

FIGURE 3C. MAXIMUM AMPLITUDE AND FREQUENCY CYCLING

Two organic fluid vapor generators were designed as backup for EPA system contractors. AEF-78 and Fluorinal-85 organic fluid vapor generators were designed to interface with the same type of combustor tested with the steam generators described above. Both used a rectangular straight tube array with machined manifolds for return bends. An all brazed construction was used with extruded internal fins incorporated to increase the heat transfer on the organic fluid side.

The results of the program proved that a low emission compact vapor generator could be developed to meet the emission and control requirements for automotive vehicles. The emission levels obtained, however, were borderline. Further development work in this concept will be required before sufficiently large emission margins were available for the normal tolerances required for vehicle applications. Among the paths available for lowering emissions are added pressure drop and addition of exhaust gas recirculation. Since these changes would increase the parasitic power demands, future work should be based upon a vapor generator optimized for a particular engine system.

2

INTRODUCTION

Rankine cycle engines are the most highly developed external combustion system with much of the world's power being generated by such power plants. However, little development progress had been made to reduce emissions and improve the system and components for application at power level suitable for automobiles. Emissions, efficiency, packaging, controls, and cost problems required solutions that could only be fully evaluated by combined component technology advancements and automobile system demonstrations. A compact low emission vapor generator with controls compatible with low emissions and automotive duty cycles is one of the major components requiring advancements. Solar, under contract to EPA, has demonstrated two different steam generators designed to meet the requirements of an automotive system. A low emission combustor based upon the results of an earlier Solar combustor demonstration program contracted by EPA (Ref. 1) has been the basis of the design described in this report. Integration of these combustor control concepts with specially designed compact vapor generators forms the basic problem attacked by this project.

The purpose of this work was to demonstrate by means of test results that a practical fully integrated steam generator had emissions below the 1976 Federal Standards. Major goals of the program are:

- High turndown range
- Compact packaging
- Low emissions during transients
- Stable vapor generator operation
- Accurate steady state control of outlet pressure and superheater temperature
- Sufficient control capability to prevent excessively high or low pressures and temperatures at the superheater outlet or burnout failures during the large amplitude and frequent steam flow demand changes required by normal automotive stop and go driving

- Low parasitic power

- Low noise

Three different fluids were required to be evaluated through the design phase of the program. Water, Fluorinol-85 and AEF-78 vapor generators were designed specifically to interface with Steam Engines Systems, Thermo Electron and Aerojets' vehicle packages. Each of these companies is on contract to the EPA to develop a complete automotive Rankine Cycle system. Solar's steam generator program was to provide backup capability for this critical component. At the end of the design phase it became apparent that the greatest gain to the technology would be for Solar to concentrate its development tests on water systems alone. This decision in no way was based on technical tradeoffs between organic based fluids and water for the automotive engine, but simply on development cost analysis. However, one of the two steam (water) generators tested was designed to specifically obtain test data on a potentially significant problem of organic vapor generators' parallel flow stability.

3

SYSTEM REQUIREMENTS

Two steam generators have been designed and tested in this program. The first unit was a test bed steam generator to evaluate its effects upon emissions, parallel flow, and the control system. Efficiency was not stressed in this unit in order to expedite construction (no extended surfaces). A second unit designed and tested placed emphasis on efficiency and elimination of parallel flow instabilities. It incorporated extensive finned tubing and single flow path in the critical vaporization and superheater tube sections. Three other units were designed for the automotive systems being developed by EPA. Each of these systems had a different fluid and required an envelope designed to interface with each of the three system contractors.

3.1 TEST BED COMBUSTOR/STEAM GENERATOR

This unit incorporated six parallel flow paths in the steam generator and bare tubes. Efficiency requirements were made sufficiently low to allow a bare tube unit that could be fabricated entirely at Solar with a minimum of lead time.

3.1.1 Combustor Requirements

- Heat release 2.5×10^6 BTU/hr based on LHV
- Turndown ratio 40:1
- Fuel: kerosene or JP-5, EPA reference unleaded gasoline was also used when it became available
- Size: 24 inches square by 20 inches high not including exhaust ducting
- Weight: 175 pounds
- Startup time to full vapor generator in less than 15 seconds from a cold start.
- Maximum electrical input to be less than 2.5 HP electrical equivalent

Emissions to be below the 1976 Federal Standards. Test results are to be compared to the limits assuming a 10 MPG fuel consumption as shown in Table II.

TABLE II

EMISSION LEVEL GOALS

Constituent	Grams/Mile	Grams/Kilogram*
Hydrocarbon (HC)	0.41	1.42
Carbon Monoxide (CO)	3.4	11.8
Oxides of Nitrogen NO + NO_2 reported as (NO_2)	0.4	1.38

*Calculated assuming 10 MPG

3.1.2 Parallel Flow-Bare Tube Steam Generator Goals

- Fluid: water
- Pressure: 1,000 psia
- Flow: 1525 lbs/hour of steam
- Temperature: 1000°F
- Efficiency: greater than 80% based on LHV, 75% based on HHV (Note actual efficiency was 78% LHV at full flow)
- Core diameter: 21.5 inches
- Core length: less than 8 inches
- Maximum air side pressure drop: 3 inches of water
- Maximum water side pressure drop: 250 psi
- Construction: bare tubes to allow rapid construction

- Flow arrangement: to be similar to an organic vapor generator with respect to air side and working fluid side temperature and flow distributions.

3.1.3 Controls

- Air-Fuel Control. An automatic control of air and fuel flow is required to maintain the equivalence ratio at optimum levels across the entire 40 to 1 turndown range.

- Steam Generator. An automatic control of feed water, fuel and air flow is required to maintain the superheater outlet at 1000°F ± 100°F and 1000 psia ± 100 psi during steady state and transients expected in an automotive operation. Although exact flow rate changes are not precisely known, high rates can be anticipated. Flow rate is basically determined by engine speed, (a relatively slow factor) and cutoff valve actuation (a fast parameter requireing only a few milliseconds for full travel). Actual test results were obtained with transients rates of as high as 900 pounds per hour steam flow change per second. These transients were made in steps as large as 80 percent of full flow.

3.2 HIGH EFFICIENCY FINNED TUBE STEAM GENERATOR

3.2.1 Combustor

Identical to the test bed combustor, see paragraph 3.1.1.

3.2.2 Steam Generator

- Efficiency: 85% based on LHV, 79.6% based on HHV (Note actual full flow was 86% based on LHV).

- Construction: finned tubes

- Flow arrangement: no parallel flow passages in superheater or vaporizer sections. This prevents "chugging" flow instabilities and simplifies the control since only a single outlet tube can be monitored for overtemperature.

- All other constraints the same as the parallel flow unit, see paragraph 3.1.2.

3.2.3 Controls

Same as test bed unit, see paragraph 3.1.3.

3.3 UNITS DESIGNED FOR EPA SYSTEM CONTRACTORS

3.3.1 Fluorinol-85 System

Fluorinol-85 Side

Flow	10,000 lbm/hr
Pressure Drop	130 psi maximum
Outlet Pressure	700 psia
Inlet Temperature	287°F (at max. power)
Outlet Temperature	550°F
Heat Transfer to Fluorinal-85	2.25 x 10^6 BTU/hr (reference)

Gas Side

Air-Fuel Ratio	25:1 (JP-5 fuel)
Flow	3740 lbm/hr
Pressure Drop	3.0 inches water column
Inlet Temperature	2500°F (mean) ± 250°F
Efficiency	81% based on HHV (reference)
	86.5% based on LHV (reference)
Outlet Temperature	427°F (reference)

NOTES:

The maximum tube wall temperature during steady state operation shall be less than 575°F. The maximum temperature was based upon an assumption that the gas side inlet temperature is 2750°F and a velocity deviation at the inlet plane of the vapor generator is 10 percent above the design mean design value.

Envelope requirements: Outside envelope dimensions were within the following configuration. A 20 inch diameter combustor section shall be oriented in the vertical firing down position with a six inch air inlet at the top. The 20 inch diameter shall extend vertically downward 10 inches to a rectangular vapor generator section. The vapor generator is designed to fit within dimensions of 15 inches by 25 inches by a core height of 10 inches (including transition). It shall be symmetrically installed below the vapor generator to give an overall height of 20 inches. Envelope parameters were held constant in the design phases.

Efficiency is defined by the relationship

$$Q = W_f \eta H$$

where Q = heat transfer rate to working fluid

η = efficiency

W_f = fuel rate

H = heating value of fuel

The fuel is assumed to be JP-5 with HHV = 19,800 BTU/lb, LHV = 18,550 BTU/lb.

3.3.2 AEF-78 Vapor Generator

AEF-78 Side

Flow	19,300 lbm/hr
Pressure Drop	50 psi goal, 100 psi maximum
Outlet Pressure	1000 psia
Inlet Temperature	396°F
Outlet Temperature	650°F
Heat Transfer Rate to AEF-78	2.02 x 10^6 BTU/hr (reference)

Gas Side

Air-Fuel Ratio	25:1 (JP-5 fuel)
Flow	3400 lbm/hr
Pressure Drop	3.0 inches of water column
Inlet Temperature	2500°F (mean) ± 250°F
Efficiency	80% based on HHV (reference) 85.5% based on LHV (reference)
Outlet Temperature	455°F (reference)

NOTES:

The maximum tube wall temperature during steady state operation shall be less than 720°F. This shall be a local temperature and shall not represent more than a small percentage of the total fluid temperature. Maximum temperature shall be based upon the assumption that the gas side inlet temperature is 2750°F, and the gas velocity at the inlet plane is 10 percent of the design mean value.

Envelope requirements. Outside envelope requirements shall be within the following configuration. A vertically downward firing combustor shall be mounted on top of the vapor generator. The assembled unit shall have an outside diameter of less than 26 inches and an overall height to the exit plane of the vapor generator of 17 inches.

3.3.3 Steam Generator

Preliminary specification for a steam generator for vehicle installation are listed below.

Water Side

Flow	1200 lbm/hr
Pressure Drop	150 psi goal, 250 psi maximum
Outlet Pressure	1000 psia
Inlet Temperature	220°F
Outlet Temperature	1000°F
Heat Transfer Rate to Water	1.58×10^6 BTU/hr (reference)

Gas Side

Air-Fuel Ratio	25:1
Flow	2670 lbm/hr
Pressure Drop	3 inches of water column
Inlet Temperature	2500°F mean ± 250°F
Efficiency	85% based on LHV 79.6% based on HHV
Outlet Temperature	462 F (reference)

The preliminary estimate of the maximum envelope allowed for this system is a horizontally firing (towards back of vehicle) combustor with a maximum diameter of 19.5 inches. Total length of the combustor/vapor generator shall be less than 16 inches.

4

SYSTEM CONFIGURATION ANALYSIS

4.1 GENERAL CONSTRAINTS AND SELECTION OF A ROTATING CUP SYSTEM

Achieving emission levels below the 1976 Federal emission levels is a challenging objective for a combustor rig operating independently. Constraints imposed by addition of practical automotive operations significantly complicate the task. Automotive requirements that have a major influence on the design include:

- Compact packaging
- High turndown ratios
- Low parasitic power
- Virtually continuously varing power level demands
- Average steam rate of approximately 10 percent of maximum in the Federal driving cycle
- Cold startup
- Rapid warm up
- Minimum superheater temperature overshoot (to prevent lubricant and seal degradation)
- Narrow band superheater outlet temperature control to maintain temperature high as is safe for maximum cycle efficiency
- Minimum overshoot in pressure control to prevent damage or loss of fluid through relief valve
- Minimum water hold up to minimize energy release hazards

A typical example of the design constraints imposed by the high turndown ratio can be seen in a brief review of the air-fuel ratio requirements. To maintain the air-fuel ratio within ±10 percent of the optimum at the critical power output of 10 to 15 percent, the valves cannot leak more than ±1 percent of their maximum rated flow values if all other errors are ignored. As a consequence new and unconventional approaches have been incorporated to allow accurate metering of the three input fluids, air, fuel and water across wide turndown ranges with compact components.

Two basic approaches are available to obtain low emission. One attractive method is to premix the air and fuel in a vapor form prior to combustion. If the fuel and air are homogeneously mixed, this method can ensure low emissions by maintaining the overall air-fuel ratio sufficiently lean (and thus low flame temperatures) to prevent the formation of significant NO_x. Emission levels an order of magnitude below the Federal level are theoretically possible with this approach. Several major problems indicate that this may not be an acceptable approach for an automotive system. Initial startup emissions of HC with cold walls are difficult to keep within limits and may represent the same order of magnitude startup problem as with the present automotive spark ignition engine. To ensure rapid vaporization and uniform mixing of air and fuel in a premixed system, large mixing volumes, high air velocities, small fuel droplets and large heat input values are required. This equates into the need for a high power consumption air atomization system, high power consumption in the combustor fan, recirculation of high temperature exhaust or combustor gases (with associated pumping losses) and the need for long mixing volumes. Since large volumes of premixed gases are necessary for correct mixing, a flashback explosion hazard is present. The required high degree of turndown necessary (40 to 1) for low fuel consumption in the driving cycle makes design of flame arrestors difficult and unreliable at very low velocities. Transient performance, as with startup emissions, is also questionable since the heat of vaporization added to the mixture must be matched to the instantaneous changes of fuel flow. If this dynamic balance is not maintained relatively closely, high inlet gas temperatures may occur or "wet wall" operation will occur. Both of these conditions are undesirable since they affect transient air-fuel ratios and can cause higher emissions.

Direct liquid fuel injection into the combustor to circumvent the above problems minimizes parasitic power and bulk. Analysis and development tests have demonstrated that fuel injection, droplet vaporization, air-fuel mixing, rich reaction and final lean burnout can achieve low emissions in an overall lean direct liquid fuel injection system.

All types of injection and atomization systems were considered. These are listed with their limitations.

- Pressure Atomizer - This system cannot form a fuel spray at the low fuel flows required (down to approximately 3 pounds per hour), it needs small orifices subject to contamination, and the high fuel pressures mean an expensive fuel pump.

- Dual Orifice Pressure Atomizer - As above but with more small orifices to reduce reliability and added filtration costs.

- Air Assist Pressure Atomizer - Requires auxiliary high pressure air compressor that can consume more parasitic power than the combustor fan. This is a key element since fuel economy is directly and strongly dependent upon the combustion system. In the Federal Driving Cycle the average roadload power is approximately 10 percent. Thus, addition of a typical 1 HP air assist compressor can cause fuel economy drops of approximately 10 percent. Air assist is also limited in turndown range thus requiring control of the air assist compressor flow as well as the main air flow into the combustor. This adds additional complexity and cost over and above the relatively expensive compressor and its drive system. It also has the limitation of a variable drop size dependent on fuel flow and a relatively narrow spray angle.

- Air Assist (Ultrasonic) - Same as above but with less proven reliability. The spider wire that holds the resonant chamber can and has, at Solar, been observed to collect spray and form large drops.

- Electrostatic and Vibrating - Auxiliary power source required, have not demonstrated capability of operating over the wide range of fuel flows. Performance not proven.

Solar's initial program for a low emission combustor (completed June 1971, Ref. 1), forms the technical basis for selecting the design configuration. A 2×10^6 BTU/hr combustor plus integrated air and fuel control system was demonstrated to have low emissions across a wide range of fuel flows. Design features determined to be of significance for low emissions were used in synthesizing the design being reported on:

- Rotating cup atomization due to its capability for wide turndown, low power consumption, insensitivity to contamination, wide spray angle uniform droplet size, low fuel pressure and good ignition characteristics.

- Fully modulated air and fuel control systems mechanically synchronized to maintain desired air-fuel ratios across the entire 40 to 1 turndown range. On-off controls result in ignition and shutdown hydrocarbon emissions during the continuously cycling operations for automotive usage.

- Emphasis on symmetric air flow from inlet through fan combustor and vapor generator to ensure the best possible uniformity of air-fuel mixtures.

- Control of air flow rate into combustor by means of a valve rather than speed changes of the fan-motor drive system since inertia lag could cause significant delays or mismatch between air and fuel flow.

The rotating cup atomization and fuel injection system selected has demonstrated that it has the following features:

- Requires essentially zero parasitic power to operate if carefully packaged into system (only several watts are necessary to accelerate and overcome fuel friction with this system). If it is coaxially driven by the combustion air fan, the additional load is difficult to measure.

- Has proven turndown capabilities of greater than 100 to 1 (Ref. 1). Spray quality and angle control do not change over this large turndown range.

- No small orifices are required thus eliminating sensitivity to contamination and improving reliability.

- No pressure drop required other than to overcome steam generator gas side pressure drop. Thus low cost standard automotive fuel pumps can be used.

- Ideal spray angle for ingition. Excellent ignition characteristics have been obtained since the fuel spray pattern can be accurately repeated and the spark plug located at the point the fuel impinges on the wall.

4.2 CONFIGURATION ANALYSIS

Integrating the above features with the specified goals (Section 3) determined the overall system configuration (Fig. 1). Emission goals dictated that the maximum possible pressure drop be utilized for mixing velocities in the combustor. Emission levels are also dependent upon combustor exit temperatures. NO formation rates are negligible below 3200°F. From previous tests (Ref. 1) an exit temperature of 2500°F ± 250°F provided an adequately conservative exit temperature to meet emission goals. With a design exit condition of 2500°F and a specified heat release of 2.5×10^6 BTU/hr an equivalence ratio of 0.62 is obtained. An air flow of 3400 pounds per hour can be calculated using these factors. During the preliminary design it was assumed that an overall electric motor-fan efficiency of 50 percent could be obtained. Therefore, ideal air horsepower available is only 1.25 HP. At 3400 pph this limits the fan pressure rise to less than 10.5 inches of water. Preliminary analysis and sizing of the air valve determined that 2.0 inches of water pressure drop was needed for air metering (see Sec. 5). Thus a total of 8.5 inches pressure drop was the maximum available for the combustor, steam generator and exhaust ducting. An allowance of 0.75 inch for exhaust leaves 7.75 inches of water.

Emission goals require that the largest portion of the available 7.75 inches of water pressure drop be allocated to the combustor. Since the air pressure drop across the steam generator is exponentially dependent upon its frontal area, it is essential to maintain the maximum frontal area. Previous experience has indicated that a straight through flow arrangement with a minimum of flow transition between the combustor and steam generator would result in the most uniform distribution of air in the combustion chamber. As a consequence, the full diameter available was used to design a tube matrix that required essentially no turns or flow transition between the combustor and steam generator. Using the maximum diameter and a compact bare tube matrix (for the test bed system), the pressure drop is 2.75 inches of water. The remaining 5.0 inches of water pressure was used to establish the combustor pressure drop.

From the above steps the steam generator and combustor diameter were established. Efficiency and pressure drop criteria determined the tube matrix depth (6.20 inches). An overall height limit of 20 inches is the only major design constraint remaining to be satisfied. A combustor emissions goal is also a major criteria at this point. To prevent combustion products from quenching before reaction is completed, it is good design practice to keep the combustor length as long as possible (particularly with low pressure drop systems). Design studies emphasizing low parasitic power, compact and symmetrical flow distribution finalized the configuration around an integrated radial flow fan coaxially mounted with the combustor and steam generator (see Fig. 1 and Section 5 for detail description). This configuration resulted in the minimum of parasitic power consumption since the same motor that drives the fan is used to drive the fuel atomization and injection cup. Fan bearing and rotating cup bearing friction losses are minimized as is mounting complexity. No external ducting is required since the fan diffuser discharges directly into a large diameter air metering valve. A large diameter valve is essential to provide low flow losses and the high degree of symmetry essential to uniform mixing at low pressure drops. The air valve uses 20 ports circumferentially spaced around the combustor outer diameter to direct air into an air swirler section. All flow is completely symmetric in the air and fuel injection systems. Non-symmetrical turns, flow areas, pressure gradients, or velocity gradients either upstream or downstream of the combustion chamber require especially careful attention to prevent maldistributions that would normally increase emissions. As a consequence of this design investigation, the 20 inches of total height was divided as follows:

• Steam generator	6.20 inches
• Fan, diffuser and air valve	1.60
• Fan inlet and drive pulley	2.00
• Primary air swirler and insulation	2.20
• Combustion chamber	8.00

5

COMBUSTOR

5.1 OVERVIEW OF COMBUSTOR SECTION

System restraints required that an integrated approach be taken in the design of the following combustor subsystems:

- Air supply distribution and control
- Fuel atomization, injection and distribution
- Combustion chamber configuration

It was necessary to treat combustion as a systems integration problem in order to meet the following major constraints:

- Ideal power limit of 0.83 HP (7 inch pressure drop at 3400 pounds per hour air flow)
- Envelope limits of 24 by 24 inches square (including electrical drive motor) and 20 inches high
- Aerodynamic and geometric physical interface with a large frontal area steam generator

As discussed in the previous section, these constrains when coupled with the approach of using a rotating cup atomization system predetermine the following combustor characteristics:

- Pressure drop: 7 inches of water total (5 inches in combustor and 2 inches across air valve)
- Diameter: 20 inches
- Length: 8 inches
- Air Flow: 3400 pounds per hour

- Fuel flow: 135 pounds per hour with JP-4, JP-5 or unleaded gasoline

These parameters were derived at the preliminary design phase of the program and remained consistent through combustor rig tests and evaluation of the integrated system with both steam generators. Since the combustor and steam generator were designed to directly interface with essentially no transition, the geometrical configuration of the combustor was essentially frozen from the beginning of the program. Pressure drop at maximum flow was similarly frozen. Emissions development thus concentrated on improving performance by relatively minor changes in mixing, flow splits, air-fuel ratios and other adjustments not requiring basic configuration modifications. This section describes the work performed to obtain the final emission test results summarized in Section 1. Initial combustor rig tests are discussed first. From these tests the total air-flow and flow split between the primary and secondary air injection ports was obtained. Next follows an analysis of the air supply fan, air control, and distribution system designed to be compatible with the combustor test rig results. A discussion of the combustor development tests for a fully integrated air supply fuel and steam generator system concludes this section on combustion.

5.2 COMBUSTOR RIG TESTS

5.2.1 Description of Combustor Rig

In order to verify all basic design assumptions, a series of full scale combustor tests were performed prior to design finalization. Figure 4 schematically depicts the combustor test rig setup. High pressure air enters the air flow measurement sections from a high pressure compressor. Air flow into the combustor is measured by means of one of three parallel orifice runs. Because of the wide turndown requirements, 40 to 1, three different orifices of 0.75, 1.5 and 3 inches diameter are used. Each orifice is sized for optimum Reynolds number at air flows corresponding to the respective fuel flows midway in the ranges of 109 to 23, 23 to 5.0 and 5.0 to 1 pounds per hour. The orifices are sharp edged, with corner pressure taps, and have upstream flow straighteners to minimize aerodynamic influence of the metering section from the upstream shutoff valves. These valves are manually operated so that air can be diverted to the metering orifice appropriate to the air flow required.

Fuel flow is measured by three variable area float type meters having ranges of 1 to 10, 10 to 110 and 50 to 170 pounds per hour. Each flow meter has been calibrated prior to use in these tests by means of a weight flow versus time measurements at three or more points across the flow range.

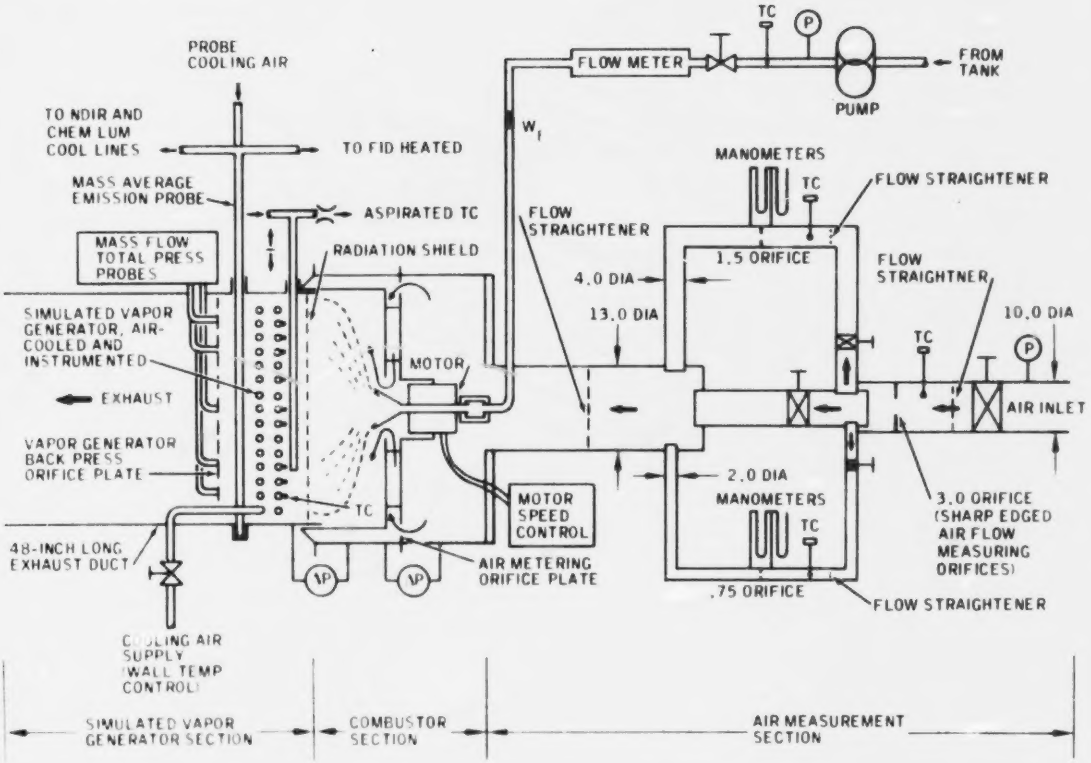
TC
P
FLOW METER
FROM TANK
PUMP
PROBE COOLING AIR
TO NDIR AND CHEM LUM COOL LINES
TO FID HEATED
W_f
MANOMETERS
TC
FLOW STRAIGHTENER
MASS AVERAGE EMISSION PROBE
ASPIRATED TC
FLOW STRAIGHTENER
MASS FLOW TOTAL PRESS PROBES
RADIATION SHIELD
1.5 ORIFICE
FLOW STRAIGHTNER
4.0 DIA
13.0 DIA
10.0 DIA
SIMULATED VAPOR GENERATOR, AIR-COOLED AND INSTRUMENTED
TC
P
MOTOR
EXHAUST
AIR INLET
VAPOR GENERATOR BACK PRESS ORIFICE PLATE
2.0 DIA
MANOMETERS
TC
TC
MOTOR SPEED CONTROL
3.0 ORIFICE (SHARP EDGED AIR FLOW MEASURING ORIFICES)
48-INCH LONG EXHAUST DUCT
ΔP
ΔP
AIR METERING ORIFICE PLATE
.75 ORIFICE
FLOW STRAIGHTENER
COOLING AIR SUPPLY (WALL TEMP CONTROL)
SIMULATED VAPOR GENERATOR SECTION
COMBUSTOR SECTION
AIR MEASUREMENT SECTION

FIGURE 4. PRELIMINARY COMBUSTOR TEST RIG

Metered air is delivered into the combustor from a plenum chamber that has provisions for installation of air metering orifices to simulate a part of the aerodynamic interaction of the air metering valve. Air is directed from this valve plate into the combustor outer case for distribution into the primary air (swirl plate) and secondary air holes located around the outside of the cylindrical portion of the combustor liner. Fuel is delivered by means of a dynamic seal into the drilled shaft of the cup motor. After passing through the rotating shaft to the cup which both atomizes and distributes the fuel in a flat spray into the 20 inch diameter combustor. Initial testing was performed with a perforated Inconel radiation shield across the exhaust plane of the combustor. The majority of tests performed including the emission results described in this report, were run without the radiation shield.

Immediately downstream of the radiation shield an asperated thermocouple probe has been installed to monitor temperature. The tip consists of a four inch long triple shielded platinum rhodium (type S) thermocouple. It is mounted on a long cooled stainless steel tube that allows the probe to be traversed across the entire diameter of the tail pipe (see Fig. 5). One-half

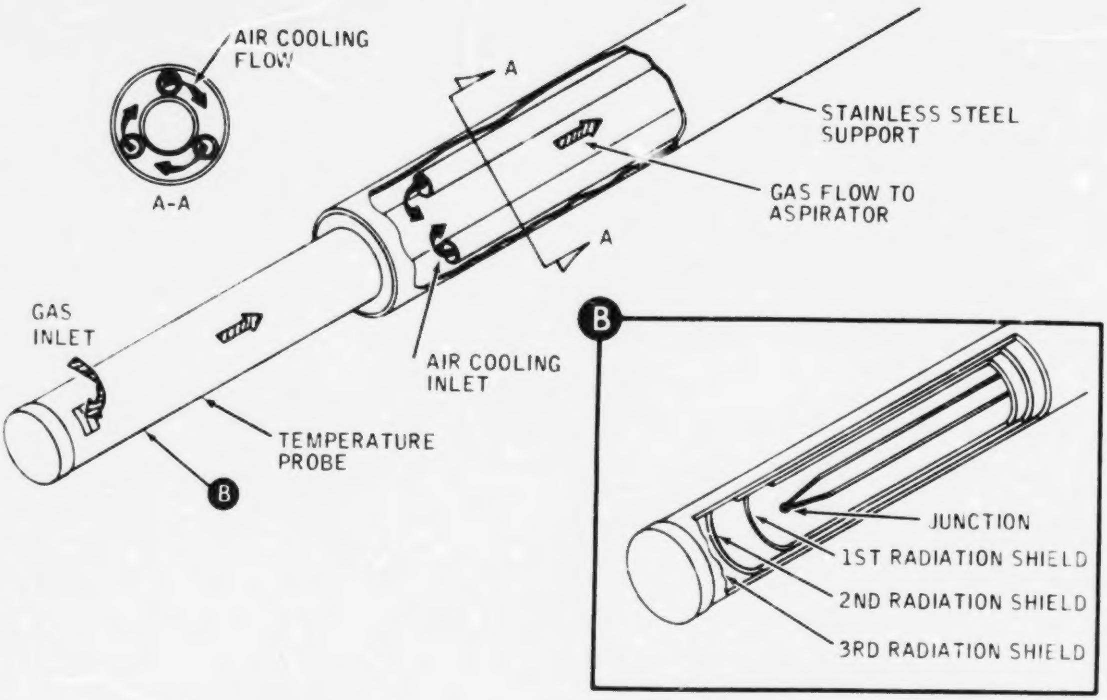
AIR COOLING FLOW
A-A
A
A
STAINLESS STEEL SUPPORT
GAS FLOW TO ASPIRATOR
GAS INLET
AIR COOLING INLET
TEMPERATURE PROBE
B
B
JUNCTION
1ST RADIATION SHIELD
2ND RADIATION SHIELD
3RD RADIATION SHIELD

FIGURE 5. SCHEMATIC OF GAS TEMPERATURE SENSOR AND MECHANICAL SUPPORT

an inch downstream of the thermocouple probe is the simulated air cooled vapor generator. Welded to the surface of the coils are twelve type K thermocouples (see Fig. 6 for thermocouple location).

An emission probe is installed at plane 4 inches downstream of the radiation shield. Figure 4 shows its installation in a twenty inch diameter duct. A total of 36 holes are used to provide equal area sampling across the 20 inch diameter tail pipe. A large diameter tube collects the gas sample for delivery to the gas analysis equipment sampling lines. Temperature of the sampling probe is controlled by cooling water flowing through passages around the probe. Three thermocouples are located along the length of the probe to ensure that the sampled gas is quenched to a sufficiently low temperature to prevent further reactions (Fig. 7). It is approximately 42 inches from the outlet of the tail pipe to prevent recirculation of fresh air into the probe.

A back pressure orifice plate is installed immediately behind the emission probe. It is a flat plate orifice with 60 holes located at radial positions to simulate a uniform flow restriction equal to the remaining flow restriction of the actual vapor generator. A 48 inch long tail pipe was used to minimize buoyancy circulation and swirl recirculation of outside air.

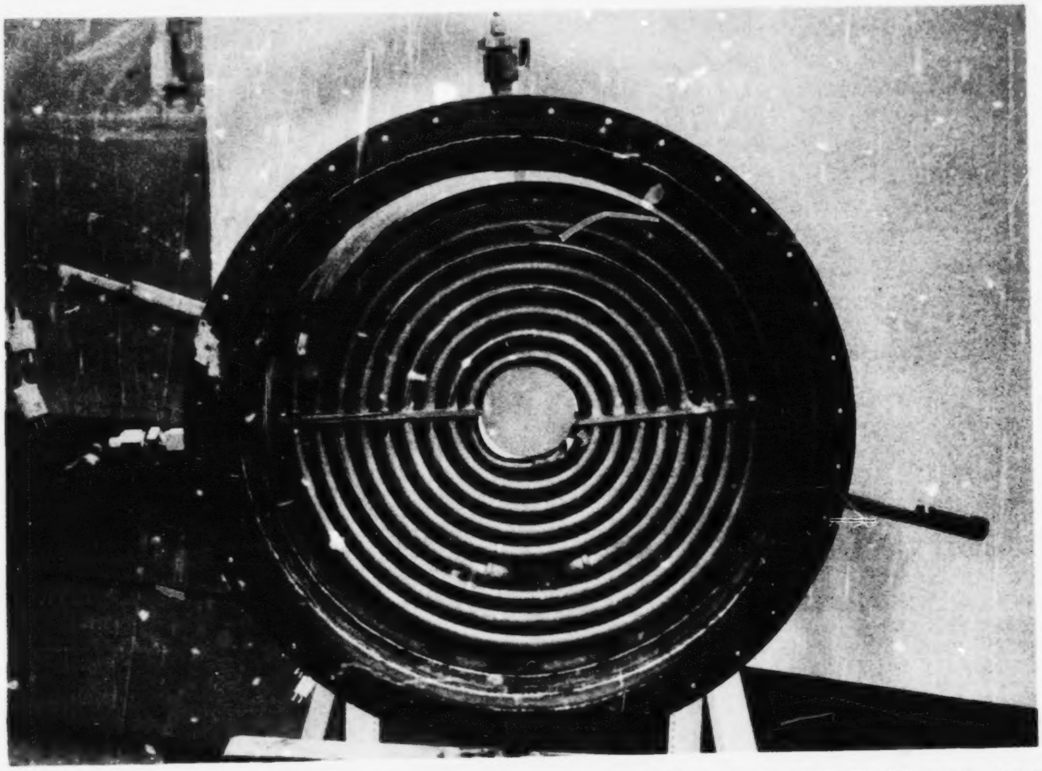

FIGURE 6. COMBUSTOR SIDE OF VAPOR GENERATOR SIMULATOR SHOWING LOCATION OF THERMOCOUPLES

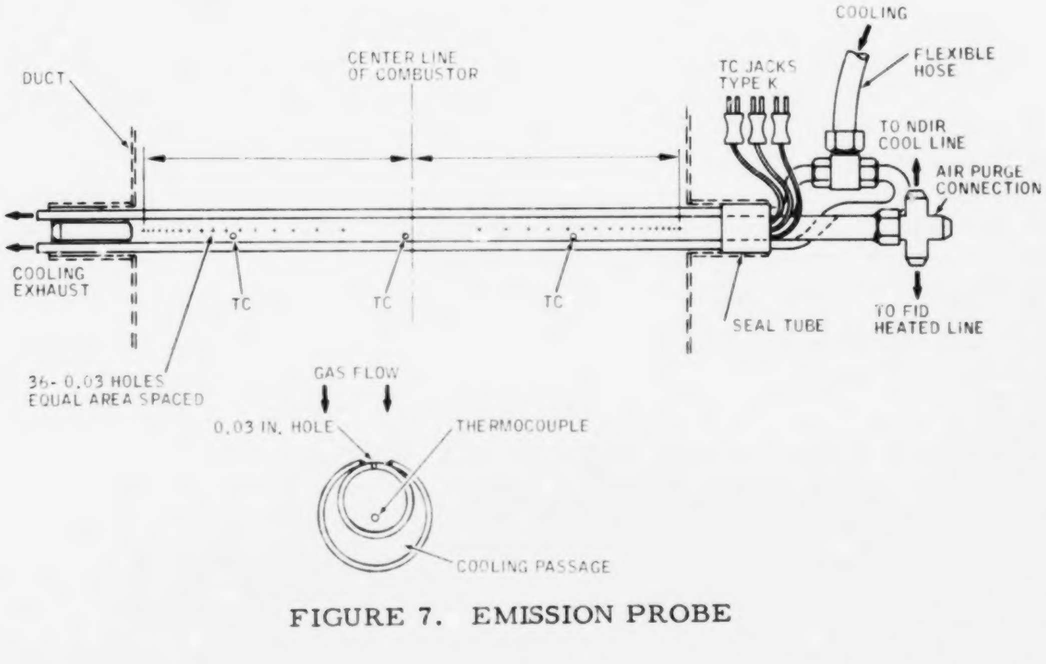
COOLING
FLEXIBLE HOSE
TC JACKS TYPE K
CENTER LINE OF COMBUSTOR
DUCT
TO NDIR COOL LINE
AIR PURGE CONNECTION
COOLING EXHAUST
TC
TC
TC
SEAL TUBE
TO FID HEATED LINE
36- 0.03 HOLES EQUAL AREA SPACED
GAS FLOW
0.03 IN. HOLE
THERMOCOUPLE
COOLING PASSAGE

FIGURE 7. EMISSION PROBE

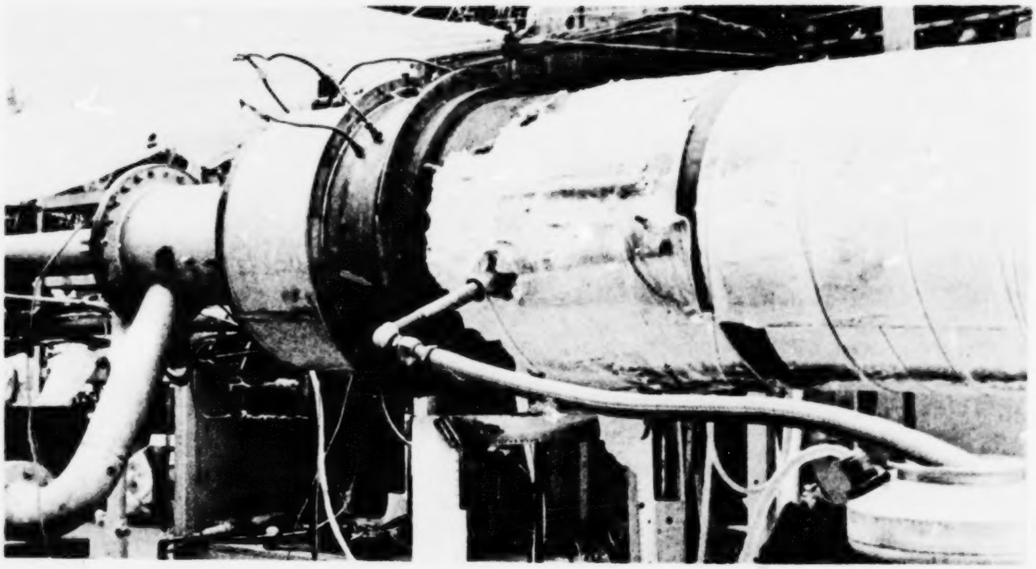

FIGURE 8. TEST COMBUSTOR INSTALLED IN RIG

Figure 8 shows the overall test rig in operation. The large diameter flange on the right is at the combustor exit plane and is used to seal the tail pipe to the combustor to prevent possibilities of air leakage into the tail pipe. Any leakage at this point could cause errors in emissions as measured by probe in tail pipe. The emission probe location is immediately downstream of the simulator (Fig. 4). All emissions were measured as described in Appendix I.

5.2.2 Control of NO_x in Combustor

Since liquid fuel (unleaded gasoline) is directly injected into the combustor the combustion process is complex. A considerable effort has been devoted to sophisticated computer modelling of the reaction kinetics of rotating cup combustors. Reference 1 summarizes this analysis. What analysis and hundreds of hours of low emission combustor development testing proves is NO_x emissions are the critical species and must be minimized by preventing reaction from occurring at high temperatures. This rate of formation of NO is:

$$\frac{dNO}{dt} = 6.62 \times 10^{14} \times e^{-\frac{67000}{T}} \left[\frac{(N_2)\,(O_2)^{1/2}\,P^{1/2}}{T^{1/2}} \right]$$

where NO, N_2 and O_2 are concentrations of nitrogen, oxygen, and nitric oxide in mole fractions, t is time in seconds, T is temperature °K, and P is pressure in atmospheres. Although this equation only holds for a homogeneous mixture, it helps explain the importance of rapid vaporization and mixing. Droplet burning and combustion during the transition from rich to lean burning both occur with local zones at stoichiometric temperatures. Only a small percentage of the fuel reacting at these temperatures will cause unacceptable high NO_x emissions.

Since the local reaction zone air-fuel ratio determines the temperature, the formation of NO as a function of air-fuel ratio and mixing versus reaction time rates are as shown in Figure 9. Because NO must be maintained well below 50 ppm, it is seen that the mixing time must be kept very low and the air-fuel ratio must be generally leaner than 20 to 1 to maintain reaction zone temperatures below 3200°F and above 2500°F to keep excessive NO from forming, but still sufficiently high to complete the oxidation of HC and CO in a reasonable volume. The important design rules and the methods of implementing used throughout the combustor development are:

- Provide rapid and uniform vaporization prior to reaction (no droplet burning). The cup causes a uniform droplet spray to be directed in a 180 degree spray pattern that has a large geometric surface area at the injection point. Use of swirl flow cause recirculation of high temperature combustion products to assist in vaporization. Cup rotation is opposite the tangential swirl component from the air injection port causing high relative velocities and consequent rapid vaporization.

- Rapid mixing of vapor with swirl air to obtain (consistent with parasitic fan power requirements) on overall lean mixture. It is a design goal to minimize reaction in this zone since the mixture must change from rich to lean in this zone. Reaction at near stoichiometric conditions would produce large amounts of NO thus mixing rates must be made faster than reaction rates to keep flame temperatures below 3200°F. By maintaining high air velocities and a high swirl cone angle around the cup's fuel spray pattern, both of the above conditions are attempted to be optimized.

- Elimination of small pockets of slowly mixing zones or high temperature reaction. High air velocities and design with complete symmetry are incorporated to eliminate this cause of NO formation.

5.2.3 Combustor Rig Test Results

Figure 10 shows the arrangement of the combustor used for rig test. Photographs of both sides of the rig test unit are shown in Figures 11

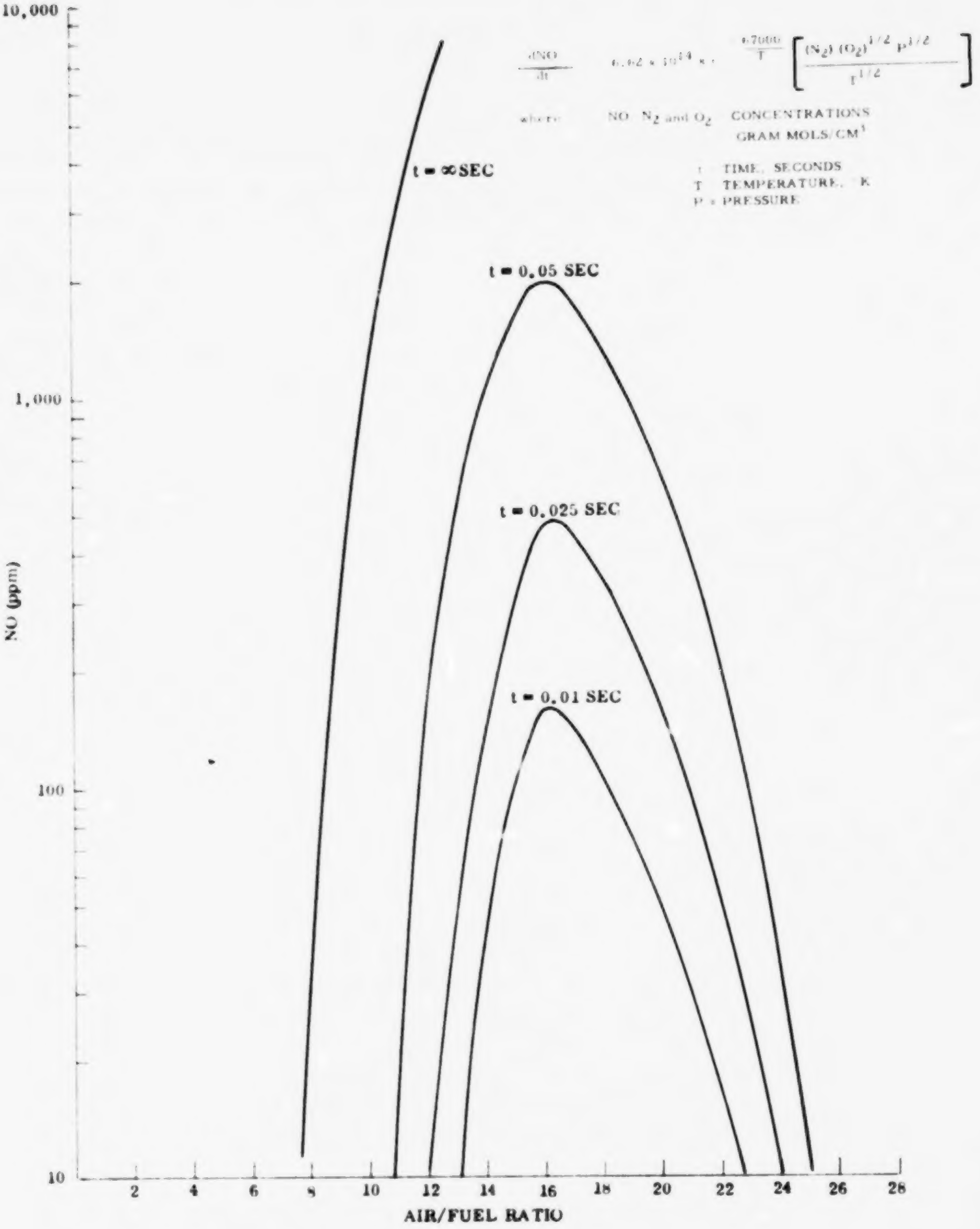

FIGURE 9. EMISSION OF NITRIC OXIDE AS A FUNCTION OF AIR-FUEL RATIO AND TIME

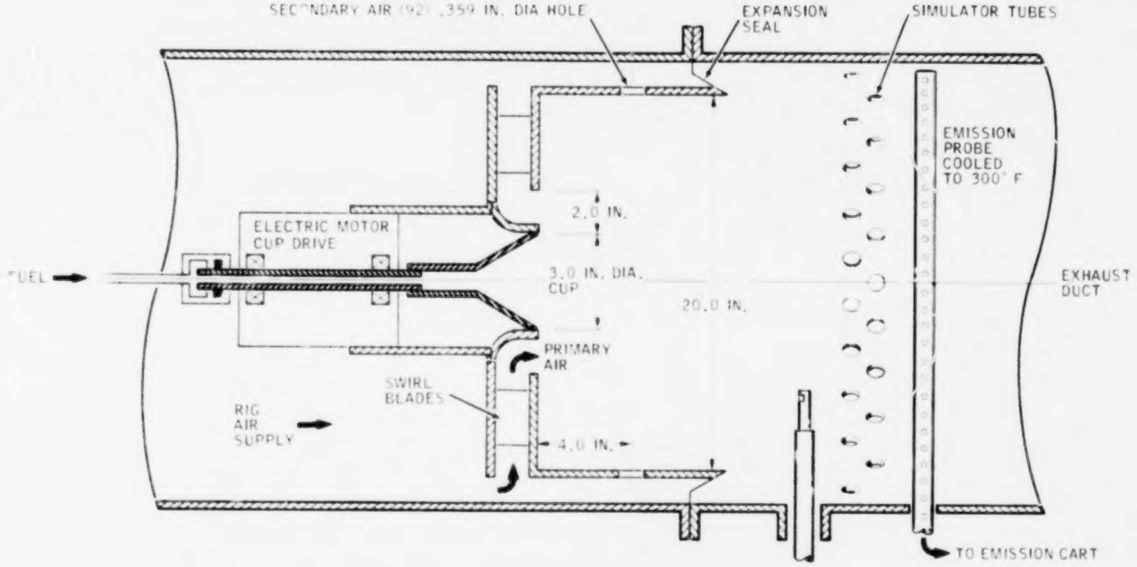
SECONDARY AIR (92) .359 IN. DIA HOLE
EXPANSION SEAL
SIMULATOR TUBES
EMISSION PROBE COOLED TO 300° F
2.0 IN.
ELECTRIC MOTOR CUP DRIVE
FUEL
3.0 IN. DIA. CUP
20.0 IN.
EXHAUST DUCT
PRIMARY AIR
SWIRL BLADES
RIG AIR SUPPLY
4.0 IN.
TO EMISSION CART

FIGURE 10. RIG TEST COMBUSTOR

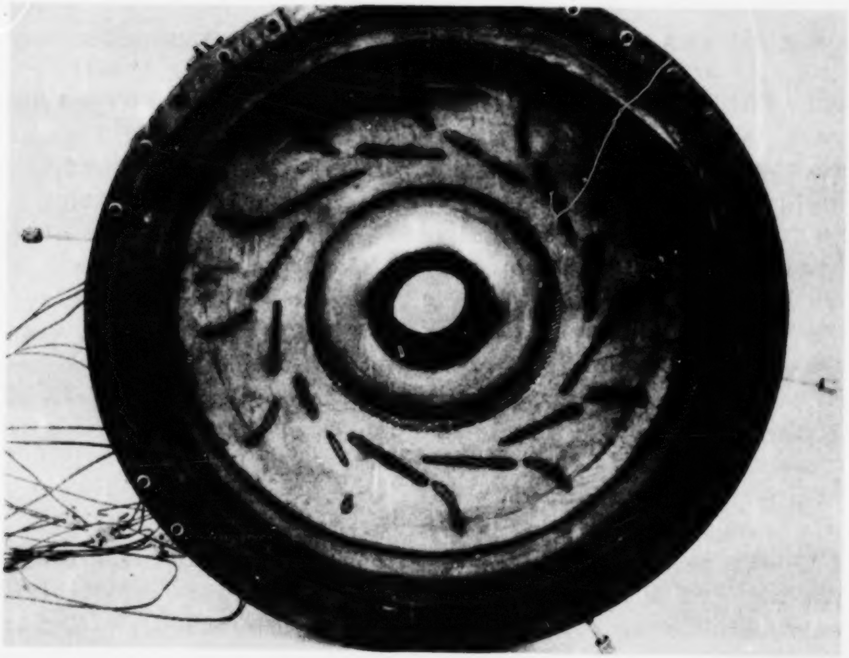

FIGURE 11. UPSTREAM SIDE OF COMBUSTOR

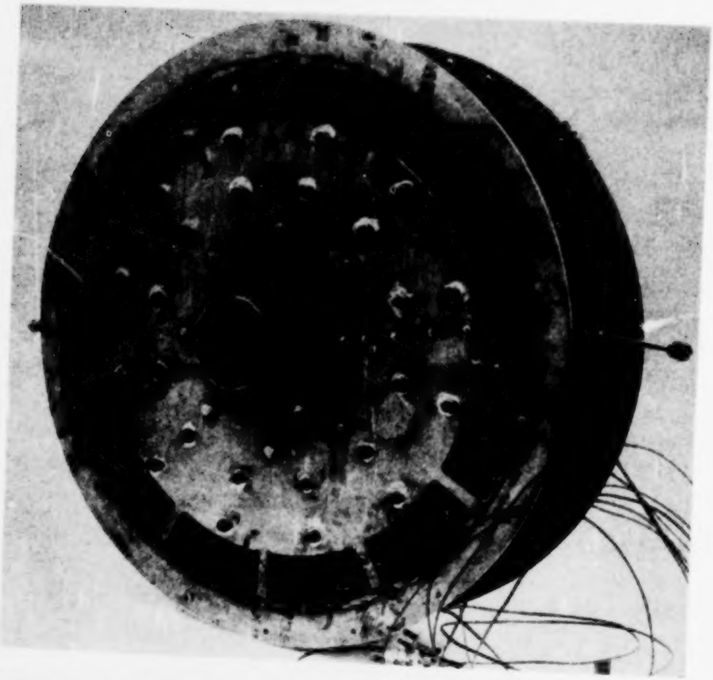

FIGURE 12. COMBUSTOR READY FOR INSTALLATION ON RIG

and 12. Rig air is supplied to an annular opening around the inlet to a swirler section. Air is accelerated inward across the swirler obtaining a rotary component as it is turned by the swirl blades. Twelve curved sheetmetal blades were used in the tests reported on in this section. Figure 11 shows the location and general shape of these swirl blades as traced by their respective weld oxidation lines on the combustor dome. A swirler exit nozzle is found by the annular opening between the outside diameter of the cup and a circular hole cut into the combustor dome. In the rig tests a 3 inch diameter cup driven by variable speed electric motor was used to atomize and distribute the fuel. A hollow armature shaft was used to supply fuel to the cup. Both JP-4 and JP-5 fuel was used with similar results. Gasoline was not, at this stage of the program, specified as the development fuel. A 20 inch diameter flame tube with a total axial length of 8 inches before the first row was used in all tests. No film cooling is provided on either the vapor dome or flame tube to avoid possible emissions complications. All cooling is by convection from the air passages on the outside or by means of radiation. Inconel 600 was used for both the dome, flame tube and flexible flame tube seal at the exit end of the flame tube. Inconel held up relatively well even at gas temperatures well above the design point of 2500°F. Oxidation was no problem but some serious distortion of the dome and cracking of the flexible flame tube to outer housing seal was observed after less than 50 hours of operation. An earlier prototype combustor fabricated from 321 stainless steel showed rapid deterioration due to oxidation and distortion.

Two basic configurations were tested on this rig combustor. Initially all of the air was supplied over the cup in the annular port around the cup. This would permit the fastest and most uniform vaporization, mixing, and reaction. However, to achieve relatively good emissions, the annular air injection port had to be reduced in area to minimize internal recirculation into the swirler. Thus the pressure drop at high flows was much greater than the maximum limit of 5 inches. In order to allow more air to be injected into the combustion zone a "secondary air" admission system was devised. A series of ports were machined into the flame tube to increase the total flow area of the combustor. Tests were performed with both configurations. Initial tests were performed without the secondary flow ports in the flame tube. All air entered around the cup through the primary or "high pressure air injection arrangement". After completion of these tests the secondary ports were machined into the combustor, thus allowing injection of air through both the primary and secondary ports simultaneously. This split flow configuration or "low pressure loss air injection arrangement" yielded data for the high fuel flow end of the power range.

Figure 13 shows the overlapping NO_x emission results with the two configurations analyzed by rig tests. With air admission through both the primary and secondary ports, the emission characteristics are seen to steadily rise as the fuel flow is decreased from 135 to 60 pounds per hour (pph). At a point near maximum allowable pressure drop of 5 inches of water, the NO_x level was well below the goal of 1.38 gm/Kgm. As the pressure drop and consequently the mixing velocities dropped with lower fuel flows, the emissions increased. At approximately 80 pph fuel flow and an air side pressure loss of 1.4 inches of water, the NO_x level exceeded the program's goals. During these tests the air cooled vapor simulator could not be kept supplied with enough air (because of rig air limitations) to keep its temperature sufficiently low to prevent it being damaged. As a consequence, it required removal at all test points above 60 pounds per hour of fuel flow. Since the emission averaging probe was fixed downstream of the simulator coils, their removal at high fuel flows effectively increased the actual combustion length by approximately 4 inches. All test points below 60 pph were with the two coils that comprised the simulator cooled to below 1000°F to provide both quenching and radiation cooling of the reaction products 8 inches from the dome.

With only the primary air being admitted into the combustor over the cup, the "S" shaped "high pressure loss" emission characteristic was obtained. At a pressure drop of 4.25 inches of water good NO_x emission levels could be obtained at a fuel flow of 70 pph. (It should be noted that a pressure drop of approximately 16 inches of water would be necessary to allow enough air into the combustor at the maximum rated fuel flow of 135 pph with this high pressure loss configuration.) As in the case of the low pressure loss configuration, the emissions increased as fuel flow and corresponding air pressure loss

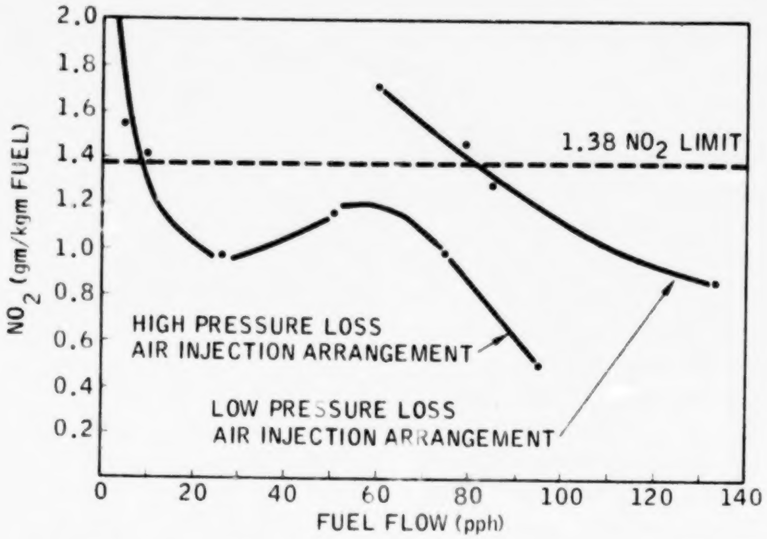

FIGURE 13. NO_2 EMISSIONS VERSUS FUEL FLOW

was decreased. A reversal of this trend occurred when the vapor generator simulator was reinstalled into the rig at flows below 60 pph. A decrease in NO_x emissions resulted until again the characteristic increase in emissions as air velocities fell to extremely low levels. NO_x emissions exceeded the limit at 10 pph fuel flow and an air side pressure drop of approximately 0.1 inch of water.

The drop in NO_x emissions when the vapor generator was installed was thought to be caused by radiation cooling by the cold walls of the combustor. Another factor that could have been important is the effects upon swirl air flow patterns and recirculation zones within the reaction zones.

CO and HC emissions were low throughout all these tests (Figs. 14 and 15). HC emissions were generally below the background levels and thus showed little or no effects of quenching problems on the vapor generator simulator tubes. At full fuel flow a temperature traverse (Fig. 16) showed good uniformity with deviations well within the ±250°F goal. The average temperature is approximately 200°F below the theoretical exit temperature. This is again within the expected limits since the combustor has a highly radiant flame that loses energy by direct radiation.

Results of these tests established the approach to be taken in the fully integrated system using fan air, control valves and the steam generator. Since integration with these components was certain to have significant effects upon emissions, further development on the rig could not be justified because of program scope limitations and lack of adequate flexibility to simulate all of the important fan, valve and steam generator effects upon performance.

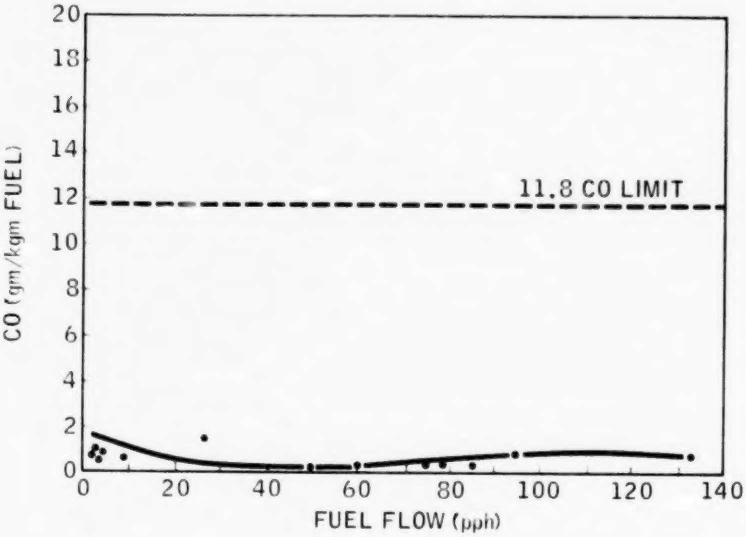

FIGURE 14. CO EMISSIONS VERSUS FUEL FLOW

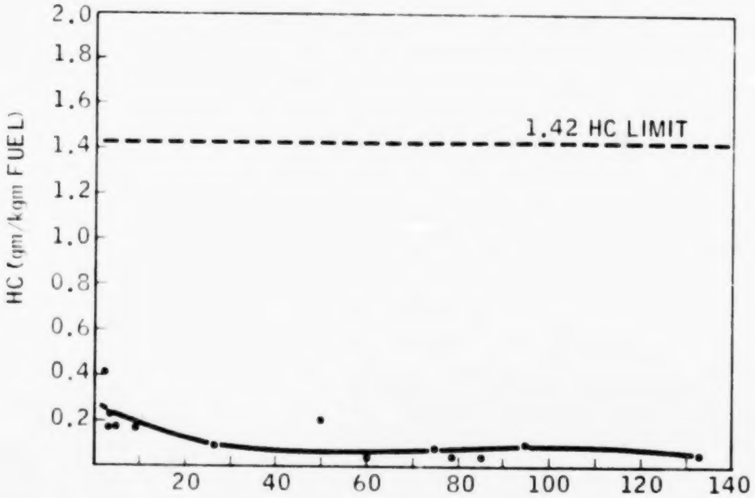

FIGURE 15. HYDROCARBON EMISSIONS VERSUS FUEL FLOW

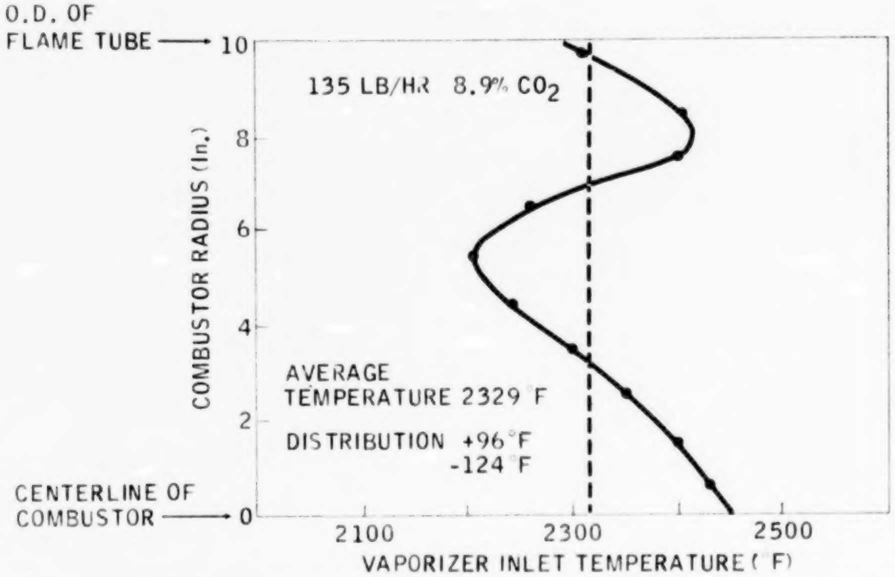

FIGURE 16. COMBUSTOR EXIT PLANE RADIAL TEMPERATURE DISTRIBUTION AT MAXIMUM FLOW

As a consequence of these rig tests a variable geometry combustor was required. From design studies a mechanically simple system, the split flow combustor, was designed and put into final integrated systems tests.

5.3 INTEGRATED COMBUSTOR PERFORMANCE

5.3.1 Design

Figure 17 is a cross section of the integrated combustor, air supply and steam generator. All test data reported from this section was with the fully integrated system. Air was supplied by the systems integral fan and the steam generator was operating at approximately 1000°F and 1000 psia. As discussed in the previous sections, parasitic power limitations required the use of a type of variable geometry combustor defined here as a "split flow" arrangement. Practical mechanization of this requirement was achieved by utilization of a simple shear valve immediately upstream of the combustor's injection passages. A detailed description of the system is given below.

Air is drawn into the unit by a fan mounted on the top of the unit on the centerline axis of the combustor tube and steam generator coils. Coaxial with the fan is the rotating cup for atomization and distribution of the fuel. Both the fan and cup are belt driven by a DC electric motor mounted to the side of the combustor within the 24 by 24 inch square envelope (see insert at bottom left of Fig. 17 and Fig. 18 and 19). Between the blade tips of the fan

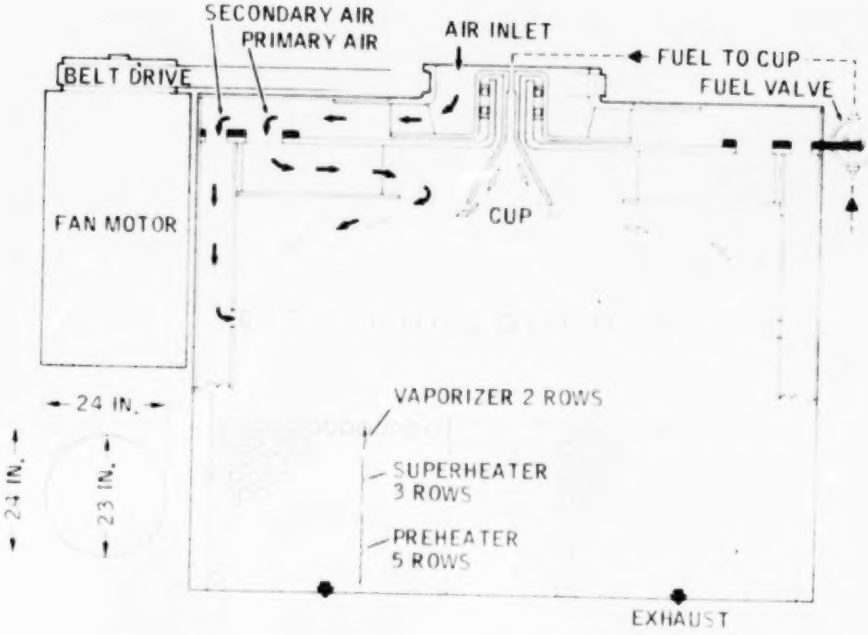
SECONDARY AIR
PRIMARY AIR
AIR INLET
FUEL TO CUP
FUEL VALVE
BELT DRIVE
FAN MOTOR
CUP
24 IN.
24 IN.
23 IN.
VAPORIZER 2 ROWS
SUPERHEATER 3 ROWS
PREHEATER 5 ROWS
EXHAUST

FIGURE 17. INITIAL INTEGRATED SYSTEM TEST CONFIGURATION WITH CONICAL CUP

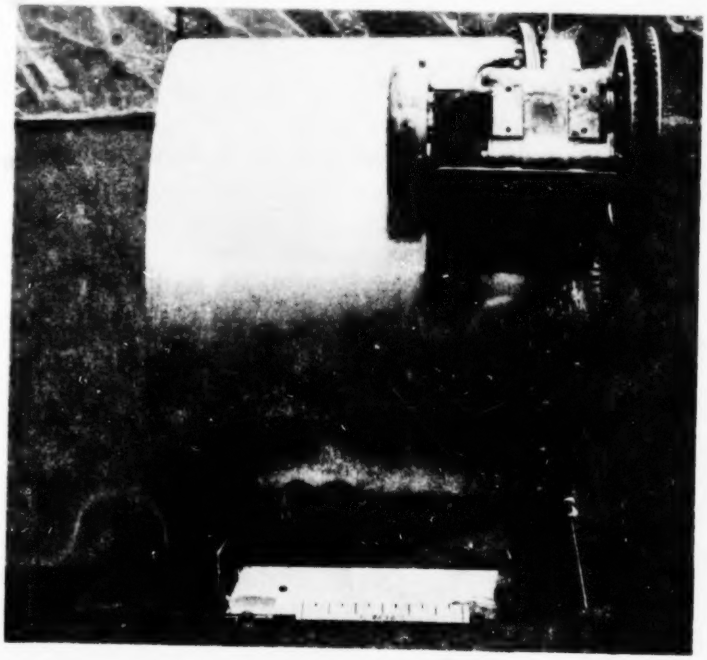

FIGURE 18. COMBUSTOR/AIR SUPPLY SYSTEM (DRIVE MOTOR SIDE)

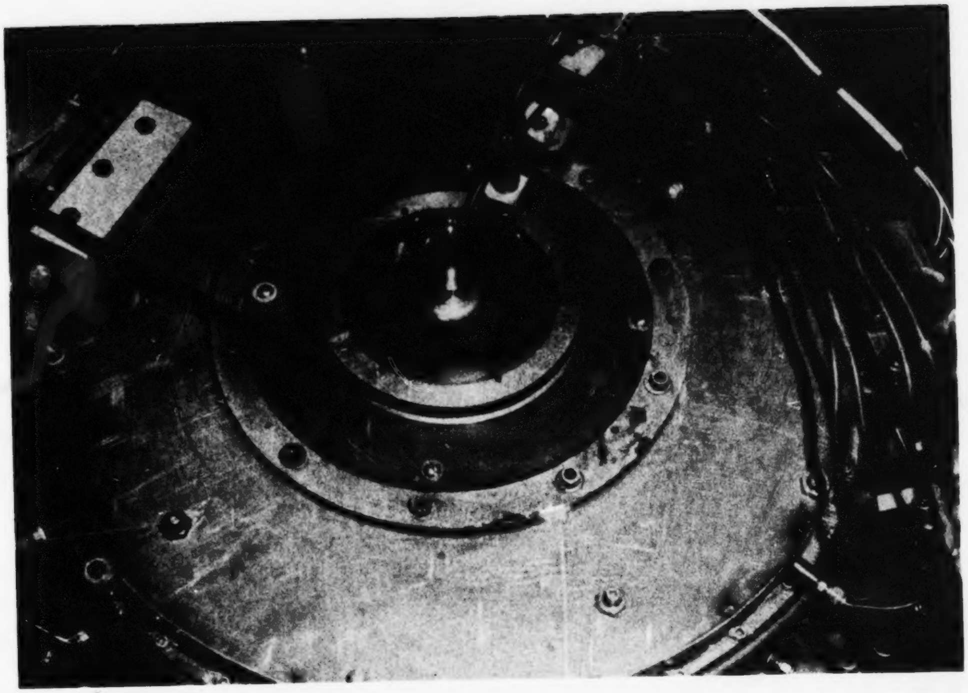

FIGURE 19. TOP VIEW OF COMBUSTOR AIR INLET TO FAN

and the air control ports a radial flow diffuser section converts velocity head to 10 inches of water (Fig. 20). Complete symmetry is maintained by spacing the ports equally around the circumference of the main valve plate. A rotary shear plate (Fig. 21) meters air to the primary at a ratio and schedule that is a function of fuel flow. After being metered by the valve, air flows radially inward through the swirler and then radially outward around the rotating cup with swirl flow. At above 50 percent power the secondary passages are also opened allowing air to flow into the combustion zone through 90 holes located 4 inches from the dome in the 20 inch diameter flame tube. Figure 22 shows the relative location of the 8.8 inch diameter primary port around a conical cup and the 90 secondary injection ports. A radiation shield is installed (Fig. 22) directly below and attached to the ID and OD of the dome plate. It is made from Hastelloy X with eight radial expansion slots to prevent thermal expansion forces being transmitted into the dome and the swirler blade assembly.

A four inch diameter conical cup (Fig. 23) was used in the initial stages of the integrated systems testing. It was a compromise size matched to the rotational speed of the fan. In combustor rig tests the best results were obtained at 10,000 rpm with a 3.0 inch diameter cup. However, satisfactory results were obtained at as low as speed as 4500 rpm. An existing fan was found to have ideal characteristics (except it operated at 5800 rpm) for both

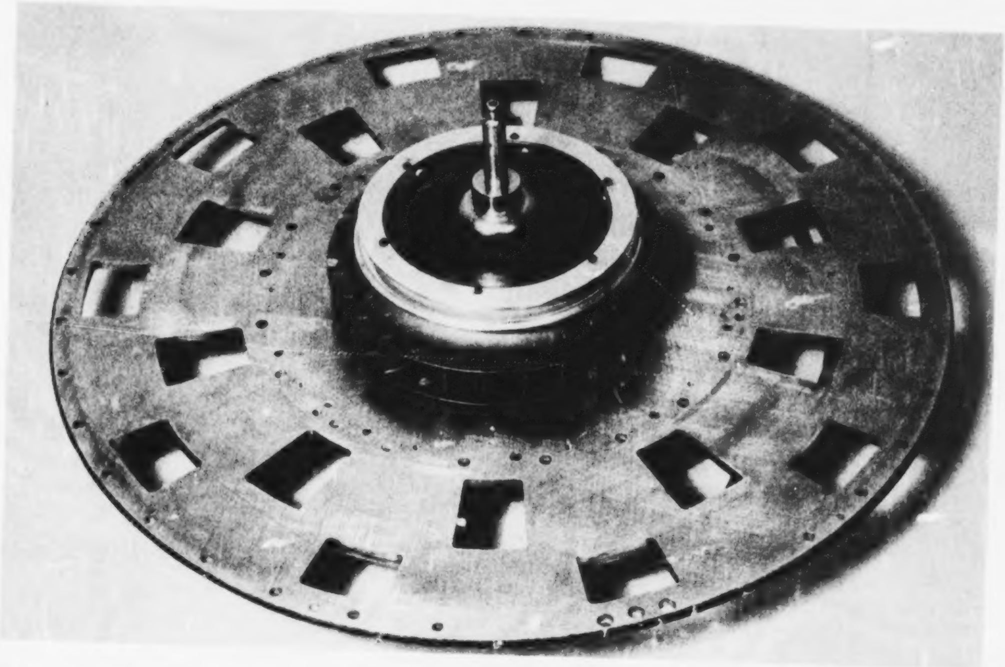

FIGURE 20. FAN MOUNTED TO CONTROL VALVE BACKUP PLATE

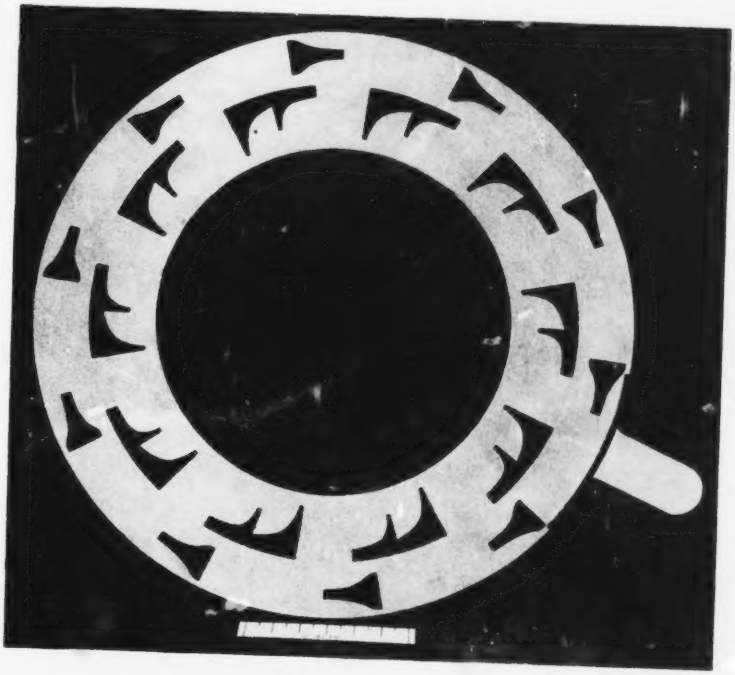

FIGURE 21. ROTARY SHEAR PLATE

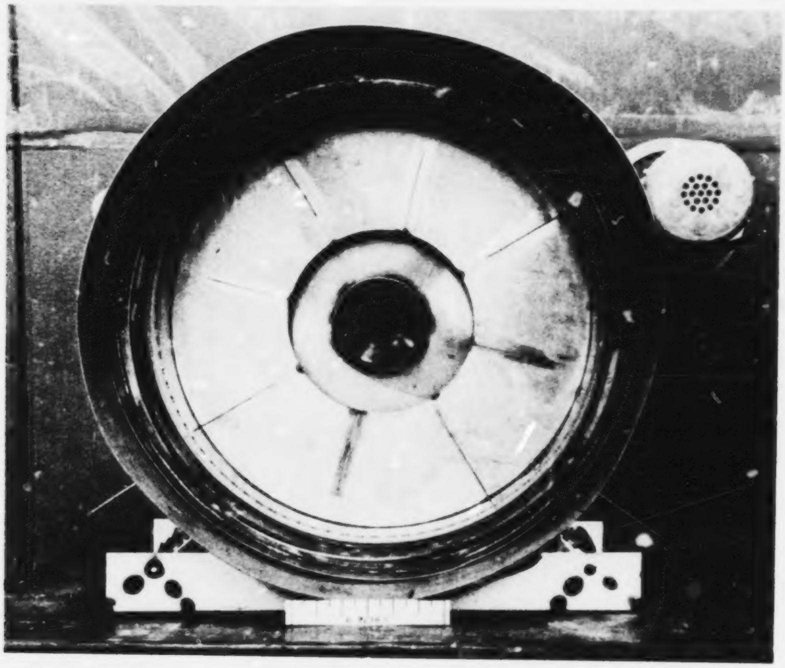

FIGURE 22. COMBUSTOR/AIR SUPPLY SYSTEM (VAPOR GENERATOR SIDE)

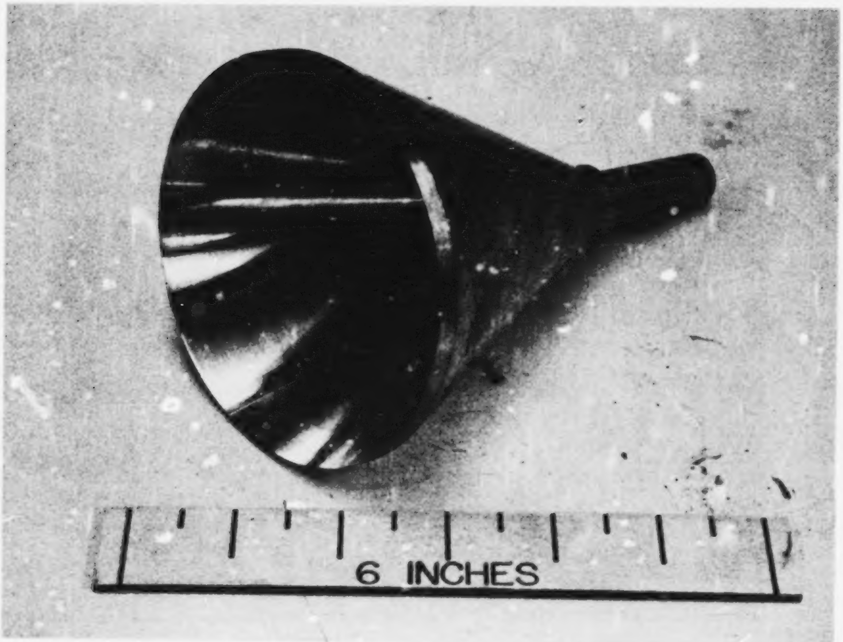

FIGURE 23. CONICAL FUEL CUP

packaging and aerodynamic integration into the system. It was decided to increase the cup diameter by one inch to more closely match the tangential velocity and droplet size used in the test rig phase of the program. Two possibly important side effects of this change were not considered as being important. One was the heat input surface area of the cup increased by over 70 percent as did the volume of reaction products in the zone immediately below the cup. As development tests progressed several modifications were made to improve emissions possibly associated with this change in diameter.

5.3.2 Air Supply System

At maximum rated conditions the air supply and control system must deliver 3400 pounds of air per hour to the combustion system. Flow control into the combustor must be symmetrical to prevent hot spots and higher emissions. A fully modulated control of air mass flow synchronized with the fuel is required across the entire 40 to 1 heat release range. In addition to these features, the air supply system must be integrated into the overall design to minimize the completed package's overall length and volume. Length can be made a minimum by using a radial fan coaxial with the combustor axis. Figure 17 shows a cross-section of a radial fan with the desired characteristics integrated into the unit. Figure 24 is a photograph of the unit after modification required for installation into the combustor. It is a standard automotive fan designed to produce minimum noise. The initial unit used was brazed to allow transmission of drive load through its shroud. Subsequent units did not appear to require brazing. It has 28 fully shrouded blades with the following parameters:

Tip diameter = 9.1 inches

Tip width = 1.15 inches

Inlet blade angle, β_1 = 57 degrees (to a radius)

Outlet, β_2 = 25 degrees (backsweep)

Number of blades, Z = 28 blades, 0.05 inch thick

A detailed analysis of its performance characteristics at several speeds is shown in Figure 25. The correct combustor flow and pressure ratio (3400 pounds per hour at 10 inches of water) can be obtained by operating the fan at 5740 rpm. At this speed and flow the efficiency map calculated for this unit indicates a total efficiency of 66 percent. Figures 26 and 27 are plots of the pressure and efficiency characteristics at 5700 rpm. Experimental pressure versus flow test points are also included in this curve.

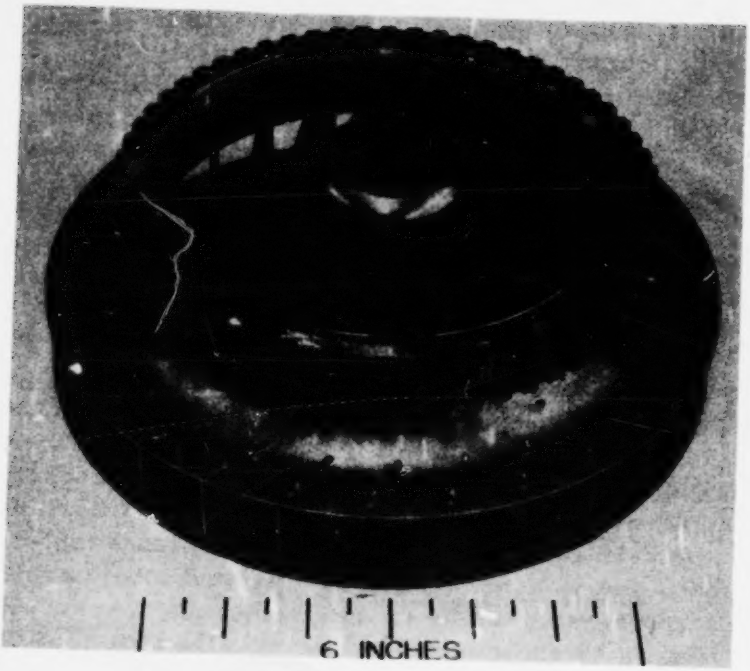

FIGURE 24. AIR SUPPLY FAN

A mechanically simple shear valve has been designed to provide the split flow characteristics required for combustion. Figure 28 schematically shows the principle of the valve. A series of twenty contour ports (Fig. 29) have been cut into a moveable plate that rotates about the axis of the combustor case. A corresponding series of matching ports have been machined into the backup plate that forms one wall of the diffuser and the support for the fan bearing mount (Fig. 30). By rotating the metering plate orifice a total of 34 degrees, the air flow is regulated from 100 percent to less than 2 percent. The arrangement and shape of the ports has been designed to provide separate control of primary and secondary air into the combustor case (secondary air) and swirl vane compartments (primary air). A seal ring is used to isolate and prevent leakage between the primary and secondary air passages. At the 50 percent flow position, the secondary air is completely shut-off and all air is directed into the primary zone through the swirler. Basically for this geometry of combustor, it was determined that a flow split of 0.55 pounds per second into the primary zone and 0.42 pounds per second of air into the secondary zone gave optimum emission performance at full power conditions (135 pounds per hour fuel flow). A maximum pressure drop of 5 inches of water was used for full flow conditions. At lower power levels tests demonstrated that mixing rates could not be maintained due to low pressure drops if fixed flow areas were maintained across the combustor. One approach that was shown satisfactory by rig tests was to inject all the air

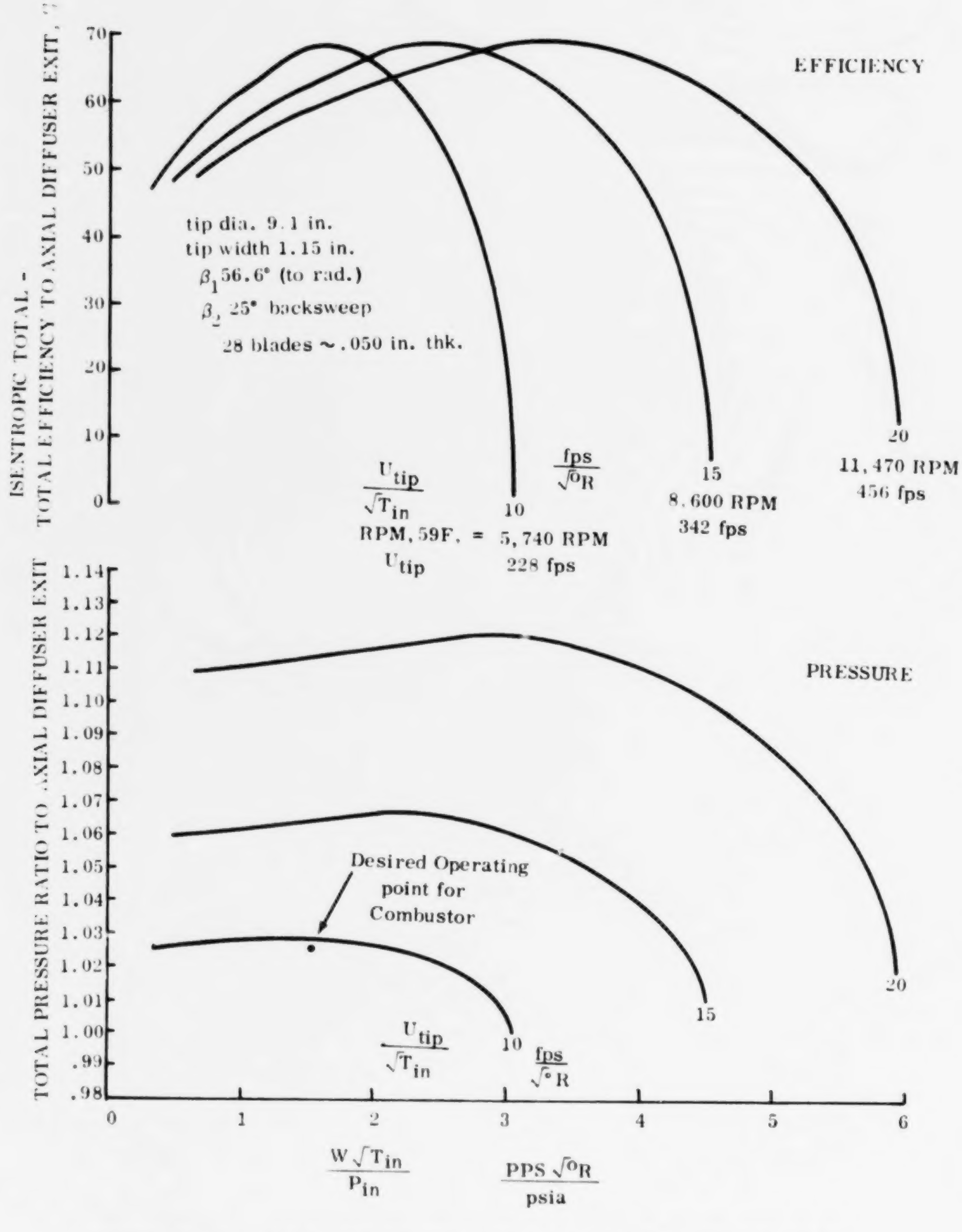

FIGURE 25. CALCULATED CHARACTERISTICS OF FAN

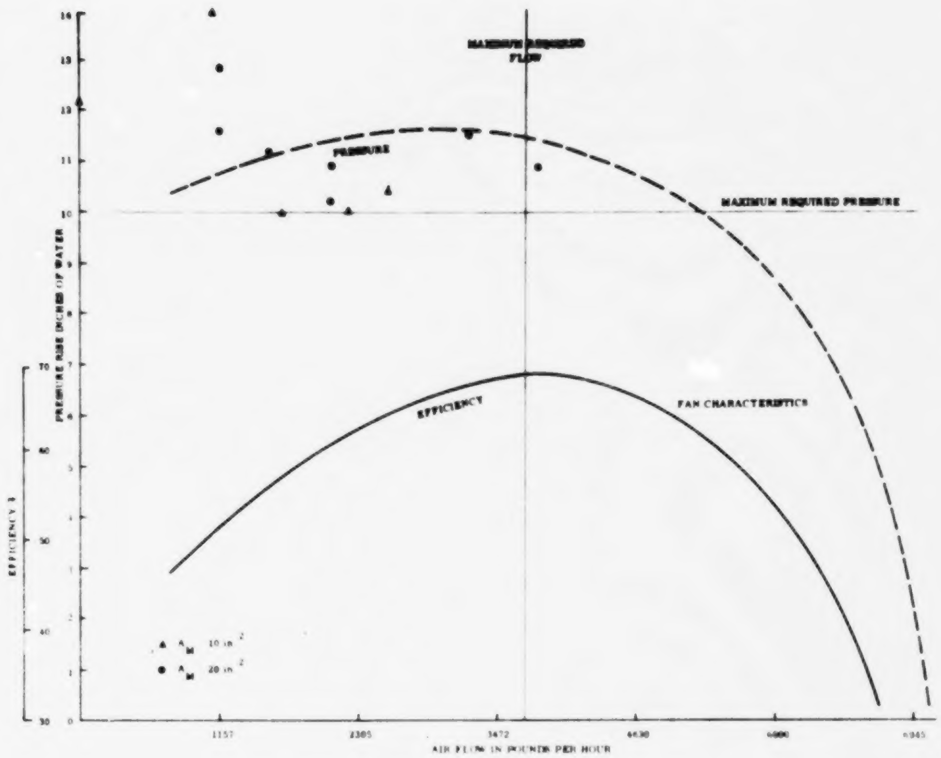

FIGURE 26. TOTAL PRESSURE RISE CALCULATED COMPARED TO TEST POINTS

through the swirler at low flows. This approach could also provide low emissions at the high flow rates but an unacceptably high pressure drop would be necessary (16 inches of water) if 100 percent of the air was injected through the swirler.

Ten primary and secondary ports are used to obtain good symmetry and uniform air distribution within the combustor. Design of the valve is dependent upon matching it with the fan, diffuser, combustor and vapor generator characteristics. Rig tests were performed to obtain the basic data necessary for design. Figure 31 was the flow rig designed to simulate the actual metering valve flow interaction with fan and diffuser. Tests results are compiled in Table III. Figure 27 gives static fan pressure rise versus flow. Figure 32 shows the variation of the coefficient of discharge, Cd, for the air metering orifices versus flow and orifice open area A_m (in.^{2}). The term, Cd, is used in the following equation for calculating volume flow across the orifice.

$$W_m = (7.617)(60)\,Cd\,A_m\,\sqrt{\gamma(P_{FS} - P_V)} \qquad (1)$$

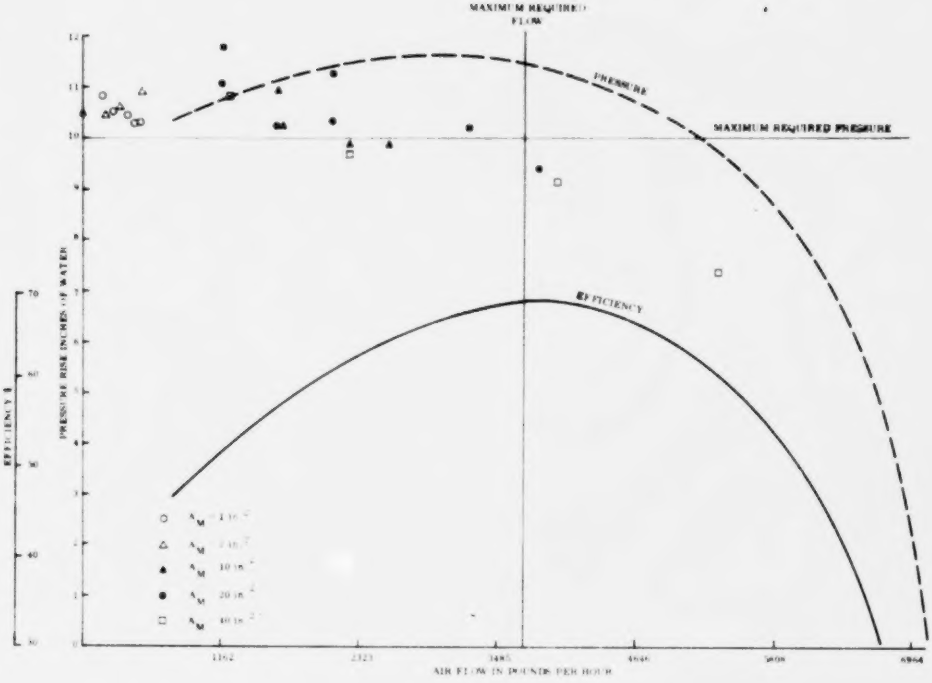

FIGURE 27. ACTUAL STATIC PRESSURE RISE COMPARED TO CALCULATED TOTAL PRESSURE

where W_m is flow across metering orifice (lb/hr)

γ is density of air in lb/ft^2

$P_{FS} - P_V$ is pressure difference across metering plate (inches of water column)

Cd is found through the above equation (1) and the relation:

$$W_m = W_V$$

where W_V is flow calculated from the downstream plenum duct pressure P_V exit area (A_V) data. The coefficient of discharge for the plenum duct orifices is assumed to be 0.65 for all cases. Figures 27 and 32 contain the important interface data necessary to design the metering valve. From Table III and Figure 27 it is seen that no significant stall characteristics exist with the fan-diffuser arrangement.

Provisions had been made to fabricate a bypass valve to prevent fan stall instabilities from causing maldistribution of air into the combustor. However, since the fan exhibits a near uniform static pressure characteristic

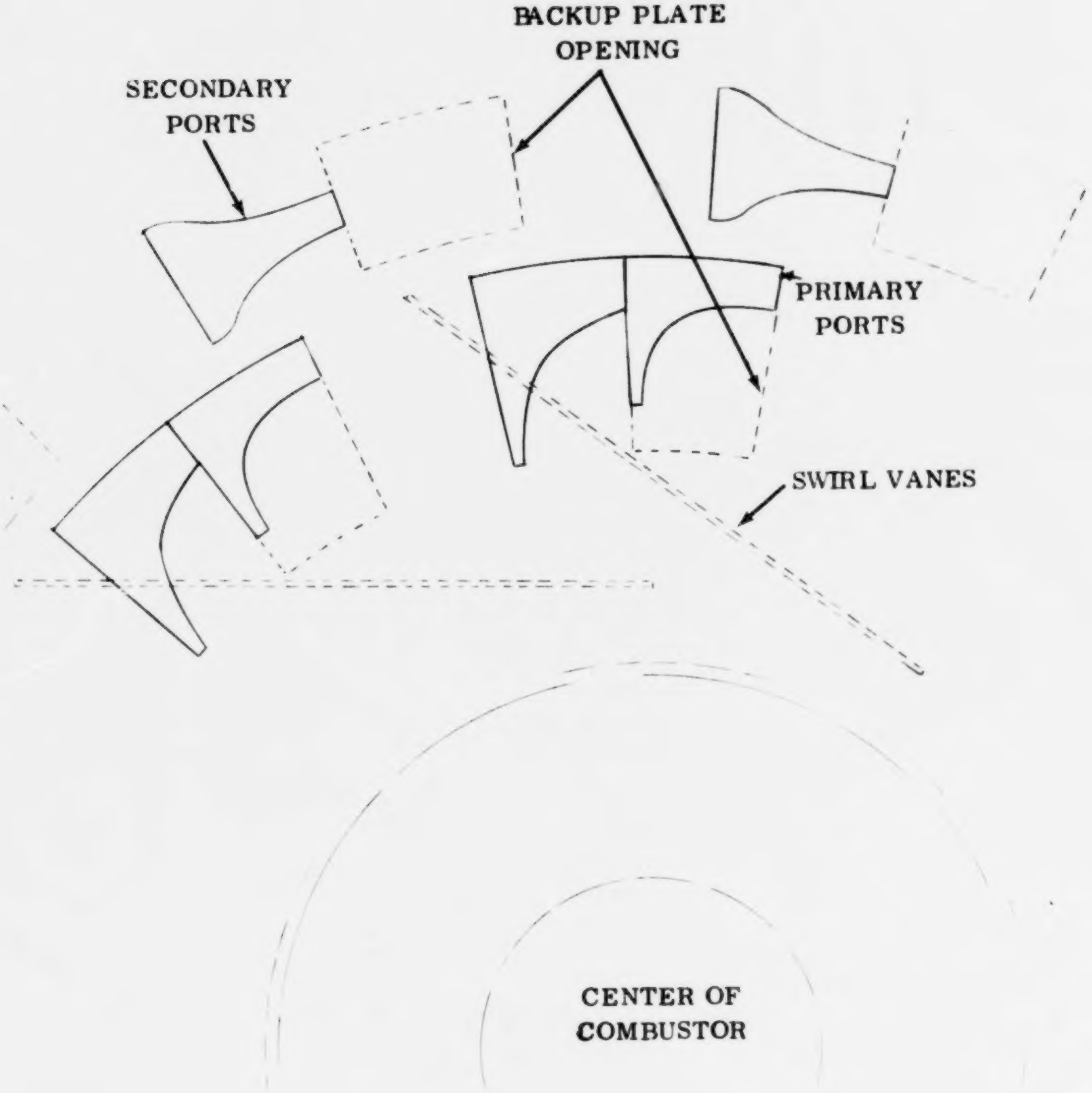
BACKUP PLATE OPENING
SECONDARY PORTS
PRIMARY PORTS
SWIRL VANES
CENTER OF COMBUSTOR

FIGURE 28. PRIMARY AND SECONDARY AIR METERING PORT CONFIGURATION SHOWN IN 50 PERCENT POWER POSITION

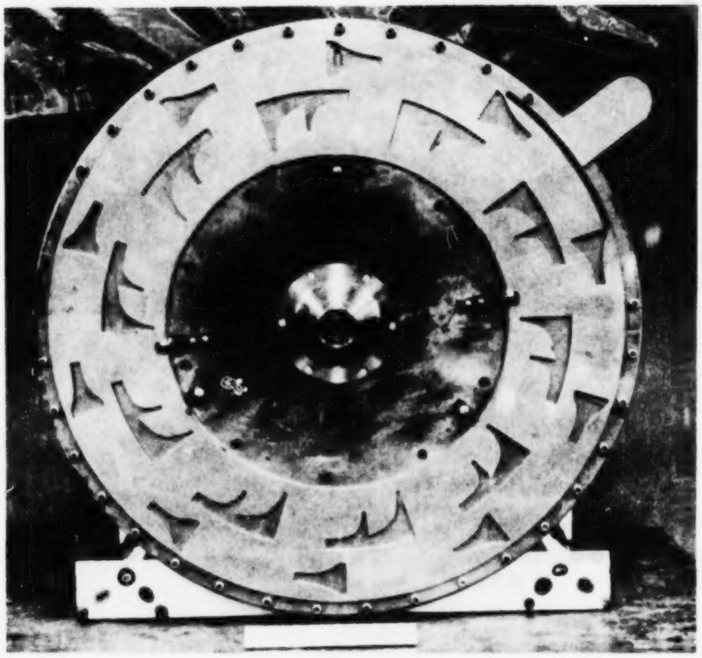

FIGURE 29A. AIR VALVE IN 2 PERCENT POSITION

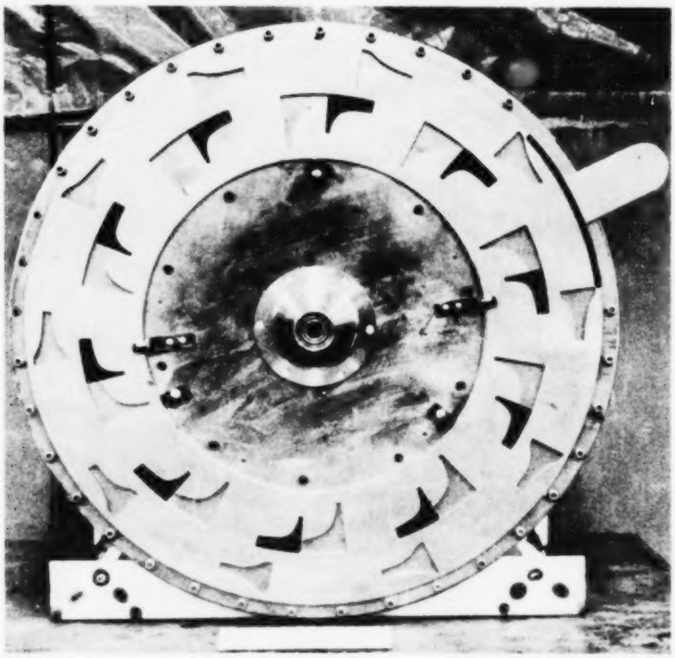

FIGURE 29B. AIR VALVE IN 50 PERCENT POSITION

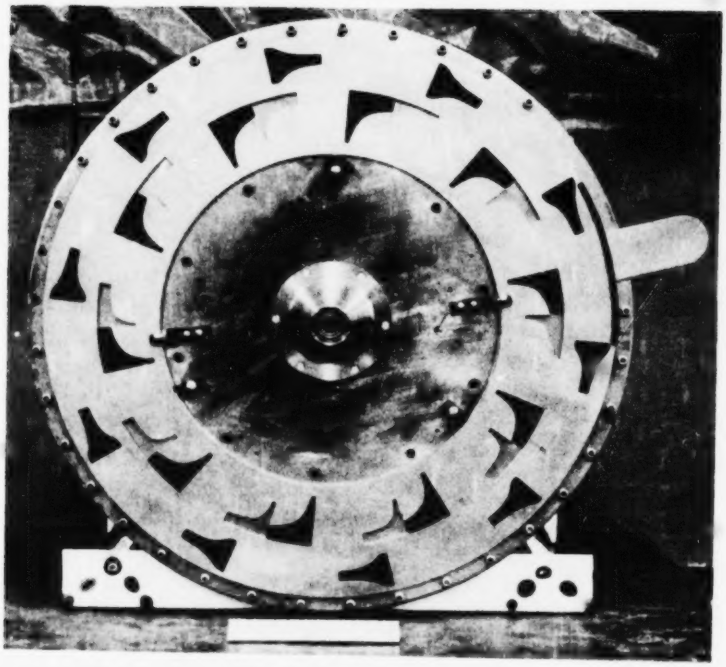

FIGURE 29C. AIR VALVE IN 100 PERCENT POSITION

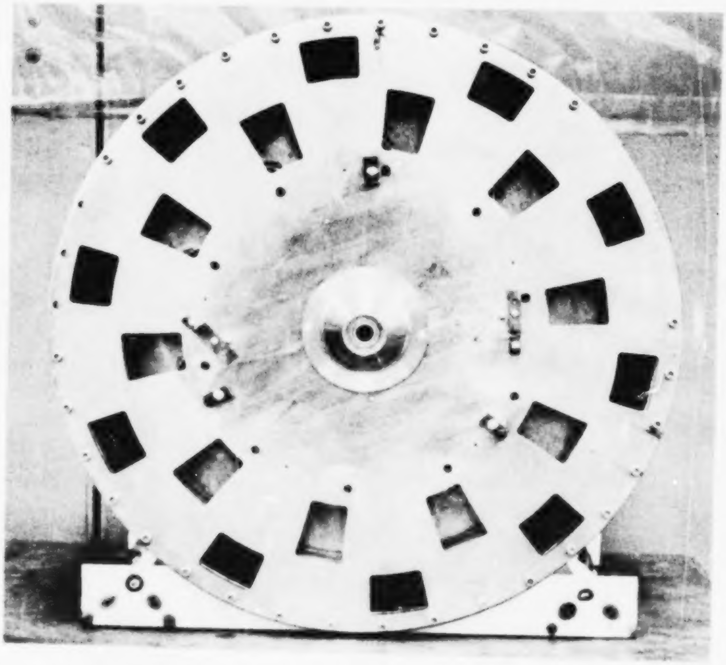

FIGURE 30. AIR VALVE BACKUP PLATE

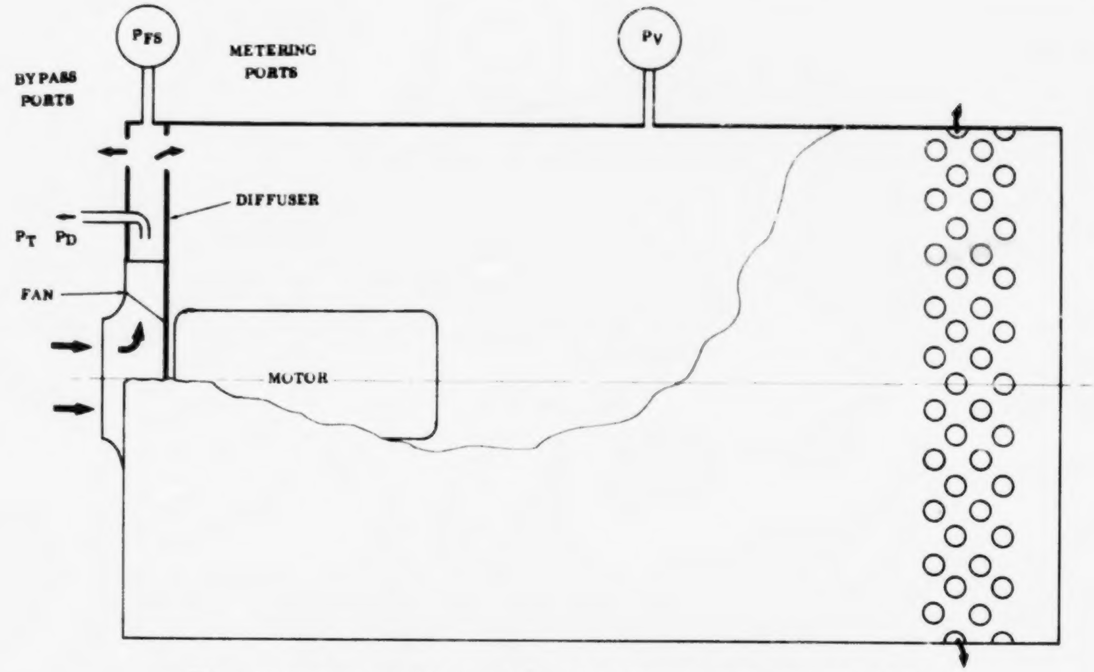
P_FS
P_V
METERING PORTS
BYPASS PORTS
DIFFUSER
P_T
P_D
FAN
MOTOR

FIGURE 31A. FAN-AIR VALVE FLOW TEST RIG

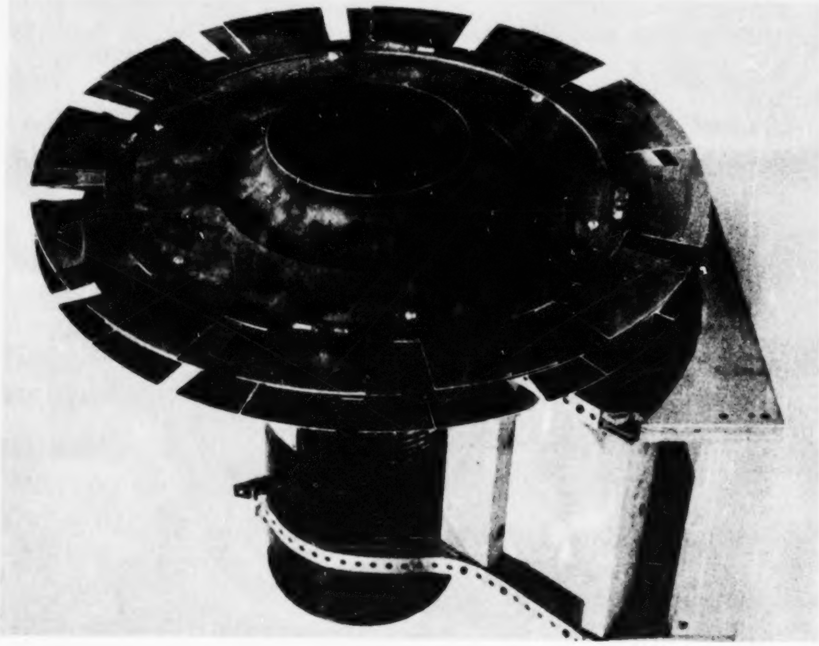

FIGURE 31B. FAN TEST RIG DIFFUSER AIR VALVE SECTION

TABLE III

FAN TEST RESULTS WITH NO BYPASS
FAN SPEED 5700 RPM

Fan Exit		Static Pressure Upstream Metering Orifice	Metering Orifice Area	Static Pressure at Duct O. D.	Duct Exit Open Area	Flow Leaving Duct	Coefficient of Discharge, Cd, for Metering Orifice
Total Pressure P_T (in. H_2O)	Dynamic Pressure P_D (in. H_2O)	P_{FS} (in. H_2O)	A_M (in.^{2})	P_V (in. H_2O)	A_V (in.^{2})	W_V (lb/hr)	
13.5	4.9	10.9	40	10.45	4.71	1230	.34
10.3	3.3	9.75	40	8.7	9.42	2244	.44
11.1	3.9	9.15	40	6.85	18.8	3975	.53
8.7	3.8	7.35	40	3.05	37.7	5319	.52
11.0	2.4	11.25	20	7.5	9.43	2100	.433
12.8	4.2	11.0	20	9.5	4.72	1180	.385
11.5	4.0	10.2	20	4.45	18.9	3240	.5397
10.9	4.1	9.4	20	1.55	37.7	3820	.545
10.2	2.1	10.35	20	7.4	9.43	2085	.485
11.6	4.4	11.05	20	9.6	4.72	1190	.395
11.2	2.2	10.2	20	8.05	7.07	1630	.444
13.9	5.0	10.95	10	8.2	4.72	1100	.530
12.2	3.6	10.5	10	10.4	0	0	
10.0	2.5	10.05	10	4.75	9.43	1670	.580
10.0	2.5	9.9	10	2.1	18.9	2330	.667
10.4	3.6	9.9	10	0.7	37.7	2560	.674
13.3	4.4	10.95	2	1.7	4.71	496	.656
12.8	3.9	10.65	2	6.05	1.57	312	.585
12.2	3.2	10.45	2	8.4	0.785	184	.517
11.8	2.7	10.35	2	10.1	0	0	----
13.1	4.2	10.85	1	6.5	0.785	162	.625
12.8	4.1	10.55	1	4.15	1.57	258	.821
12.6	4.2	10.45	1	0.95	4.71	371	.969
12.4	4.2	10.35	1	0.3	9.42	417	1.05
12.4	4.2	10.35	1	0.1	18.8	480	1.21
12.4	4.1	10.4	1	0.0	37.7	----	

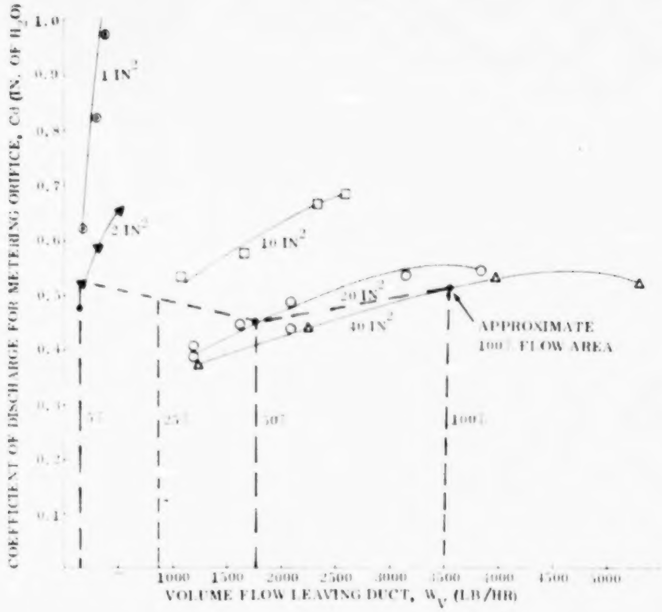

FIGURE 32. Cd VERSUS FAN FLOW FOR SEVERAL METERING PLATE ORIFICE AREAS

from 100 percent down to complete shutoff of the air valve, it was possible to design a simple single shear plate valve without the complexity of a bypass valve. Prior to final sizing of the valve ports, it was necessary to establish the actual coefficient of discharge and its variation with flow and port opening (Fig. 32). Since the velocity of approach is relatively high from the diffuser to the ports and at 90 degrees to their flow orientation, a nonuniform Cd is expected. Figure 32 indicates the variation between a 40 to 1 area ratio of port sizes is acceptable and is within ±10 percent of a Cd of 0.5 at the area size approximately proportional to the required flow shown by dotted lines.

Port sizing is based upon a Cd of 0.5 and application of the flow equation (1). To permit a reasonably small radial valve dimension a full flow pressure drop of 2 inches of water has been used. With this pressure drop the full flow areas for primary air (0.55 pounds per sec) is: 22.3 in^2 and secondary air (0.45 pounds per sec) is 16.9 in^2 for a total flow area of 39.2 in^2. Ten ports each are used for the primary and secondary flow control areas. Ports are equally spaced around the valve to provide symmetrical air flow. In the case of the primary air the ports are located to individually feed air into 10 separate swirl chambers to further ensure uniform air distribution (see Fig. 28). A linear response to valve position is provided by contouring the ports to account for the variation of pressure drop across the valve at reduced flow conditions. A constant fan discharge static pressure of 10 inches of water is maintained across the entire flow range by use of a nearly constant speed 28 volt compound wound DC motor. At full power the pressure drop is 10 inches of water, 2 inches across the air metering valve, 5 inches across combustor and 3 inches across the vapor generator. At the 3 percent power level there is nearly zero pressure drop across combustor and vapor generator with the full ten inches pressure drop taken across the metering valve. Linear response is obtained by calculating the open area for each valve position using the power level dependent pressure drop across the valve. Resulting contours are thus high at the 100 percent flow side and low at the reduced power positions (Fig. 29).

A DC electric motor drives the fan through a belt. A search for a compact motor with good efficiency resulted in selection of a Model 1000 Hoover Electric unit. Availability, small size (Fig. 33) and light weight (13 pounds) were the primary factors used to finalize its selection. Efficiency at maximum rated conditions is only slightly better than 60 percent (see Fig. 34). Since the ideal air horsepower is 1.2 HP and the fan is 68 percent efficient, the shaft power into the fan is 1.8 HP. From Figure 34 the electrical power input for 1.8 HP is 2120 watts or 2.8 HP (electrical equivalent). This is slightly above the goal of 2.5 HP but could be improved to less than 2.5 HP if a motor with an efficiency of greater than 72 percent were installed. Although aircraft motors can be made in this range, no automotive motor of this efficiency has been located and may require special design.

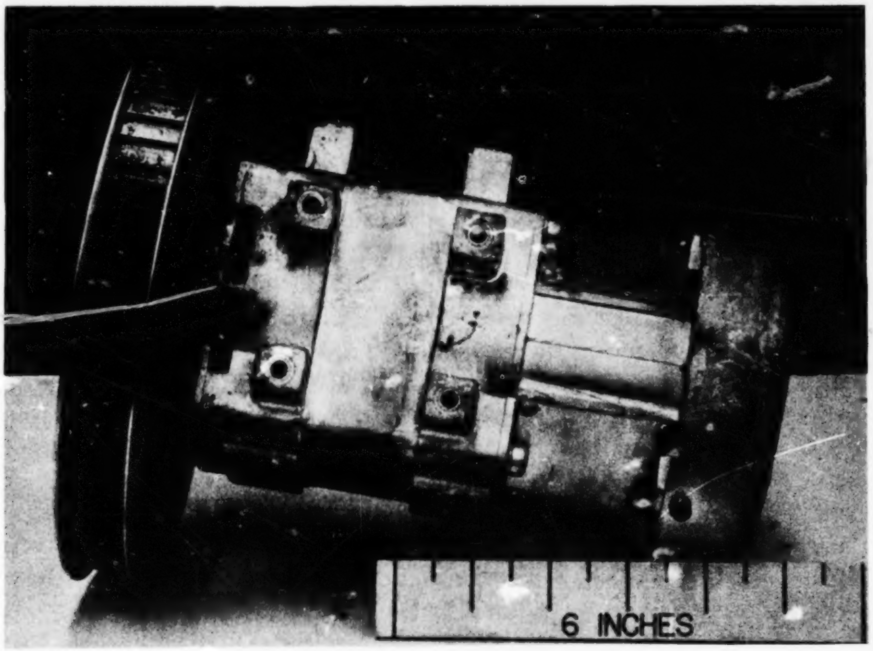

FIGURE 33. FAN DRIVE MOTOR

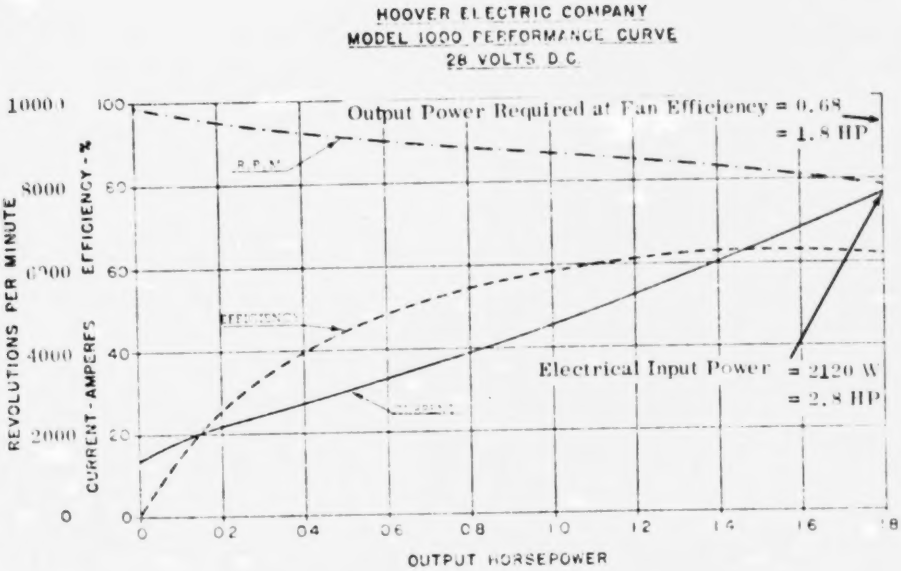

FIGURE 34. FAN DRIVE MOTOR CHARACTERISTICS

5.3.3 Flame Performance

An initial step in the evaluation of the integrated system was a visual examination of the flame. Symmetry and flame length can be quickly evaluated by this procedure. These tests were performed in a horizontal position with all system components installed except for the steam generator.

Figure 35 is a schematic of the test arrangement and instrumentation used to make a preliminary evaluation of the closely coupled air supply and combustor. At a given air valve setting fuel flow was varied to obtain optimum flame performance as determined by visual inspection. Static pressure rise across the fan and pressure drops across the primary and secondary ports of the combustor were measured by three manometer readings each (located approximately 120 degrees around the circumference of the unit). Current and voltage to the drive motor were recorded as was the fan speed. Figures 36 through 40 are records of flame performance during the integrated systems tests. In general the results were acceptable from visual symmetry and flame length considerations. Potential problems such as diffuser instabilities and flow separation due to interaction between fan, diffuser, air valve and swirler did not appear to occur, or were not significant enough to cause apparent asymmetry or downstream hot or cold patterns in the flame. Good correlation between design point and actual pressure drops across metering valve and combustor were also recorded. One major

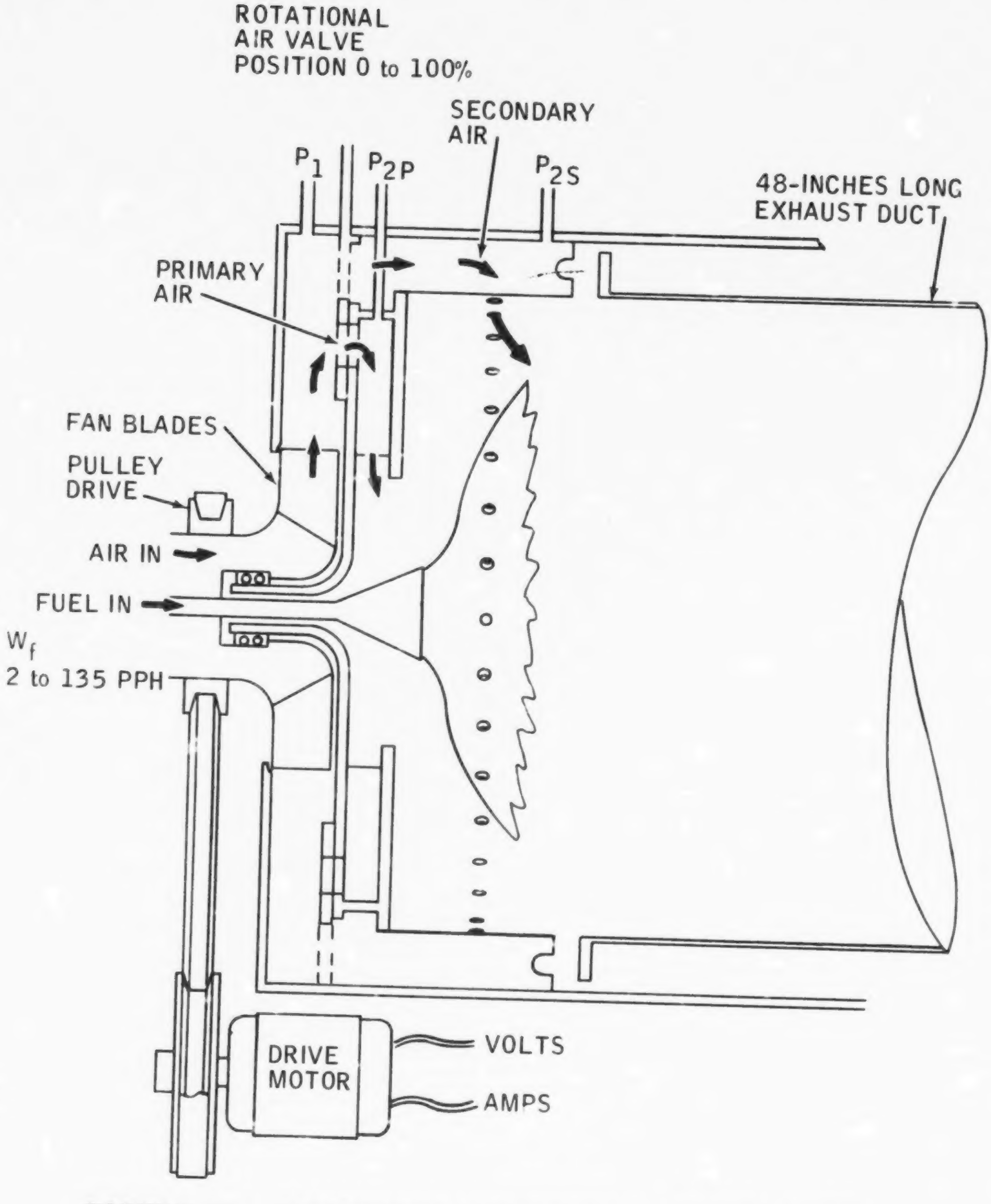
ROTATIONAL
AIR VALVE
POSITION 0 to 100%
SECONDARY
AIR
P_1
P_{2P}
P_{2S}
48-INCHES LONG
EXHAUST DUCT
PRIMARY
AIR
FAN BLADES
PULLEY
DRIVE
AIR IN
FUEL IN
W_f
2 to 135 PPH
DRIVE
MOTOR
VOLTS
AMPS

FIGURE 35. COMBUSTOR/AIR SUPPLY SYSTEM TEST ARRANGEMENT

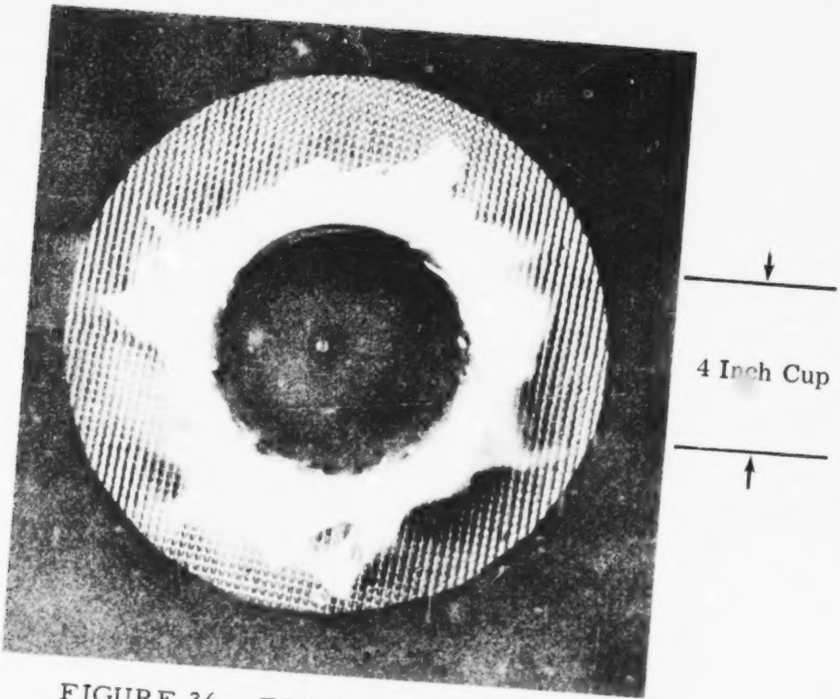

FIGURE 36. FLAME AT 1.5 PPH

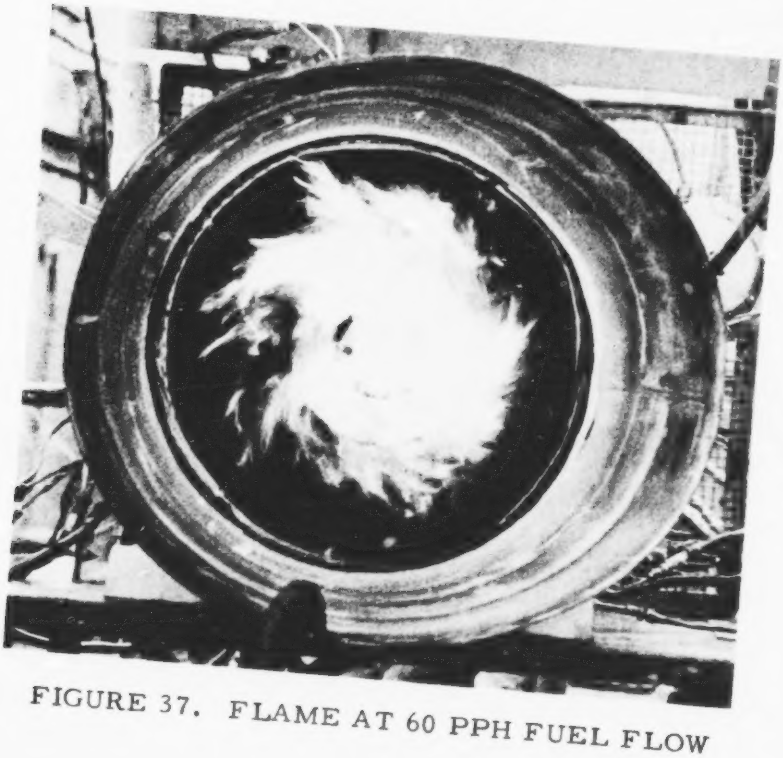

FIGURE 37. FLAME AT 60 PPH FUEL FLOW

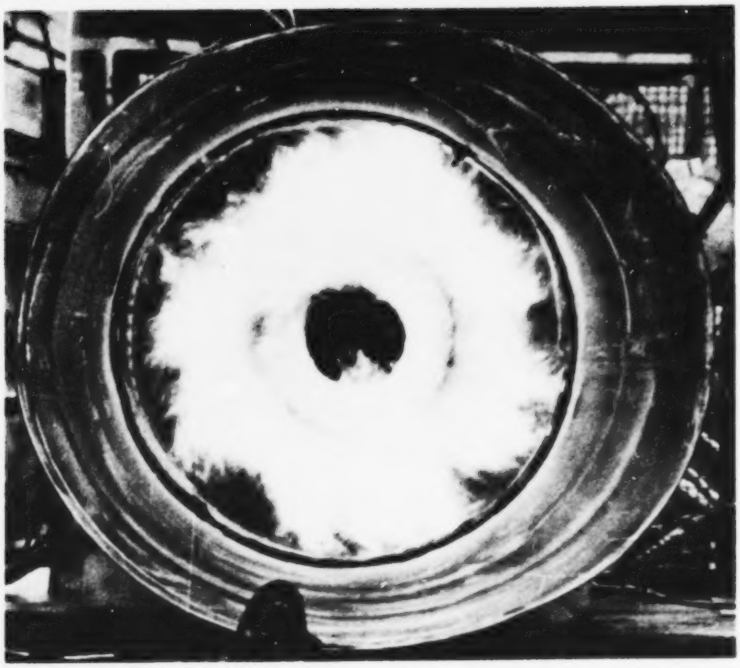

FIGURE 38. FLAME AT 80 PPH FUEL FLOW

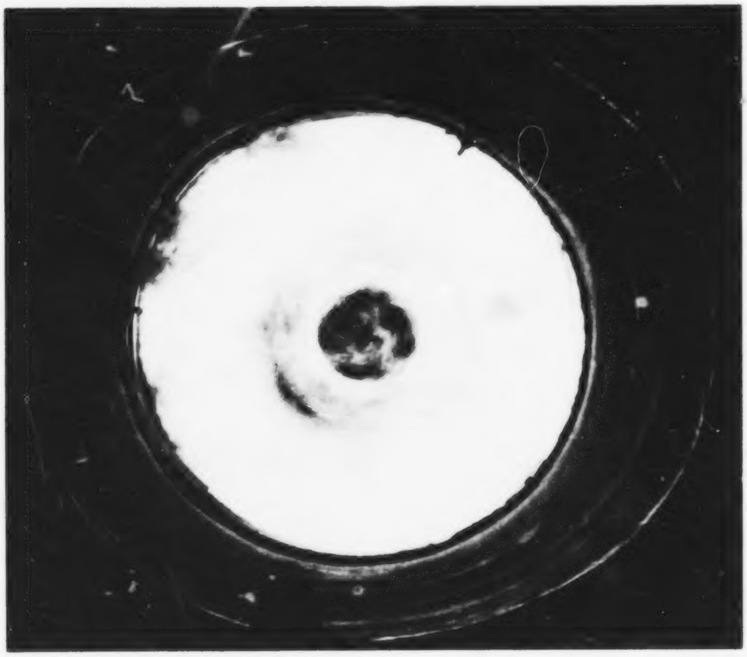

FIGURE 39. FLAME AT 100 PPH FUEL FLOW

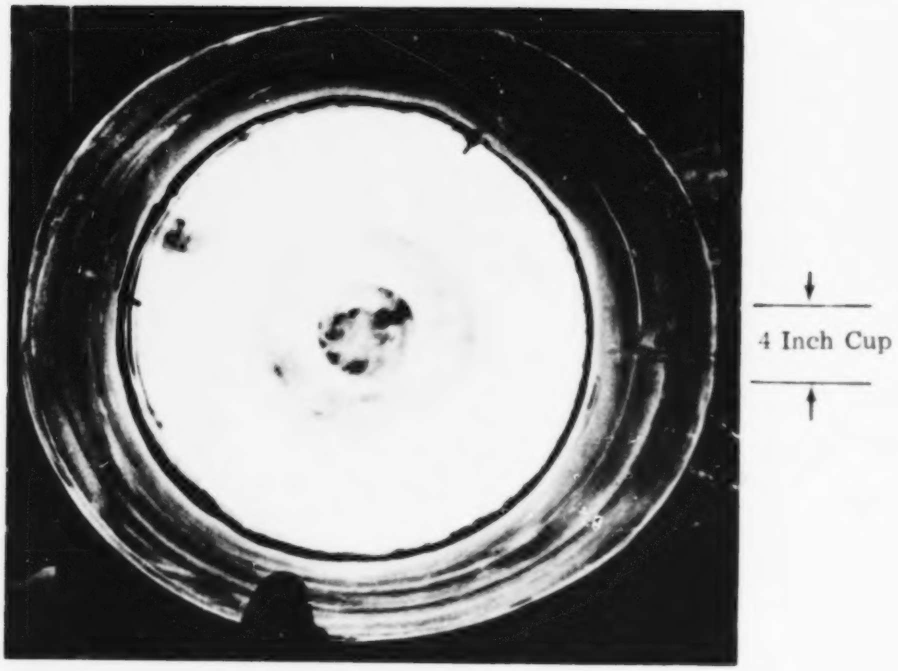

FIGURE 40. FLAME AT 130 PPH FUEL FLOW

problem discovered was with the matching of fan and motor characteristics. Electrical input power (see Table IV) ranges from 1100 watts (1.5 HP) at 3 percent flow to 2360 watts (3.2 HP) at 96 percent flow. At 22 percent power (near the average duty cycle requirements) the electrical power required was 1.7 HP. All of the input power levels were well above calculated values. Analysis of the problem indicates that a mismatch between the fan load speed characteristic and the motor speed-voltage-current relationships was the cause. In order to operate the fan at 5700 rpm voltages below design point were necessary. As a consequence, higher than design currents were recorded, increasing I^2R losses and reducing efficiency. A new pully drive ratio was installed to obtain a better speed match and has reduced the input power requirements by allowing the motor to operate at higher speeds and voltages (28 volts).

Table V lists results of several of the test cell operations with complete system including the vapor generator. Current values range from 55 to 73 amps with the new pulley arrangement. Previous results in the same flow range varied from 70 to 100 amps or a reduction of approximately 30 percent.

TABLE IV

INITIAL COMBUSTOR PLUS FAN AIR SUPPLY TEST RESULTS

Power Level %	Fuel Flow (lb/hr)	Air Valve Position % Open	Fan Discharge Static Pressure (in. of water)	Combustor Pressure Drop (in. of water)		Fan Speed (rpm)	Motor Input Power	
				Primary P_{1p}	Secondary P_{2s}		(Volts)	(Amps)
3	4	5	10.3	<0.1	<0.1	5900	21	53
7.5	10	10	11.2	<0.1	<0.1	6150	22.8	60
22	30.3	20	10.5	<0.2	<0.1	5900	23	55
48	65	40	9.5	1.2	<0.1	5750	23	70
55	75	60	8.4	5	-	5500	23	80
59	80	60	8.1	4.5	0.4	--	22.5	83
74	100	80	7.6	4.5	2.4	5400	22.5	91
85	115	90	7.1	4.9	3.9	--	22.5	100
96	130	97	7.0	4.9	4.6	--	22.5	105

TABLE V

FAN POWER WITH HIGH RATIO PULLEY

			Run No.			
			#1	#2	#3	#4
	Air Valve Position	%	46	69	82	90
	Fuel Flow	PPH	56.5	83	94	101.5
Fan	Fan Speed	RPM	5700	5700	5680	5680
	Volts	Volts	24	25	25	25
	Amps	Amps	55	65	71	73
Water	Flow	PPH	1600	1600	1600	1600
	Press In	PSIG	370	580	660	690
	Press Out	PSIG	260	460	530	590
	Temperature Out	°F	400	454	468	473
Air	Fan Out	In. of W.C.	8.7	8.6	8.5	8.5
	Primary	In. of W.C.	1.0	5.5	5.5	5.5
	Secondary	In. of W.C.	0.25	1.0	2.3	3.0
	V.G.	In. of W.C.	0.4	0.8	1.0	1.15

5.3.4 Integrated System Emissions Evaluation

Initial combustor test and development was performed with all the systems and components assembled as shown in Figure 17. Steam conditions at the outlet of the unit were kept at design conditions to ensure quenching radiation effects and aerodynamic recirculation of the steam generator were correct for emissions analysis.

The emission probe was located two inches downstream of the vapor generator in an exhaust plenum (Fig. 41). It has 36 sampling ports located across the major diameter of the vapor generator. A Beckman Model 315A infrared analyzer (using a 41 inch long 150 ppm full range nitric oxide NDIR analyzer) was used for NO, CO and CO_2 measurements. Beckman's Model 402 FID hydrocarbon analyzer was used for HC emissions. Thermo Electron Corporation's Chemiluminescent Analyzer Model 1CA equipped with a high temperature-thermo-reactor was used to measure NO and NO + NO_2. Values of NO_2 reported were recorded by the chemiluminescent analyzer. Beckman's NDIR nitric oxide analyzer was operated in parallel with the chemiluminescent unit as a double check by an independent measurement method. Good correlation between the two methods of measurement were observed throughout the tests. In general, the NDIR would be two or three parts per million higher than the chemiluminescent analyzer. This bias is caused by the much greater sensitivity of the NDIR to water vapor in the exhaust. By replacing the "Drierite" filter immediately upstream of the NDIR analyzer every few minutes the high bias of the NDIR could be eliminated. Difficulties due to water condensation with the chemiluminescent analyzer have been resolved by use of a water preheater and an electrically heated sampling line. Water condensation on the last rows of the vapor generator and in the sampling and analyzing portions of the system were an emissions measurement problem during the first weeks of testing. Addition of a water preheater to the feed water circuit increased the inlet temperature to over 185°F. This temperature simulates the condenser outlet temperature in an automobile. At 185°F the tube wall temperature was well above the dew point of water vapor in the exhaust and no further problems were observed with either NO_x of HC measurements.

Little or no NO_2 formation has been observed in the exhaust from the vapor generator. Two or three parts per million of NO_2 have been observed in some of the initial tests but normal test results show only a scatter that is probably inherent in the instrument's basic accuracy. (See Appendix I for a more detailed discussion of the emission measurement instrumentation.)

The initial rig tests used a three inch diameter cup normally operating at 10,000 rpm. Design of the integrated combustor air valve, fan and vapor generator required the fan and cup shaft to operate at a speed between 5,000 and 6,000 rpm to match fan characteristics. From variable speed tests and analysis of the three inch diameter cup, it was determined that good atomization

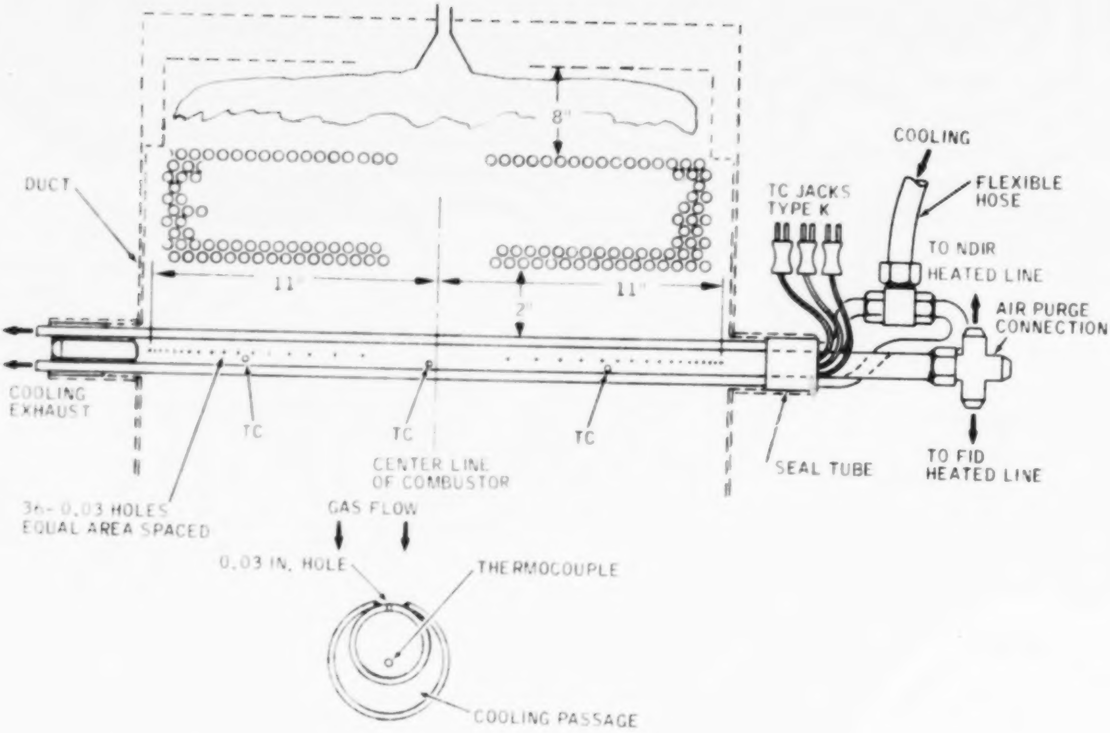
8"
DUCT
11"
11"
2"
COOLING EXHAUST
TC
TC
TC
CENTER LINE OF COMBUSTOR
36-0.03 HOLES EQUAL AREA SPACED
GAS FLOW
0.03 IN. HOLE
THERMOCOUPLE
COOLING PASSAGE
TC JACKS TYPE K
COOLING
FLEXIBLE HOSE
TO NDIR HEATED LINE
AIR PURGE CONNECTION
SEAL TUBE
TO FID HEATED LINE

FIGURE 41. EMISSION PROBE LOCATION AND CONFIGURATION

could be obtained at lower speeds but a larger diameter cup would be required. A four inch diameter conical cup was incorporated and tested in the complete system. Emissions of HC and CO were well within limits, however, NO_x emissions were slightly above limits. At fuel flows of less than approximately 20 pounds per hour, it was not possible to lower emissions of NO_x below the 1976 limits. Analysis of these results indicated that the probably cause of the problem was a lack of adequate mixing rates because of the low pressure drop across the combustor's air swirler at low air flows. In particular it was theorized from flame observations, that a relatively slow burning mass of fuel vapor was reacting in a "dead" region immediately downstream of the cup. It was believed that fuel vapor was trapped in this low velocity zone and consequently reacting stoichiometrically thus driving the NO_x above limits as the fuel vapor reacted from rich through to overall lean. Correction of this problem has been based upon the basic requirements to minimize NO_x. Essential for low emissions in a combustor in which fuel is introduced as a liquid, is the need to complete combustion with an overall lean air-fuel ratio. Production of NO_x is exponentially dependent upon local temperatures, and availability of oxygen. Since fuel is injected as a liquid, some zones of stoichiometric (maximum temperature) will occur prior to transition to an overall lean condition unless mixing rates are made sufficiently fast. A key feature of the combustor is to obtain a large area (wide spray angle) interface between liquid fuel and air at a zone that has very high shear velocities. Under these conditions, vaporization and mixing can occur extremely rapidly. Since chemical reaction rates are relatively slow compared to the high mixing rates possible, when a high pressure drop is used, NO_x production is minimized by reducing stoichiometric conditions. In the actual combustor, the mixing rates and thus the formation of NO_x is, to a large extent, dependent upon the pressure drop available. Thus a fundamental tradeoff between parasitic power limitations and acceptable NO_x levels has been made. Ideal power required for this combustor has been established at 1.2 HP (approximately 2.5 HP electrical input). In addition to the basic pressure drop-mixing rate tradeoff, it is essential that little or no droplet burning take place and that no pocket of vaporized fuel is allowed to mix slowly and react stoichiometrically.

Improvements of emissions at the low fuel flows is thus dependent upon achieving three goals.

- Rapid and uniform vaporization proper to reaction (little or no droplet burning)
- Elimination of pockets of stoichiometric fuel and slow mixing
- Increasing mixing and vaporization rates

All of these goals can be completely dependent upon mixing rates and recirculation or they can be independent as in the case of atomization and droplet control. Three modifications have been incorporated to assist to reduce NO_x formation.

- Double heat shield (see Figs. 42 and 43)

  Two heat shield discs with a dead air space between have been incorporated to prevent excessive vaporization from cup surfaces and consequent carbon buildup. This may also assist in the mixing since excessive fuel vapors generated in the cup are not accelerated tangentially at the lip of the cup as are the liquid droplets. This gaseous fuel may mix slowly down stream of the cup in a dead zone or be entrapped in local recirculation zones inside the swirler.

- Auxiliary Air Swirler

  Approximately 3 percent of rated air flow has been routed through an auxiliary air swirler (Fig. 42). High velocity mixing rates can be provided by this method since the full fan discharge air

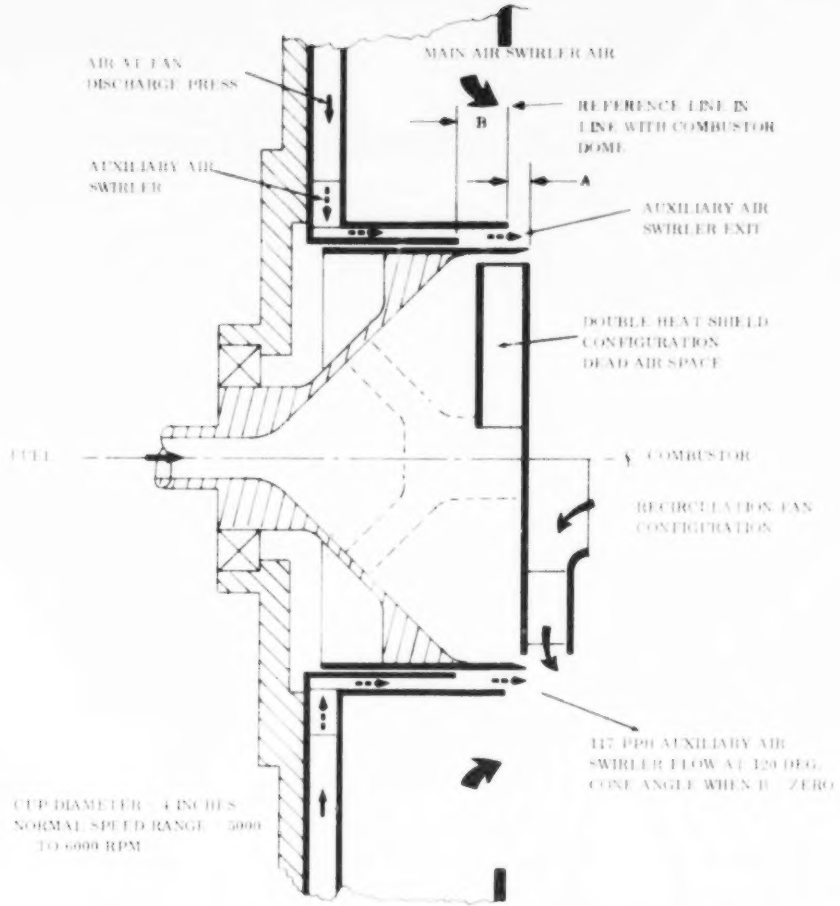
MAIN AIR SWIRLER AIR
AIR AT FAN DISCHARGE PRESS
REFERENCE LINE IN LINE WITH COMBUSTOR DOME
B
AUXILIARY AIR SWIRLER
A
AUXILIARY AIR SWIRLER EXIT
DOUBLE HEAT SHIELD CONFIGURATION DEAD AIR SPACE
FUEL
℄ COMBUSTOR
RECIRCULATION FAN CONFIGURATION
117 PPH AUXILIARY AIR SWIRLER FLOW AT 120 DEG. CONE ANGLE WHEN B = ZERO
CUP DIAMETER = 4 INCHES
NORMAL SPEED RANGE = 5000 TO 6000 RPM

FIGURE 42. CYLINDRICAL CUP CONFIGURATION FOR EMISSION TESTS

pressure (10 inches of water) is maintained across this auxiliary air swirler. In addition, the swirler provides a wide spray angle and recirculation in the critical fuel to air interface region adjacent to the lip of the cup. Measured air flow at 10 inches of water pressure drop is 117 pounds per hour at a 120 degree cone angle when "B" dimension equals zero. Figure 1 shows schematically the flow route from fan discharge to auxiliary air swirler passage. Air short circuits the air valve through 20 ports (see

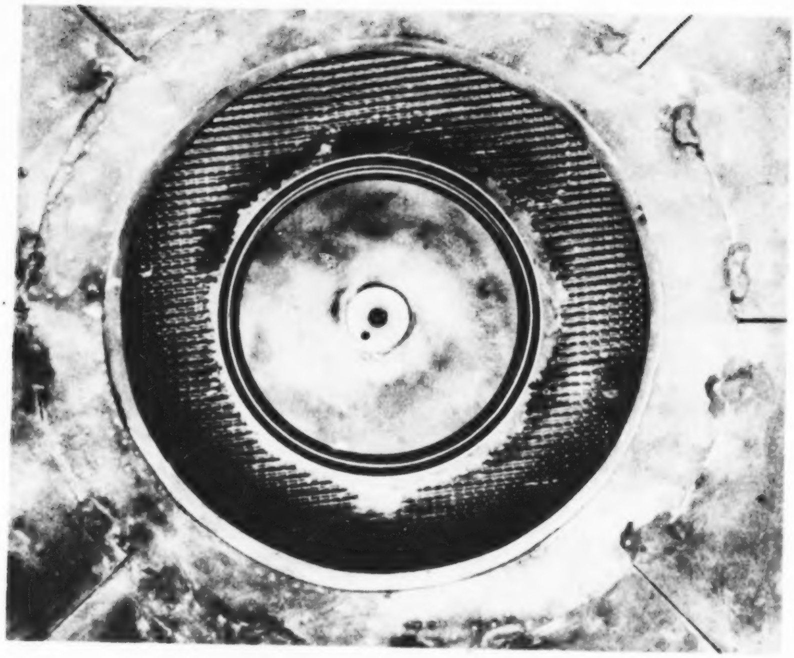

FIGURE 43. CYLINDRICAL CUP WITH DOUBLE HEAT SHIELD

Figs. 1 and 44). An air seal between the primary air passage and auxiliary air passage prevents leakage between the high pressure in the auxiliary swirler into the primary swirler. Figure 45 is a closeup view of the auxiliary air system. Tangential slots machined into the base of the auxiliary swirl tubes produce the desired high velocity swirl air. Figure 45 shows the air flow turning tabs mounted to the primary air ports. Their purpose is to convert some of the dynamic head of the pressure loss to tangential flow and thus increase mixing rates at low flows.

- Recirculation Fan

A small internal recirculation fan (Figs. 42 and 46) has been mounted to the cup. Its purpose is to help eliminate the "dead" zone downstream of the cup and to pump high temperature recirculated products to the interface with atomized fuel droplets for rapid vaporization and mixing at low fuel flows.

All of these modifications were tested in the fully integrated combustor/vapor generator both individually and combined. Initial tests of the recirculation fan concept were made with the 4 inch diameter conical cup. The fan in this configuration also acted as a heat shield. Tests results were encouraging. Figure 47 shows these results graphically. For each data point the NO_x was

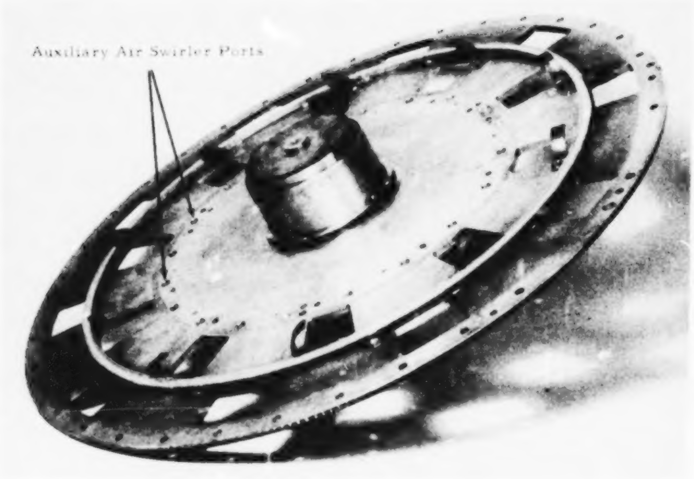
Auxiliary Air Swirler Ports

FIGURE 44. AUXILIARY AIR SWIRLER PORTS

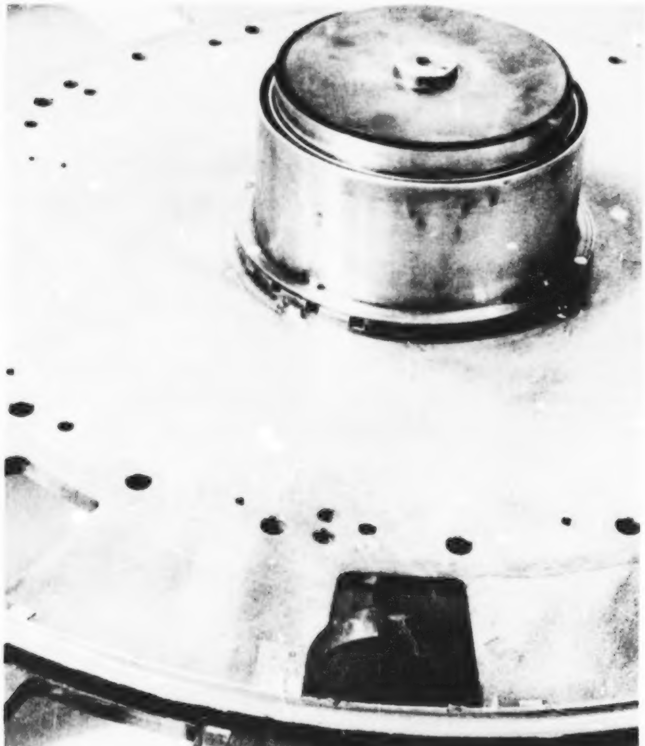

FIGURE 45. TANGENTIAL SLOTS AT BASE OF AUXILIARY AIR SWIRLER

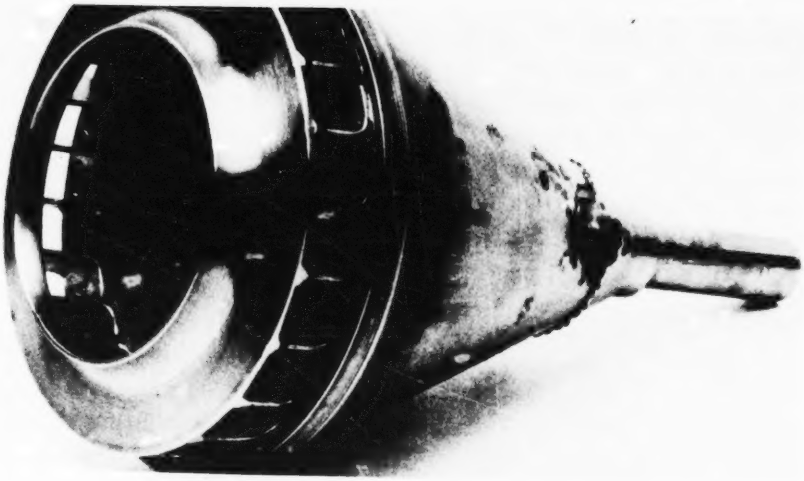

FIGURE 46. RECIRCULATION FAN ON CONICAL CUP

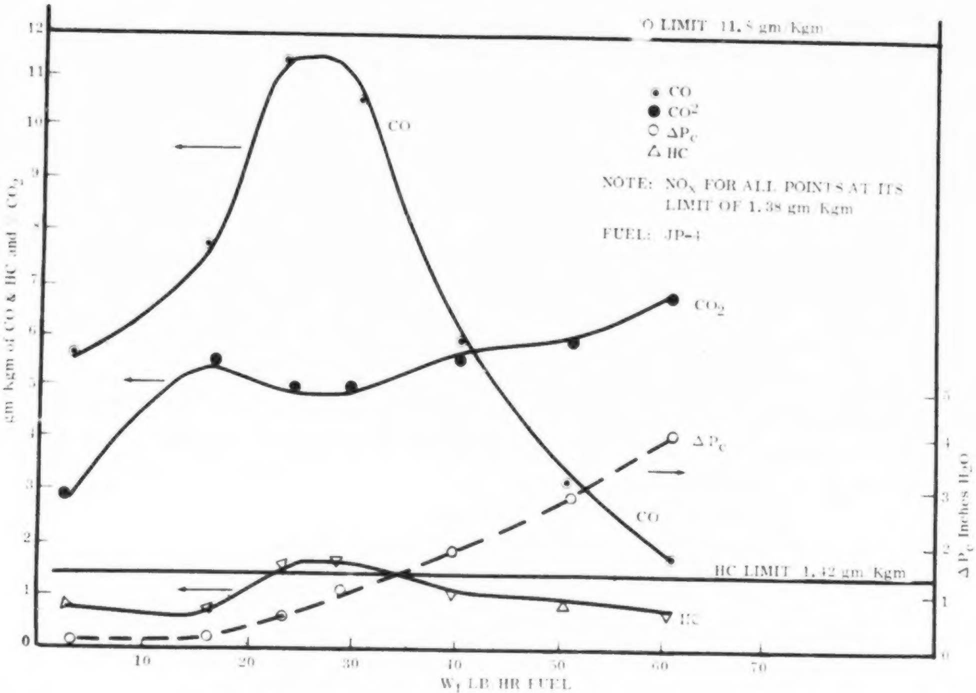

FIGURE 47. CONICAL CUP EMISSIONS WITH RECIRCULATION FAN (CO_2 ADJUSTED TO MAINTAIN NO_x AT 1.38 GM/KGM)

maintained at its limit of 1.38 gm/kgm by adjustments to the air-fuel ratio. CO and HC emissions were good down to fuel flows as low as 2.8 pounds per hour. This is the lowest fueling rate at which all emissions have been brought within the limits. An emissions peak at 30 pounds per hour has not been fully explained but may be an atomization problem associated with fuel impingement on the cup or its shroud. Another possible problem is the counter rotation of the fan swirl from the main air swirler which will produce lower mixing velocities at a specific air flow.

To obtain a flexible cup atomizer and incorporate heat shields, auxiliary air swirler and a recirculation fan the cup was redesigned to a cylindrical configuration shown in Figure 42. A more stable bearing stack was also incorporated to eliminate a wobble that was noted with the conical cup. A cylindrical cup configuration was chosen for better control of vaporization and to allow wakes from the center support spider be uniformly distributed prior to atomization. A number of different fuels have been tested with this final configuration. Auxiliary swirler dimensions A and B have been found to be critical variables. With "A" small it has been observed that the fuel can be drawn back into the auxiliary swirler causing impingement on the outer lip of the auxiliary air swirler. Since the fuel accumulates into large drops and then reatomizes from the swirler with relatively large droplets, the emissions increase.

Test results are graphically shown in Figures 48 through 55. Initial tests and developments, including rig tests were mainly performed with JP-5 and JP-4. JP-4 was the initial fuel used for combustor development on the integrated combustor steam generator tests. Figures 45 through 49 show emission test results with JP-4. Since the NO_x emissions are close to the limit, most of the test points recorded were obtained by adjustments of the fuel-air ratio to obtain best NO_x or CO emission levels. In general, this was accomplished by moving the air valve to the desired flow position. The mechanically linked fuel valve would also move to the same percent flow position giving a nominal air-fuel ratio of 25 to 1 or approximately a CO_2 reading of 8.3 percent. By adjusting the fuel pressure across the fuel metering valve, the air-fuel ratio could be changed to a richer or leaner point. A direct tradeoff between NO_x and CO emissions can be made by adjustments of the fuel-air ratio at a particular air valve setting. As the air-fuel ratio decreased (CO_2 increased) the level of CO emissions can be drastically reduced. This is due to an increase in temperature in the CO burnout zones resulting in more complete reaction. A corresponding but less sensitive increase in NO_x results from a decrease in air-fuel ratios. In these tests the data points were obtained by adjusting the fuel-air ratio while monitoring and trading-off NO_x against CO levels. In general, two readings were obtained at each power level. One data point recorded was the NO_x level with the CO level allowed to approach its maximum specified limit. A second point was

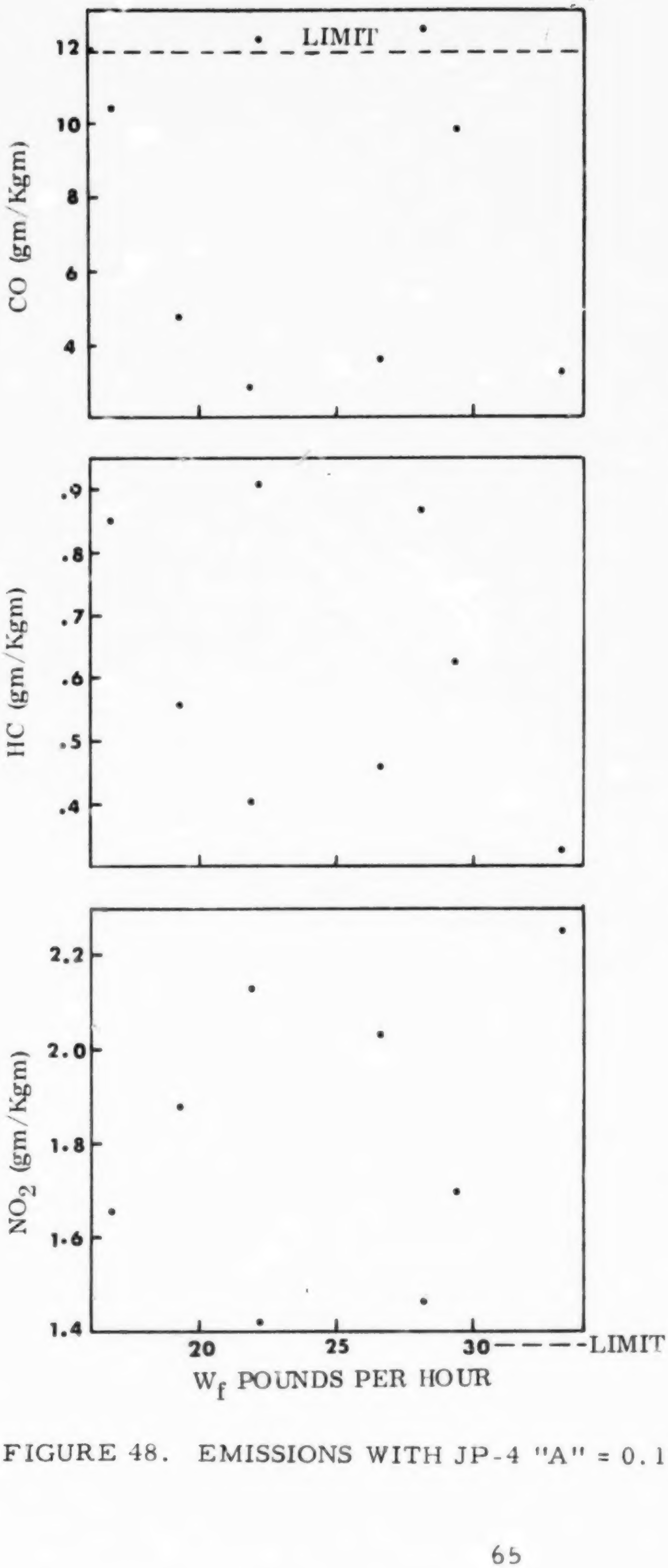

CONFIGURATION

Fuel - JP4
Auxiliary Air Swirler (None)
2 Heat Shields
A = 0.125
B = Zero
Carbon: Not Recorded

FIGURE 48. EMISSIONS WITH JP-4 "A" = 0.125 AND 2 HEAT SHIELDS

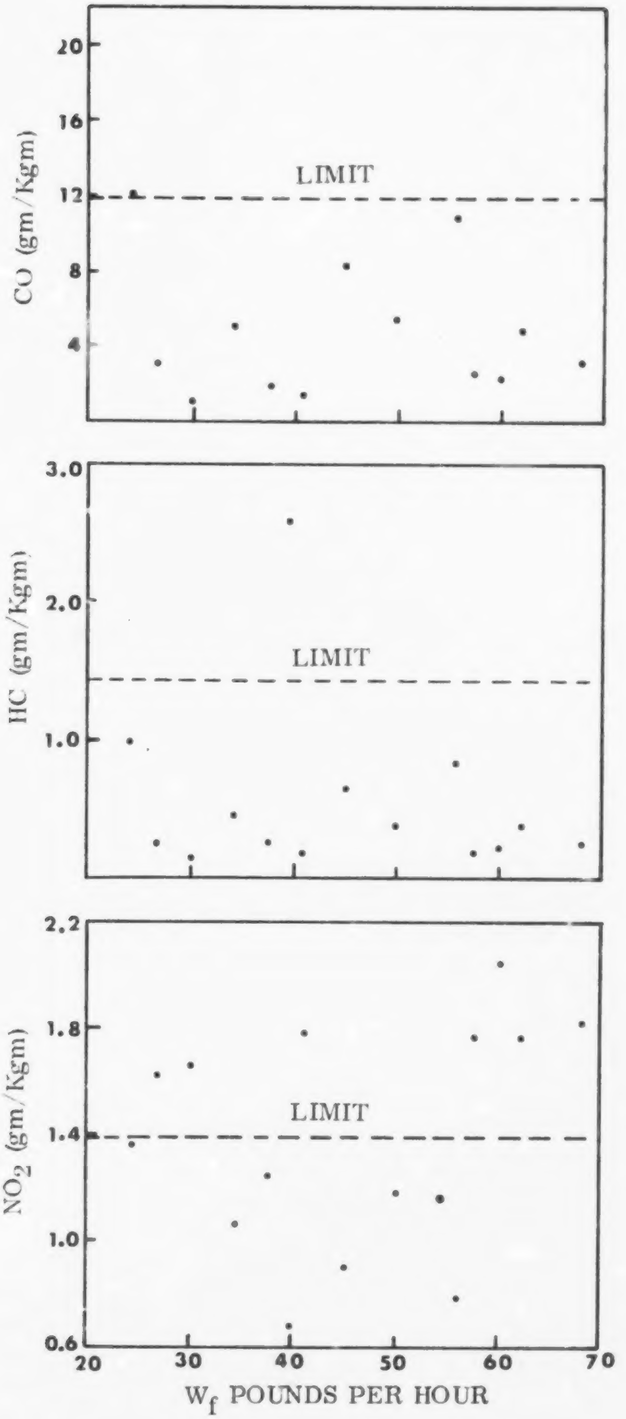

CONFIGURATION

Fuel - JP4
Auxiliary Air Swirler
2 Heat Shields
A = 0.125
B = Zero
Carbon: Cup Clean
Auxiliary Swirler
Coated

FIGURE 49. EMISSIONS WITH JP 4, "A" = 0.125 WITH AUXILIARY AIR SWIRLER

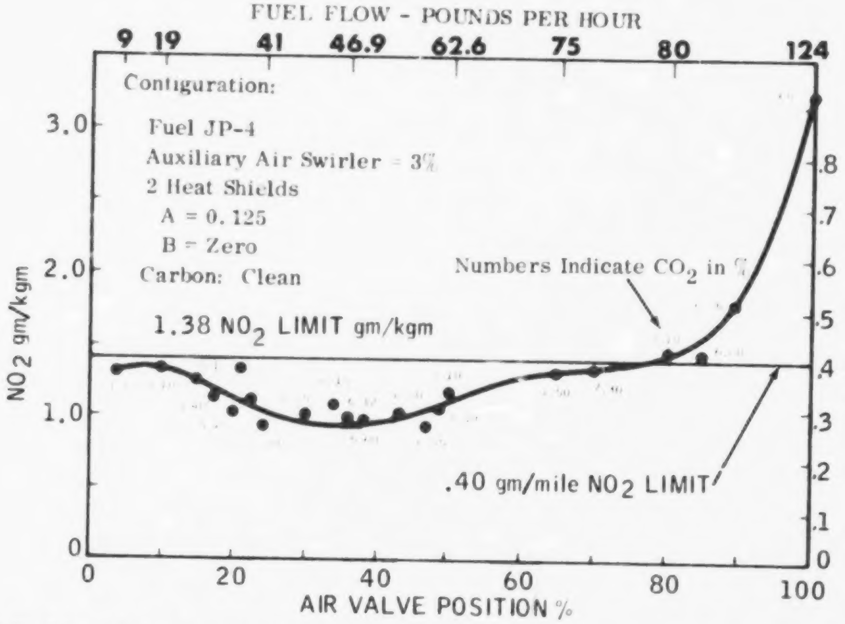

FIGURE 50. NO_2 EMISSIONS WITH A = 0.192, 2 HEAT SHIELDS AND AUXILIARY AIR SWIRLER

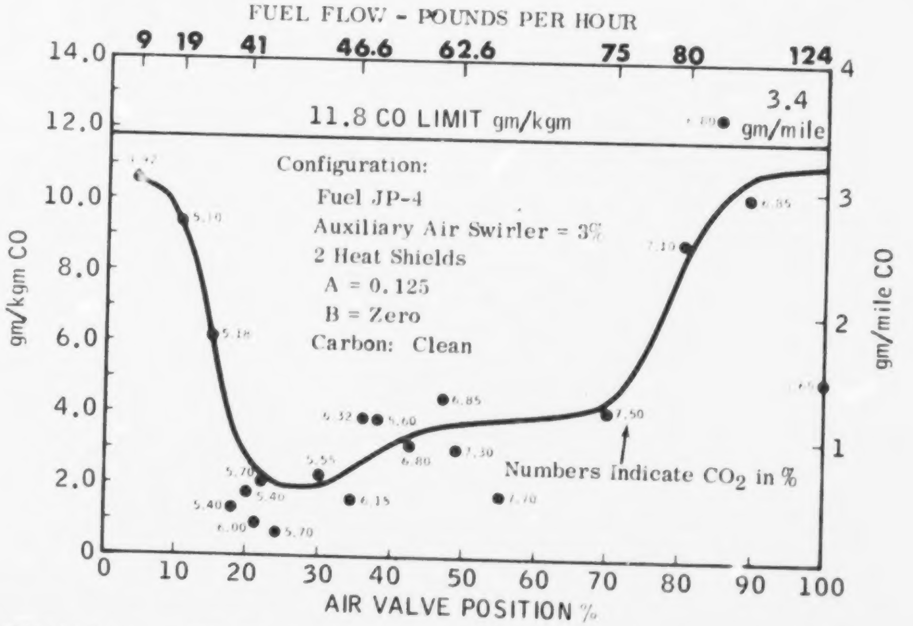

FIGURE 51. CO EMISSIONS WITH A = 0.192, 2 HEAT SHIELDS AND AUXILIARY AIR SWIRLER

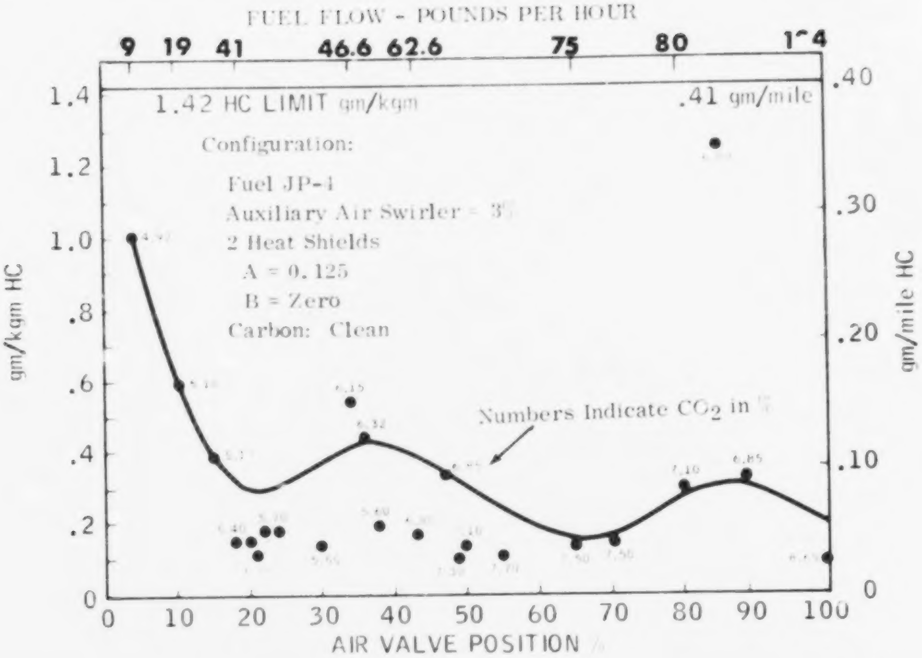

FIGURE 52. HC EMISSIONS WITH A = 0.192, 2 HEAT SHIELDS AND AUXILIARY AIR SWIRLER

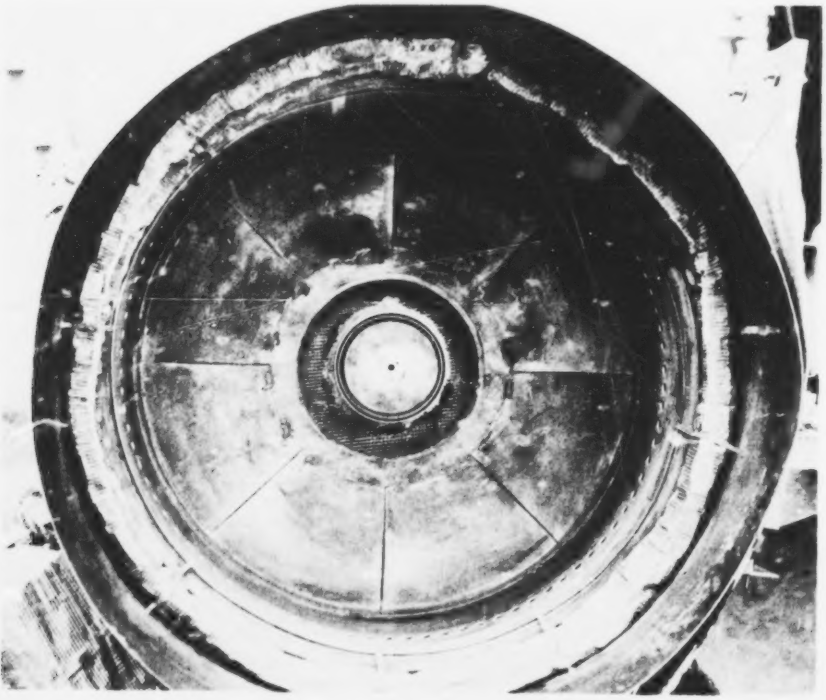

FIGURE 53. COMBUSTOR POST TESTS RECORDED IN FIGURES 50, 51 AND 52

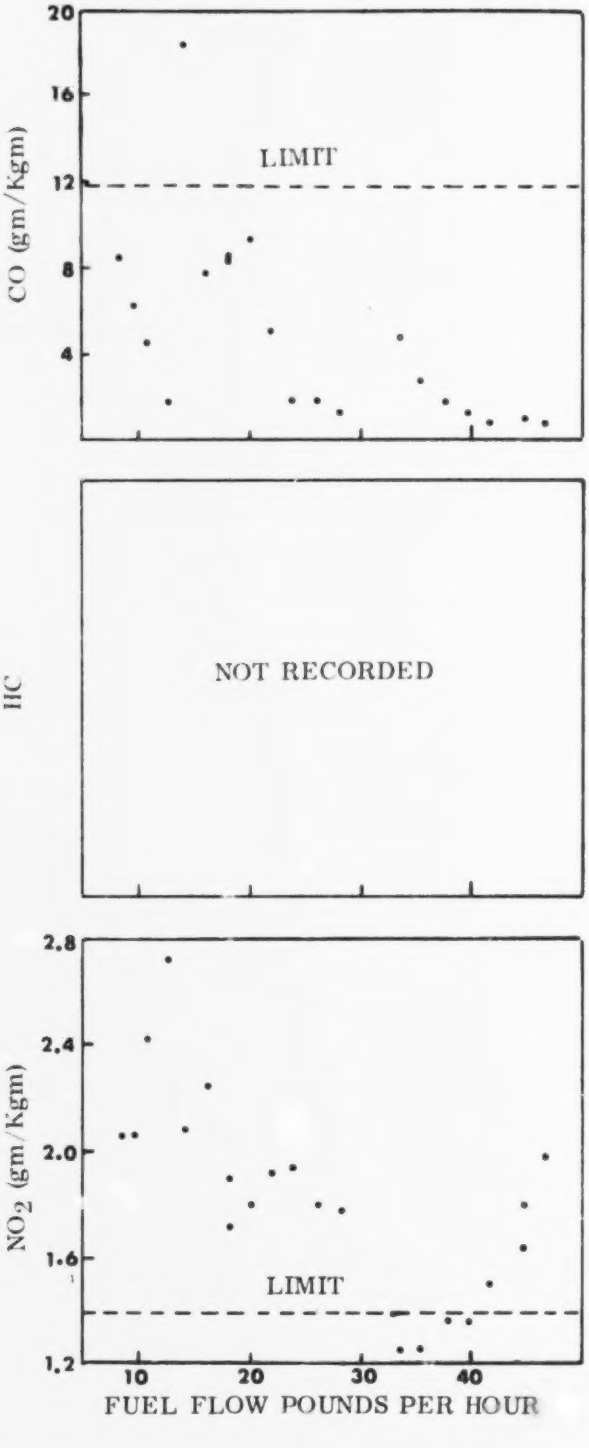

CONFIGURATION

Fuel - Gasoline
Auxiliary Air Swirler = 3%
2 Heat Shields
A = 0.192
B = Zero
Carbon: Inside of Cup and indication of combustion on outer lip of cup

FIGURE 54. EMISSIONS WITH GASOLINE, A = 0.192 AND 2 HEAT SHIELDS

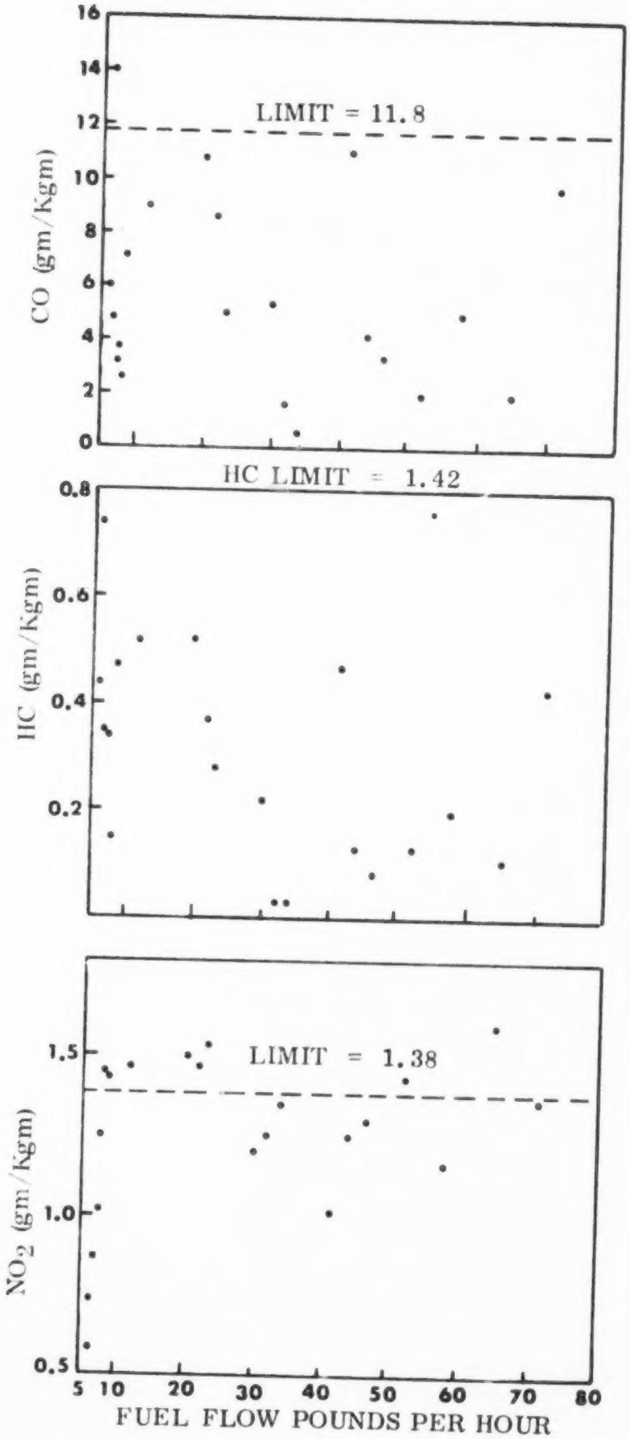

CONFIGURATION

Fuel: Gasoline
Auxiliary Air Swirler = 3%
Recirculation Fan
A = 0.03
B = 0.5
Carbon: Clean

FIGURE 55. EMISSIONS WITH GASOLINE, A = 0.03, AUXILIARY AIR SWIRLER AND RECIRCULATION FAN

the NO_x level with low CO reading. By analyzing these limits it is possible to obtain approximate values of the tolerance band within which the controls are required to hold the air-fuel ratio to obtain low emissions across the full range.

The first tests using the cylindrical cup and dual heat shield were disappointing. Figures 48 and 49 show the emission levels for fuel flow ranges between 16.8 and 70 pounds of fuel per hour. The first data point on Figure 48 was at 16.8 pounds per hour with the air-fuel ratio adjusted to move the CO level to near its maximum allowable limit of 11.8 gm/Kgm. The CO_2 reading at this point was 4.8 percent. At this condition the emissions of NO_x were well above the limit (1.65 compared to a limit of 1.38 gm/Kgm). The next points recorded were obtained by decreasing the air-fuel ratio to a CO_2 reading of 5.45 resulting in an order of magnitude drop in CO levels while relatively small increases in NO_x were recorded. The general appearance of widely scattered data points is a result of the continual adjustments made to CO_2 levels to obtain best emission levels or control band information. No auxiliary air swirler flow was used for the test points of Figure 48. Addition of 3 percent auxiliary air swirl is shown in Figure 49. Many of the NO_x emission data points were well below the limit indicating a significant gain by addition of the auxiliary air swirler. However, it was not possible to reduce NO_x emissions below the limits with this configuration at fuel flows below 25 pounds per hour. Visual examination of the combustor after the test indicated carbon on the auxiliary air swirler. This accumulation was indicative of fuel impingement caused by excessive recirculation over the cup lip due to the auxiliary air swirler. By moving the cup away from the immediate discharge of the swirler, this problem appeared to be resolved as shown by the emission results plotted in Figures 50 through 52. The "A" dimension (Fig. 42) was increased from 0.125 to 0.192 inch to permit emission levels to be held within limits down to 9 pounds per hour of fuel flow. Although this change reduced the beneficial effects of the air swirler, it prevented impingement. By adjustment of the air-fuel ratio (as shown by the $\%CO_2$ readings adjacent to the data points) emissions of NO_x and CO were traded off to obtain the "best" results shown in the curves on Figures 50, 51 and 52. In order to maintain NO_x below the limits the air-fuel ratio was increased (low CO_2 values on curves) at the low fueling rates. A rapid increase in the main tradeoff parameter of CO is illustrated by the rapid rise in CO at low fueling rates as the overall air-fuel ratio is made leaner. In the mid-fuel flow ranges, ample margins exist to allow NO_x and CO to be well below the limits. At fuel flows above 80 pounds per hour it was no longer possible to adjust the air-fuel ratios and keep both CO and NO_x below their limits. At 100 percent air valve setting the unit was operated at its design air-fuel ratio of 25 to 1 to do full flow vapor generator calibrations of efficiency and stability. At these conditions, the CO was less than 1/2 of its limit but NO_x was approximately twice. In general it can be assumed that the emissions at flows above approximately 25 pounds per hour have little effect upon the steady state simulation of the Federal Driving Cycle. If an assumption of 10 mpg fuel economy is used, the emissions at a fueling rate of 12 to 15 pounds per hour dominate the results. As a consequence the greatest effort has been placed upon lowering the emissions at these low fuel flow rates. Inspection after emission tests shown in Figures 50, 51 and 52 showed the cup and swirler to be free of carbon. Figure 53 is a post test inspection after approximately 15 hours of operation with this configuration that results in the lowest emissions.

Upon completion of tests with JP-4, the best configuration (Figs. 50 through 52) was tested with commercial automotive unleaded gasoline. Results are shown in Figure 54. Emission levels were worse. This was unexpected since the greater volatility of gasoline should have been an asset in vaporization and rapid mixing. Inspection after these tests revealed carbon on the swirler and burn marks on the outer diameter of the cup as far back as the distance it extended from the swirler. To correct this tendency for gasoline vapors to be sucked back toward the swirler, the inside ring of the swirler was cut back 0.5 inch (dimension "B" on Fig. 42) and the cup was extended only 0.03 inch from the swirler ("A" dimension). In addition, a recirculation fan was installed in place of the dual heat shield to assist in controlling the flow of vaporized gasoline and recirculated products of combustion. Results of these tests showed a considerable improvement (Fig. 55). Emissions were well within limits at low fuel rates of 6.5 pounds per hour. However, at the critical fuel flows of 12 to 15 pounds per hour, the emissions of NO_x could not be brought within limits even though CO was allowed to increase towards its limits. At these fuel flows the NO_x was approximately 10 percent above the limits with CO approximately 20 percent below its limit. It appears that the recirculation fan is, as in the tests with JP-4 and the conical cup, producing good emissions performance at the very low fuel flows as anticipated. However, a hump in the emissions at fuel flows from 10 to 25 pounds per hour exists that is not aleviated by the use of the auxiliary air swirler. Cold flow tests with water through the cup instead of fuel has shown an interaction between auxiliary air swirler's jet and the fan discharge jet that causes liquid to impinge on the swirler. Modifications incorporated to eliminate this interaction by changing the swirl angle of the auxiliary air swirler are discussed below.

Efforts to improve the systems emission in the low fuel flow range (5 to 15 pph) were attempted. A series of cold flow tests with water used in place of fuel resulted in the selection of an optimum auxiliary air swirler and recirculation fan configurations. Visual observation of the water spray pattern was made by removing the combustor section from the vapor generator coils. An optimum configuration was defined as one in which no water impingement was observed on any combustor surface except the side walls. Spray angles were observed visually with the widest angle being considered the best. Two configurations had excellent spray patterns. Figures 42 and 56 show the geometry arrangements between the cup, the auxiliary air swirler and the recirculation fan. With the "C" dimension at 0.06 and "A" at 0.075 inch a

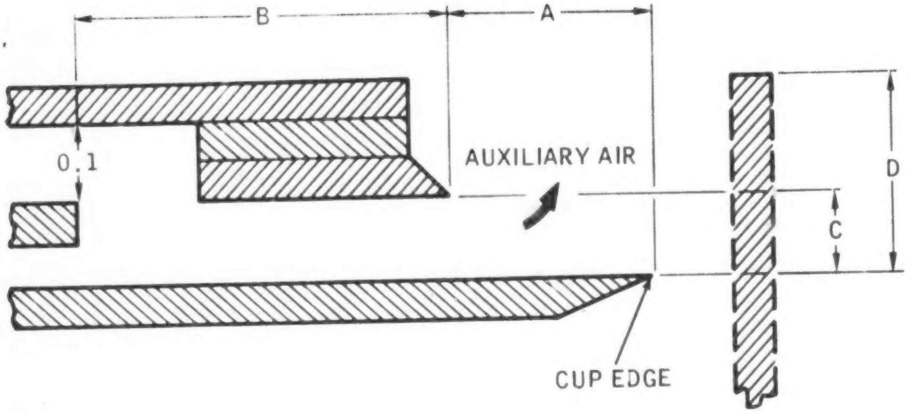

FIGURE 56. AUXILIARY AIR SWIRLER CONFIGURATION VARIATIONS

180 degree spray pattern of air and water could be obtained with only a slight impingement on the combustor dome. This condition was with auxiliary air flow but no fan. When the fan was added the "A" dimension had to be increased to 0.137 inch to prevent impingement on the swirler. With that configuration no impingement on the dome was observed. An ideal spray and air flow pattern results from high down to flows of 2 or 3 pounds per hour. As the "A" dimension is decreased, water impingement on the outer lip of the auxiliary air swirler was observed. As "C" dimension is increased, the swirl angle is increased (since the axial velocity component goes down) and a greater tendency to send water back into the auxiliary swirler was observed.

Emission tests with both secondary air swirl, recirculation fan and combination of both were performed, results were not as good as the emission levels reported above. With "A" at 0.075, "B" at 0.5 and "C" at 0.06 inch without a recirculation fan but with a double heat shield, emissions within limits were obtained at fuel flows above 16.5 pounds per hour (tests run up to 43 pph). At lower flows NO was above limits. Inspection of the unit after runs indicated considerable carbon on the cup and on the outer lip of the secondary swirler. It was thought that the carbon formed as a result of high velocity recirculation of partially burnt products across the edge of the cup. A baffle 0.1 inch greater than the OD of the cup lip was installed to eliminate this edge effect (see dimension "D" in Figure 56). Results of emission tests with the baffle installed were good with respect to carbon formation. A small amount of carbon formed within the cup but all exterior surfaces remained clean. However, emissions were not as good as without the baffle.

Tests with the "best" swirler configuration and with the recirculation fan were also disappointing. A large amount of carbon formed and emissions were all above limits. Some of these poor results were believed to be associated with the discontinuity caused by the auxiliary swirler on the main air swirlers flow path. The auxiliary air swirler was removed and tests were performed with and without the recirculation fan. In both cases the emissions of NO were generally borderline or well above the limits.

None of these tests showed an improvement of the configurations reported in Figures 50 through 52. In all the tests without the auxiliary air swirler, there was a carbon buildup on the inside and outside of the cup. This indicates the main swirler is not flowing full and that a central recirculation across the edge of the cup back into the swirler exit draws fuel vapor back into this zone. Carbon deposits on the outside of the cup indicate that fuel vapor burns in this area. Heat from the recirculation flow and the combustion reaction on the outside of the cup compounds the problem by generating more fuel vapors prior to leaving the cup as a spray. Oxide layer buildup has indicated cup temperatures in excess of 600°F.

Another series of tests with the main swirl vanes 80 percent blocked allowed measurements to be performed with high pressure drop and low fuel flows. As in the above series of tests, this resulted in excessive recirculation and burning around the fuel flows of 10 to 15 pounds per hour. However, the safety margin was only abour 10 percent. It was decided to rebuild the combustor back to the configuration that resulted in the best emissions with gasoline (Fig. 55). Although these results were not entirely satisfactory a combination of the auxiliary air swirler and recirculation fan resulted in below requirement from 6.5 pounds per hour to 10 pounds per hour emissions. From 10 to 20 pounds per hour the emissions of NO were approximately 10 percent above limits (Fig. 55). This configuration has been retested with the addition of the double heat shield using the EPA reference gasoline. Test results show a similar pattern with emissions of NO_x 4 or 5 ppm within limits at 8.5 pounds per hour and reaching the limit at 14 pounds per hour. From 14 to 30 pounds per hour the emissions of NO_x were approximately 3 or 4 ppm above the limit (23 ppm limit).

Inspection after approximately 70 hours of operation with the EPA reference gasoline showed an extremely clean combustor and steam generator. Figure 57 shows the overall view of the combustor after 70 hours. All surfaces were clean with the exception of a small accumulation of carbon near the exit of the main swirler and on the outer tube of the auxiliary swirler (Fig. 58). Local recirculation patterns into the inner core of the main swirler appear to have been the cause of these carbon formations. Time limitations have not permitted the necessary redesign to eliminate these slow reacting pockets. By eliminating these slow mixing, rich pockets (indicative of near stoichiometric temperatures), a considerable improvement in the emission characteristics will be achieved.

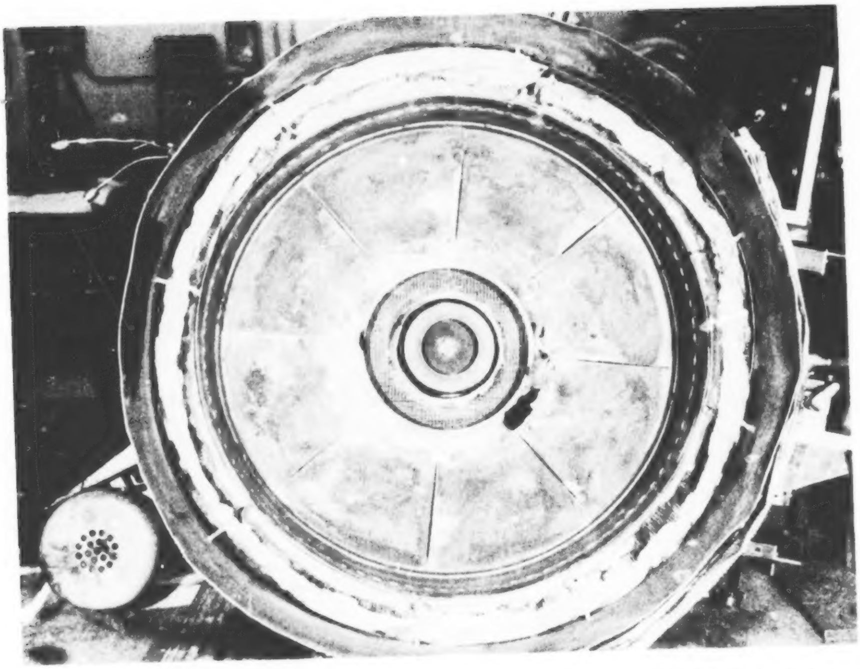

FIGURE 57. COMBUSTOR AFTER 70 HOURS OF OPERATION ON EPA REFERENCE GASOLINE

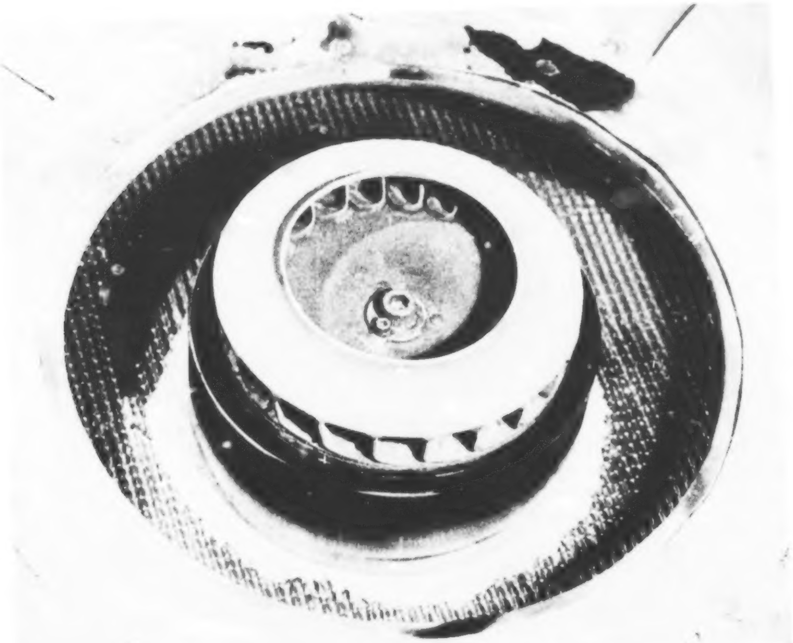

FIGURE 58. AUXILIARY AIR SWIRLER AFTER 70 HOURS OF OPERATION WITH EPA REFERENCE GASOLINE

One approach to significantly reduce emissions below the limits is to use exhaust gas recirculation or water injection. Injection of water can also give a qualitative analysis of the mechanism of NO_x formation. Water injection was used with the best configuration (Fig. 50, 51, 52) to assist in analysis.

The rotating cup was well suited to modification for water injection. A water line was tied into the fuel line just ahead of the pickup on the cup shaft, as shown in the schematic below. The water was run through a flowrator, then through a needle valve, which controlled the water flow rate, just ahead of the tee.

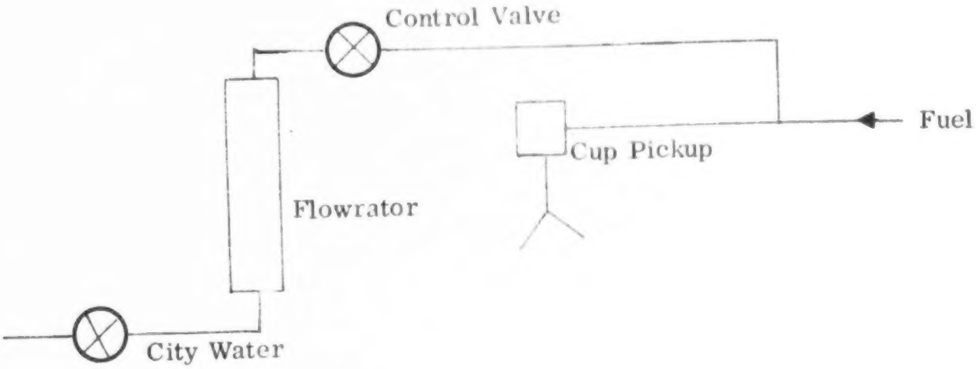

It was found that this simple injection device was capable of producing drastic reductions in NO_x emissions, especially at low fuel flows, where combustor pressure drop is low. At fuel flows on the order of 10 lbm/hr, the injection of one pound of water per pound of JP-4 fuel was sufficient to reduce NO_x levels down to less than 1/2 the level required by 1976 standards. Water injection allowed the average flame temperature at low loads to be greatly increased over its permissible value for acceptable NO_x emissions without water injection. CO levels were down to about ten percent of their values without water injections, as would be expected from the higher average flame temperatures.

The mechanism by which water injection reduces NO_x emissions is fairly well known. Primarily, the water acts to reduce the local flame temperature by absorbing heat as it vaporizes and as its temperature increases. At high flame temperatures it also absorbs heat as it dissociates. The dissociation reaction

$$H_2O + O \longrightarrow OH + OH$$

also tends to reduce NO formation by competing with nitrogen for oxygen radicals, thus interferring with the Zeldovich mechanism through which NO is formed, that is,

$$O + N_2 \longrightarrow NO + N$$

$$N + O_2 \longrightarrow NO + O$$

From the foregoing, it is apparent that water injection cannot interfere with the formation of NO_x unless the water is present in the gas phase in the regions where NO_x is being formed.

Water is considerably less volatile than the JP-4 fuel which was used for these tests, so it is reasonable to assume that in regions where the water is primarily in the gas phase, so is the fuel. If diffusion burning from excessively large droplets was a significant factor in NO_x formation in the present burner, as was thought to be one of the possible problems, water injection would be unlikely to significantly reduce NO_x emissions. In zones where significant fuel is present in the liquid phase, there would be unlikely to be much water present in the gas phase.

The water tests therefore seems to confirm that NO_x formation in the test combustor is due to poor mixing in the gas phase, allowing near stoichiometric pockets of fuel to persist for significant amounts of NO to form. This problem is probably compounded by the formation of recirculation zones in the main swirler close to the cup producing NO through much the same mechanism as near stoichiometric pockets in the flow outside the main swirler.

5.3.5 Temperature Pattern

Evaluation of the combustor outlet temperature pattern was made during performance analysis of the steam generator. A triple shielded and asperated thermocouple (Fig. 5) was used to measure the temperature. It was positioned at one inch increments across the full 20 inch diameter of the flame tube. Axial position was 8 inches downstream of the rotating cup (immediately upstream of the first row of the steam generator). Fuel flow and steam conditions (1000°F and 1000 psi) were held constant throughout the temperature traverse. The top curve of Figure 59 records the temperature pattern at 100 percent steam flow (1200 pounds per hour), the maximum rated condition for the high efficiency monotube unit (see Section 7). EPA reference gasoline was the fuel, with a measured fuel rate of 104 pounds per hour. An average temperature of 2350°F was recorded with the maximum peak temperature of 2625°F measured 4 inches from the centerline of the combustor. A minimum temperature of 2135°F was recorded near the wall of the flame tube. A total temperature spread of +275 and -215°F around the mean results at full flow. This is slightly above the initial goal of ±250°F but an acceptable deviation when considering the steam generator heat transfer assumptions. The theoretical flame temperature at these conditions (neglecting radiation effects) is approximately 2500°F. Radiation heat transfer

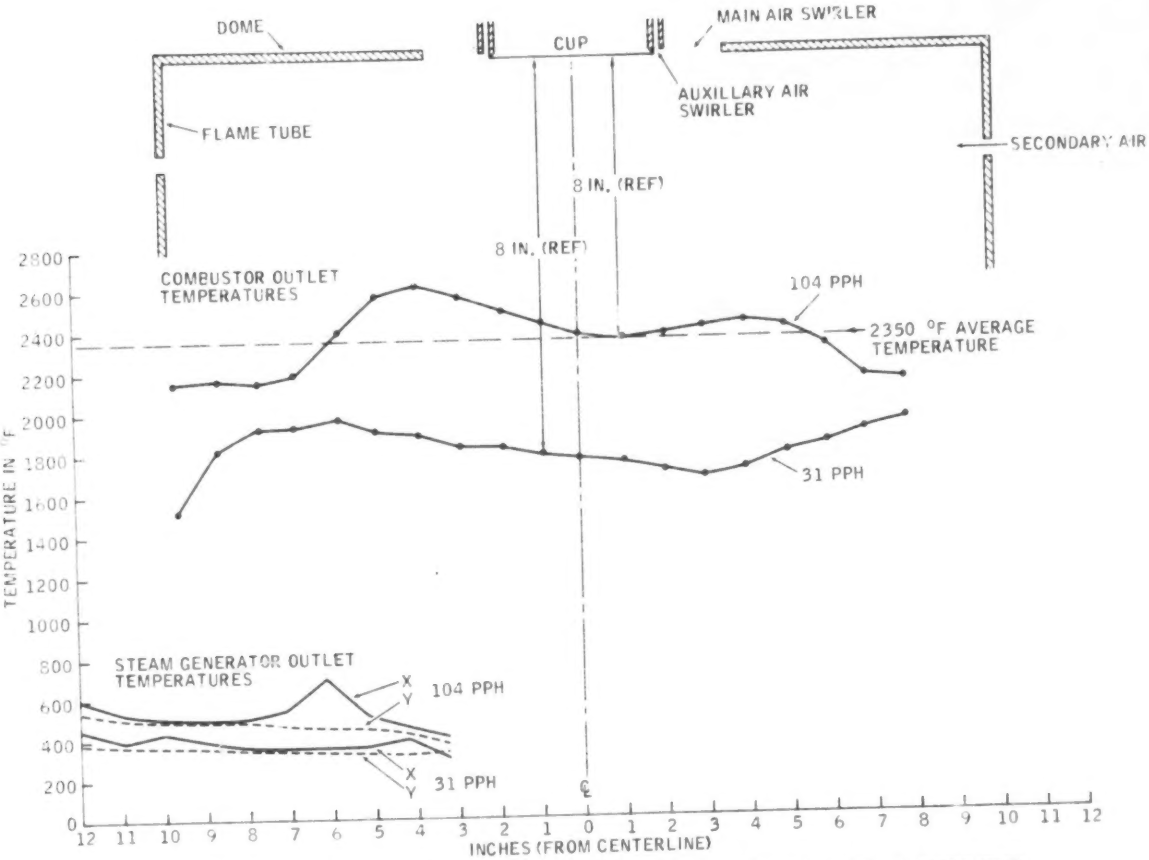

FIGURE 59. COMBUSTOR AND STEAM GENERATOR OUTLET GAS TEMPERATURES

from the highly luminescent flame into the relatively cool (540°F) first row of tubes was expected to be high. Thus the gas temperature drop of 150°F below the theoretical level is indicative of the expected high flame emissivity.

A typical temperature distribution at lower flows with leaner air-fuel ratios is shown by the second curve. It was recorded at the same station (8 inches from the cup) at the identical positions across the combustor's diameter. Fuel flow was 31 pounds per hour. The temperature profile at this flow is considerably different than at the higher flows. A major factor in explaining this difference is the entirely different air flow arrangement between the two flows. At 104 pounds per hour fuel flow, approximately 50 percent of the air is being admitted into the combustor through a ring of 90 ports located 4 inches downstream of the fuel injection cup station. The lower temperatures near the flame tube wall at high flows is probably due to inadequate penetration and mixing from these jets. Temperatures recorded at the fuel flow of 31 pounds per hour were with no secondary flow. All air is admitted through the main air swirler. As a result, the characteristic distribution of temperatures is considerably different. The low temperature recorded at about 0.1 inch from the flame tube wall may be a result of a small amount of secondary air flow due to air valve leakage.

Although the temperature profiles are acceptable with regards to steam generator performance, they do not look ideal for low emissions. Of particular concern is the lack of symmetry. As was discussed earlier in this section, emissions at 100 percent flow is well above the goal. The asymmetrical shape of the temperature distribution indicates that some degree of non-uniform fuel-air ratio distribution is taking place, and thereby contributing to formation of NO_x.

The four temperature curves at the bottom of Figure 59 were taken at a station one inch downstream of the steam generator. Two thermocouples mounted at 90 degrees to each other recorded temperatures from approximately 3 inches (a six inch diameter insulated manifold is in center of steam generator to the wall of the exhaust plenum). Good distribution was observed except for one temperature spike in the x plane at 104 pph. This may be indicative of a local gas blowby causing a reduction in the efficiency of the steam generator (see Section 7).

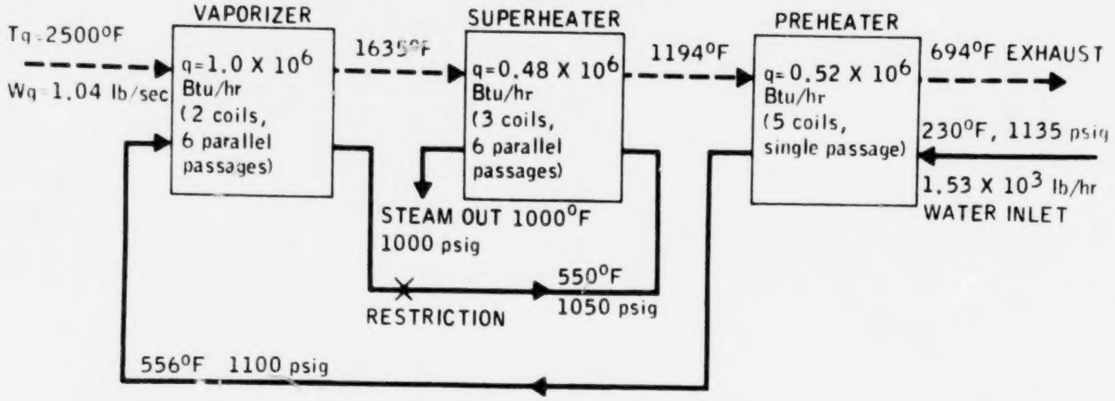
Tq 2500°F
Wq 1.04 lb/sec
VAPORIZER
q=1.0 X 10^6 Btu/hr (2 coils, 6 parallel passages)
1635°F
SUPERHEATER
q=0.48 X 10^6 Btu/hr (3 coils, 6 parallel passages)
1194°F
PREHEATER
q=0.52 X 10^6 Btu/hr (5 coils, single passage)
694°F EXHAUST
230°F, 1135 psig
1.53 X 10^3 lb/hr WATER INLET
STEAM OUT 1000°F 1000 psig
550°F 1050 psig
RESTRICTION
556°F 1100 psig

FIGURE 60. TEST BED VAPOR GENERATOR - WATER WORKING FLUID

- Tube size throughout unit: 0.5 inch OD, 0.035 inch wall, 321 SS all welded construction
- Heat transfer area (gas side) 62 ft^2
- Tube nest size: 21.5 inches OD, 6.25 inches high
- Gas side pressure drop: 2.8 inches of water
- Water side pressure drop: 135 psi
- Tube weight: 106 pounds
- Water holdup: 30 pounds
- Triangular axial and transverse tube pitch with the pitch equal to 1.25 tube diameter

Each of the five preheater rows consists of five, flat spiral coils. Connections at each end of this coil are made by specially designed fittings (bottom of Fig. 61). Both vaporizer and the three superheaters rows are each constructed from six flat spiral coils (Fig. 62) connected in parallel by the fittings shown in Figure 63.

6.2 CONSTRUCTION

A test bed unit was constructed to minimize lead times. All tubing is 321 stainless steel (0.5 OD, 0.035 inch thick wall) with welded construction throughout. A total of 10 rows of flat spiral coils each 21.5 inches outside diameter make up the tube matrix.

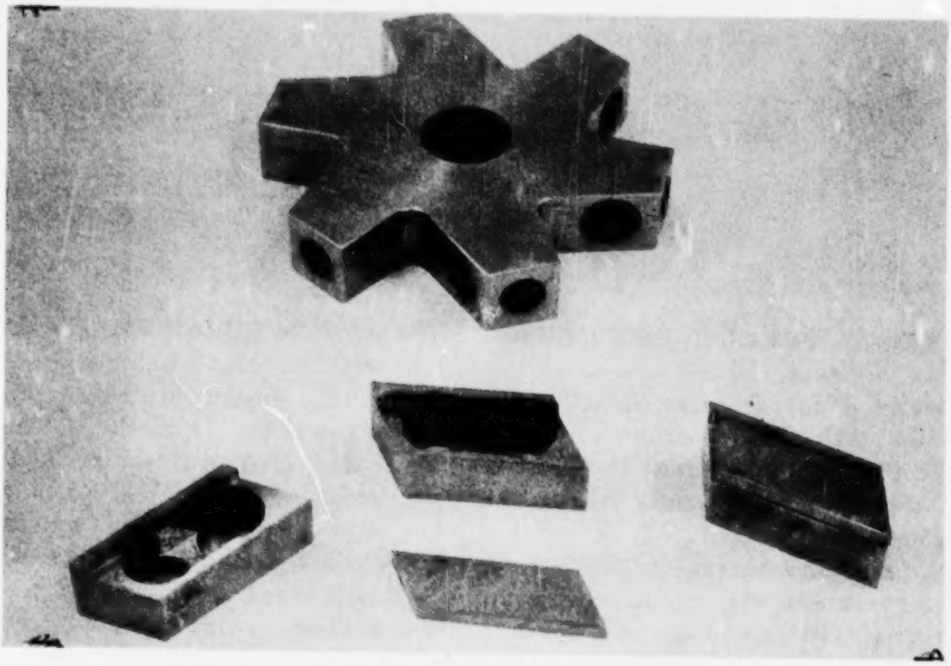

FIGURE 61. VAPOR GENERATOR COIL CONNECTORS

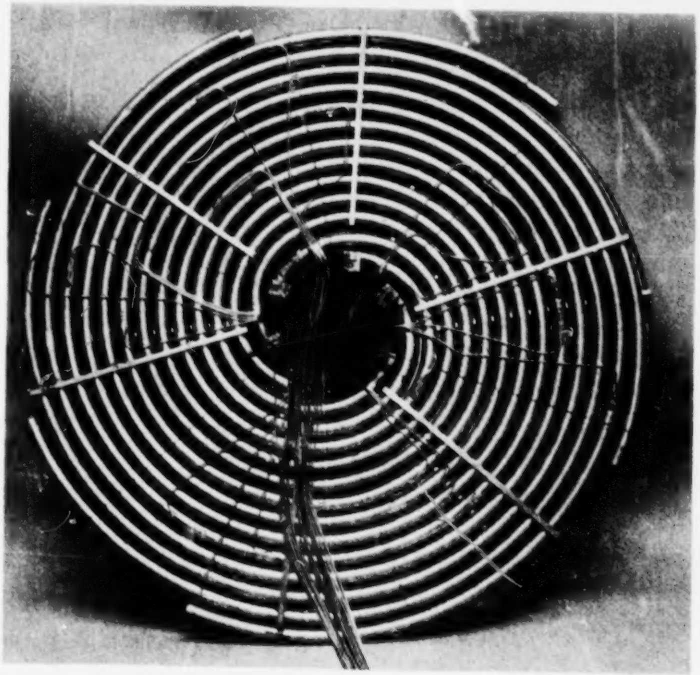

FIGURE 62. VAPORIZATION COILS (6 PER ROW)

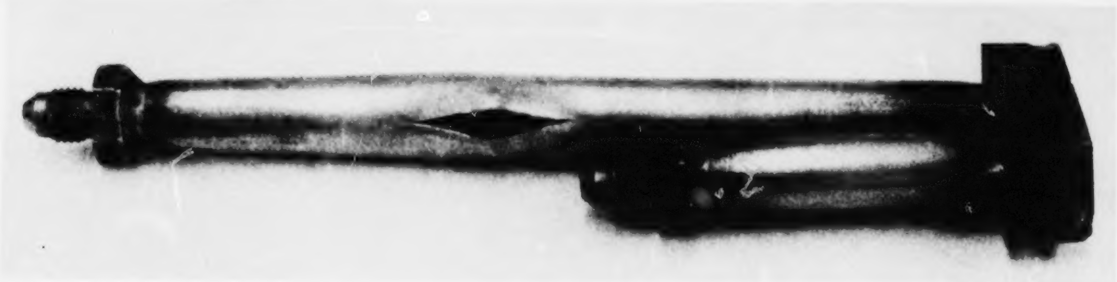

FIGURE 63. SPECIAL BOX CONNECTION AFTER BURST PRESSURE TEST

Figure 64 schematically identifies the flow arrangement and row numbering system. Inlet water enters the first row (row number 1) on the exhaust gas side of the flow system at the center of the coil. It then flows radially outward along the single tube spiral coil that forms row 1 for a total length of approximately 50 feet. Tubes within each row and the next row are staggered with 1.25 times outside tube diameter axial and radial pitch. Two of the preheater rows are staggered with respect to each other in Figure 65. Special welded box fittings (Figs. 61 and 63) connect each row to the next row on both the outside and inside of each coil to form a compact preheater section consisting of rows 1 through 5 with a total stack height of 3.125 inches and a total monotube length of approximately 250 feet. A monotube flow arrangement was acceptable because water velocities can be maintained low in the preheater and thus a reasonable pressure drop (35 psi) was the maximum required. A counter flow arrangement has been utilized in the first five rows of tubing.

A more complex arrangement was necessary in the remaining five rows. To ensure against potential burnout and hotspots in the superheater, the counter flow arrangement was modified to place the two vaporizer rows 10 and 9 immediately adjacent to the combustor. Additionally the need for large surface area with compact tubing arrangement dictated that small diameter tubes be maintained in the vaporizer and superheater sections. As a result, water side velocities were high and a parallel flow arrangement became necessary (a total pressure drop of 100 psi was used for rows 6 through 10). Each row 6 through 10 consists of six parallel flow passages connected in a manner to form a single flat spiral. Construction of double rows 6-7 and 9-10 are identical. Each row consists of six flat spiral coils connected at the center to the next row by means of a special welded box fitting (Fig. 62 views the downstream side of rows 9 and 10). A manifold in the exhaust duct distributes water from the last row of the preheater to six feed lines connected to the six coils forming row 10. Water flows radially inward and connects to the inside of row 9 giving a parallel flow arrangement in the two vaporizer coils. From the outlets of row 9 six 0.25 inch diameter lines connect to six adjustable restrictor valves used to balance flow in each of the flow paths (flow paths are not interconnected except for final outlet of superheater).

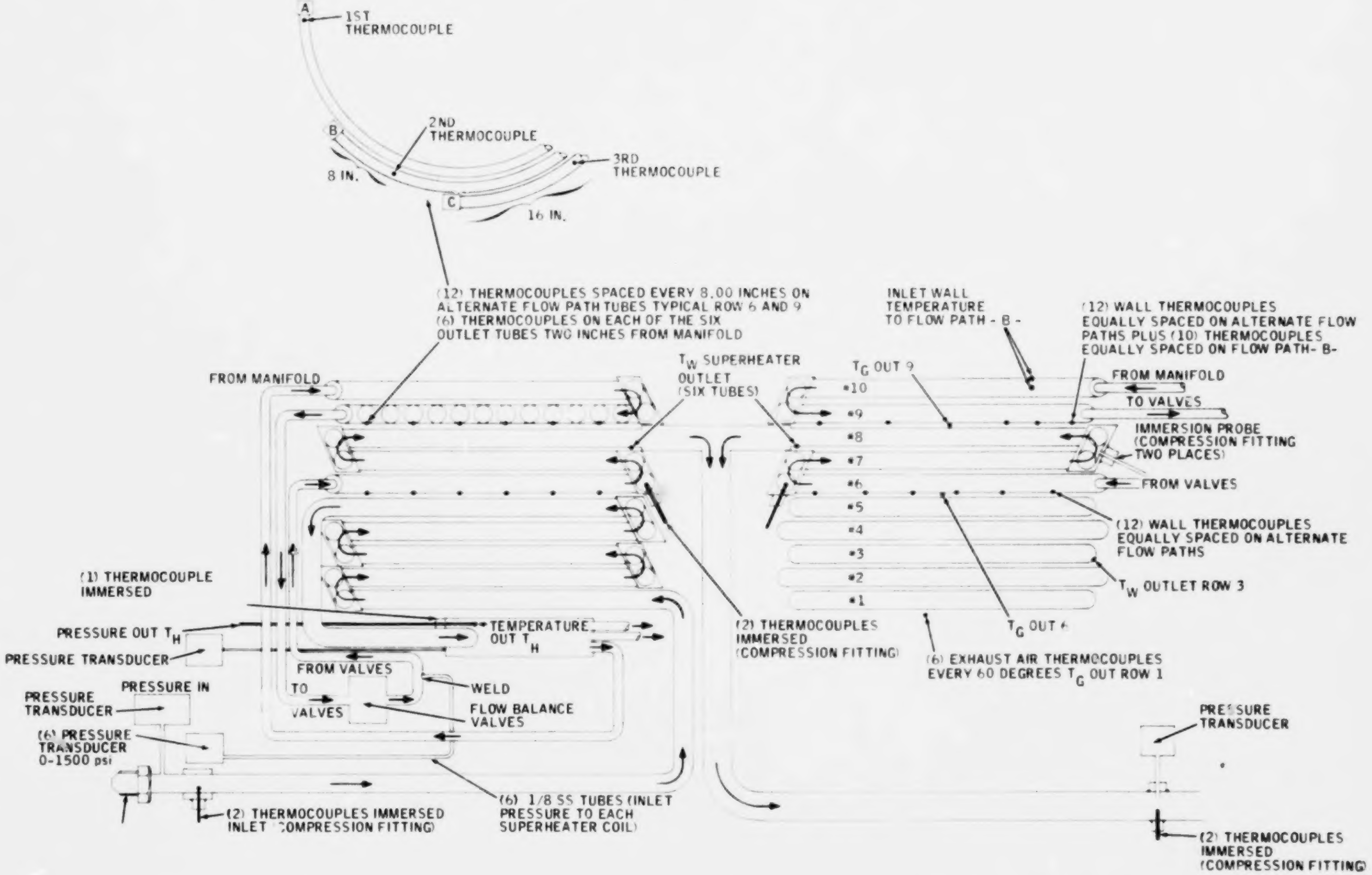
A
1ST THERMOCOUPLE
B
2ND THERMOCOUPLE
3RD THERMOCOUPLE
8 IN.
C
16 IN.
(12) THERMOCOUPLES SPACED EVERY 8.00 INCHES ON ALTERNATE FLOW PATH TUBES TYPICAL ROW 6 AND 9 (6) THERMOCOUPLES ON EACH OF THE SIX OUTLET TUBES TWO INCHES FROM MANIFOLD
INLET WALL TEMPERATURE TO FLOW PATH - B -
(12) WALL THERMOCOUPLES EQUALLY SPACED ON ALTERNATE FLOW PATHS PLUS (10) THERMOCOUPLES EQUALLY SPACED ON FLOW PATH- B-
FROM MANIFOLD
T_W SUPERHEATER OUTLET (SIX TUBES)
T_G OUT 9
#10
#9
#8
#7
#6
#5
#4
#3
#2
#1
FROM MANIFOLD
TO VALVES
IMMERSION PROBE (COMPRESSION FITTING TWO PLACES)
FROM VALVES
(12) WALL THERMOCOUPLES EQUALLY SPACED ON ALTERNATE FLOW PATHS
T_W OUTLET ROW 3
(1) THERMOCOUPLE IMMERSED
PRESSURE OUT T_H
PRESSURE TRANSDUCER
TEMPERATURE OUT T_H
(2) THERMOCOUPLES IMMERSED (COMPRESSION FITTING)
T_G OUT 6
(6) EXHAUST AIR THERMOCOUPLES EVERY 60 DEGREES T_G OUT ROW 1
FROM VALVES
PRESSURE IN
PRESSURE TRANSDUCER
TO VALVES
WELD
FLOW BALANCE VALVES
(6) PRESSURE TRANSDUCER 0-1500 psi
PRESSURE TRANSDUCER
(2) THERMOCOUPLES IMMERSED INLET COMPRESSION FITTING)
(6) 1/8 SS TUBES (INLET PRESSURE TO EACH SUPERHEATER COIL)
(2) THERMOCOUPLES IMMERSED (COMPRESSION FITTING)

FIGURE 64. VAPOR GENERATOR FLOW AND INSTRUMENTATION

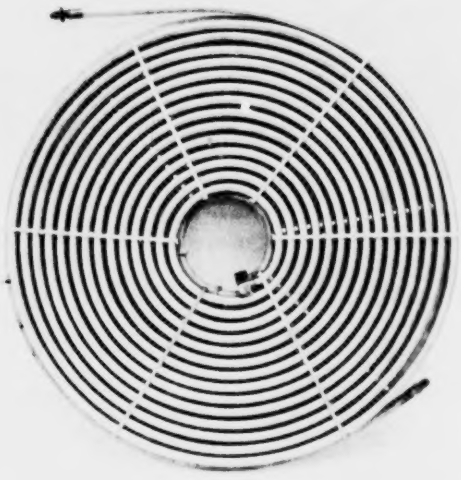

FIGURE 65. ASSEMBLY OF TWO PREHEATER COILS WITH SPECIAL CONNECTOR WELDED AT INSIDE OF COILS

From the restrictor valves a 0.25 inch tube connects the flow into the first row of the superheater (row 6). Flow in this row is again inward and back-outward through row 7 where special welded connectors direct the flow into row 8 where a central collection manifold finally connects each of the six flow paths to a single 0.75 inch diameter outlet tube (Figs. 66 and 61).

A proof pressure of 3000 psi was applied for 20 minutes as a leak check prior to installation in the test cell. Weight of the assembled vapor generator is 104 pounds including instrumentation and restrictor valves.

Instrumentation was installed to monitor steam generator performance; the most important and useful measurements are listed below:

- Input and Output Conditions

  Two immersed thermocouples, closed Inconel sheath, 0.06 inch, type K thermocouples were located at the inlet and outlet of the vapor generator. Two were used for redundancy for these critical parameters. A pressure tap is also located at the inlet and outlet.

- Outlet Temperature in Each of the Six Parallel Superheater Flow Paths

  Six surface thermocouples are installed two inches from the outlet of each tube in the superheater row 8 (Fig. 66). These

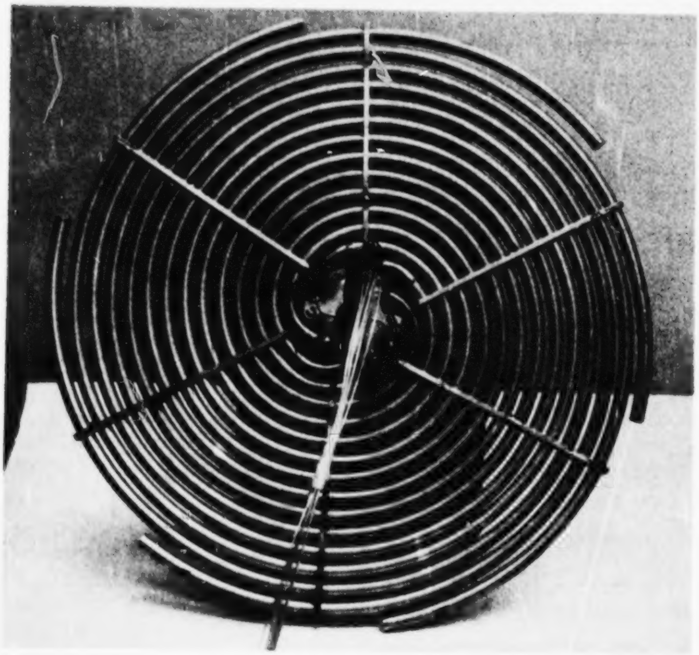

FIGURE 66. SUPERHEATER OUTLET ROW SHOWING THE SIX THERMOCOUPLES

were used to monitor outlet temperature in each flow path for stability.

- Superheater Thermocouples

  Four immersion type thermocouples are located in the superheater. Two are at the 33 percent and the other two at the 66 percent point along the flow path.

- Water Flow Rate

  A high response turbine flow meter with direct digital readout in pph installed in the inlet line of the vapor generator was used to measure water flow rates.

6.3 PERFORMANCE TESTS

Steam generator performance, emissions and control system tests were all performed with the same basic test loop. Operation of the test loop is shown by the flow schematic (Fig. 67). Untreated city water in the test cell supply line is passed through four deionization bottles.

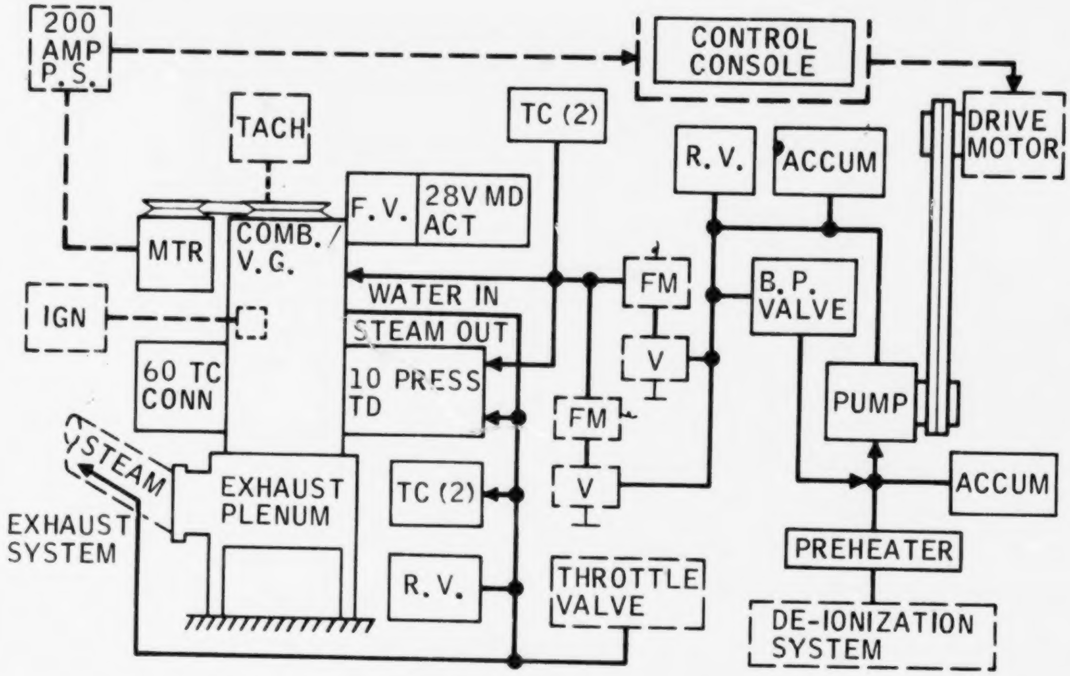
200 AMP P.S.
CONTROL CONSOLE
DRIVE MOTOR
TACH
TC (2)
R.V.
ACCUM
F.V.
28V MD ACT
MTR
COMB./V.G.
WATER IN
STEAM OUT
FM
B.P. VALVE
IGN
V
60 TC CONN
10 PRESS TD
FM
PUMP
STEAM
EXHAUST PLENUM
TC (2)
V
ACCUM
EXHAUST SYSTEM
PREHEATER
R.V.
THROTTLE VALVE
DE-IONIZATION SYSTEM

FIGURE 67. TEST CELL FLOW SCHEMATIC

After deionization the water goes to a preheater that discharges it at a regulated temperature between 180 to 190°F. An insulated suction line is connected to the inlet of a Union DX-10 triplex pump. A variable diameter pulley belt drive from an electric motor allows remote control of the pumps speed. Prior to the installation of the automatic electronic control system pumps, speed was used to adjust the water flow control steam outlet temperature. Accumulators on the inlet and outlet reduce pressure and flow pulsations from the piston pump to acceptable levels for accurate control. A relief valve protects the pressure side of the pump circuit from overpressure. Some of the outlet flow from the pump is bypassed by a valve (B.P. valve of Fig. 67) to the inlet to the pump. A bypass was necessary at this point to allow a match between the pump speed characteristics and the speed range of the variable speed drive system. Water inlet flow is measured by turbine flow meters (FM) immediately ahead of the inlet to the steam generator. Two turbine meters are necessary to cover the flow range of interest. Both are checked periodically by means of a weight of flow versus time to ensure their accuracy. Under steady state conditions the inlet water is identical to the steam rate. Difficulty with exact measurements of steam flow directly have resulted in the use of water inlet flow measurement for the steam rate. The only difficulty with this approach has been the extremely long times at low flows required to obtain true steady state values. At some control conditions, a true steady state condition did not ever appear to be established. Generally, when the rate of change of temperature for a specific flow was only 1 or 2°F per minute the condition was considered steady state.

The blocks labeled COMB/V.G. schematically represents the test unit. Inlet water temperature are measured in the 0.5 inch diameter feed line downstream of the reverse flow check valve. Exhaust gases, after passing through the unit, discharge into an exhaust plenum and then into a 15 inch duct for venting into the test cell's exhaust stack. Steam rate is controlled by the setting of a throttle valve. Between the steam generator and throttle valve a safety relief valve (R.V.) and thermocouples (TC) are installed. From the throttle valve the superheated steam is vented into the test cells exhaust system.

All functions of the system were regulated from the test cells control panel (Fig. 68). Fuel flow, water flow, and air flow can each be independently regulated remotely from the control panel. Steam flows were established at the control panel by manually adjusting the setting of the throttle valve. Ignitor and fuel solenoid controls are also manually controlled from the face of the panel. After installation of the steam generators control system, the position of the air valve could be controlled automatically or manually from the control room. Water rate was also capable of being manually or automatically regulated by either automatic or manual remote positioning of the input to the differential pressure regulator (see Section 8). Fan speed was adjustable by changing the voltage to the fan drive motor . Important instrumentation

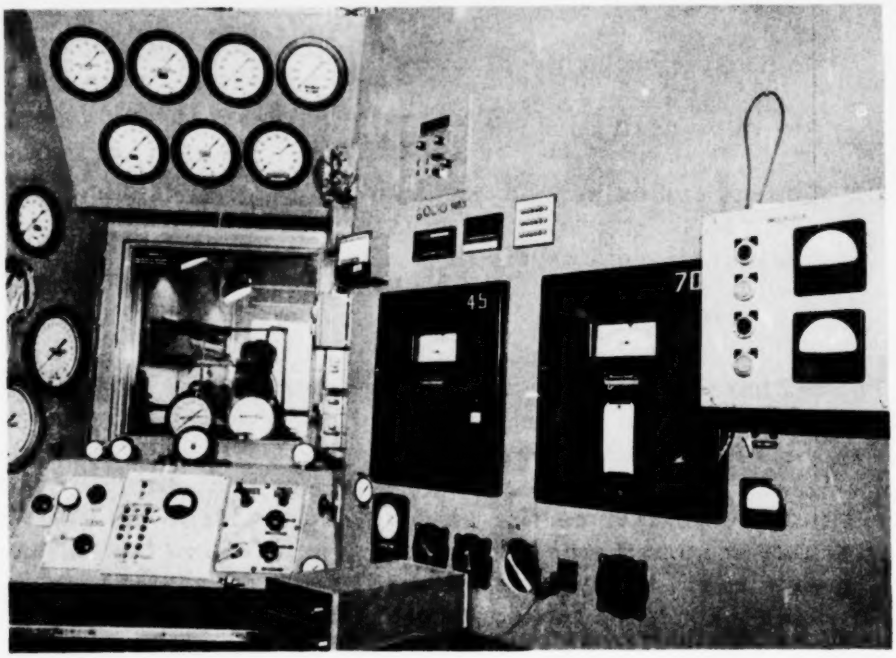

FIGURE 68. TEST CELL STEAM GENERATOR CONTROL PANEL

and control functions in the control room included:

- Speed of water feed pump
- Fuel pressure and flow
- Superheater outlet temperature
- Six parallel flow paths outlet temperatures
- Inlet and outlet pressure of steam generator
- Water flow
- Fan speed
- Fan discharge pressure
- Primary and secondary air pressures
- Combustor pressure
- Temperature of inlet air to fan
- Combustor outlet temperature
- Air valve position
- Voltage and current to fan motor
- Pressure regulator position

6.3.1 Mechanical Integrity

The six parallel flow passage steam generator has been operated more than 500 hours in emissions, controls and performance development tests. In all these tests the unit was operated at near rated temperature and pressure. Two leaks developed after approximately 70 hours of preliminary tests. Both leaks were in the vaporizer section at weld joints made to the tubes accidently by a weld arc-over from a tube spacer. Figure 65 shows the six tube spacers installed in each row. Each end of the tube spacer is welded together to hold the spacer closely about the tubes. In both leakage failures a small crack formed about the weld nugget between the tube spacer and the tube wall. It had been anticipated that the thermal strain would cause this type of problem and the design required that the tubes be free to move slightly within each spacer. Errors in welding proved the importance of not restricting the tubes with a limited number of highly stressed weld joints. After repair, no further leaks developed during more than 400 hours of testing. The only physical damage noted during the final inspection of the unit was distortion and failure of several of the spacers and flow blockage plate at the center (Fig. 69 and 70). These failures were due to insufficient depth to the first spacer row and use of a weld joint between the center plate and the six spacers. A slip joint and an increase in depth of 0.25 inch on the second high efficiency unit has corrected this problem. The deposits shown on the center sections of the coils were rust color and apparently were residual elements in the fuel and air. Table VI shows the results of a spectrographic analysis of the deposits on the first row of tubes. Carbon deposits are seen on the outside of the coils and were thought to be the result of ignition failures.

6.3.2 Flow Stability

It has been demonstrated that it is possible to operate a six parallel flow steam generator at water flows up to rated conditions without serious water flow maldistributions in the superheater tubes, and without the consequent overheating of the tubes. Successful operation has been achieved without any flow restrictors in the water flow passages. Balanced flow seems to depend on maintaining near rated outlet pressure at all flows, and

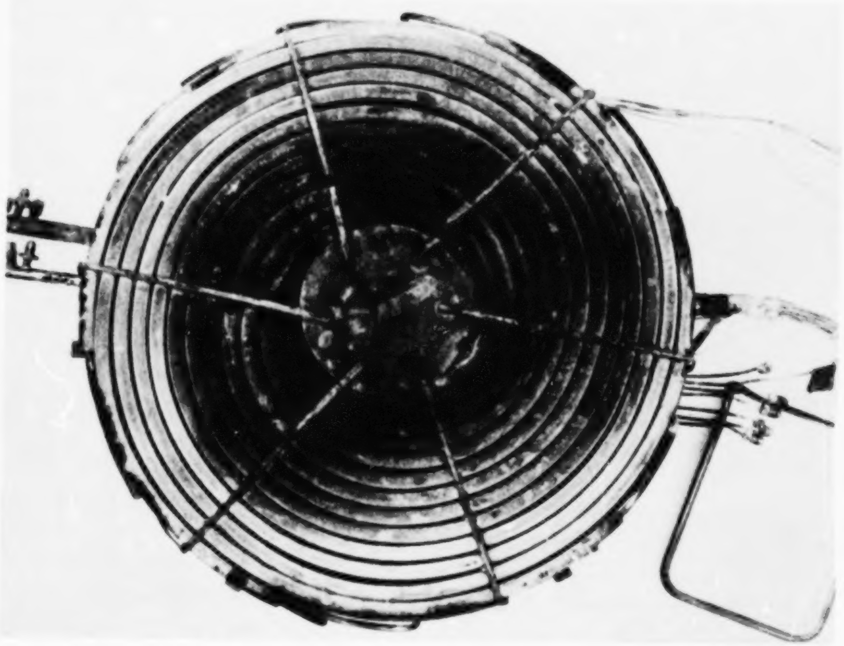

FIGURE 69. STEAM GENERATOR AFTER 500 HOURS OF EMISSION AND CONTROL SYSTEM TESTS

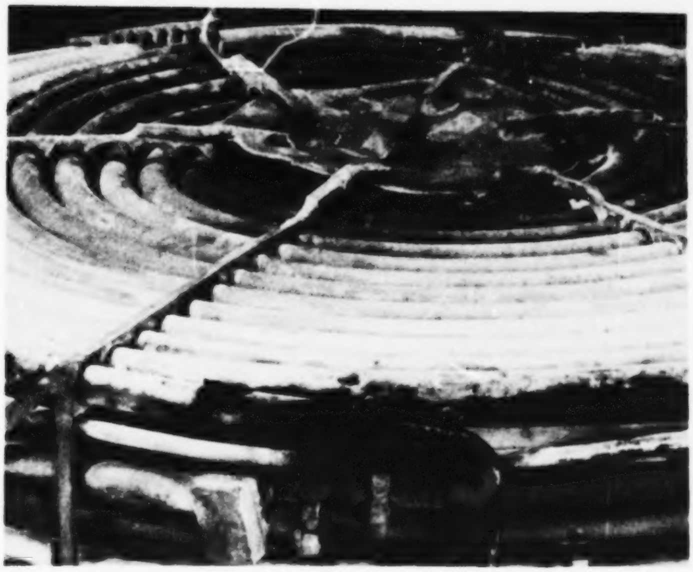

FIGURE 70. VAPORIZER SPACERS AFTER 500 HOURS OF OPERATION

TABLE VI

RESIDUE REMOVED FROM FIRST ROW OF STEAM GENERATOR
(Chemical Analysis by X-ray Fluorescent Spectrography)

Elements Detected (Approximate %)			
Al	>0.20	Ni	>0.15
Ca	>1.00	P	>0.50
Cd	>0.08	Pb	>1.00
Cr	>0.25	S	>6.00
Cu	>0.25	Si	>11.00
Fe	>0.75	Zn	>0.30
K	>0.03		

on adjusting water flow so that the preheater outlet liquid is within a few degrees of the saturation temperature. It appears to be impossible to achieve stable operation of the unit unless these two conditions are simultaneously met.

The effect of preheater outlet temperature is illustrated quite clearly in the traces of Figure 71. At the left hand side of the trace, the preheater outlet temperature is only 410°F, about 75°F below the saturation temperature at the outlet pressure of 610 psi. The six traces shown represent steam temperature at superheater outlet for each of the six parallel flow superheater tubes. It can be seen that two of the tubes have a much lower temperature than the other four, and that the temperature in these two tubes undergoes a sustained oscillation in temperature. It is believed that there is considerable liquid phase flow in the tubes shown by these temperature oscillations, even near the superheater outlet. This is also shown by the mixed mean superheater outlet temperature, which was quite low, in spite of the high wall temperature, which fluctuated between 480 and 620°F. It was found that with oscillations such as those shown on the left hand side of the trace, it was impossible to achieve anything like the rated superheater outlet temperature of 1000°F without producing excessive wall temperatures in the superheater tubes.

At the right hand side of the trace, one sees the effect of an increase in the preheater outlet temperature. Preheater temperature is now 455°F, only about 45°F below saturation temperature. As preheater outlet temperature is increased, the wall temperature oscillations disappear, and the wall temperatures of all six superheater tubes become nearly equal. Superheater temperature was steady, without the 40°F oscillation observed at the left hand side of the trace.

An explanation of the importance of the preheater outlet temperature and other parallel flow stability criteria has been discussed in the literature A brief review helps explain the performance of the unit. There are several types of two phase flow instability which must be considered and, in general avoided, if the performance of the steam generator is to be considered satisfactory. They are to be avoided for two reasons. First, they can cause disastrous overheating of the tube walls, even though steady state calculations indicate that wall temperatures should be satisfactory. Second, they can produce oscillations in steam generator outlet temperature and pressure even though there has been no change in steam demand, air flow, or fuel flow. This tends to complicate the controls problem. Flow instabilities can be classified according to whether they are periodic or aperiodic.

A periodic instability results when the flow conditions are such that an increase in flow produces a reduction in pressure drop. For this type of instability, a high loss factor for the flow tends to be stabilizing, as does a

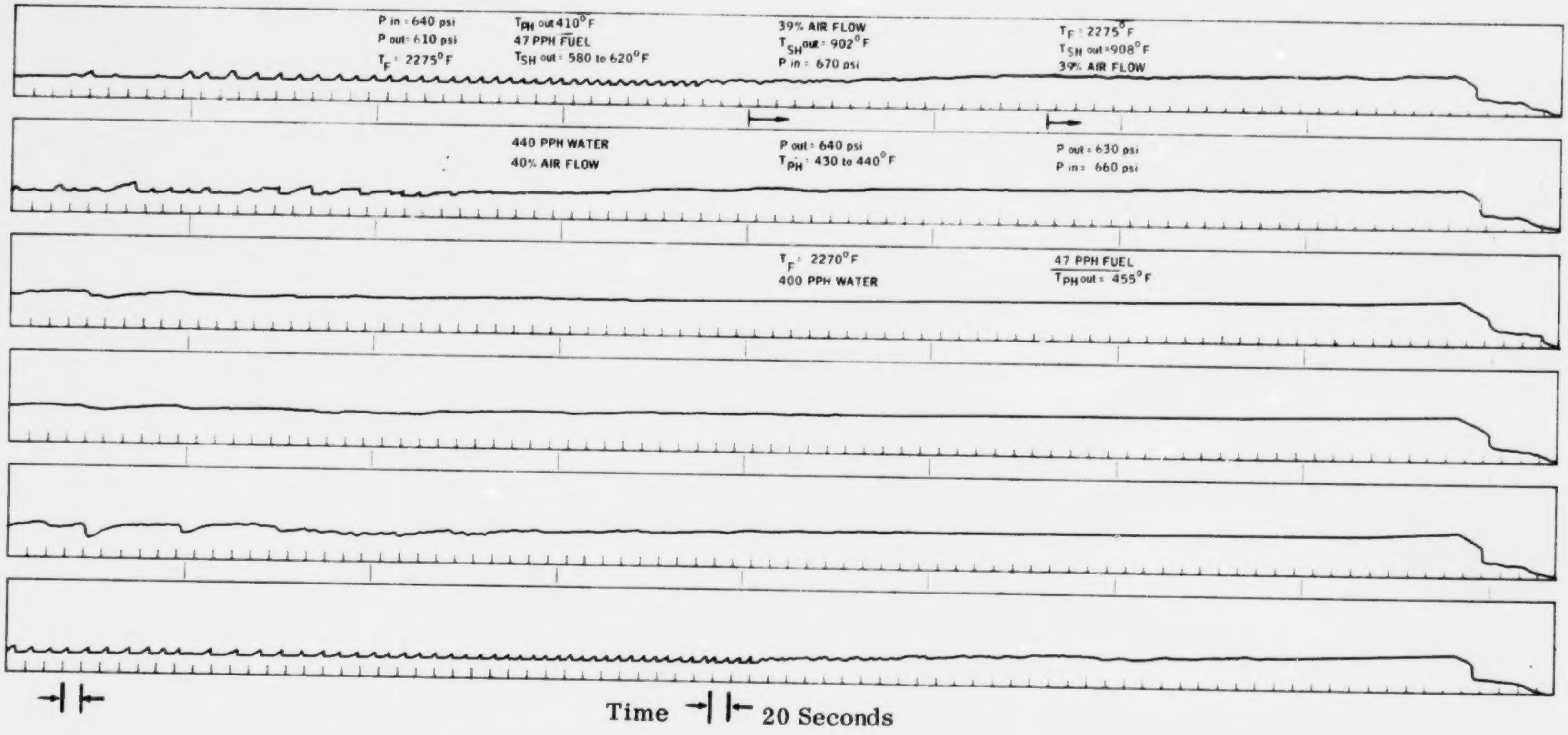

FIGURE 71. SUPERHEATER OUTLET TUBE WALL TEMPERATURE (SIX FLOW PATHS)

small difference in specific volume between the liquid and the vapor phases. Inlet subcooling has a definite destabilizing effect. A good discussion of these tendencies is given in chapter 7 of Tong (Ref. 2). It should be mentioned that any inflection point in the curve of the pressure drop versus flow is likely to cause difficulties in parallel flow units. If the stability is marginal, then large changes in flow rate can result from small differences between the tubes in heating rate or loss factor. This can cause serious flow maldistributions with its accompanying overheating of some of the tubes, as they become starved for water.

Periodic flow instabilities are usually the result of coupling between thermal and hydrodynamic forces. They tend to be more troublesome in parallel flow units than they are in monotube units. In a parallel flow unit, oscillations can occur in one tube without significantly affecting the others. When this is the case, other parts of the loop, such as accumulators and throttle, have less chance to damp the oscillations. Periodic instabilities can occur in systems which are stable against aperiodic instabilities. They can have highly undesirable interactions with the boiler automatic controls, if this possibility is not carefully eliminated in the design. In general, those factors which increase the aperiodic stability also increase the periodic stability. Some other considerations are: (1) a high heat input aggravates instability; and (2) an orifice at the inlet strongly increases the stability, while increased resistance at the outlet is strongly destabilizing. Periodic flow instabilities can sometimes be caused by a shifting back and forth between different two-phase flow regimes, for example, slug flow and annular flow.

While the analysis of flow instabilities is quite complicated and, at best, only approximate, it is nevertheless fairly clear what the designer must do to eliminate the danger of two phase flow instabilities. The approach to the solution of this problem in the high efficiency unit discussed in the next section is outlined below:

1. The preheater is designed so as to give a very slight amount of vaporization before the flow enters the vaporizer. The inlet subcooling for the vaporizer is therefore zero. Under such circumstances, it is theoretically impossible for aperiodic instabilities to exist, because the inlet subcooling is negative. Collier and Pulling (Ref. 3) say that their experiments indicate that with two phase flow at the inlet, periodic instabilities are unlikely to occur.

2. There is a restriction at the inlet to the vaporizer section. This has a further stabilizing effect.

3. The number of parallel passages in the vaporizer and superheater sections will be kept as low as possible, so that other parts of the loop will have the maximum possible damping effect.

4. The flow will be mixed in manifolds at both the inlet and exit of the vaporizer tubes. This will minimize the effect that flow instabilities in any one section have on the other sections. It also ensures a very stable flow in the superheater section, where tube wall temperatures are expected to be highest.

5. Mass flow rates are chosen so that the transition from one type of two phase flow to another is not likely to take place over a large length of tube all at the same time.

6. The final design will be analyzed by the method presented by Quandt (Ref. 4) in order to determine the degree of periodic flow stability, and the frequencies involved. Such information will be useful in the design of the controls.

Experience with the parallel flow steam generator tends to confirm the results which would be expected from a study of the literature. Inlet subcooling has been seen to have a definite destabilizing effect. The flow is less stable at high heat inputs than it is at low heat inputs. Increasing the outlet pressure, hence reducing the volume change due to vaporization, has tended to stabilize the flow. Since test results confirm results predicted in the literature, this literature is believed to be a reliable basis for design.

Steady state performance data have been obtained at fuel valve settings ranging from 10 to 98 percent. The results are shown in Figure 72. At full load, the performance is very close to theoretical predictions based on 2500°F flame temperature and zero heat loss to the surroundings. The rise in efficiency with decreasing load is much less than theory predicts, however. There is considerable scatter in the data at low load.

It is believed that the low efficiency at low load is primarily due to the fact that it is necessary to lean the combustor at low fuel flows to reduce NO_x causing a drop in flame temperature as the load is decreased. While at full load the flame temperature based on CO_2 measurements is in the range 2500-2700°F, at 20 percent air valve position it drops down to 1800-2000°F. The lower temperature would cause a noticeable loss in boiler efficiency.

The scatter in the low load data points is thought to be primarily due to the fact that backlash in the fuel-air valve linkage used with the six parallel flow passage unit occasionally cause rather large differences in flame temperature corresponding to the same setting. A contributing factor to the scatter may be the difficulty of obtaining steady state operation at low loads.

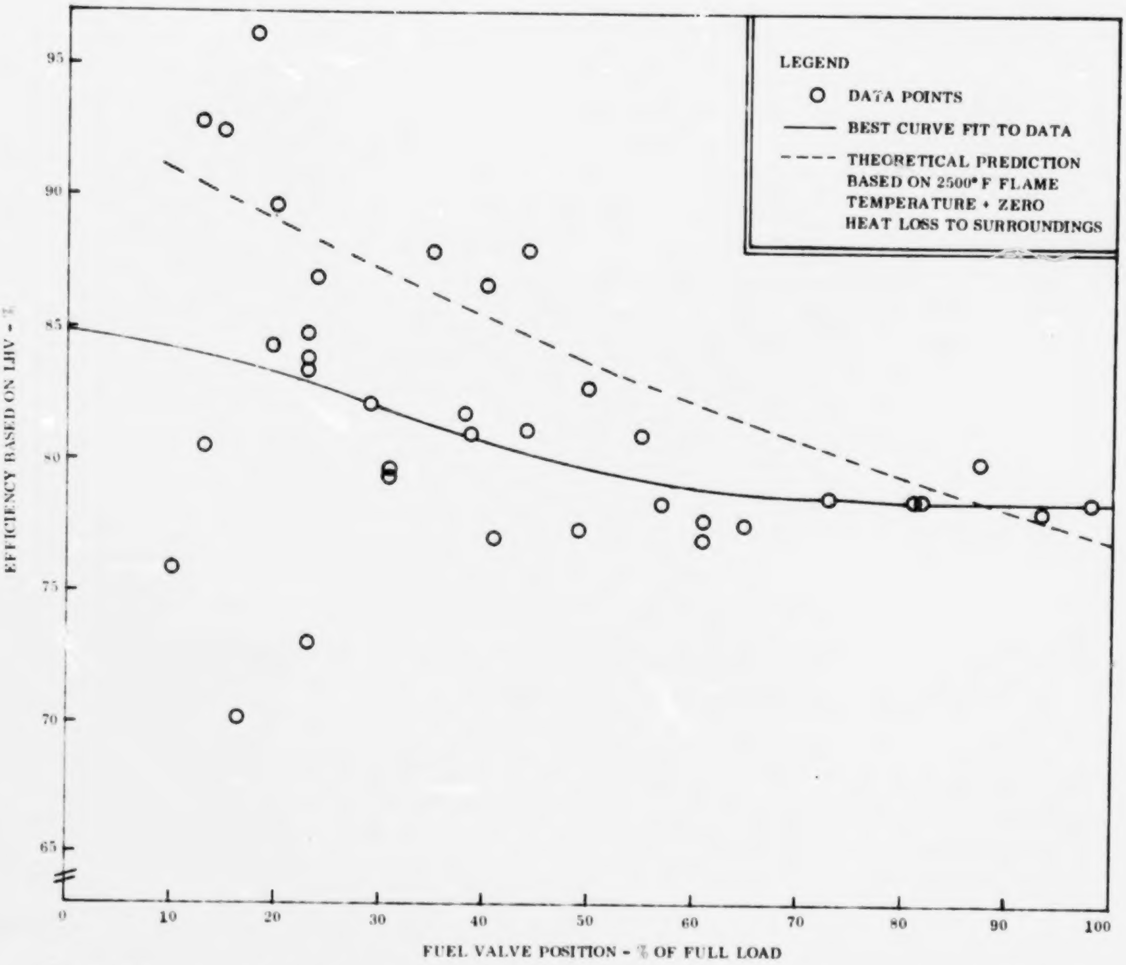

FIGURE 72. TEST BED VAPORIZER STEADY STATE PERFORMANCE

A change in superheater temperature of only 2°F per minute can apparently mean that the unit is still well away from steady state at low loads. A continual high frequency fluxuation in the water inlet flow recorded by the turbine flowmeter used to measure water rate is also thought to be a possible factor contributing to the scatter of the data (see Section 8).

The unit seems to have only limited hydrodynamic stability at high loads. Even at superheater temperatures in excess of 1000°F, a definite sustained oscillation in superheater temperature can frequently be observed at loads in excess of 80 percent of the design load. The poor stability also seems to be reflected in worsening flow distribution in the superheater tubes as the load is increased. This is shown in the charts of Figure 73. At the high load point, the difference between hottest and coldest tube is slightly

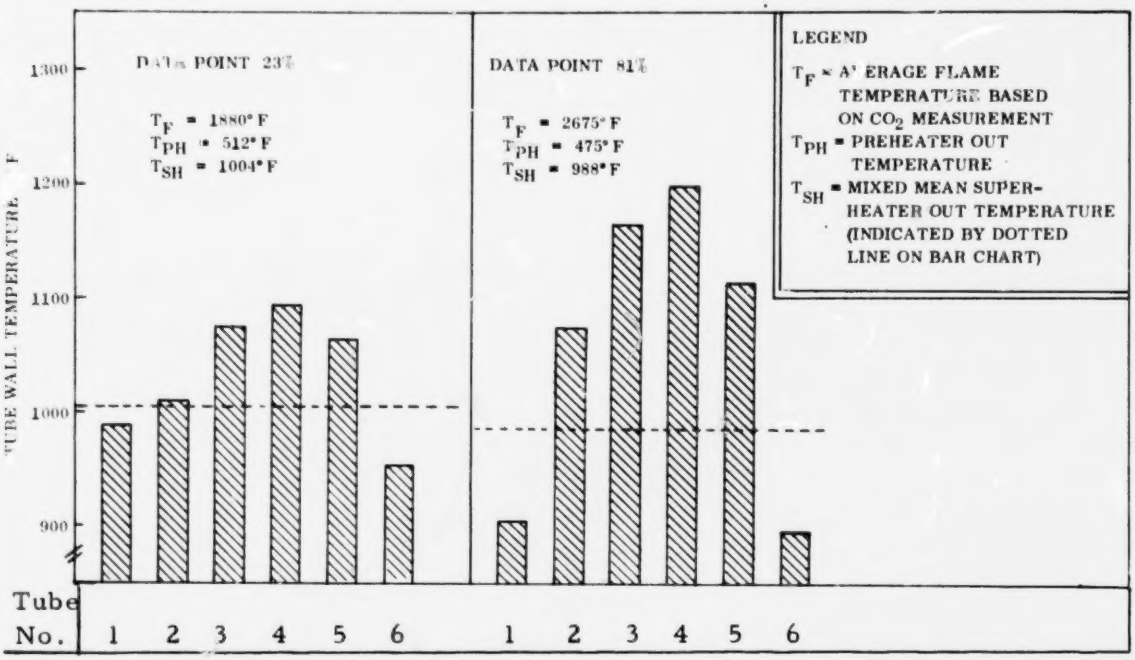

FIGURE 73. TEST BED VAPORIZER. TUBE WALL TEMPERATURE AT SUPERHEATER OUTLET

over twice what it is at the low load point. The difference between hottest tube wall temperature and mixed mean superheater temperature is also slightly over twice as great at high loads. Although these stability characteristics were present, hundreds of hours of emission tests and closed loop control system tests do indicate that a practical parallel flow system can be achieved. The main problem is controls. Steady state and most transient controls do not present much of a problem. It appears from the results that only an initial startup stability is of major concern. Although not worked out in demonstration tests, it does appear as though a controlled schedule in the rise of pressure and temperature would allow satisfactory automatic startup of a parallel flow unit. Additional control measurements would probably be required to give adequate reliability. By measuring each of the parallel flow outlet temperatures and restarting if chugging occurred during transient operation, a high degree of reliability against burnout failures would be ensured. Although it turned out to be unnecessary with the automatic control system, the six parallel flow passages temperatures were continuously monitored to prevent damage to the unit during all test cell operations.

7

HIGH EFFICIENCY SINGLE FLOW PATH STEAM GENERATOR

A second steam generator incorporating fins for high efficiency and light weight was designed and tested. It also incorporated essentially a monotube flow arrangement (only two parallel flow passages in the dryer) for improved stability. To achieve high efficiency, 'low weight, low water holdup and low gas side pressure drop, small diameter finned tubing was used in the design. The dominant thermal resistance is on the gas side. Fins allow this resistance to be reduced by adding heat transfer area which is not highly stressed, as are the tube walls. Since the fins are unstressed, they can be made of very light gage metal thus saving weight. In the preheater, the fins account for only 61.9 percent of the total weight, while providing 85.9 percent of the total heat transfer area. Because of the small hydraulic diameters attainable with fins, heat transfer coefficients are much higher, providing a further saving in weight. Heat transfer coefficients in the finned tube parts of the exchanger are about half again as high as the bare tube parts of the exchanger.

Gas side pressure drop is low because fins present a surface with a high ratio of drag to form factor. Friction drag allows a much higher heat transfer per unit pressure drop than does form drag, since the viscous dissipation in the turbulent wake does not contribute to the heat transfer process.

Finned tubes help reduce water hold up, because they allow a large gas side heat transfer surface for a given tube length with only a small volume of tube.

The effect of changing tube diameter on water hold up and matrix weight is derived in Appendix II. Both hold up and matrix weight increase slightly more rapidly than in direct proportion to the tube diameter. For finned tubes, fin weight increases in proportion to the square of tube diameter.

The basic constraints used for the unit were to have an efficiency of at least 85 percent LHV at full load of 1200 pounds per hour of steam and that it fit in the same combustor used for the first steam generator (21.5 inch steam generator OD).

Table VII shows the flow arrangement and fluid conditions of the steam generator. In general, the overall flow arrangement that proved out well on the test bed unit was incorporated in this improved steam generator. Placement of the vaporizer tubes upstream of the dryer and superheater gives protection against burnout failures and high tube wall temperatures that would result in a pure counterflow unit. Table VIII is a summary of the units performance and construction features.

TABLE VII

FLUID CONDITIONS

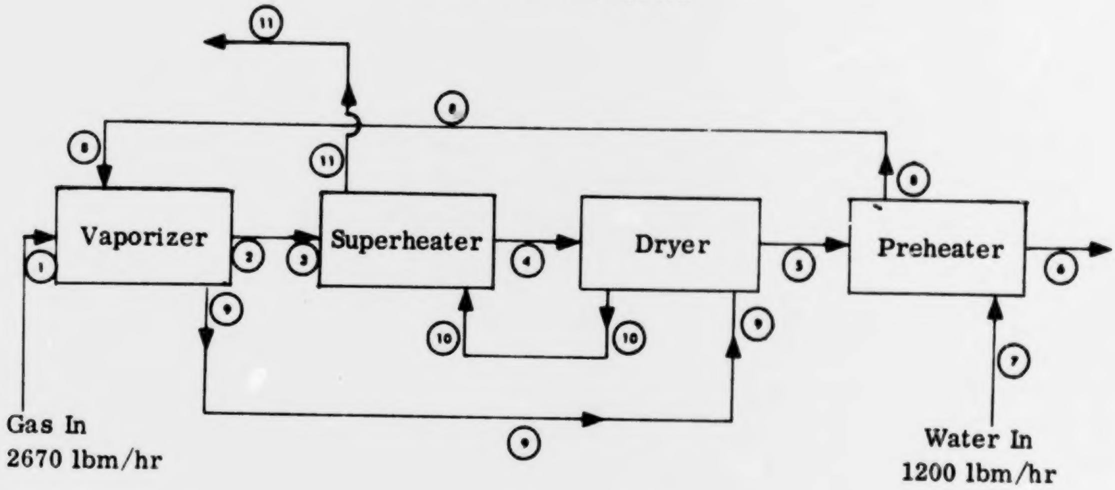

Station	Temperature (° F)	Pressure
1	2500	Atmospheric
2	2017	↓
3	1985	
4	1714	
5	1090	
6	306	Atmospheric
7	160	1194 psia
8	561 (3.9% quality)	1148 psia
9	559 (57.3% quality)	1126 psia
10	696	1064 psia
11	999	1000 psia

A comprehensive summary of the monotube steam generator design including sizing, heat balances, part load-performance, dryer heat transfer, burnout, air side pressure drop, and parallel flow-passage stability is contained in Appendix III.

TABLE VIII

SUMMARY OF PERFORMANCE PARAMETERS

Maximum Steam Rate	1200 lbm/hr
Maximum Heat Transfer Rate	1.651×10^6 BTU/hr
Boiler Efficiency	
(API 56 Gasoline, S.G. = 0.755 HHV = 20,160 BTU/lbm; LHV = 18,840 BTU/lbm)	
100% load	84.4% (HHV); 90.1% (LHV)
5% load	90.0% (HHV); 96.3% (LHV)
Gas Exit Temperature	
100% load	306 F
5% load	172 F
Gas Inlet Temperature	2500 F
Gas Side Pressure Drop	1.318 in. H_2O at 100% load
Feedwater Inlet Pressure	1194 psia
Steam Outlet Pressure	1000 psia
Maximum Fin Temperature	999 F
Maximum Tube Wall Temperature	1031 F
Total Matrix Metal Weight	66.0 lb
Matrix OD	21.5 in.
Total Matrix Depth	6.65 in.
Water Hold up	6.76 lbm

Construction

Preheater: Three rows of single flow passage flat spiral coils in cross counter flow, 0.375 inch outside diameter, 0.028 inch thick 321 stainless steel tubes with 15 copper fins per inch. Fin outside diameter is 0.625 inch with a thickness of 0.012 inch. Transverse pitch 0.717 inch, axial pitch 0.784 inch.

Dryer: One row of two parallel flow passage flat spiral coils 0.375 inch outside diameter, 0.028 inch thick Hastelloy X tubes with 15, 304 stainless steel fins per inch. Fin outside diameter 0.625 inch with a thickness of 0.012 inch. Transverse pitch 0.717, axial pitch 0.784 inch.

Superheater and Vaporizer: Both are two rows of bare 0.627 inch, 0.042 inch wall thickness 321 stainless steel tubes in single flow passage arrangement. The transverse and axial pitch is 0.9375 inch. Superheater is in cross counter flow and the vaporizer is in cross parallel flow.

7.1 CONSTRUCTION

Flow arrangements, matrix spacing and materials are defined in Tables VII and VIII. All welded construction is used with the exception of the fins. Fins were brazed to tubes after coiling. Figure 74 shows a copper finned preheater coil prior to brazing. Three coils make up the preheater. Flow is cross counter flow with each of the 0.375 tubes being joined in series by special welded connectors. The only parallel passage row in the unit is the dryer located immediately above the preheater. Two coils with twice the transverse pitch (Fig. 75) of the preheater are intermeshed to form a single dryer row with the same transverse pitch as the preheater but with two parallel flow passages. Tube material in the dryer was Hastelloy X. Under normal conditions stainless steel would be adequate but the unit was designed to be failure proof with regards to parallel flow instabilities. Stress temperature characteristics are sufficiently great to allow successful operation with zero flow through one of the two dryer coils. Analysis of stability characteristics indicated a high degree of stability in this area. Tests confirmed the analysis but did show a 60°F difference in the outlet temperature between the separate flow paths.

Outlet water from the preheater bypasses the dryer and superheater and enters the first row of the vaporizer adjacent to the combustor. A vertical tube in the center core (Fig. 76) brings the preheater outlet water up to a special welded connector on the inside end of the top coil. At the outside of the spiral coil a special welded U-connection (Fig. 77) into the second row of the vaporizer section. At the inside core a jumper line brings the outlet from the vaporizer section down past the two superheater rows to the dryer. Flow is divided at this point into the two dryer coils where it flows from the center out to two jumper tubes. These tubes bring the steam down around the outside (see tube at far right of Fig. 76) of the preheater section and across the bottom of the unit and back up to the first row superheater through the center core. In the center core the flow is combined in a manifold and flows through the superheater coils in a single flow path. Steam from the first superheater row is coupled by a "U" connection (Fig. 77) to the final superheater row for discharge through an outlet tube that directs superheated steam down the center core and out across the bottom of the unit.

Immersion thermocouples were installed at the inlet and outlet of each section of the unit. Figure 77 shows the installation of a thermocouple that records temperature on the outlet of the first row vaporizer and one that measures temperature at the outlet of the first superheater row. Two wall temperature probes were installed within 3 to 4 inches of the outlet of the superheater's last row. Both of these units agreed well with the immersed superheater thermocouple, but always indicated slightly higher as was expected.

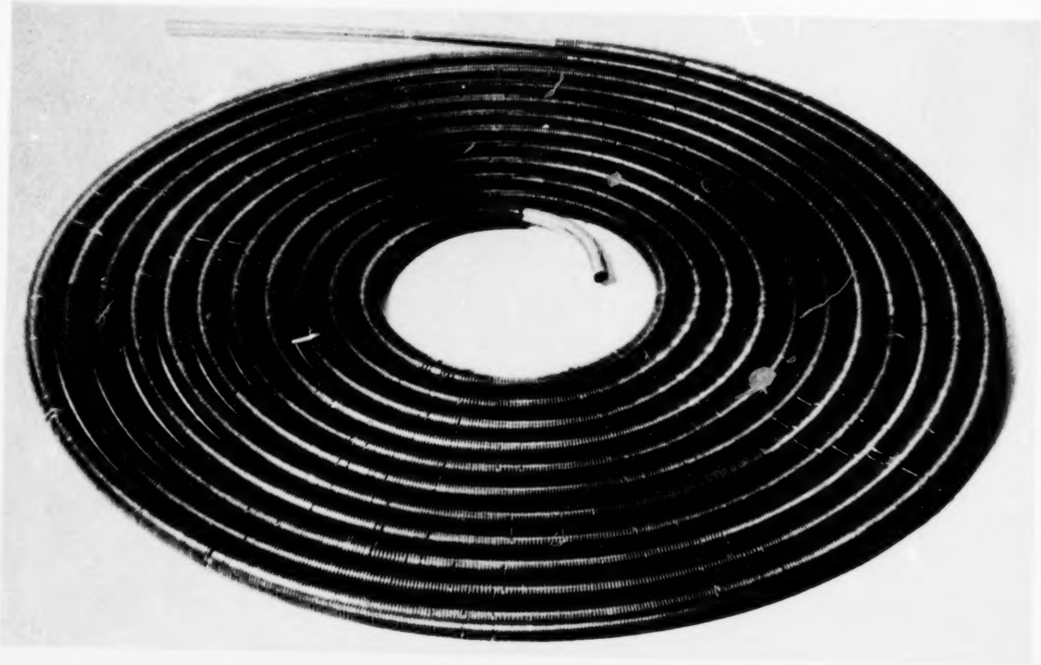

FIGURE 74. PREHEATER COILS WITH COPPER FINS

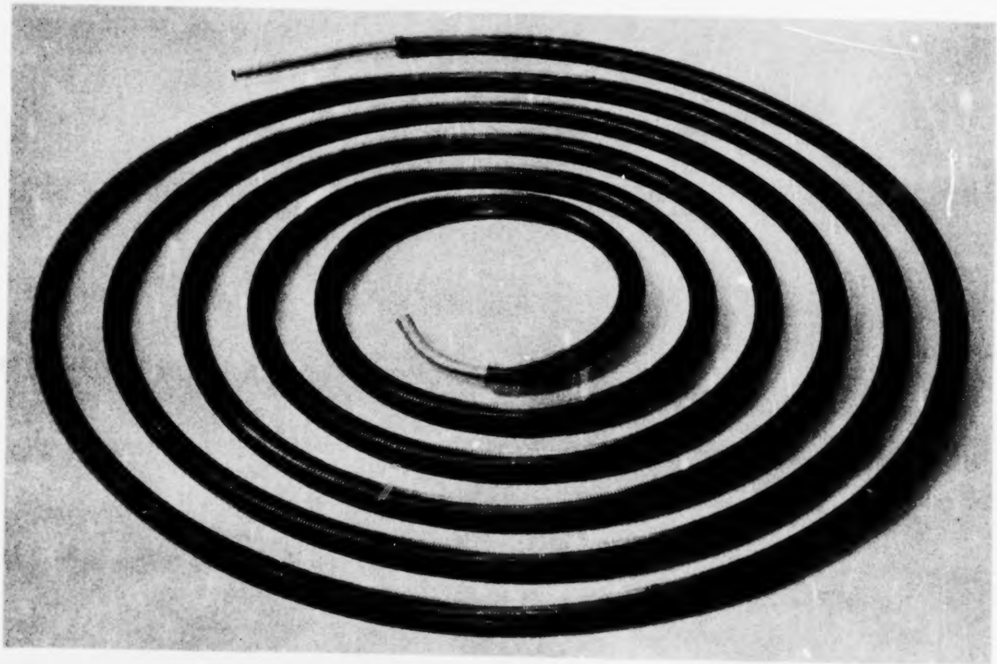

FIGURE 75. ONE OF THE TWO DRYER COILS

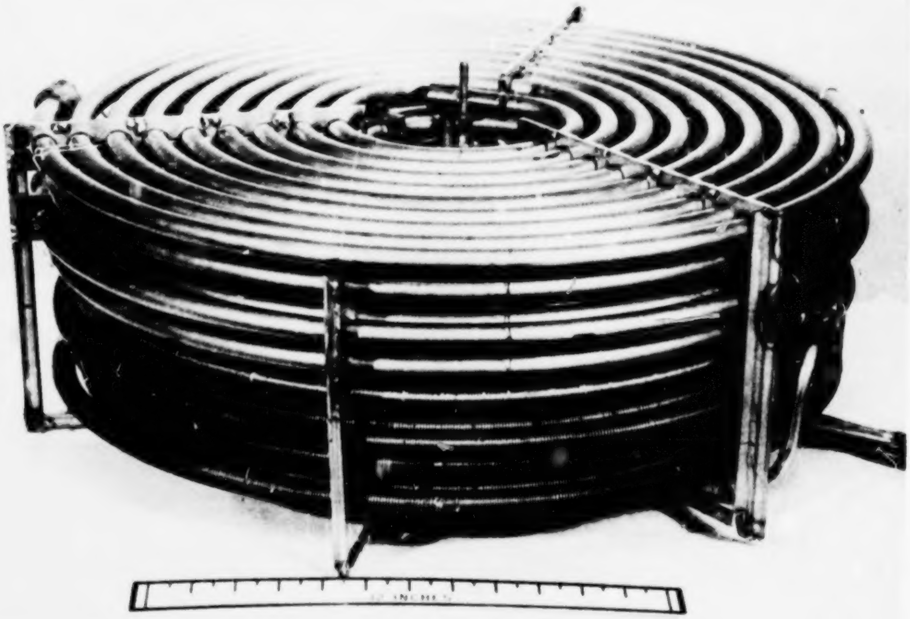

FIGURE 76. ASSEMBLED STEAM GENERATOR

FIGURE 77. STEAM GENERATOR U CONNECTIONS

7.2 STEADY STATE PERFORMANCE

The high efficiency finned tube steam generator has been calibrated for steady state efficiency at fuel flows from 15 to 105 pounds per hour fuel flow, corresponding to steam rates from 240 to 1200 pounds per hour at 1000 psia and 1000°F. The unit was stable with little or no difficulty in holding a particular steady state point. As a consequence, little scatter in the data was observed.

The design goals for this unit are listed below.

- Maximum Steam Rate: 1200 pph @ 1000°F and 1000 psia
- Efficiency (LHV) at full load 85%
- Water Side Pressure drop at full load - 250 psi maximum

The steady state efficiency is shown on the curve of Figure 78. As can be seen, the design goal is slightly exceeded at full load, and well exceeded at fuel flows representative of those encountered during the Federal Driving Cycle.

At the maximum steam flow measured, 1245 pph, the water side pressure drop was 320 psi. This corresponds to a water side pressure drop of 297 psi at a flow of 1200 pph, which is slightly higher than the design goal of 250 psi. It is thought that this increase is due to the fact that the manifolding system in the present unit is slightly more restrictive of the flow than was originally estimated.

Although the unit meets the design goals regarding efficiency, it does not measure up to the efficiency predicted for it by analysis, and gas side pressure drop was also significantly lower than predicted. These three factors; low measured efficiency, high exhaust temperature, and low gas side pressure drop combine to indicate that the poorer than expected performance is due to significant blowby being short circuited around the tube coils, so that not all the combustion gases pass through the coils. It seems quite possible that if the blowby can be stopped, full load efficiency can be brought close to the 90 percent level.

As was predicted by analysis in Appendix III, flow in the parallel passages of the dryer was quite stable. No tendency toward chugging was observed. Flow through the boiler was much more nearly constant at steady state than it was for the original six parallel path unit. The maximum temperature spread between the dryer outlets was 57°F, as compared with 300°F for the six parallel path unit, as reported in Section 6.

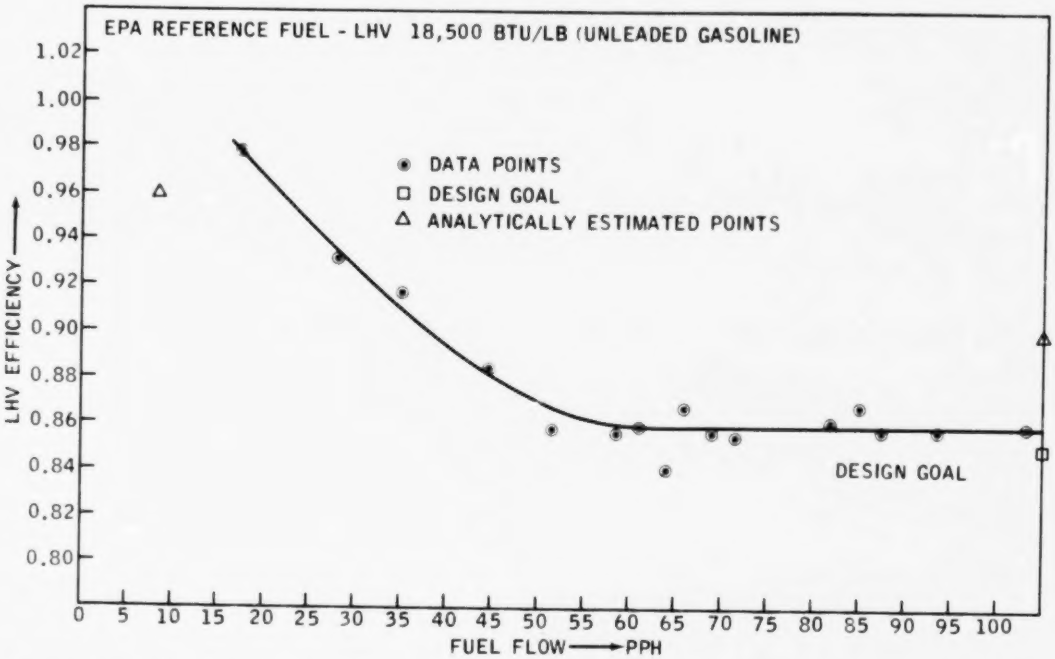

FIGURE 78. HIGH EFFICIENCY FINNED TUBE STEAM GENERATOR STEADY STATE EFFICIENCY MEASUREMENTS

Inspection of the steam generator after approximately 70 hours of operation revealed no damage or accumulation of deposits. EPA reference unleaded gasoline was used as the fuel. Both steady state efficiency measurements and severe transient cycling tests were performed during the operating period. No leakage or distortion occurred during operation of this unit, although temperatures and pressures in excess of 1200°F and 1200 psi occurred during some transients. Figure 79 illustrates the condition of the top row just below the combustor. Vaporization takes place in this and the next row at an average temperature of 550°F. As a consequence, the tubes still retain a bright appearance with little traces of oxidation even though gas temperatures in excess of 2600°F (see Fig. 79) entered the tube matrix at this row. Two rows below the last superheater coil had a relatively dark but thin oxide coating typical of operation of 321 stainless steel at about 1100°F wall temperature. A 1/8 inch thick Hastelloy X center core baffle plate indicated a relatively heavy oxide layer but little distortion. No direct connection between this plate and the three tube spacers was made in this installation. Additionally, the depth of the tube spacers was greater than the unit described in Section 6. As a result of these two improvements no breakage or distortion occurred in the first row tube spacers on this unit.

Figure 80 illustrates the condition of the last row preheater from the exhaust duct. Both the stainless steel tubes and copper fins were in a brigh metal condition with little indication of either oxidization or deposits.

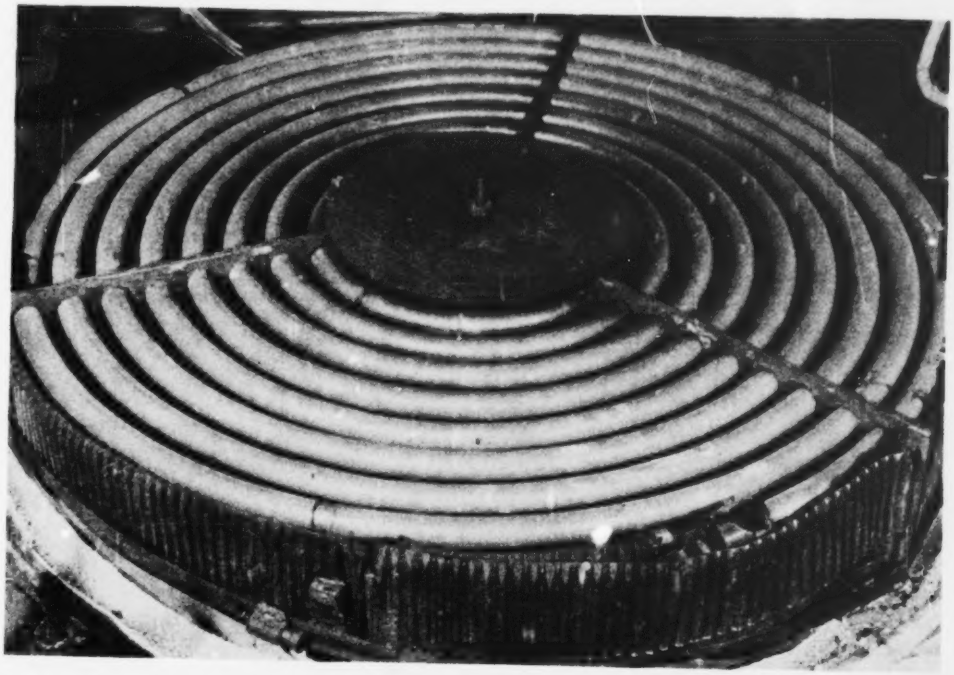

FIGURE 79. TOP COIL (VAPORIZER) AFTER 70 HOURS OF OPERATION

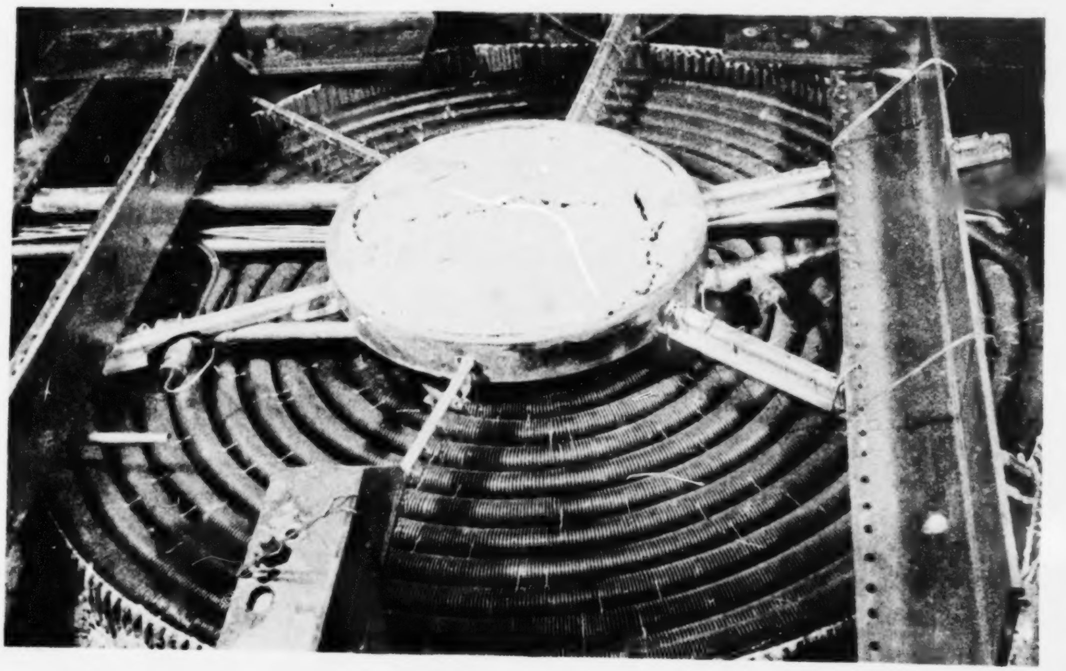

FIGURE 80. BOTTOM COIL (FIRST ROW PREHEATER) AFTER 70 HOURS OF OPERATION

8

CONTROL SYSTEM

A unique automatic control system was evaluated as an integral part of the combustor steam generator test program. Requirements for an automotive steam generator control can be summarized as:

- Maintain a fixed schedule of air-fuel ratios across the full operating range of the combustor to ensure low emissions, correct outlet temperature and prevent flame out.

- Maintain outlet steam pressure at constant value of 1000 psia (tolerance goal of ±100 psi)

- Maintain steam outlet steam temperature at a constant value of 1000°F (tolerance goal of ±100°F).

An automatic control was synthesized to maintain these functions under the virtually continuously varying steam demands of an automotive city driving cycle. Inherent in the requirements are large turndown ratios with rapid and frequent power level demands.

System synthesis was based upon first providing a positive synchronization between the fuel and air flow control subsystems. Secondly, it was determined that the transient requirements for steam flow and the slow thermal response of the unit required an open loop schedule of fuel and water to be instantaneously responsive to steam flow. By providing this anticipatory feature in the control loop, a relatively limited authority was needed in the closed loop temperature and pressure trim control circuits. Response characteristics observed during manual operation of the test bed steam generator indicated that the best control response occurred when firing rate (fuel-air flow) was used as the trim control input to correct pressure errors. Water flow rate changes were used to correct temperature errors. In both cases outlet steam pressure and temperature were the only parameters in addition to steam rate required as inputs to the control system. Fuel flow, water flow and air flow were the only outputs of the control system. Components to allow open loop synchronized scheduling of air, fuel and water were specially designed to be integrated into the system. Electronic sensing, positioning and compensation was used in the integrated system since its flexibility lends itself to a highly developmental controls program.

Preceding page blank

8.1 SYSTEM DESCRIPTION

Operation of the basic open loop schedule control (anticipatory type steam generator control) is simple and straight-forward. Output steam flow rate is controlled by a throttle valve that has a pressure ratio above critical flow at all times. It is a simple variable orifice contoured to provide a linear change in flow area with input position. Thus, if the pressure in the steam generator is relatively constant, the steam flow is directly proportional to the "manual throttle position". An electrical position transducer measures this position and thereby provides an electrical signal directly proportional to flow. In an actual automobile installation this signal could be synthesized from the engine speed and cutoff valve position or a direct measurement of flow. A closed loop position control subsystem (Fig. 81) automatically moves the triple valve actuator to a position that will give the desired steady state temperature and pressure while balancing the heat input to the steam rate. The gain of the control system is approximately 600,000 BTU/sec. (It takes approximately two seconds to move from 0 to full flow.)

Closed loop trim control on output steam pressure is provided by an electronic system. Outlet pressure is sensed by a strain gage transducer. Comparison between actual pressure and the desired setpoint of 1000 psi is made in an electronic controller having a simple proportional output. A wide adjustment of gain is provided in this controller to assist in establishing the best gains to be used with the system. From the controller the signal is operated on by a pressure trim gain compensator that scales the control signal proportionally to steam flow (position of the steam throttle valve). For example, if operating at 5 percent steam flow the pressure circuit would have an actual authority of ±2 percent. At 50 percent steam flow the corresponding authority of the pressure trim circuit would be ±20 percent. The compensated pressure trim signal is then summed together with the main open loop position control signal (proportional to steam flow) to trim the triple valve actuator position from its basic position assumed as a function of steam flow.

Temperature trim is provided by a completely independent electronic system. Outlet steam temperature is sensed by a thermocouple and a proportional plus integral and derivative controller which trims the temperature by adjustments to the feedwater rate. For a given set of conditions, reducing the feedwater rate decreases the water level. When the water level (dryout zone) drops the most significant effect is to increase the length of the superheater, thereby increasing outlet steam temperature. Since the feedwater metering valve is mechanically linked to the air and fuel valves, it is necessary that a controller independent of the triple valve actuator be incorporated. The method selected was to independently regulate the pressure drop across the water metering valve.

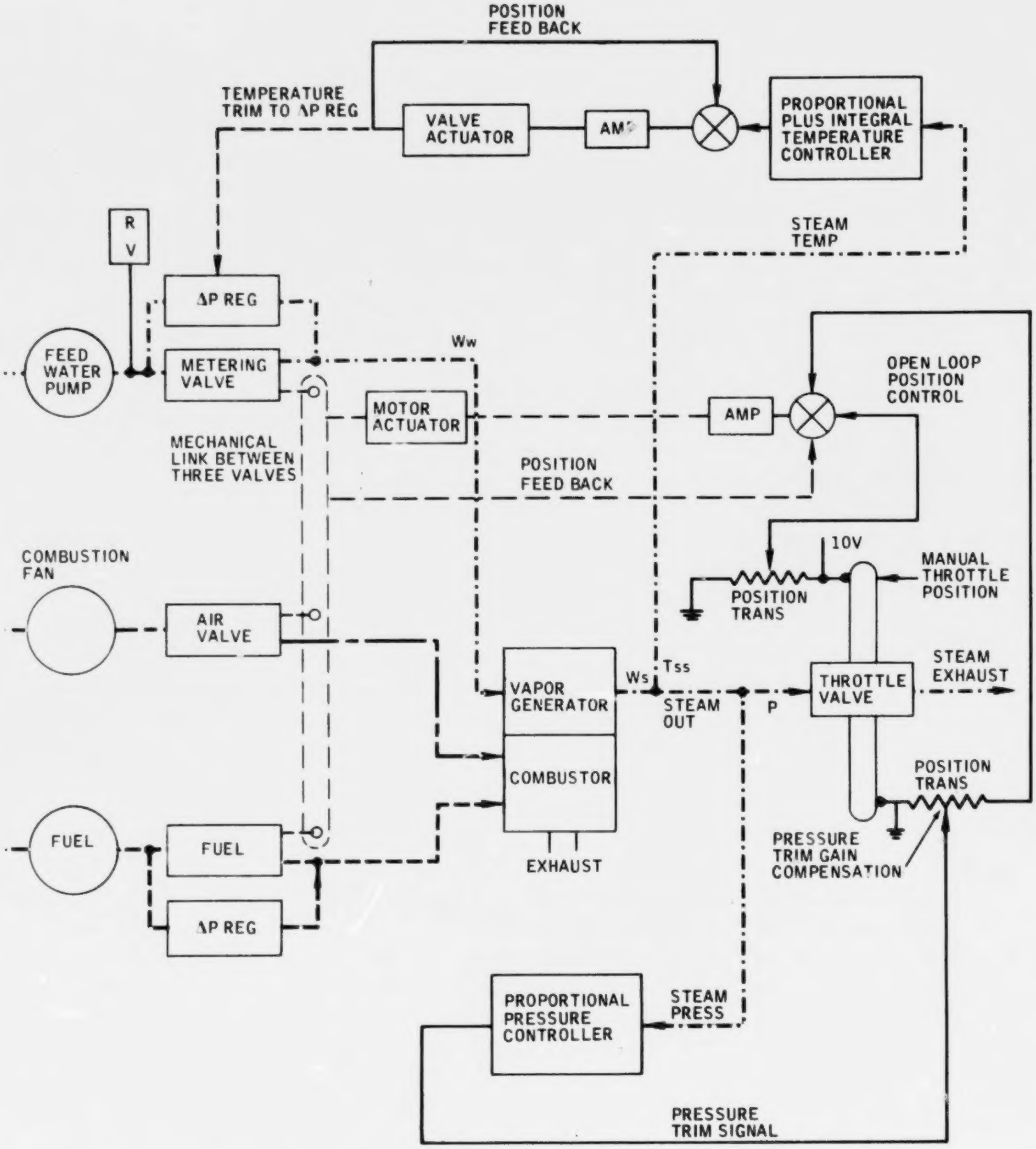
POSITION FEED BACK
TEMPERATURE TRIM TO ΔP REG
VALVE ACTUATOR
AMP
PROPORTIONAL PLUS INTEGRAL TEMPERATURE CONTROLLER
STEAM TEMP
R V
ΔP REG
FEED WATER PUMP
METERING VALVE
Ww
MOTOR ACTUATOR
AMP
OPEN LOOP POSITION CONTROL
MECHANICAL LINK BETWEEN THREE VALVES
POSITION FEED BACK
10V
MANUAL THROTTLE POSITION
POSITION TRANS
COMBUSTION FAN
AIR VALVE
Ws
Tss
STEAM EXHAUST
VAPOR GENERATOR
THROTTLE VALVE
STEAM OUT
P
COMBUSTOR
POSITION TRANS
FUEL
FUEL
EXHAUST
PRESSURE TRIM GAIN COMPENSATION
ΔP REG
PROPORTIONAL PRESSURE CONTROLLER
STEAM PRESS
PRESSURE TRIM SIGNAL

FIGURE 81. COMBUSTOR/VAPOR GENERATOR CONTROL SYSTEM

8.2 SYSTEM COMPONENTS

8.2.1 System Flow Arrangement

Figure 82 schematically describes the operation of all major fluid flow components. The basic control approach is to mechanically schedule fuel, air and water as a function of steam demand. A triple valve actuator operates each of the metering systems from a signal from the electronic controller. Linkage between the large diameter rotary air shear valve (see Section 5) drives through cams the fuel and water metering valves. Both valves are spool type with slotted orifices. The water metering valve is pressure balanced to minimize actuation loads. A constant pressure drop of 16 psi is used to control fuel. Thus flow is a function of the valve's position only. The mechanical linkage and cam drives allow a fixed schedule of fuel flow to air flow for emissions requirements. Water flow orifice area is controlled by the triple valve actuator but the pressure drop is regulated by an electronic temperature trim actuator. A bypass differential pressure regulator controls the pressure drop across the water metering orifice. Pump flow must be at least 20 percent greater than the actual steam demand to allow proper functioning. As pressure is increased on the upstream side the piston of the valve moves to the right against the balance spring force. The bypass orifice opens up until the pressure drop across the piston and metering valve is equal to the spring force balance. By adjusting the spring force with an electric position actuator the pressure drop and thus the flow can be adjusted. An electronic temperature trim circuit adjusts the flow to maintain a constant outlet temperature.

8.2.2 Air Valve and Triple Valve Mechanization

A complete description of the rotary shear valve is given in Section 5.3.2. Rotary positioning of the valve is accomplished by the attached actuation tab shown on the upper right hand corner of Figure 29. This tab projects through a seal in the combustor case wall. The tip of the air valves actuation tab is visible at the top of Figure 83. Rotation of the air valve is accomplished by a linear screw jack actuator driven by an electric motor. A bolt drives the rotary shear valve through a bearing mounted in a slotted cutout in the tab. Two cams on the bottom of the linear actuator carriage operate the fuel (inboard) and the water metering valves. In Figure 83 the fuel metering valve is installed. Valve position is controlled by the contour of the cam which drives the spool down reducing the fuel metering area as the air valve reduces the flow area into the combustor. Since constant voltage is maintained to the fan motor, its speed and pressure are relatively constant. Thus air flow is always in correct synchronization with fuel flow; the ratio depending upon the shape of the cam. Figure 84 shows the triple valve actuator with both the fuel and water metering valves in operating positions of 100 percent power output. Microswitches installed on the actuator

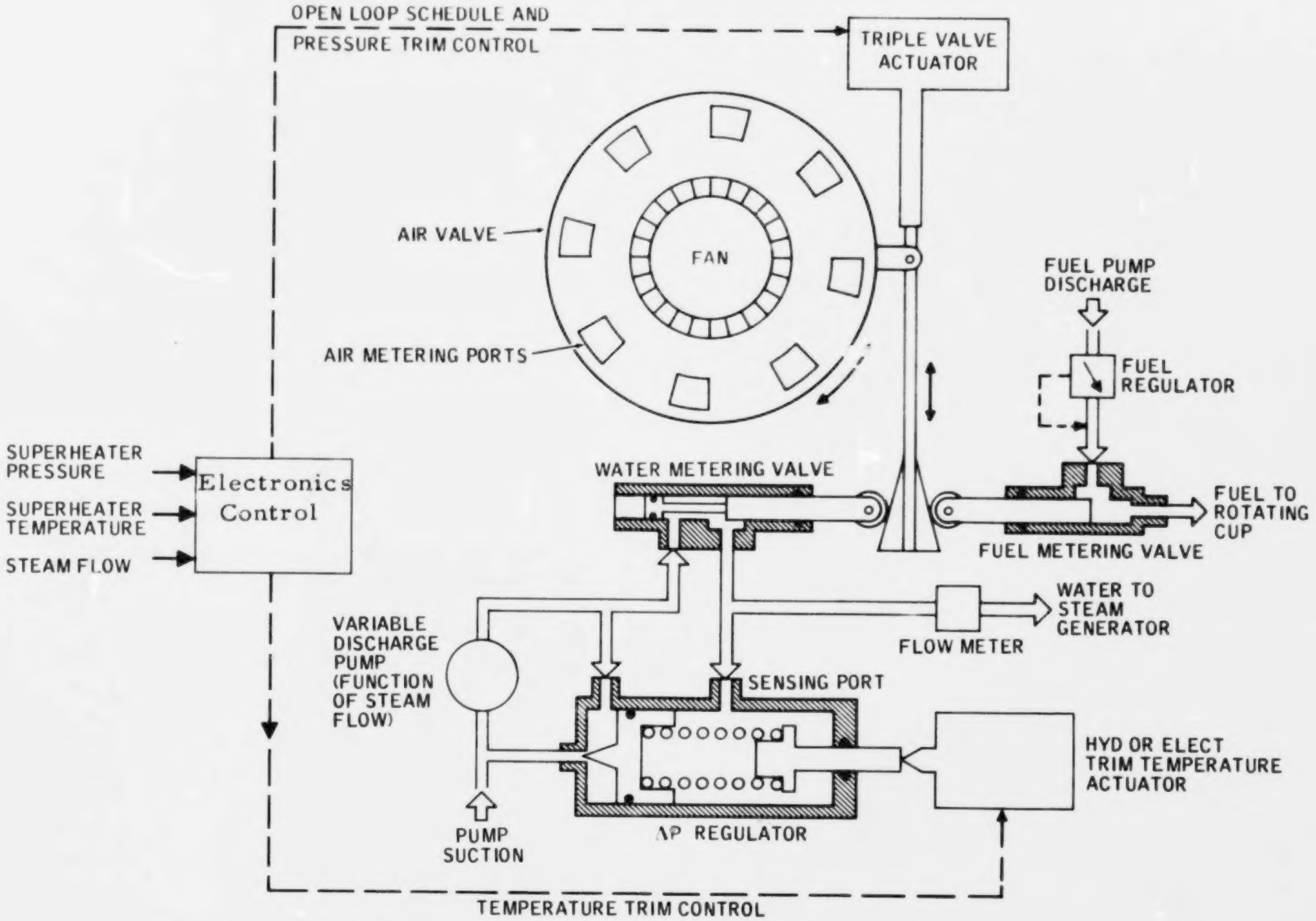
OPEN LOOP SCHEDULE AND
PRESSURE TRIM CONTROL
TRIPLE VALVE ACTUATOR
AIR VALVE
FAN
AIR METERING PORTS
FUEL PUMP DISCHARGE
FUEL REGULATOR
SUPERHEATER PRESSURE
SUPERHEATER TEMPERATURE
STEAM FLOW
Electronics Control
WATER METERING VALVE
FUEL TO ROTATING CUP
FUEL METERING VALVE
WATER TO STEAM GENERATOR
FLOW METER
VARIABLE DISCHARGE PUMP (FUNCTION OF STEAM FLOW)
SENSING PORT
HYD OR ELECT TRIM TEMPERATURE ACTUATOR
PUMP SUCTION
ΔP REGULATOR
TEMPERATURE TRIM CONTROL

FIGURE 82. CONTROL SYSTEM FLOW SCHEMATIC

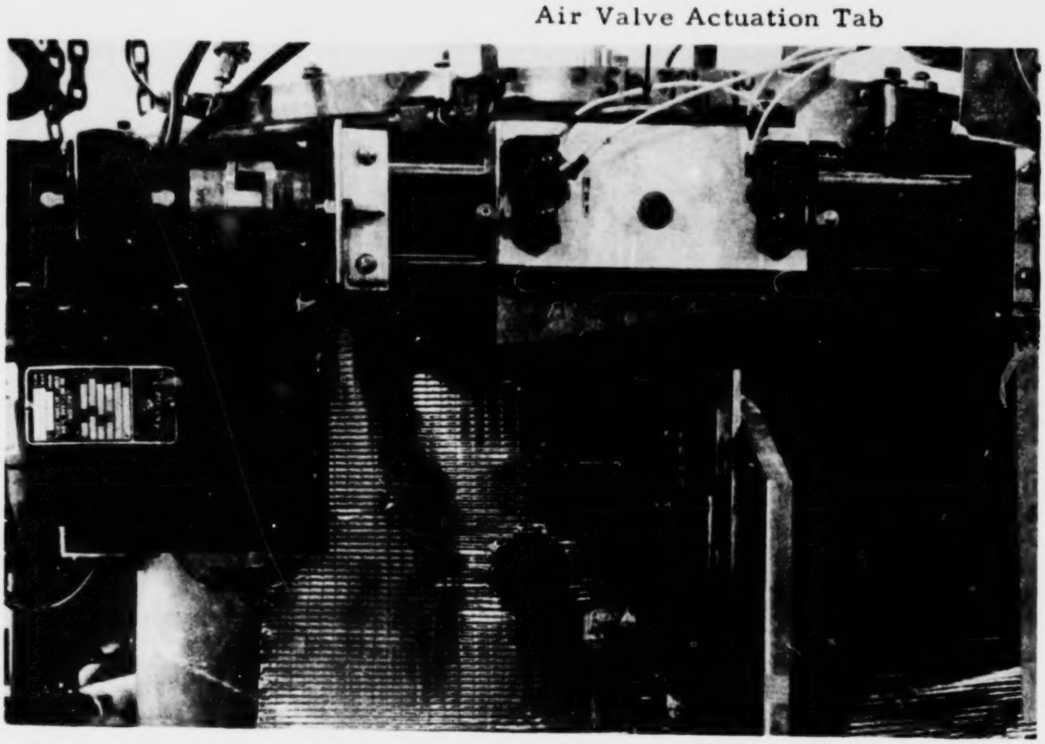
Air Valve Actuation Tab

FIGURE 83. TRIPLE VALVE ACTUATOR SHOWING AIR VALVE ACTUATION TAB

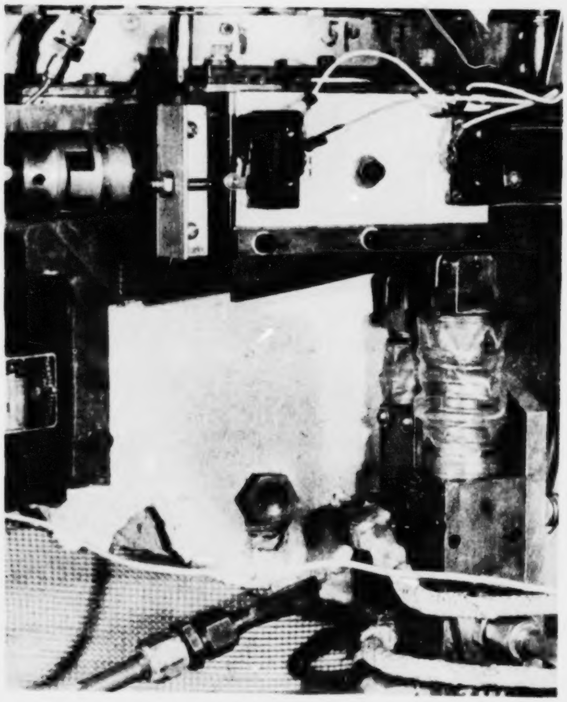

FIGURE 84

TRIPLE VALVE ACTUATOR WITH FUEL AND WATER VALVES INSTALLED carrier electrically limit travel at full and low flows. A rotary position transducer attached to the screw drive shaft provides a position feedback signal.

8.2.3 Air Valve (see Section 5)

8.2.4 Fuel Valve

A technical challenge exists in providing a linear fuel valve having a 40 to 1 turndown range. A goal of maintaining at least ±10 percent accuracy in the fuel-air ratio schedule means that the valve must be repeatible within better than 10%/40 or ±0.25 percent of the full range at the final turndown position. To make the valve insensitive to contamination and allow use of low pressure automotive pumps, a low pressure drop (15 psi) was used in its design. Figures 85, 86, 87 and 88 illustrate the design of the valve. A rectangular slit forms the fuel metering orifice. Flow area is controlled by the position of a cam driven plunger.

For accuracy at these low flows (down to 3.5 pounds per hour) it is important to size the valve metering orifice to make it insensitive to viscosity changes caused by temperature and blending. For normal practice a Reynolds number greater than 4000 will ensure a relatively constant coefficient of discharge.

Reynolds number is:

$$R_e = \frac{\frac{W_f}{A} \quad \frac{4A}{P}}{\mu}$$

where

W_f is mass flow (lbm/sec)

A is flow cross section area (ft^2)

P is perimeter of flow slot (ft)

μ is kinematic viscosity of fuel

($\mu = 1.70 \times 10^{-5}$ lb sec/ft^2 for JP-4 and $\mu = 1.02 \times 10^{-5}$ lb sec/ft^2 for gasoline at 70°F)

$4A/P$ is the hydraulic diameter of flow orifice

One hundred percent fueling rate is

137 lb/hr = 0.0381 lb/sec

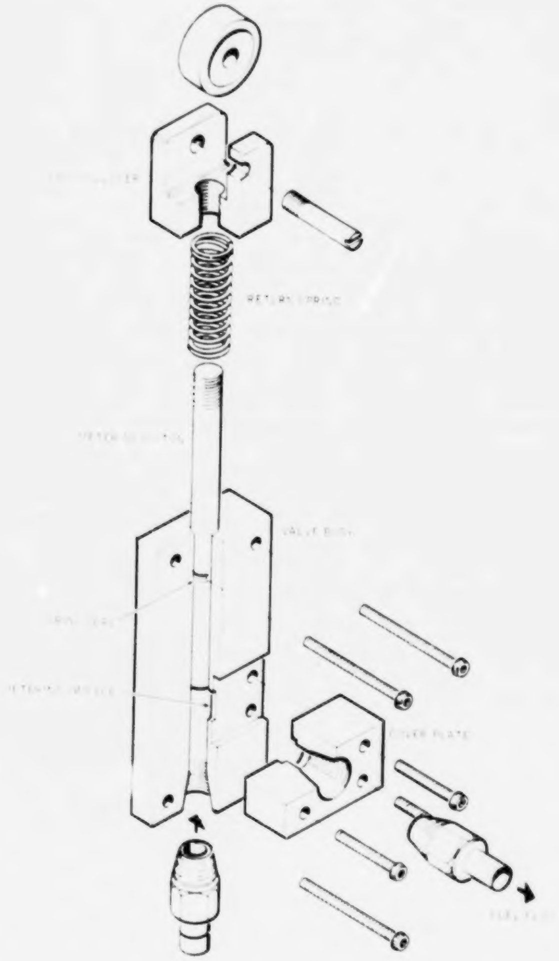
RETURN SPRING
METERING PISTON
VALVE BODY
COVER PLATE

FIGURE 85. EXPLODED VIEW OF FUEL VALVE

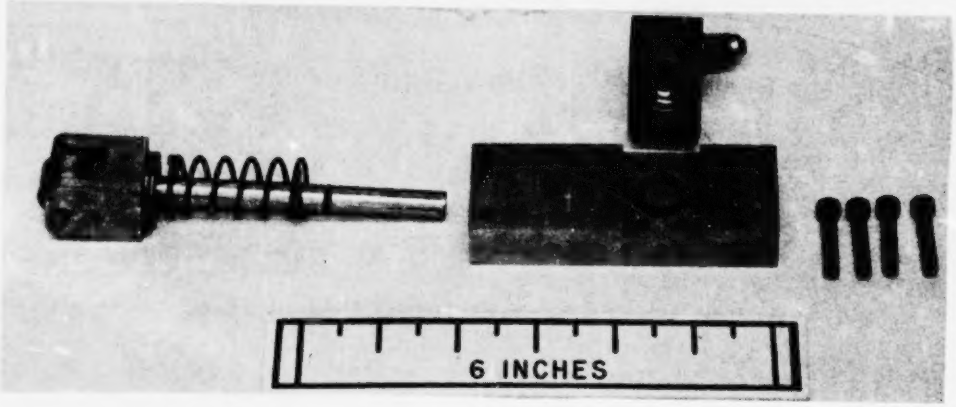

FIGURE 86. FUEL VALVE COMPONENTS

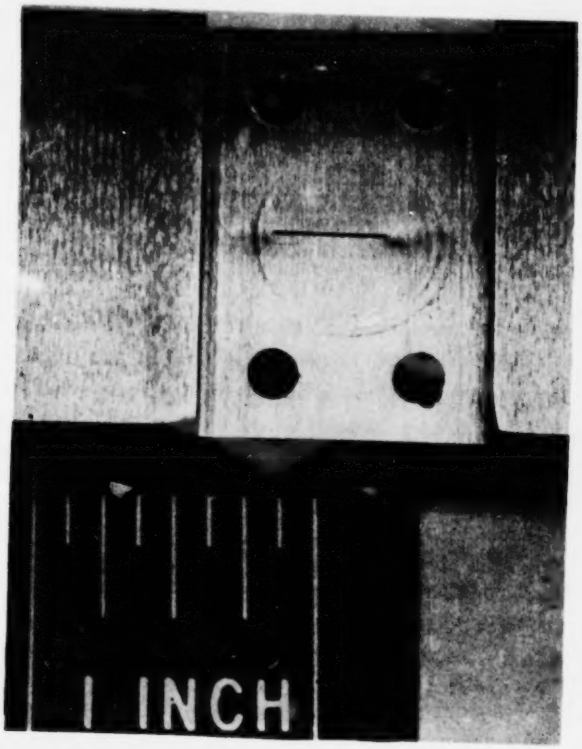

FIGURE 87. METERING SLOT

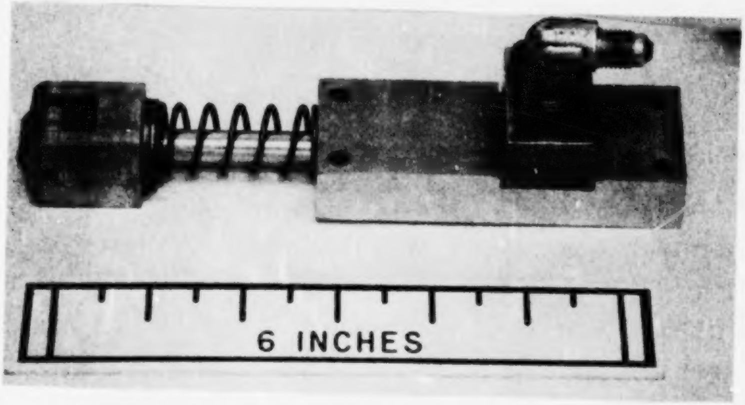

FIGURE 88. ASSEMBLED FUEL VALVE

Assume JP-4 as a fuel and slot dimensions of 0.008 in. x 0.40 in. at 100 percent

$$\text{Reynolds} = \frac{4 \times \dfrac{0.038}{32.17}}{\dfrac{0.816}{12} \; 1.7 \times 10^{-5}} = 4087$$

Figure 89 shows Reynolds number for JP-4 fuel at the low range lies in the transition zone (R_e = 2000 through 4000) from laminar to turbulent flow. The valve was sized this way such that slot dimensions did not become too small and impair accurate function of valve. Low flow valve operation will be experimentally investigated to determine if this has an unacceptable effect on fuel flow. For gasoline (the normal fuel to be used) the Reynolds number is well above the transition zone across the entire operating range.

Flow test calibrations confirmed the analysis of the valves characteristics. Lapsed time to accumulate an accurately measured weight of fuel was used to provide an absolute calibration of the valve. Figures 90 and 91 plot the data points against axial position of the valve's spool. Linearity with ±5 percent is exhibited across the 40 to 1 range. Relatively linear characteristics are maintained down to 0.9 pph. Valve gain was 368 pph per inch of stroke.

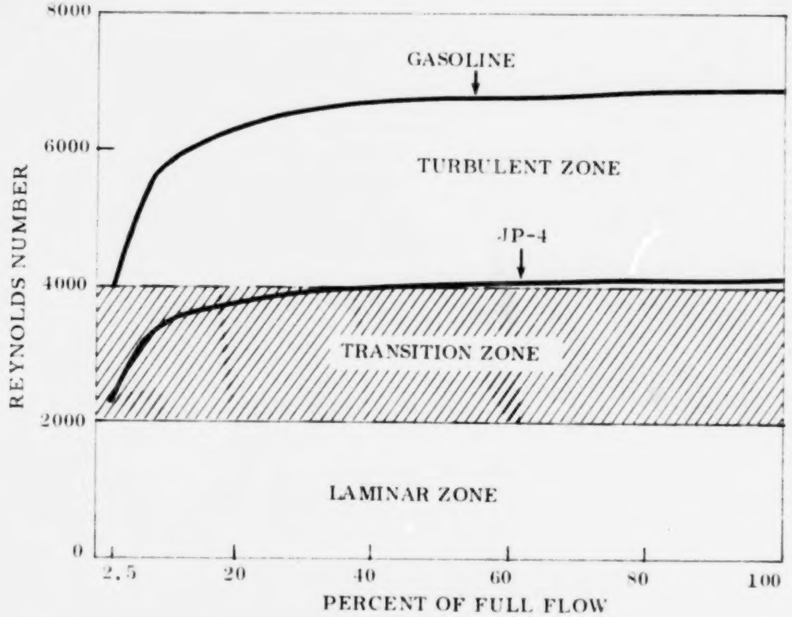

FIGURE 89. REYNOLDS NUMBER VS. PERCENT FUEL FLOW FOR JP-4 AND GASOLINE; 40 to 1 Turndown Ratios; Slot Dimensions 0.40 Inch by 0.008 Inch

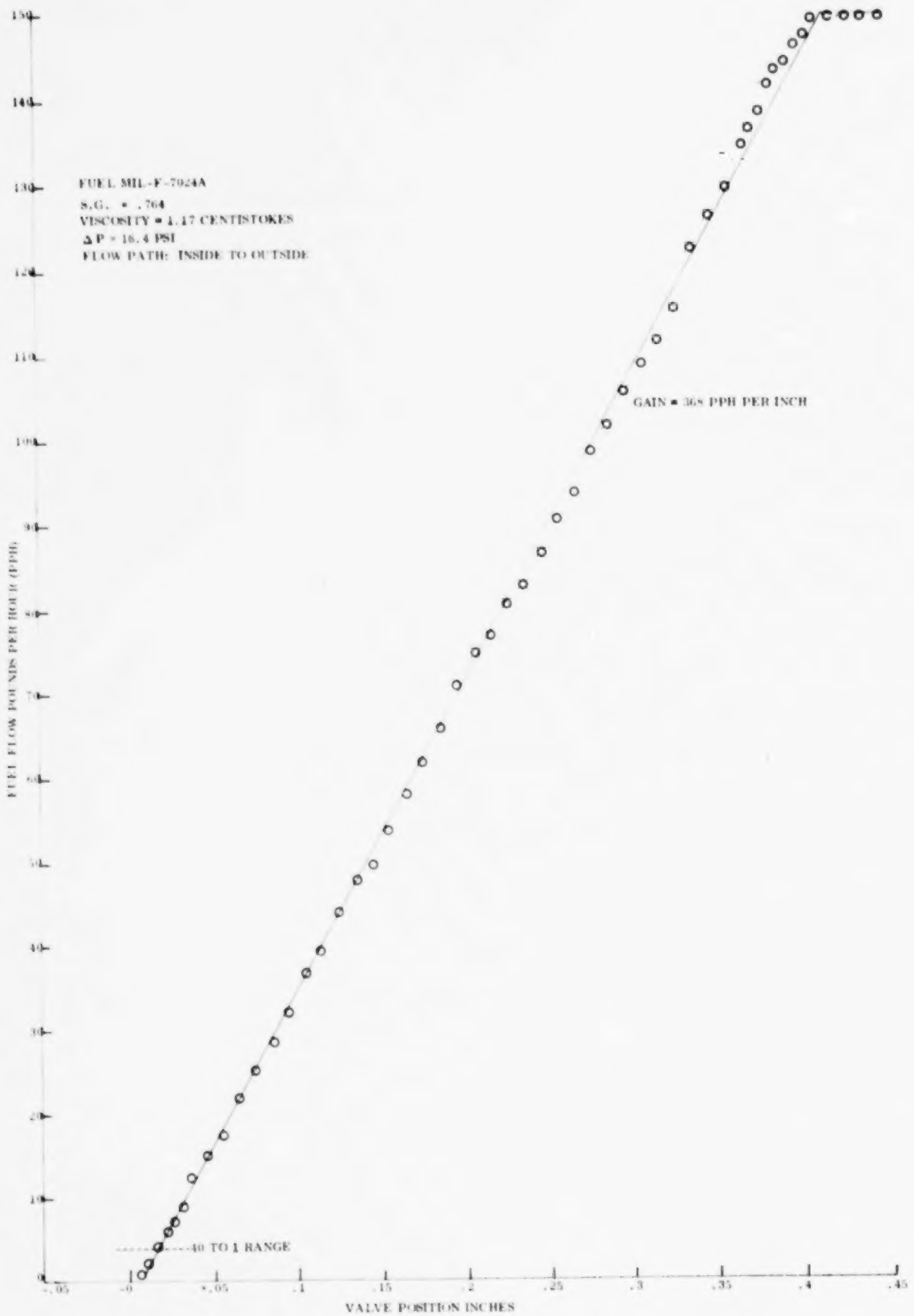

FIGURE 90. FUEL VALVE CALIBRATION

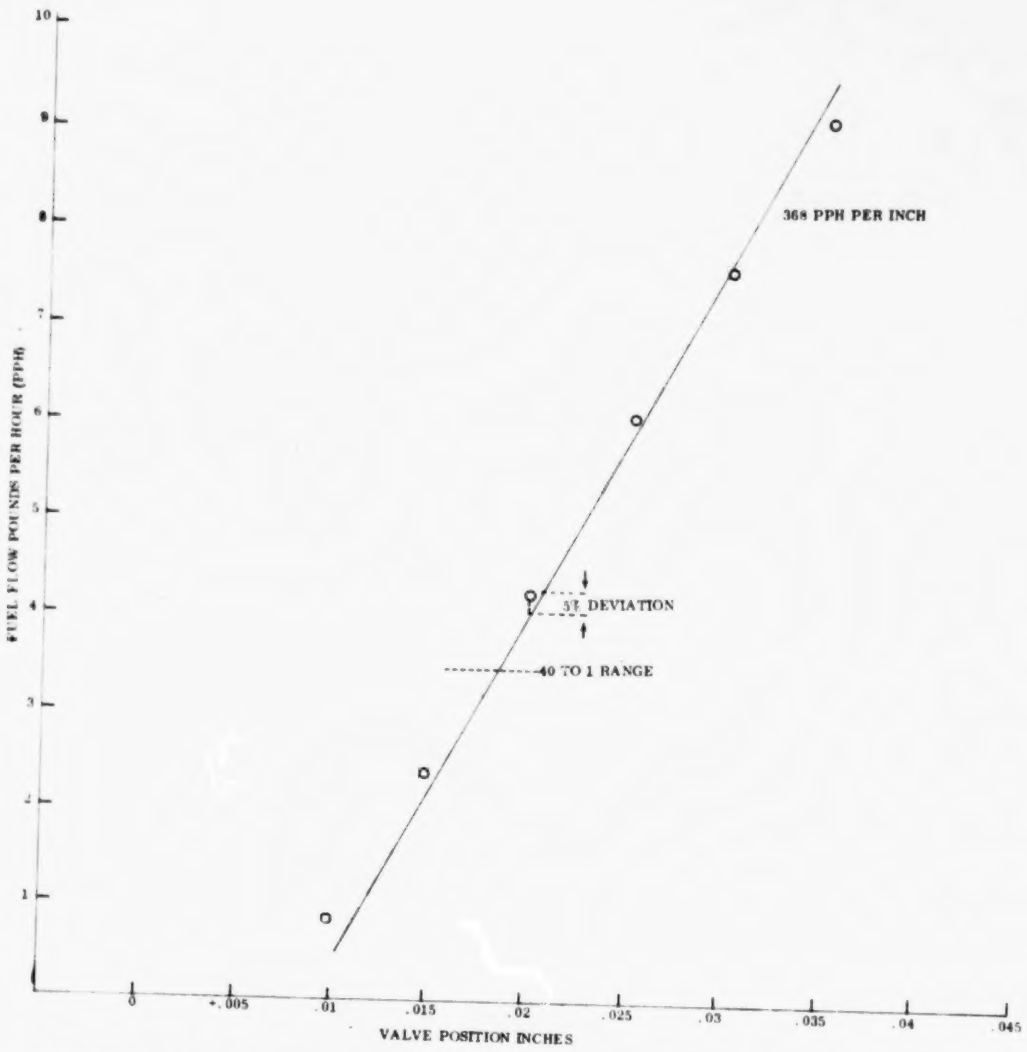

FIGURE 91. FUEL VALVE CALIBRATION 1 TO 10 PPM RANGE

8.2.5 Water Metering System

Water flow to the steam generator is controlled by a valve similar to the fuel valve in concept. A slotted orifice area (Fig. 92) is controlled by the position of a spool land actuated by a cam. Because the operating pressure is over 1250 psia at maximum steam flow a pressure balanced spool (Fig. 93) was incorporated. Water from the feed pump enters the right hand side port of Figure 94 and flows around a reduced spool diameter flow passage. It then passes through the variable orifice to the steam generator. Flow rates are a function of the position of the spool and the pressure drop across the valve. Calibrations of the valve were made at a

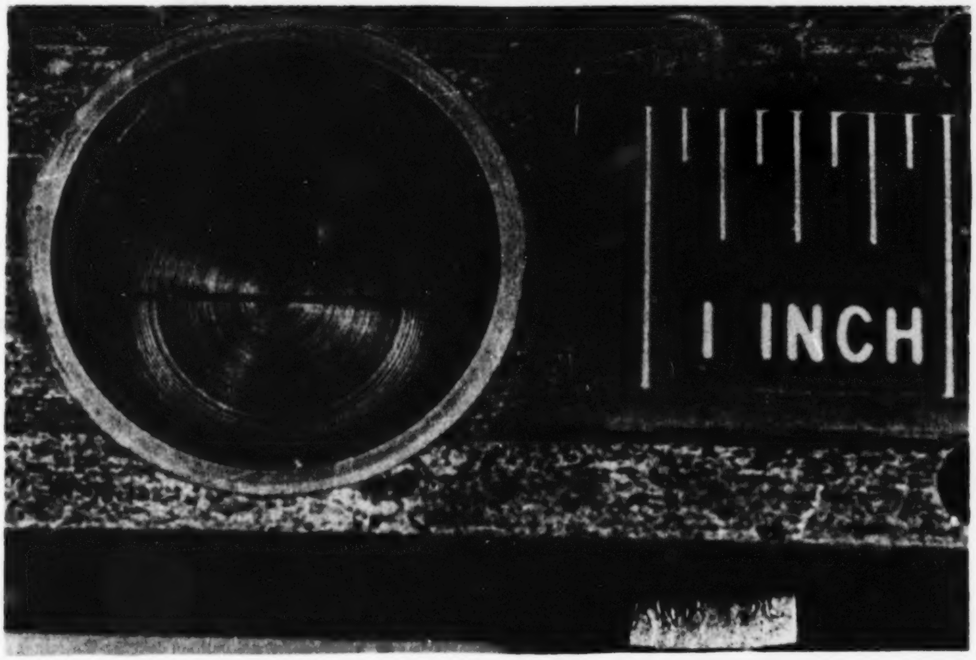

FIGURE 92. WATER METERING VALVE ORIFICE

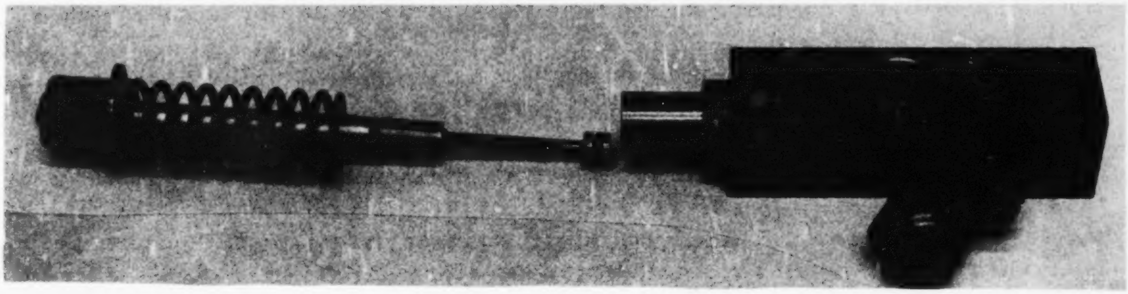

FIGURE 93. COMPONENT PARTS OF THE WATER METERING VALVE

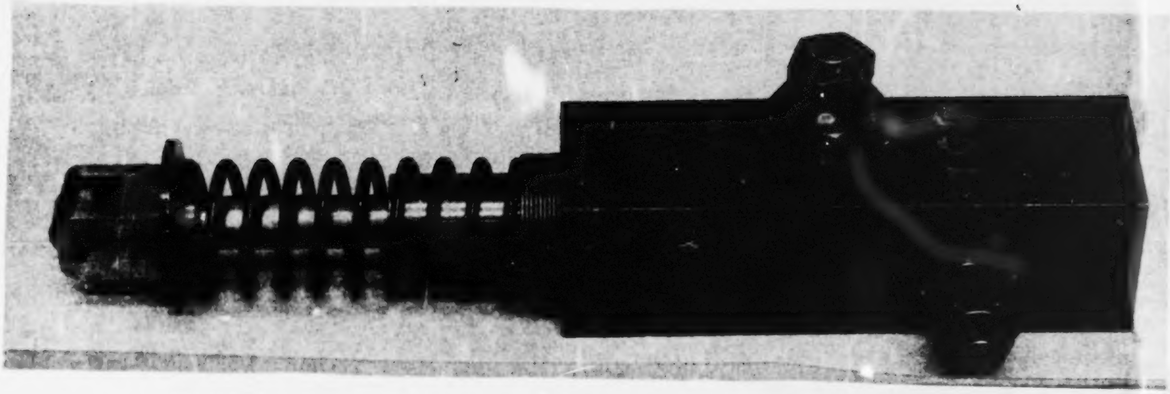

FIGURE 94. ASSEMBLED WATER METERING VALVE

constant 50 psi differential pressure with water. For each position of the spool calibrated, an absolute flow rate was established by measuring the weight of water flowing through the valve during a known period of time. Figure 95 is a plot of the flow rates measured versus valve spool position. From 1507 to 34 pounds per hour the standard RMS deviation from a straight "best fit" line was 18 pounds per hour.

As was discussed earlier in this section, closed loop temperature trim is providid by controlling the pressure differential across the water metering valve. As a consequence the temperature of the outlet steam can be regulated independent of the firing rate. A specially designed differential pressure control valve was designed to perform this function. Water from the pump enters a chamber on the high pressure side of the valve's piston from the pump discharge. Pressure from the downstream side of the metering valve is connected by a small sensing line to the opposite side of the piston. Downstream pressure plus the spring force balance the piston causing it to bypass excessive pump flow into the pump's suction line through a needle orifice valve. A needle orifice and a large diameter piston were used in this prototype system to ensure stability of the valve in the pulsating flow of the test cells large triplex pump. Much smaller sizes appear quite practical even with a triplex pump. An electric actuator positions the spring carrier (thus controlling differential pressure) in response to closed loop position control signals from a temperature trim circuit (Fig. 97). In a system that employs a variable displacement pump, the differential pressure could be controlled by regulating the displacement of the pump. It should be noted that the differential pressure regulator has no direct effect upon the steam pressure. Differential pressure across the metering valve is controlled from 15 psi to 70 psi. Valve design is established to make the differential pressure controller insensitive to input pressure requirements of the steam generator. However, its operation becomes non-linear at pressures below 300 psia steam generator pressure. The inlet pressure to the steam generator is only a function of steam demand, firing rate and flow pressure

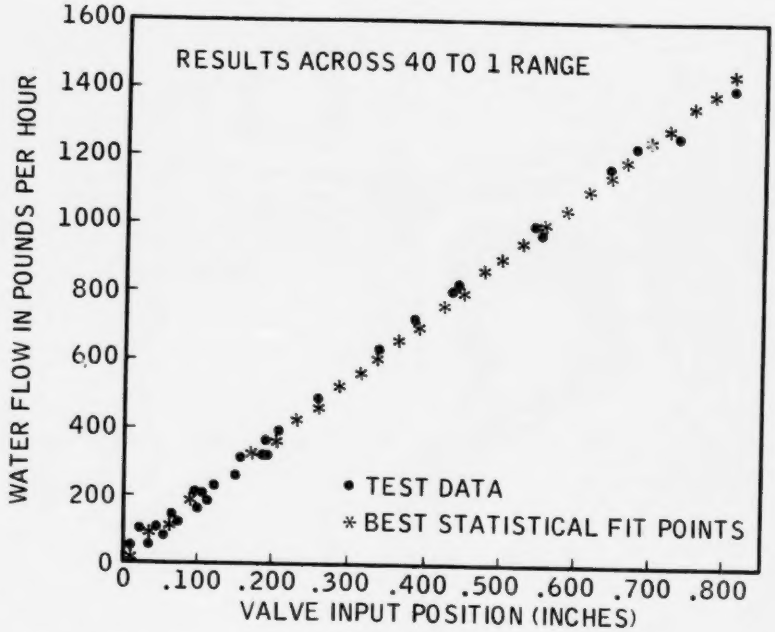

FIGURE 95. WATER METERING VALVE CALIBRATION AT 50 PSI DIFFERENTIAL

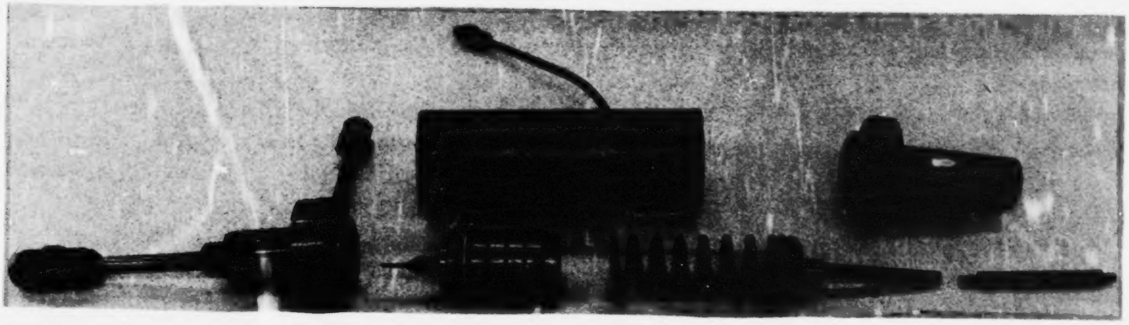

FIGURE 96. DIFFERENTIAL PRESSURE CONTROL VALVE COMPONENTS

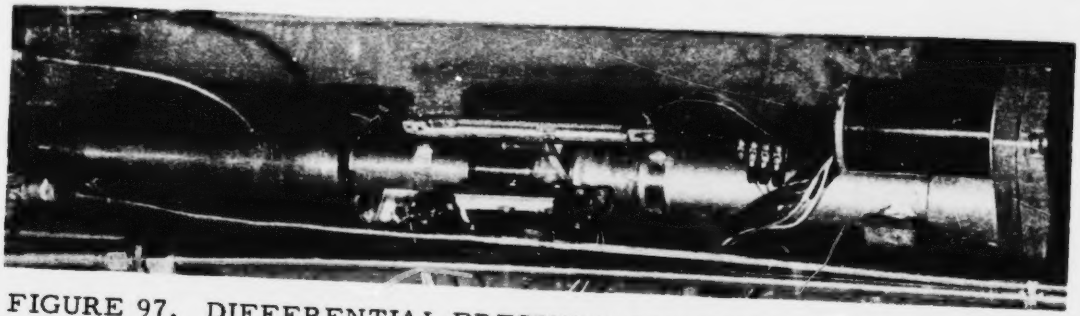

FIGURE 97. DIFFERENTIAL PRESSURE CONTROL VALVE ASSEMBLED WITH ELECTRIC ACTUATOR

drop across the tube matrix. Valve performance in the system was good with no apparent instabilities.

8.3 ELECTRONIC CONTROLS

The functional arrangement of the electronic system is shown in Figure 81. For all tests performed, a breadboard system was used. It consisted of two commercially available electronic controllers integrated into a breadboard system to perform the necessary functions discussed earlier in this section. A Barber-Colman Model 260T pressure controller was used in the pressure controller block. A Barber-Colman Model 523C Digital Temperature Setpoint controller was used in the block labeled as temperature controller. Both of these units had adjustable proportional bands and set points. Each also had an integral compensation in the forward control loop. Summing amplifiers, actuator position, null setting position feedback and signal conditioning circuits were breadboarded around these two components to form the complete control system. Most of the features required in the commercial controllers are not necessary in an integrated system. However, their wide flexibility with respect to gain ranges and control modes makes their use more effective in optimizing control functions and gains. After gains and control compensations were established an integrated electronic package was fabricated to perform all of the functions of the electronic portions shown in Figure 81. Only four circuit boards were necessary to obtain the necessary electronic functions. Figure 98 shows the arrangement of these components. Program time allowed some limited bench testing of these circuits but problems with temperature drift, comparator circuit operations, and thermocouple reference junction compensation were not worked out of these circuits. As a consequence, no complete systems tests were performed using the actual circuits shown in Figure 98. However, they do show the relatively few number of components necessary to perform the electronic functions necessary, and they do perform the same functions of the system breadboard successfully used to control the steam generator.

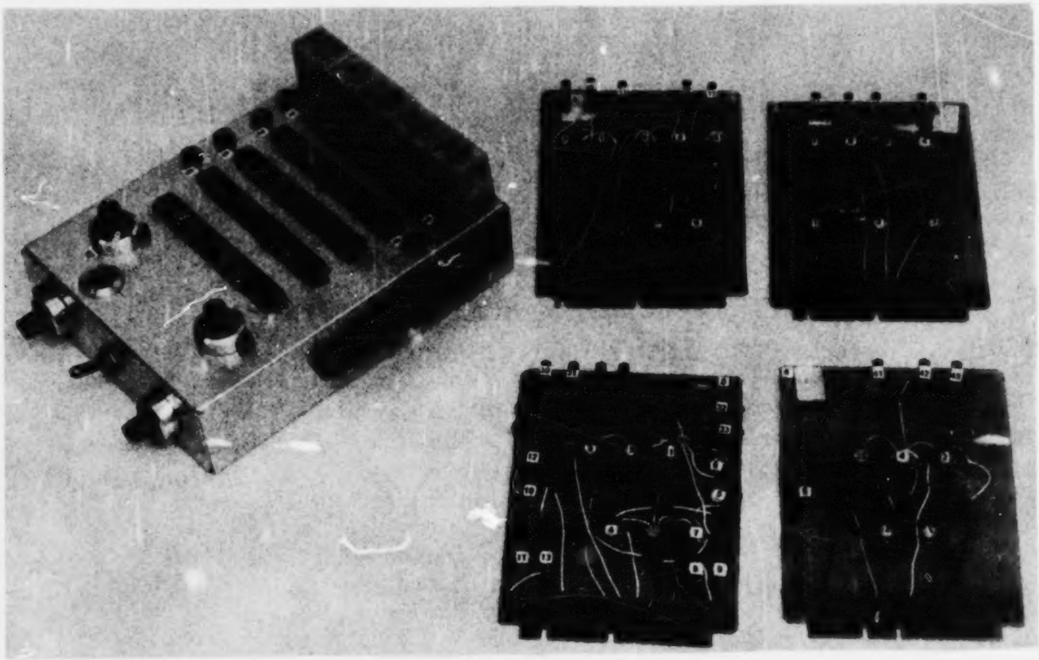

FIGURE 98. ELECTRONIC COMPONENTS REQUIRED TO PERFORM CONTROL FUNCTIONS

8.4 TEST RESULTS WITH PARALLEL FLOW STEAM GENERATOR

8.4.1 Fxplanation of Test Results

Initial control system tests were performed with the combustor discussed in Section 5 and the steam generator described in Section 6. Test cell components were essentially the same as described in Section 6.3. Important transient control system data was recorded on a high response six channel Sanborn chart data system. Figures 99, 100, 101 and 102 are reproductions of the Sanborn strip chart traces. At the top outlet steam pressure is recorded from a strain gage transucer connected several inches from the outlet tube of the steam generator. Each major ordinate division is 0.5 cm, scales are all based on Sanborn calibrations. Pressure is scaled at 250 psia per cm. Next trace is the steam throttle position. Steam flow is controlled by the position of the throttle valve. A contoured needle plunger allows the throttle valve to control steam flow directly proportional to valve position. Throttle valve position (steam flow rate) is the control system "disturbance" for transient tests and also establishes steady state flows. Total system volume between the outlet of the steam generator and the throttle valve is 40 cubic inches. Two linear position transducers are mounted on the throttle valve drive mechanism. Output voltage from one transducer supplies the main input to the electronic control system. This

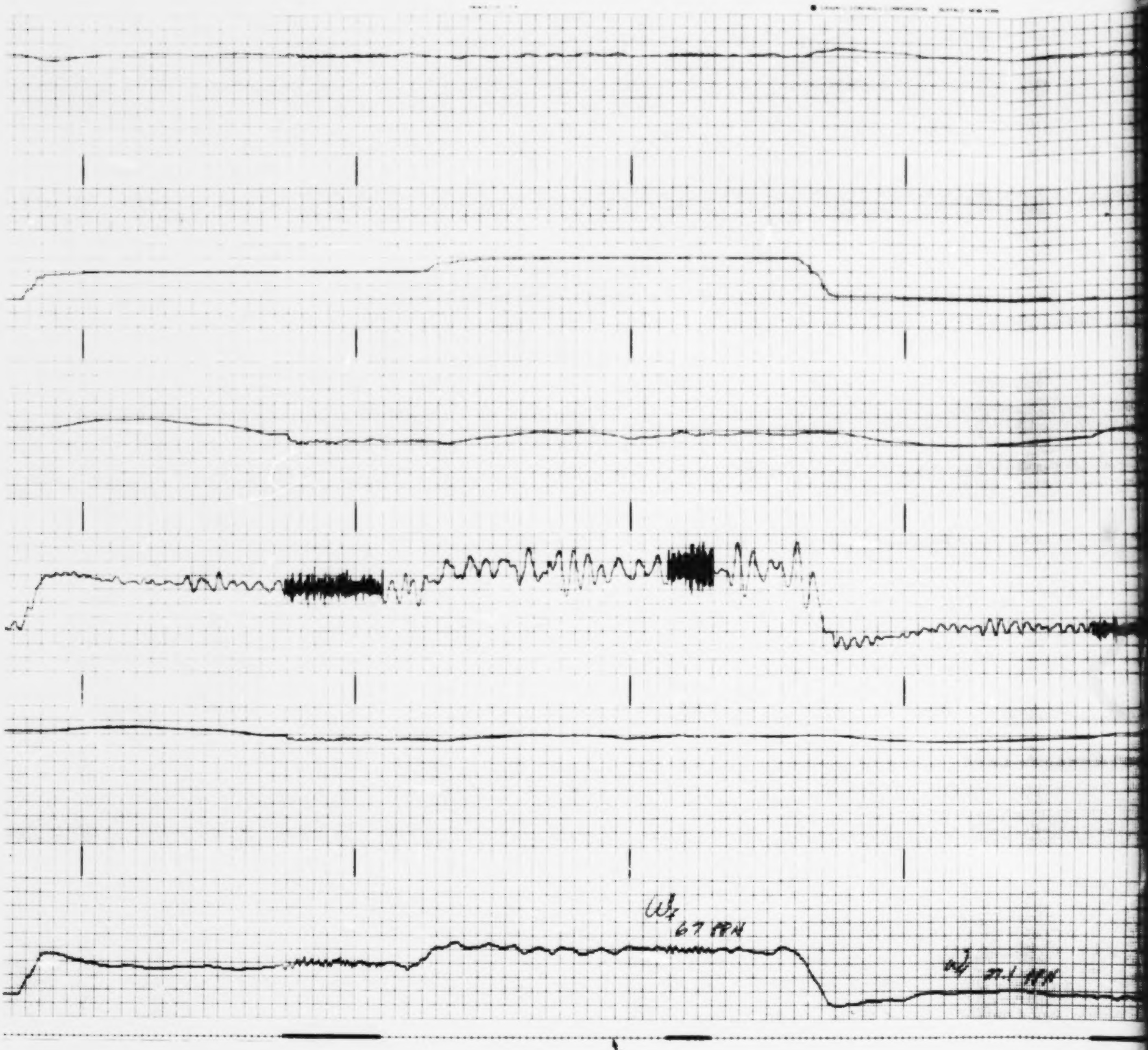

TIME IN SECONDS PER MARK

Preceding page blank

A

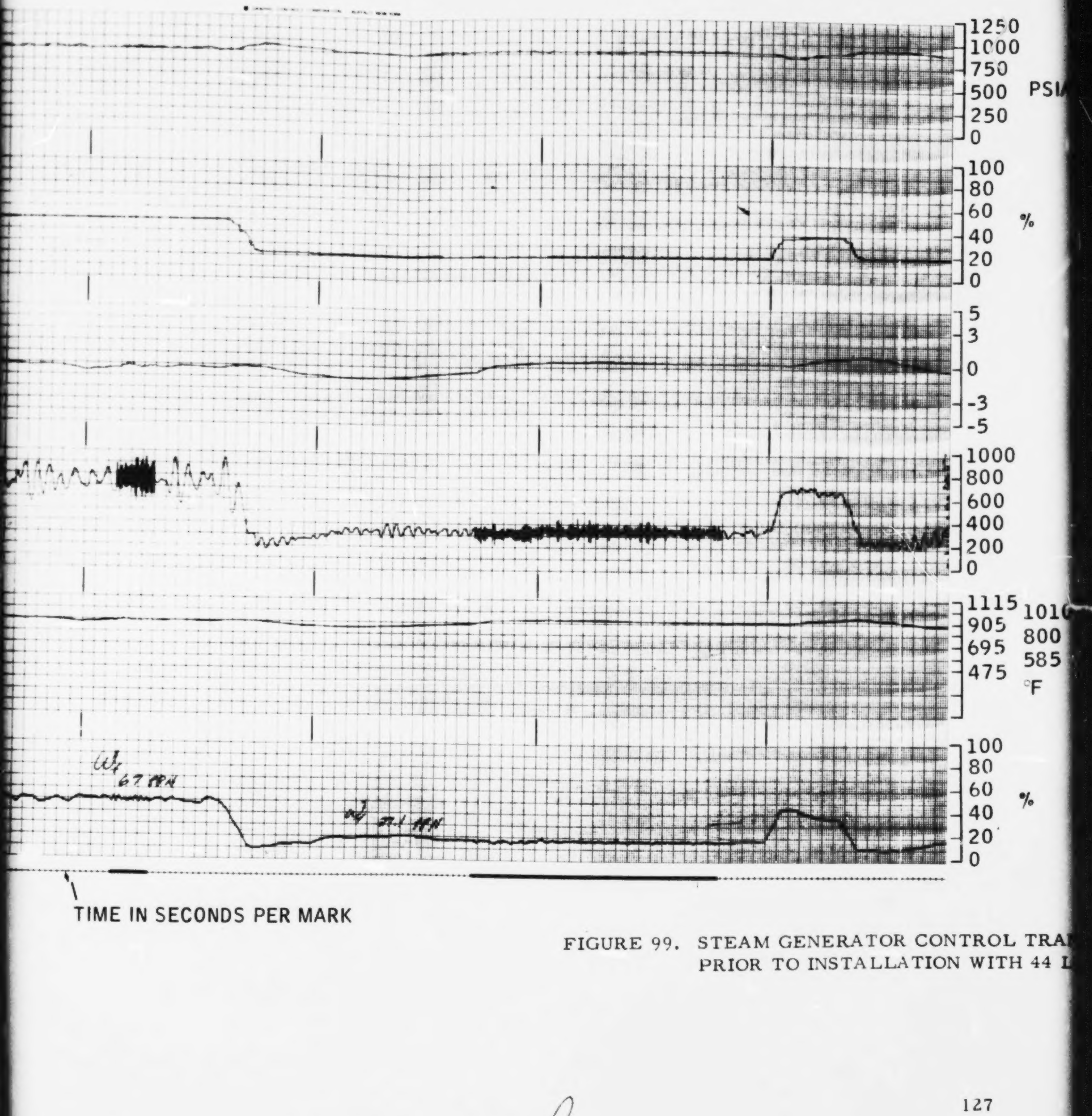

FIGURE 99. STEAM GENERATOR CONTROL TRA
PRIOR TO INSTALLATION WITH 44 L

B

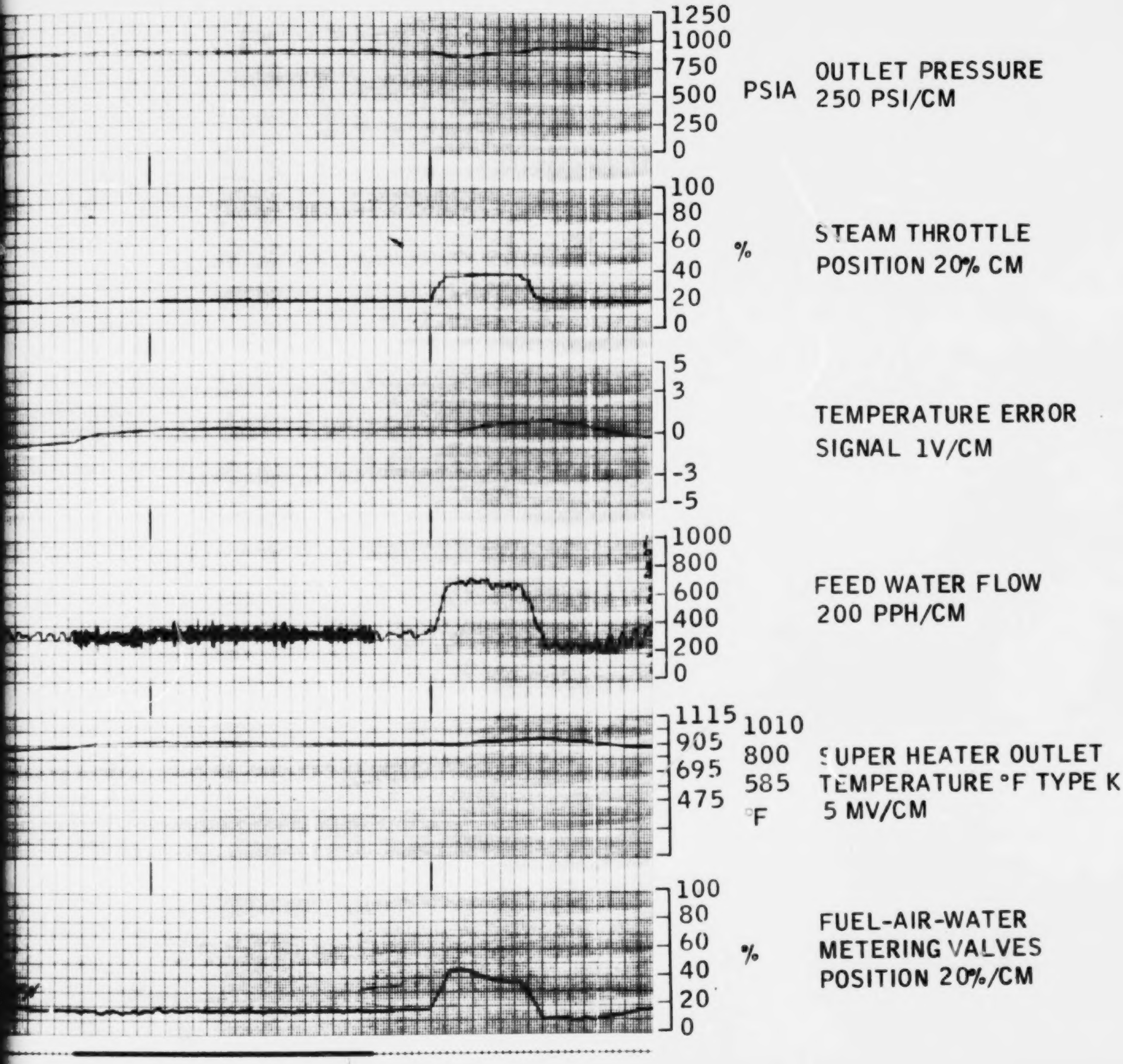

FIGURE 99. STEAM GENERATOR CONTROL TRANSIENTS, STEP CHANGES PRIOR TO INSTALLATION WITH 44 LB/IN SPRING IN ΔP VALVE

B

C

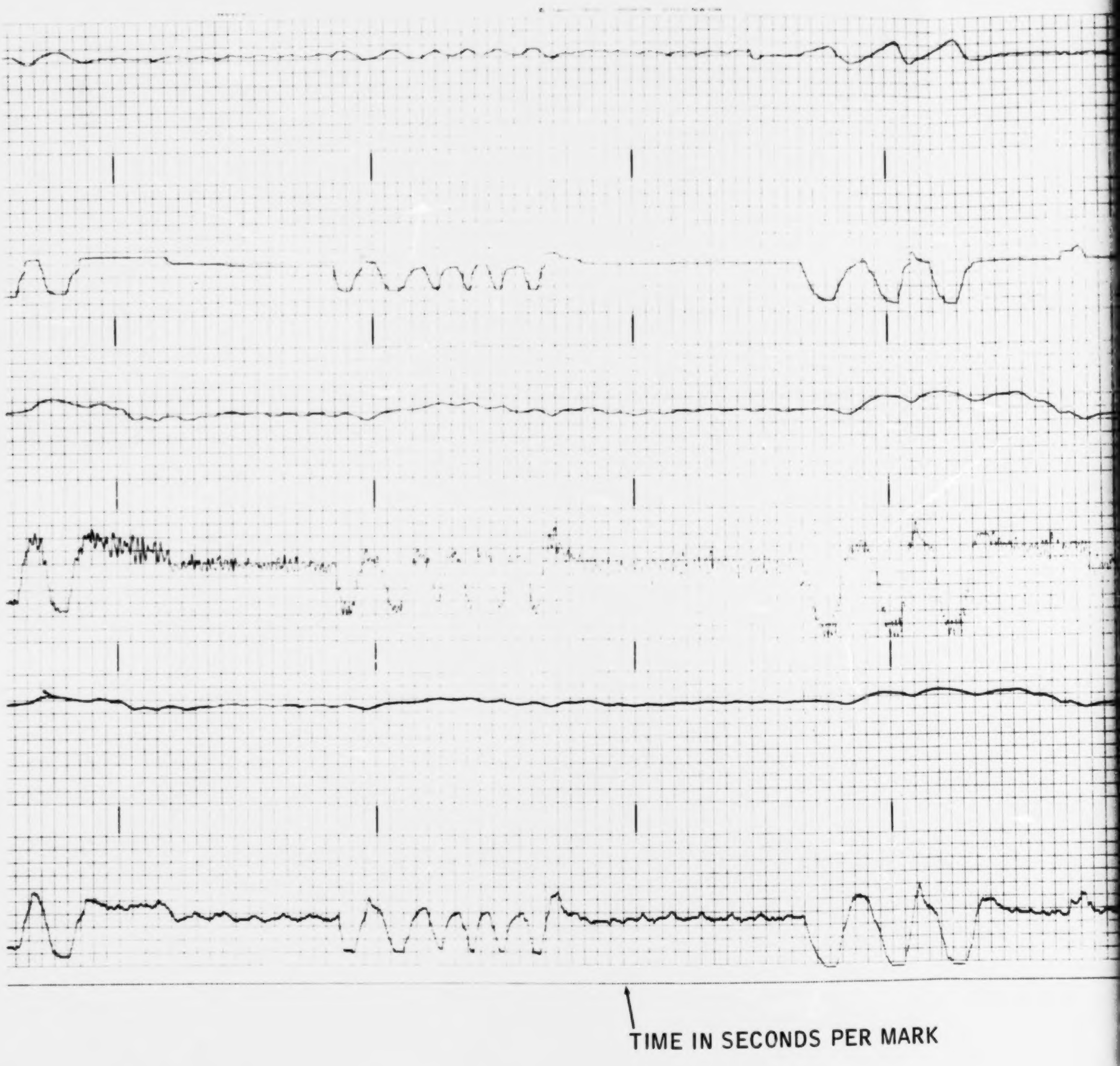

TIME IN SECONDS PER MARK

Preceding page blank

A

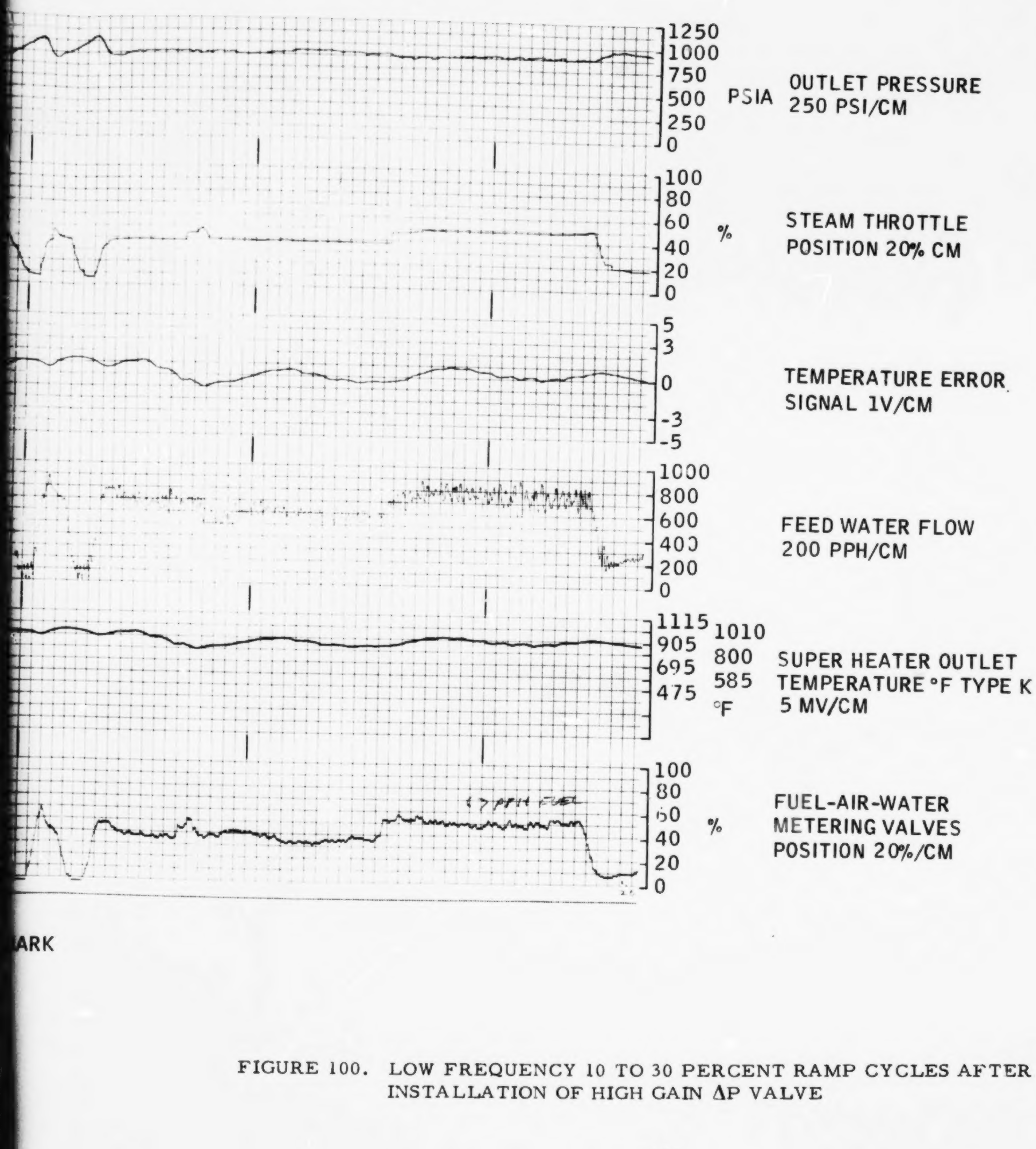

FIGURE 100. LOW FREQUENCY 10 TO 30 PERCENT RAMP CYCLES AFTER INSTALLATION OF HIGH GAIN ΔP VALVE

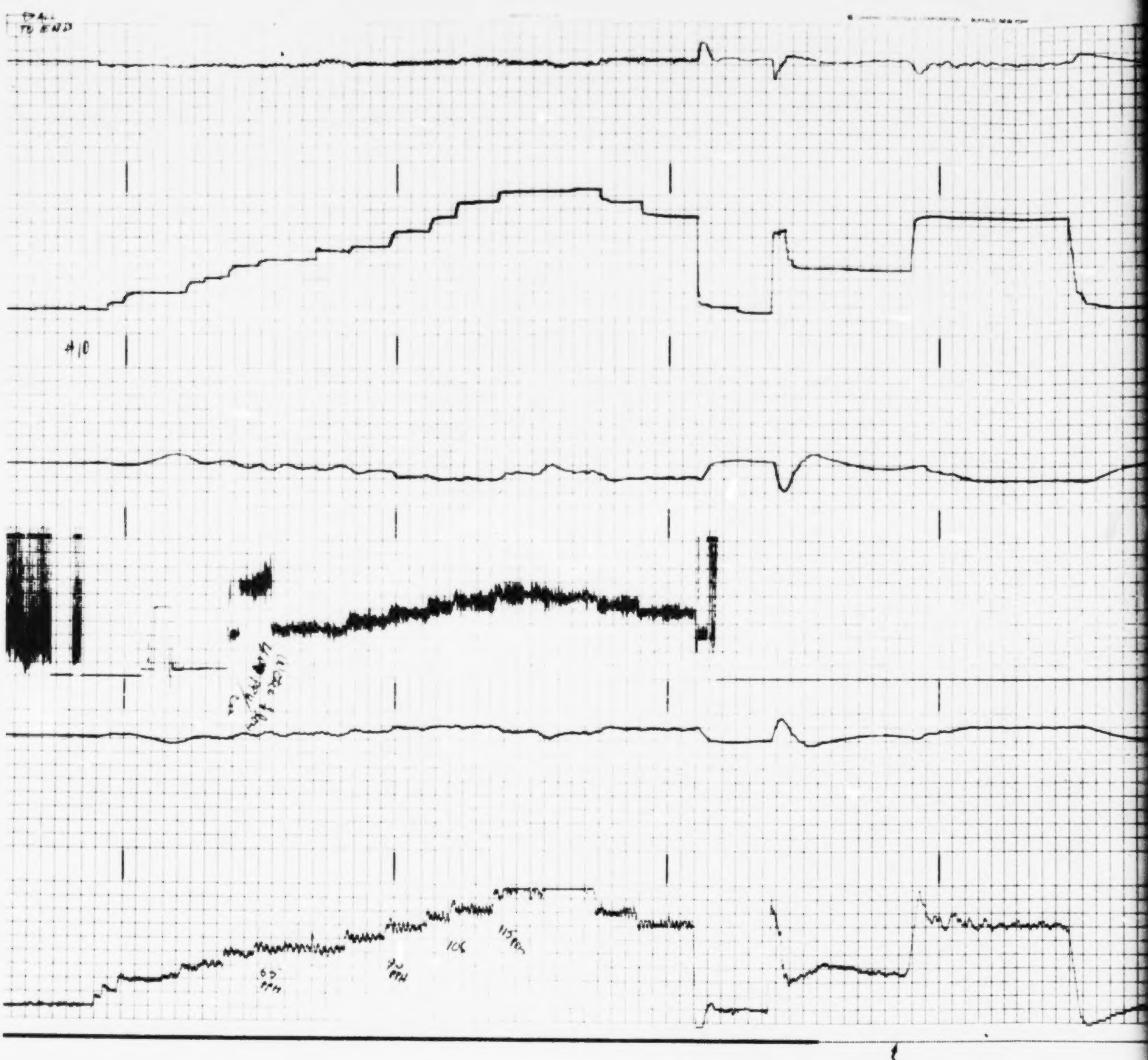

TIME IN SECONDS PER MARK

Preceding page blank

A

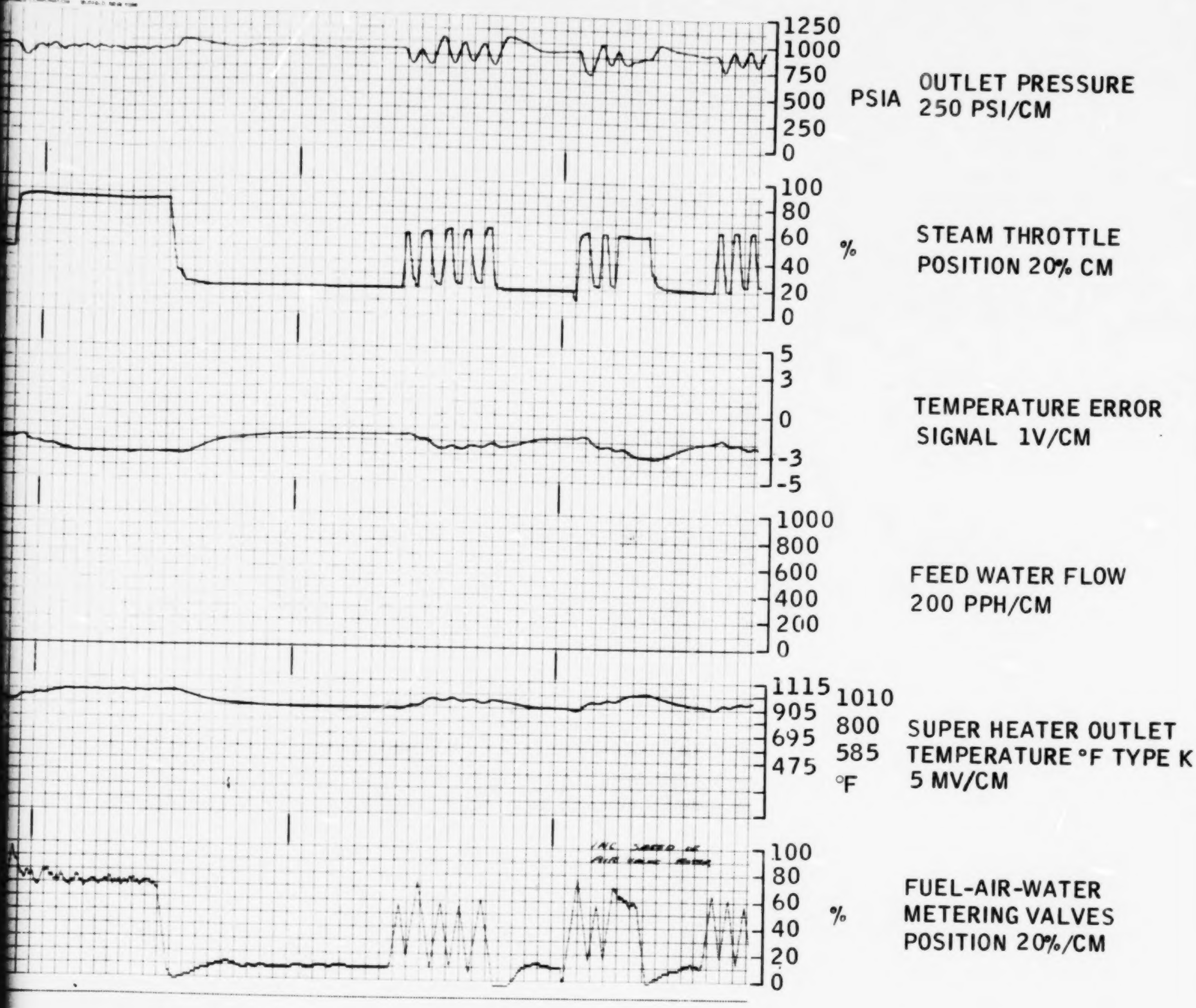

FIGURE 101. FULL POWER STEADY STATE PERFORMANCE WITH STEP TRANSIENTS IN STEAM FLOW

B

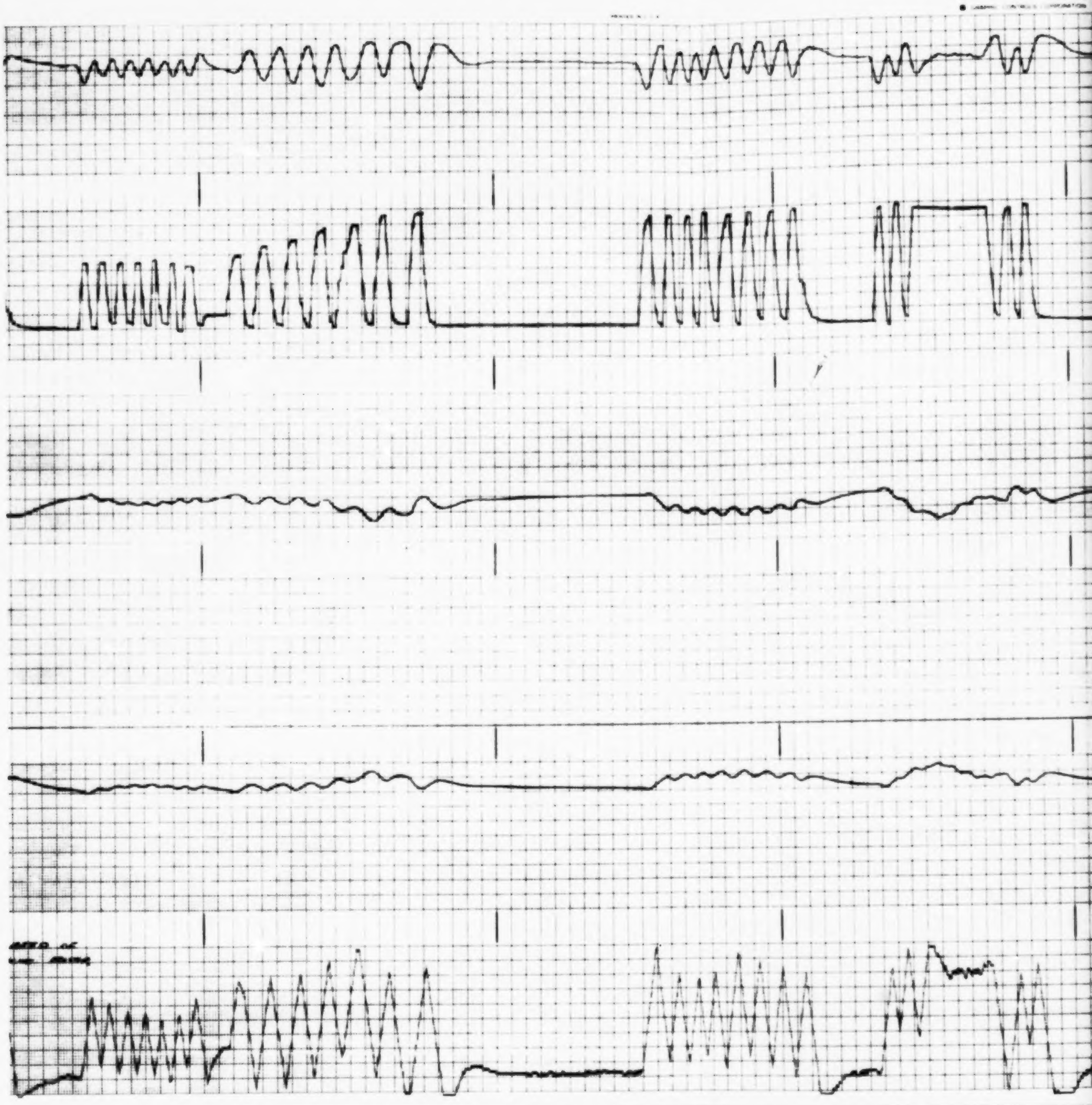

TIME IN SECONDS PER MARK

FIGURE 1

page blank

A

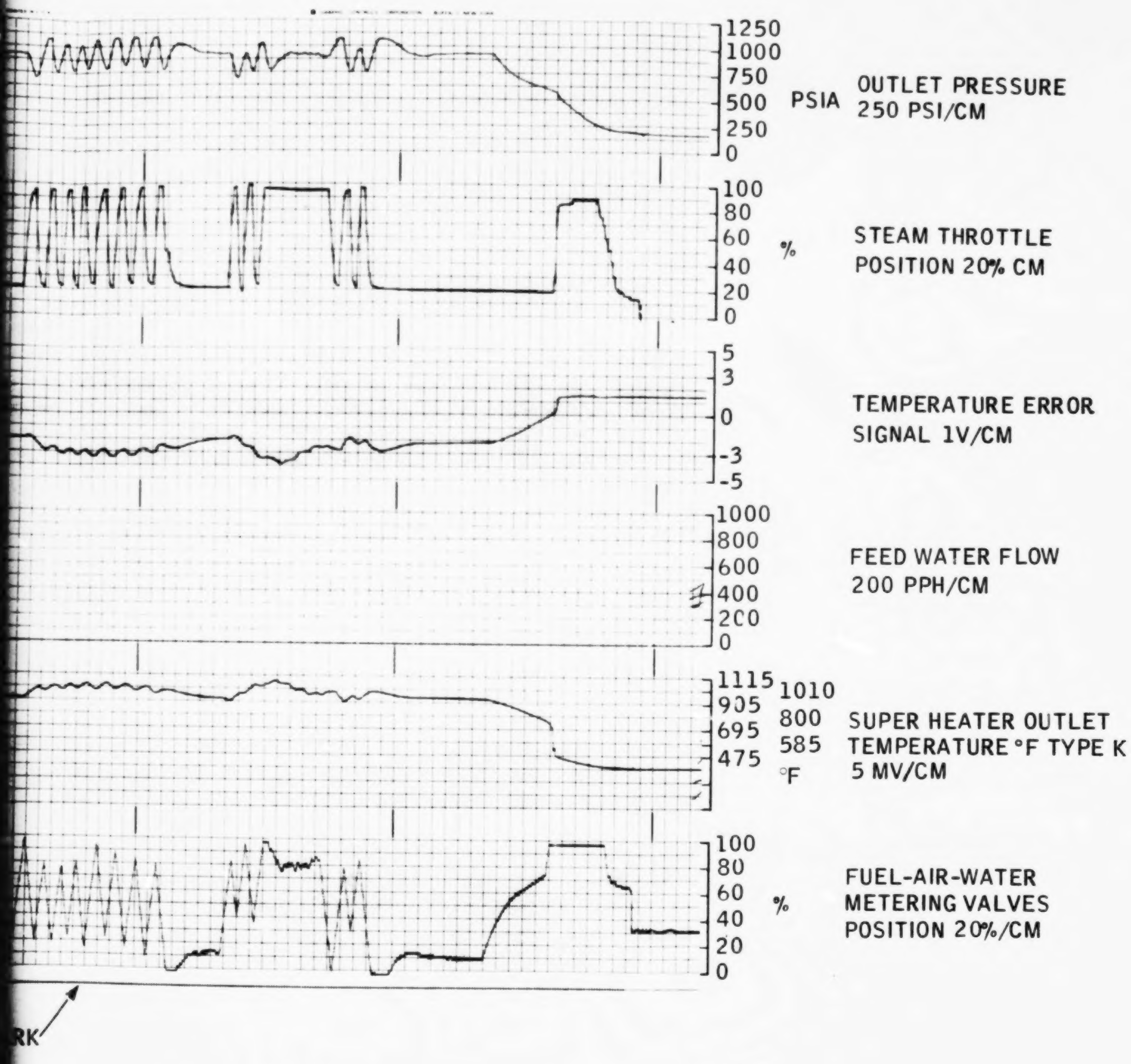

FIGURE 102. HIGH AMPLITUDE AND MAXIMUM FREQUENCY STEAM FLOW CYCLING SYSTEM RESPONSE

B

signal represents "steam flow input signal" to the basic open loop position control circuit of the triple actuator servo. A feedback position transducer on the triple valve actuator provides a nulling signal to the loop. Its position is recorded on the bottom trace with the ordinate labeled fuel-air-water metering valve position 20 percent per cm. As it can be seen from these three traces, pressure control is obtained by operation of the triple valve actuator in response to an open loop signal from the steam flow error signal (second trace labled steam throttle position) and a closed loop pressure error signal providing a proportional trim adjustment of the triple valve actuators position.

Analysis of the ramp steam flow change in the middle of Figure 99 will illustrate the basic pressure loop control sequence. Pressure prior to the steam flow change was constant at an average value shown on the data trace of 890 psia. For the controls development tests the normal setpoint used for the pressure system was 900 psia. A value lower than the design value of 1000 psia was selected to prevent possible test disruptions from overpressure safety circuit shutdowns or relief valve blowdowns. Temperature setpoint for controls experimentation was also reduced slightly below the design value to 900°F to prevent possible damage in these highly developmental phases of the program. Neither of these changes is believed to have had significant effects on the conclusions drawn from the dynamic or steady state controls tests. From the steady state operation at 890 psia a ramp disturbance in steam flow was introduced by opening the steam throttle. At a rate of approximately 5 percent per second the steam flow was dropped from 50 percent to 32 percent in approximately four seconds. It should be noted that the time scale is the bottom line on the trace. Each space between marks on this line is one second of time. Portions of this line that show up as a heavy solid line indicate the chart speed was reduced to more than one second per mm (each small division is one mm). From the chart it is seen that as soon as the steam valve is moved (thus changing steam flow) the fuel-air-water (triple valve actuator) follows with the same slope, 5 percent valve movement per second. A delay or dead time of 1.5 seconds in the steam generator's pressure response can be seen in the top trace. At 1.5 seconds from the initiation of steam flow reduction a rise in steam pressure starts its maximum overshoot in 6 seconds. At 1.5 seconds the closed loop pressure error signal adds to the open loop ramp function command and increases the slope of the triple valve actuator to 8.5 degrees per second. A maximum overshoot to 950 psia produces a sufficient error signal to cause the triple valve actuator to move to 10 percent position. Gains in the pressure loop were adjusted to have a 50 psia error signal result in a 50 percent trim correction signal applied to the triple actuator. As pressure error is corrected, the fuel-air-water metering valve proportionally follows and settles itself in approximately 16 seconds to a zero error position of 20 percent with the steam pressure stable at 890 psia.

Three of the record traces in Fig. 99 were not discussed in the above analysis of the response characteristics of the pressure loop. These three charts are basically associated with the steam temperature control loop. Superheater outlet temperature measured immediately at the outlet of the steam generator is recorded on the second from bottom trace. A type K thermocouple with an Inconel sheath 0.06 inch in diameter inserted in the steam flow is used in this measurement. It also provides a feedback signal to the temperature trim circuit. A non-linear temperature scale (for type K thermocouple) is superimposed on the mV data recorded from the temperature sensor. Temperature error (the difference between the setpoint and feedback signal) is displayed in the third from top trace. It is scaled as 1 V per cm and was used to investigate control system characteristics. Voltage recorded on this trace essentially duplicates the superheater outlet temperature variations but multiplied by a gain factor. Feedwater flow is the last trace to be discussed and is located fourth from the top. It records the linearized output from a turbine water flow meter located in the steam generator inlet water line. It is a high response measurement system and the oscillations shown in the trace appear to be actual water flow. Weight calibrations of the turbine flow meter with all conditions similar except no steam being generated in the unit do not show these oscillations. Also during startups and shutdowns, the high amplitude oscillations start and disappear with the beginning and termination of boiling in the steam generator. In addition, when the high efficiency steam generator (described in Section 7) was installed, the amplitude of these oscillations were observed to be lower by a factor between 2 to 5. A 50 cubic inch displacement accumulator is installed down stream of the pump to dampen pressure oscillations. Normal pump speed is approximately 120 rpm and being a triplex pump, its output pressure and flow oscillation is normally 6 pulsations per second. Figure 99 shows a flow oscillation an order of magnitude slower (approximately 0.5 per second). The accumulator did an effective job of damping out the normal pump oscillations. Below the prechange pressure of 400 psia, high amplitude pump oscillations were observed. When the accumulator was unseated at 400 psia oscillations disappeared. Water flow can be seen (Fig. 99) to follow the triple valve actuator position. Temperature trim effects are difficult to detect in Figure 99 since temperature variations are relatively small. Overall performance of the closed loop control system as shown in Figure 99 is a control band of ±50 psi about a pressure setpoint and a band of ±40°F about a setpoint. These are well within the goals of the program and are considered good since the transients are representative of normal driving requirements.

8.4.2 Cycling and Step Transient Performance

Figure 100 records the closed loop performance with cycling and steady state dwells. Steam flow rate is the only external disturbance to the system. Output steam flow is manually varied by opening and closing the steam throttle valve. Steam rate was 8 and 40 percent six times within 70 seconds in the center trace that produced the most severe excusions in pressure and temperature. It should be noted the time base for Figure 100 is 1 mm per second. Maximum pressure overshoot in these traces was 120 psi and 75°F above the setpoint. It should be noted that a mechanical stop was reached on the main metering valve (shown by the saturation lines at -2 percent valve position) during some of the cycles. At this condition the pressure loop is saturated, thus causing an increase in pressure. Because of introduction of auxiliary air swirler with fixed flow and the desire to maintain a fixed air-fuel ratio, fuel flow was 8 pounds per hour under this condition. As a consequence, the steam rate was actually less than the controlled corresponding mechanically limited firing rate. This was a significant contributor to the pressure overshoot at the low steam flows.

Steady state control from 10 to 100 percent is recorded in Figure 101. The time base on the left side of the trace was 0.1 mm per second for steady state performance and 1.0 mm per second during cycling transient analysis. Steam flow was stepped up from 18 to 100 percent in 5 to 10 percent increments. Steam flow was left constant for approximately 100 seconds to allow the temperature and pressure controls settle. Pressure remained within a ±25 psi band around the setpoint during this calibration. Temperature control exhibited a positive offset in the steady state control of 100°F between the setpoint at 10 percent and the controlled temperature at 100 percent. If the set point were defined at the 50 percent flow condition, a steady state temperature control accuracy of ±50°F could be assigned to the system. This offset change as a function of load was typical of all testing performed. It was apparently caused by the fact that the water metering cam had significant steady state errors with respect to the fuel metering cam profile. A high proportional loop gain would eliminate this mechanical error, however, a relatively low gain was necessary to prevent oscillations during transients. Addition of integral mode control also gave significant improvements (some results showed control within ±10°F), however, it was also destablizing and was only used at very low gains.

Transient response tests were performed by stepping the steam rates from high flows. The feedwater flow meter was disconnected from the Sanborn during these tests since a manual valve was required to connect two different turbine flow meters into the system to measure both high and low flow ranges. Flow was only passed through the large turbine meter to prevent damage to the low flow unit. As it is seen from the trace, the noise output from the large meter is of high amplitude when the flow goes below 300 pph. Step changes show the typical overshoot in pressure expected in a test loop with low volume (40 cubic inches) between the steam generator and throttle valve. Upon closing the throttle steam flow drops almost instantaneously. However, generation of steam is still at original levels until the fuel flow is dropped and energy distributions in the metal tube matrix can be rebalanced. As a result steam pressure rapidly rises causing an error signal to trim the triple valve actuator to further reduce fuel flow. A pressure overshoot of 150 psi above the 900 psia setpoint occurs when rapidly closing the steam throttle from 85 to 20 percent. The bottom trace shows the overshoot to saturation that occurs due to the high pressure signal driving the valve into its mechanical stop. Exactly the opposite sequence of events occur when the throttle valve is rapidly opened. From Figure 101 the magnitude of the pressure drop is seen to be -150 psi before the control system restores the output pressure to its new steady state valve. From the traces it is apparent that the pressure loop is highly damped with no tendency to oscillate.

An explanation of the major cause of the pressure overshoot and undershoot can be seen in the transient cycles at the right of Figure 101. The throttle valve was opened and closed as fast as the screw jack actuation mechanism would allow. Throttle valve rates as high as 50 percent per second were recorded. The first five cycles the triple valve actuator speed was 15 percent per second (or only about 30 percent as fast as the throttle valve). A small increase in actuator velocity gain was made in the last few cycles by changing the drive motor output speed from the control panel. A small but significant reduction in the magnitude of the pressure overshoot resulted by this gain change. It is theorized that the magnitude of the pressure overshoot is associated with the lag between the rate at which steam flow is changed and the corresponding response of the triple valve actuator. As the actuator velocity is increased, a better instantaneous match between output steam flow and input firing rate is achieved. Variation in temperature and pressure are normal and cannot be fully eliminated with a single control mode. Water level for steady state operation moves towards the inlet of the unit as steam rate is decreased (see Appendix VII). Thus a rapid closing of the throttle valve from high steam flow conditions to low flow results in the steam generator operating at a low power condition with a water level higher than normal steady state levels. As a consequence, outlet steam temperature will be lower than normal until the controls correct the situation. The opposite sequence occurs in going from low to high power rapidly. Water levels with an increasing power step transient are now lower than steady state thereby giving effectively greater length to the superheater. As a consequence, outlet steam temperature will increase until corrections to the closed loop temperature control system raise the water level back to the normal high power level. It should be noted that these corrections require many seconds since the changes in water level are dependent on feedwater flow rates. Another factor to be noted is that with a fully modulated control the response time at low powers is much lower since feedwater trim control rates are made proportionally lower to allow stable operation. As can be seen from the temperature traces, these are inherent characteristics of the system with a single control mode (feedwater rate only). These can be partially eliminated by use of a separate trim control with an auxiliary water injection for desuperheating. However, the control is sufficiently accurate to not require the added complexity and efficiency loss associated with desuperheating.

Maximum possible steam flow cycling rates were imposed on the system as a final proofing for the controls. Operation of the steam throttle was limited to the cycling rates shown in Figure 102 by its manual screw jack actuation fixture. However, these cycles are considered more severe than could be imposed by an automotive service. Dwells at high and low flows after a series of cycles were maintained until the controls stabilized pressure and temperature. From the performance trace it is seen that peak to peak pressure excusions were at levels of as high as ±200 psi with normal peaks about ±150 psi. Temperature variations were less than ±100°F about a mean temperature line although they reached a peak of 150°F above the nominal setpoint of 900°F.

Evaluation of the transient response characteristics of the fuel and air control systems performance was made during the high velocity cycling. Each of the emissions was plotted by a strip chart recorder during the eight high velocity steam flow transients in the center of Figure 102. Figure 103 shows the results with zero time starting on the right hand side. The relatively constant emission line at the right of each figure is a record of the emissions during the steady state operation of the unit with the steam throttle at 21 percent (see Fig. 102). Eight cycles between 21 and 96 percent steam throttle position follow. As was discussed in Section 5, a cam drive between the air valve and fuel valve schedules the air-fuel ratio leaner at low powers. This is a programmed variation and is best analyzed by reference to the CO_2 trace. As it is seen, the syncronization between the air and fuel control system is relatively good. The rounding off of the minimum and maximum peaks is indicative that the CO_2 cell cannot respond rapidly enough to give an exact value of the instantaneous CO_2, but it does fall within the bounds normally expected for the steady state values of CO_2 at the extremes of the cycling. It should be noted that the variation in CO_2 (air-fuel ratio) peak values follows very closely the triple valve actuator position on the bottom trace of Figure 102. The first peak (left one on Fig. 102 and right one on Fig. 103) are both the highest with the fourth one being the next highest. This type of correlation indicates good syncronization between air and fuel flow controls. Emissions are placed on Figure 103 in order of response of the particular analytical system. NO_x measurements by chemiluminescent techniques (Appendix I) were the slowest and are shown at the top of the figure. As discussed in Section 5, decreasing the air-fuel ratio (increasing CO_2) causes an expected increase in NO with a decrease in CO and HC. Corresponding data points are shown on the curves with emission limits shown in the table. As it can be seen, only NO is a problem during these severe transients. However, its characteristics

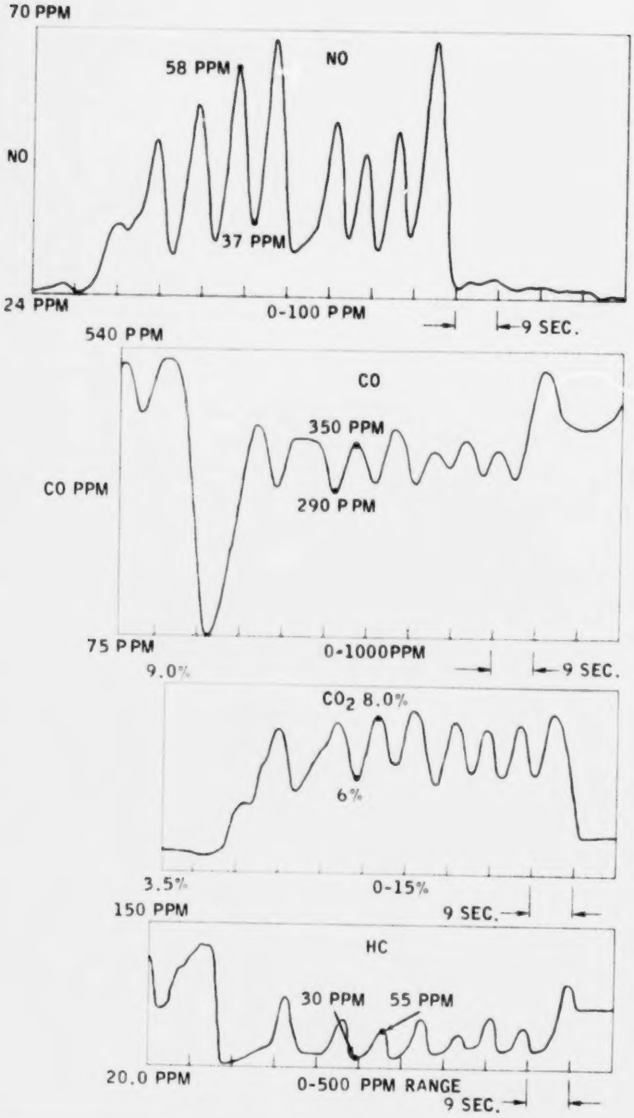

Power Level (%)	CO_2 (%)	CO (ppm)		NO (ppm)		HC (ppm)	
		Actual	Limit	Actual	Limit	Actual	Limit
90	7.7	290	462	60	31	30	120
20	6.15	350	377	35	26	60	84

FIGURE 103. TRANSIENT EMISSIONS DURING PEAK STEAM GENERATOR CYCLING (See Fig. 102)

are very similar to the steady state situation in which the emissions are borderline at low flows and exceed limits at high flows. From this it is concluded that the air-fuel ratio control is basically satisfactory and can maintain reasonably accurate control of air-fuel ratios during severe and continuous transient operation.

8.5 HIGH EFFICIENCY MONOTUBE STEAM GENERATOR PERFORMANCE

Initial tests with the monotube steam generator indicated slower than expected response characteristics. Open loop tests were performed to measure some of the characteristics. A steady state condition was obtained on the steam generator with both temperature and pressure loops opened. While at a steady state temperature and pressure the water flow was manually increased by 50 percent for approximately 10 seconds. Through these step tests the triple valve and the throttle valve were maintained at fixed positions of 20 percent. Figure 104 shows the results. Temperature had a 30 to 40 second dead time before effects of the step change were observed. Pressure responds in approximately 10 seconds. A sinusoidal open loop response test was also performed (Fig. 105). Both pressure and temperature loops were opened. A sine wave voltage signal was imposed on the amplifier controlling the position of the differential pressure regulator. Feedwater input to the steam generator follows the sinusoidal in phase.

Output response of the steam generator is shown by the sinusoidal disturbance to the outlet temperature. Input frequency was set at 0.01 cycle per second to cause a sustained response from the steam generator. Note that a high frequency input had no effect upon temperature. The amplitude of the temperature response to the flow variation input was ±15°F. A phase lag of 135 degrees in the temperature response was measured. These tests and closed loop transient response indicated the need for a lead compensation in the temperature control loop. A derivative amplifier operating the proportional error signal added anticipation into the circuit to improve performance and stability. Figure 106 shows the improvements made by addition of rate compensation in the foreward temperature control loop. In the center of the trace a step change in throttle position from 15 to 52 percent shows a typical temperature transient characteristic with a relatively low gain derivative circuit. During the next step up in steam flow the derivative circuit was removed leaving only a proportional amplifier in the system. As it is seen, the addition of a relatively low gain derivative compensator significantly reduced the magnitude of the overshoot and reduced the settling time to approximately one half of the value in the uncompensated characteristic. Further development optimization of this circuit was not possible due to time schedules, but significant improvements seem likely.

Figure 107 shows the response of the control system on the monotube unit to high velocity cycling of the steam throttle. As in the discussion of the parallel flow unit, the speed of response of the triple valve actuator is not sufficient to prevent a large mismatch between steam flow rates and firing rates. This factor combined with the low discharge volume between the steam generator and throttle valve produce the pressure oscillations in the output steam. Higher response and a larger volume (test volume was 40 cubic inches in tubing to throttle valve) will reduce the magnitude of the pressure excusions. Temperature responded in a similar manner to the parallel flow with the inherent water level mismatch between high and low flow contributing to temperature fluxuations. Response to step changes in throttle valve position are shown by Figure 108. Good pressure loop characteristics are shown in these results but a tendency to oscillate in the temperature loop. It should be noted that some experiments with integral compensation were being performed in this test sequence causing greater tendencies to oscillate.

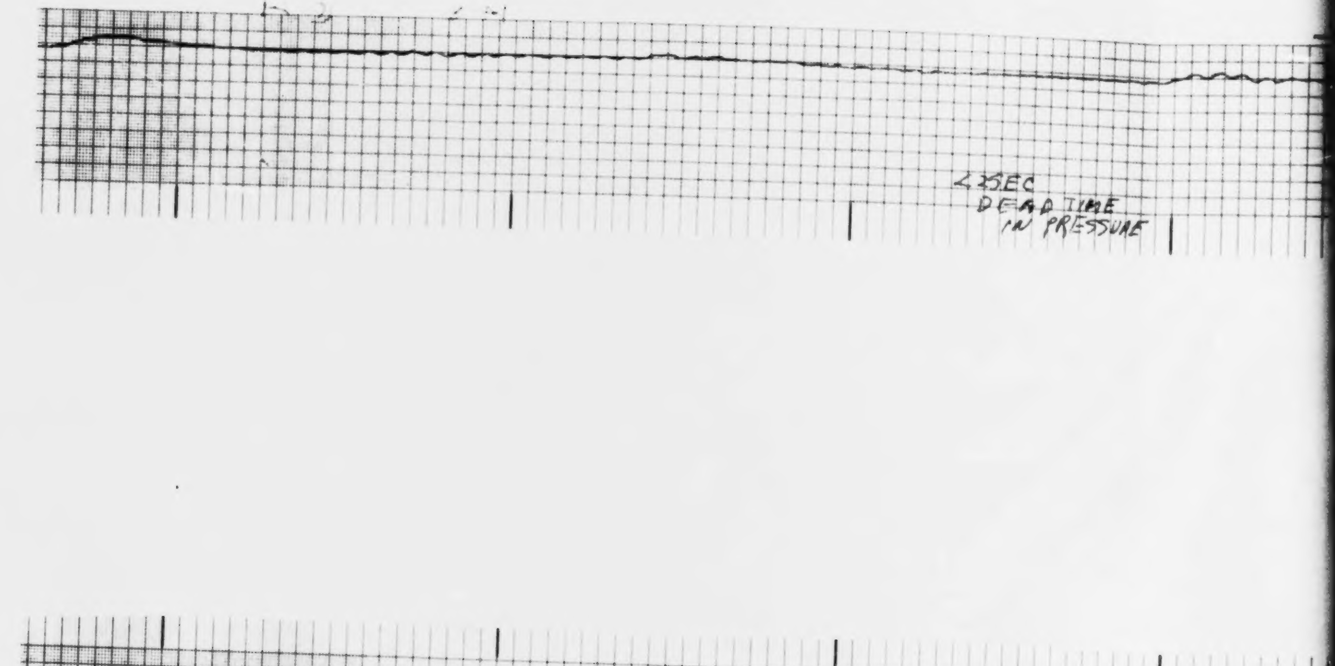

TIME IN SECONDS PER MARK

Preceding page blank

FIGURE

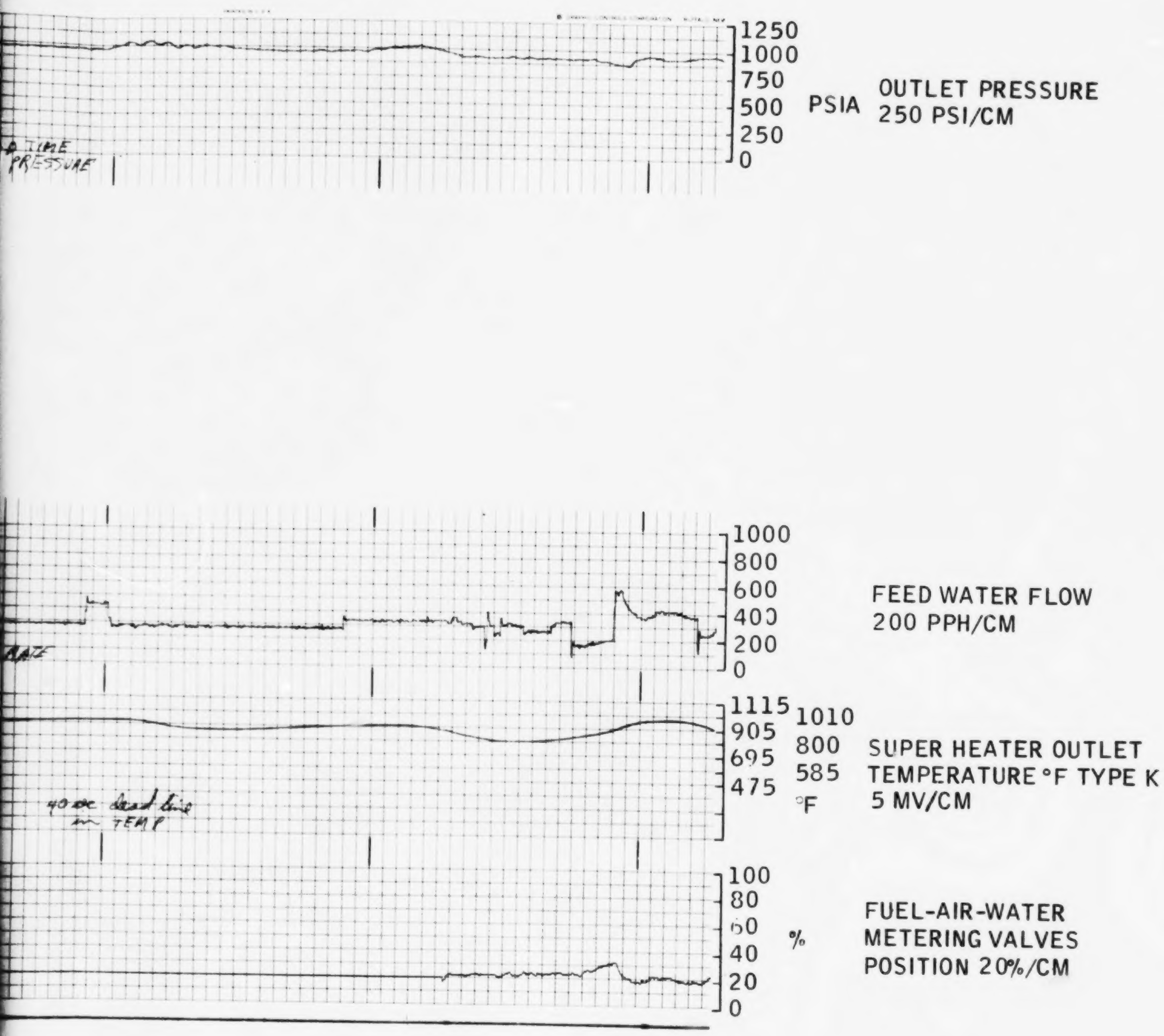

NDS PER MARK

FIGURE 104. OPEN LOOP CHARACTERISTICS TO STEP INPUTS IN WATER RATE

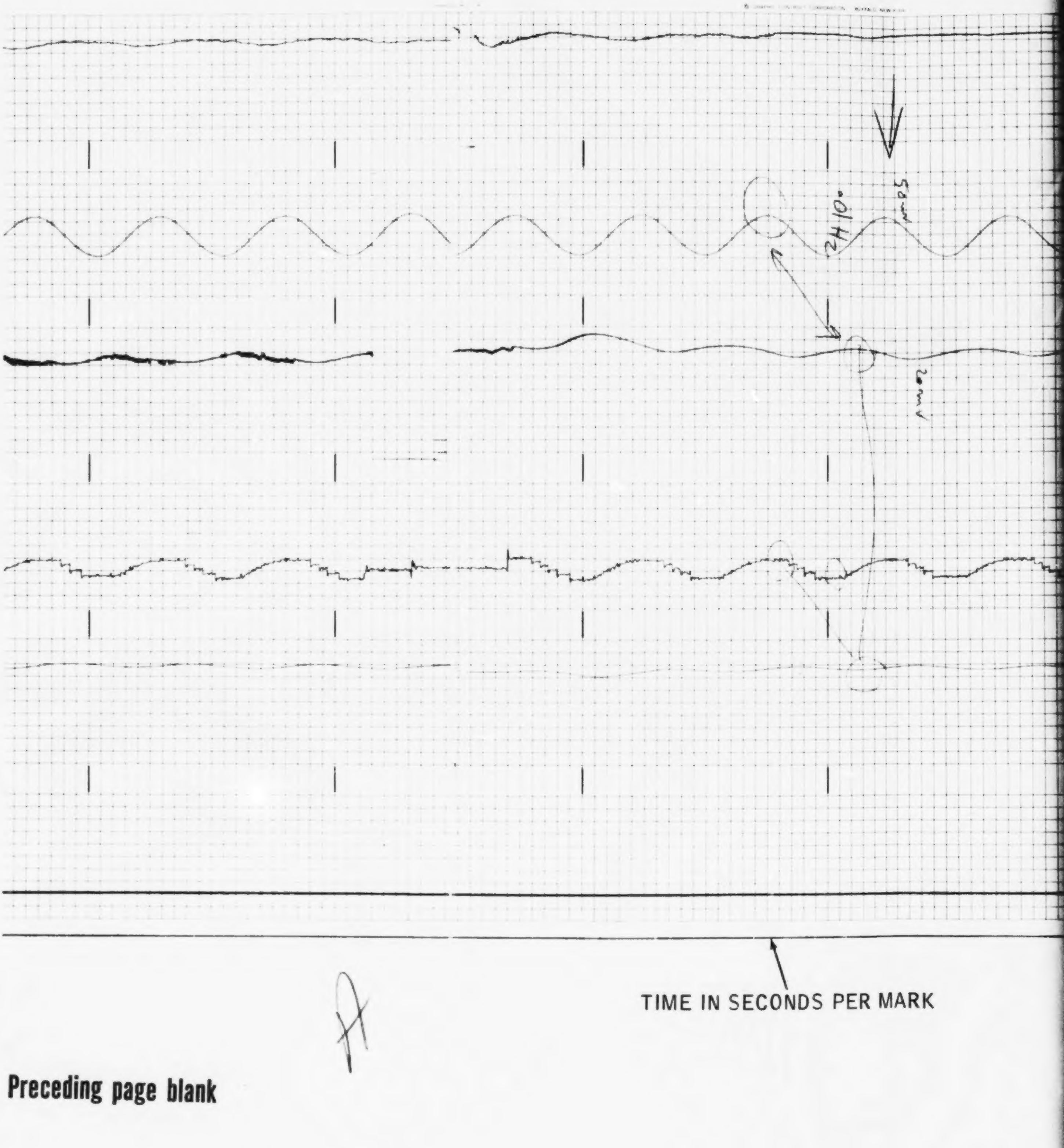

TIME IN SECONDS PER MARK

Preceding page blank

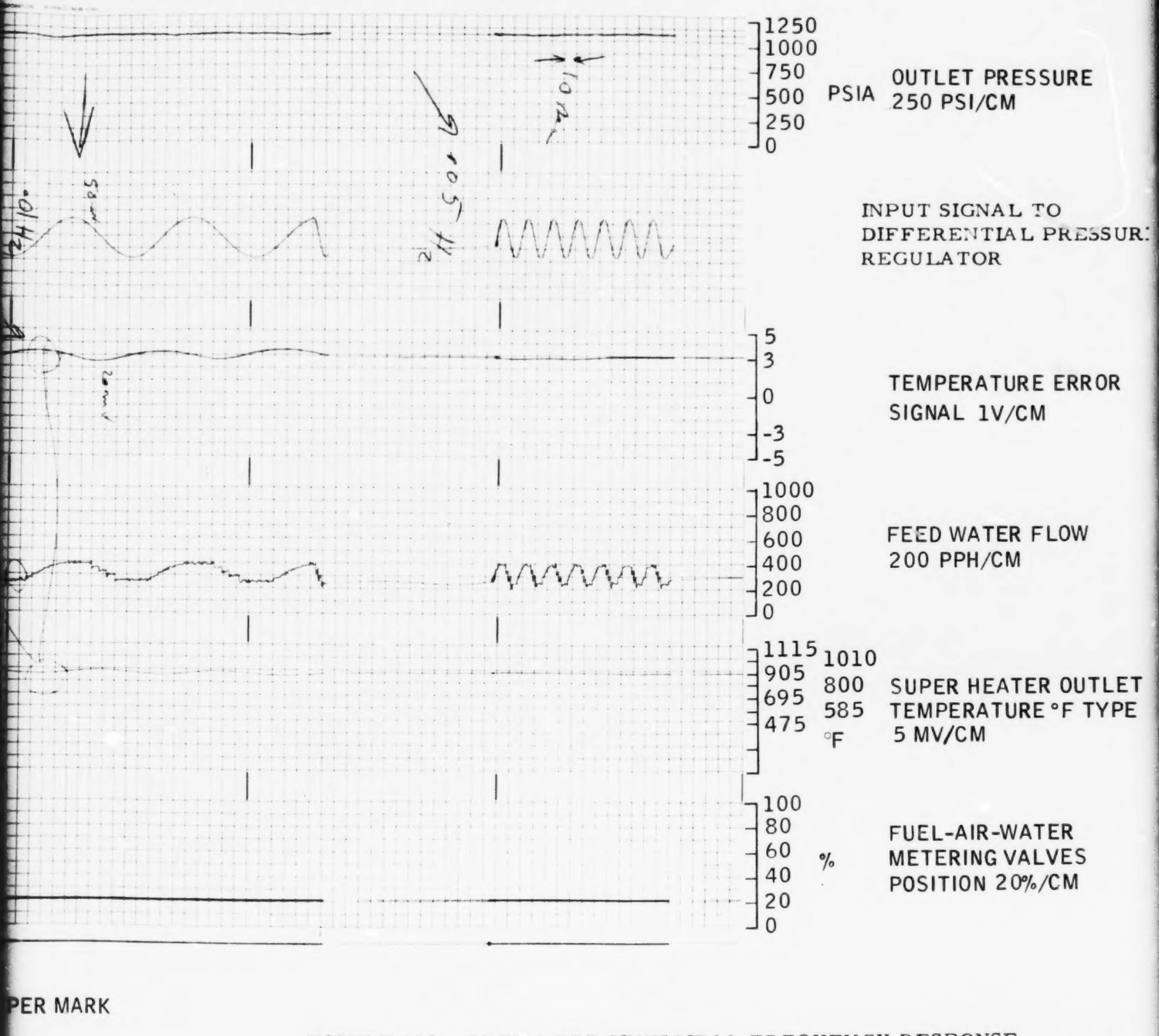

FIGURE 105. OPEN LOOP SINUSOIDAL FREQUENCY RESPONSE

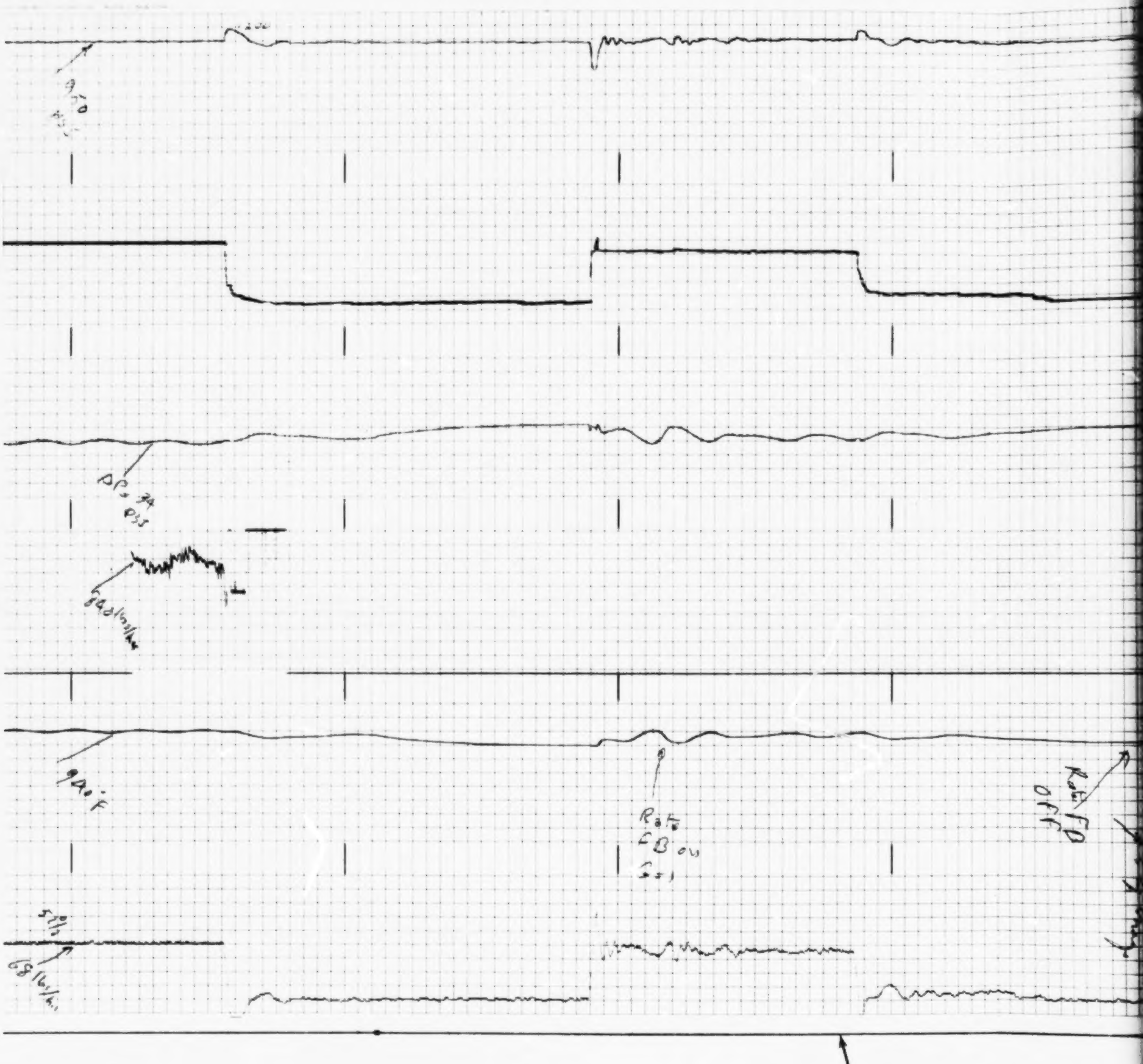

Preceding page blank

A

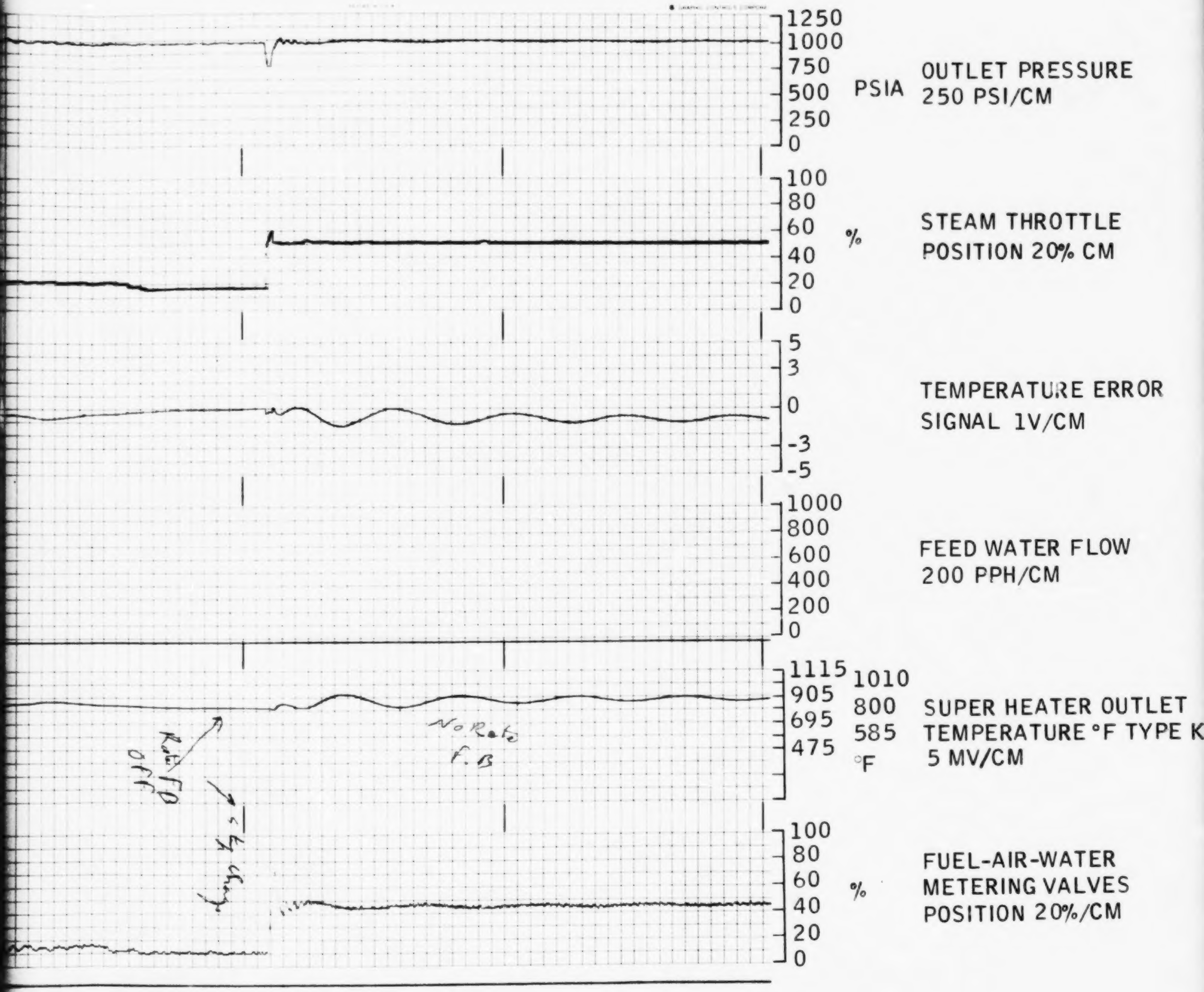

ER MARK

FIGURE 106. CLOSED LOOP TRANSIENT RESPONSE WITH AND WITHOUT DERIVATIVE COMPENSATION

B

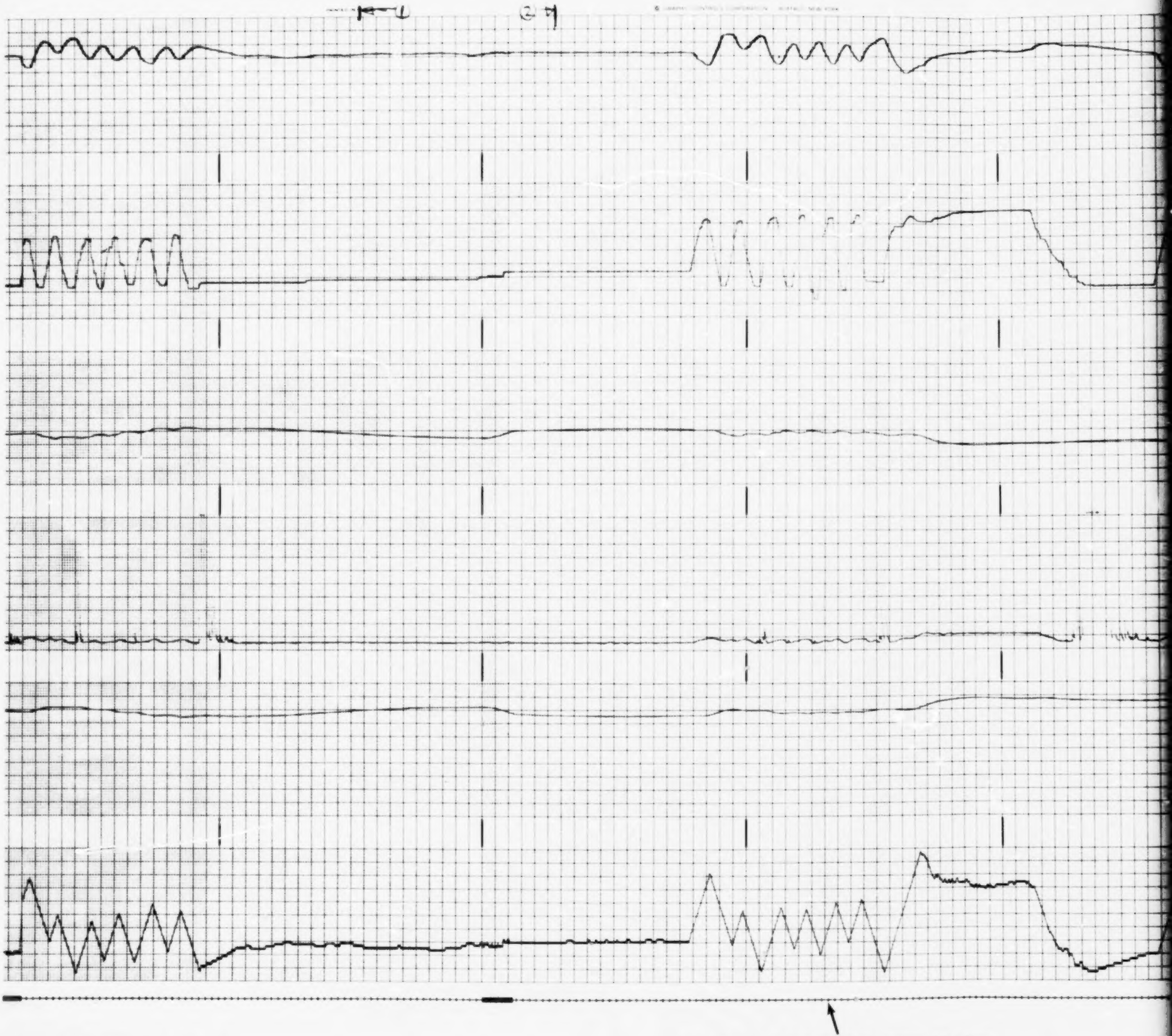

TIME IN SECONDS PER MARK

Preceding page blank

A

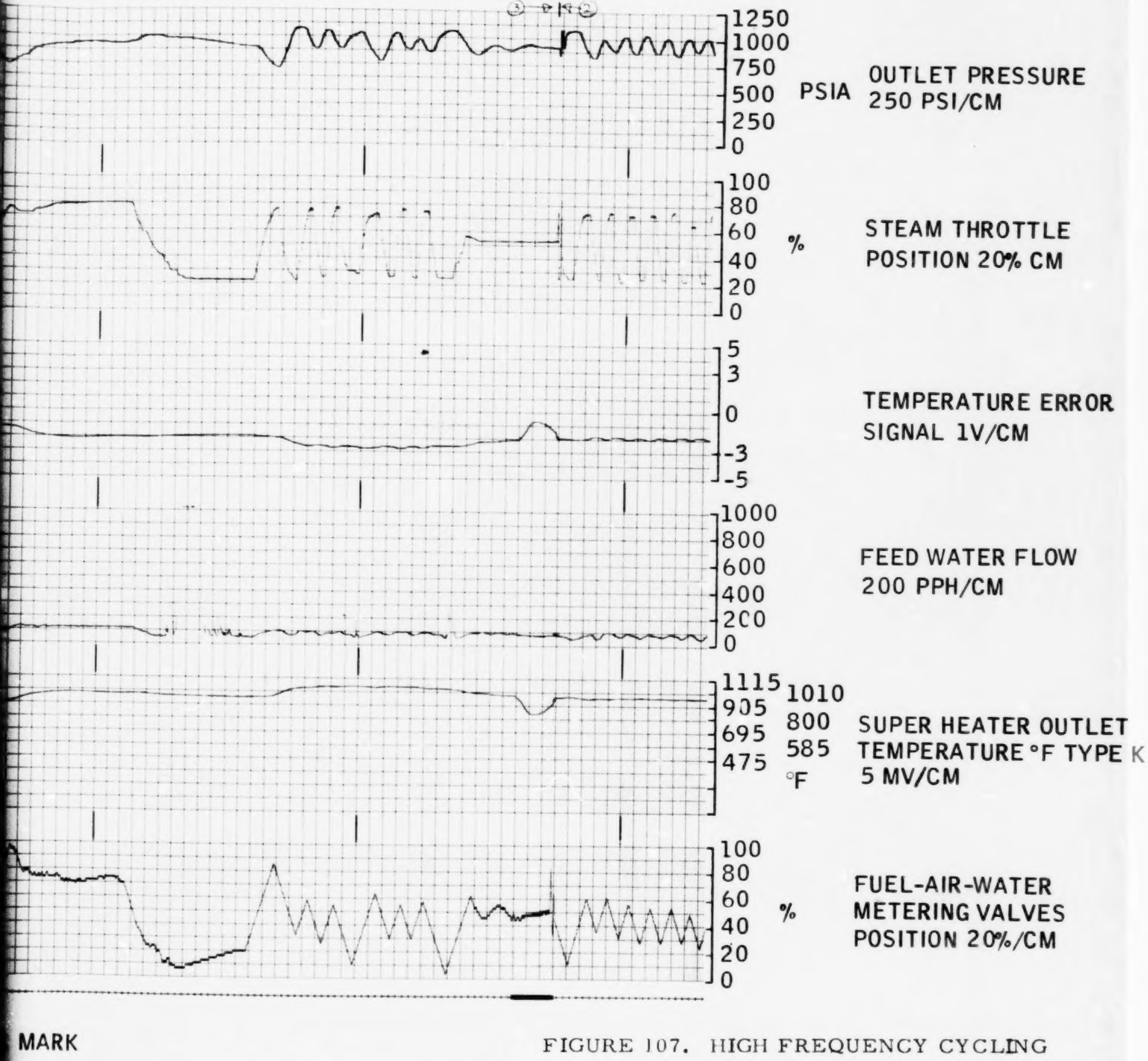

FIGURE 107. HIGH FREQUENCY CYCLING

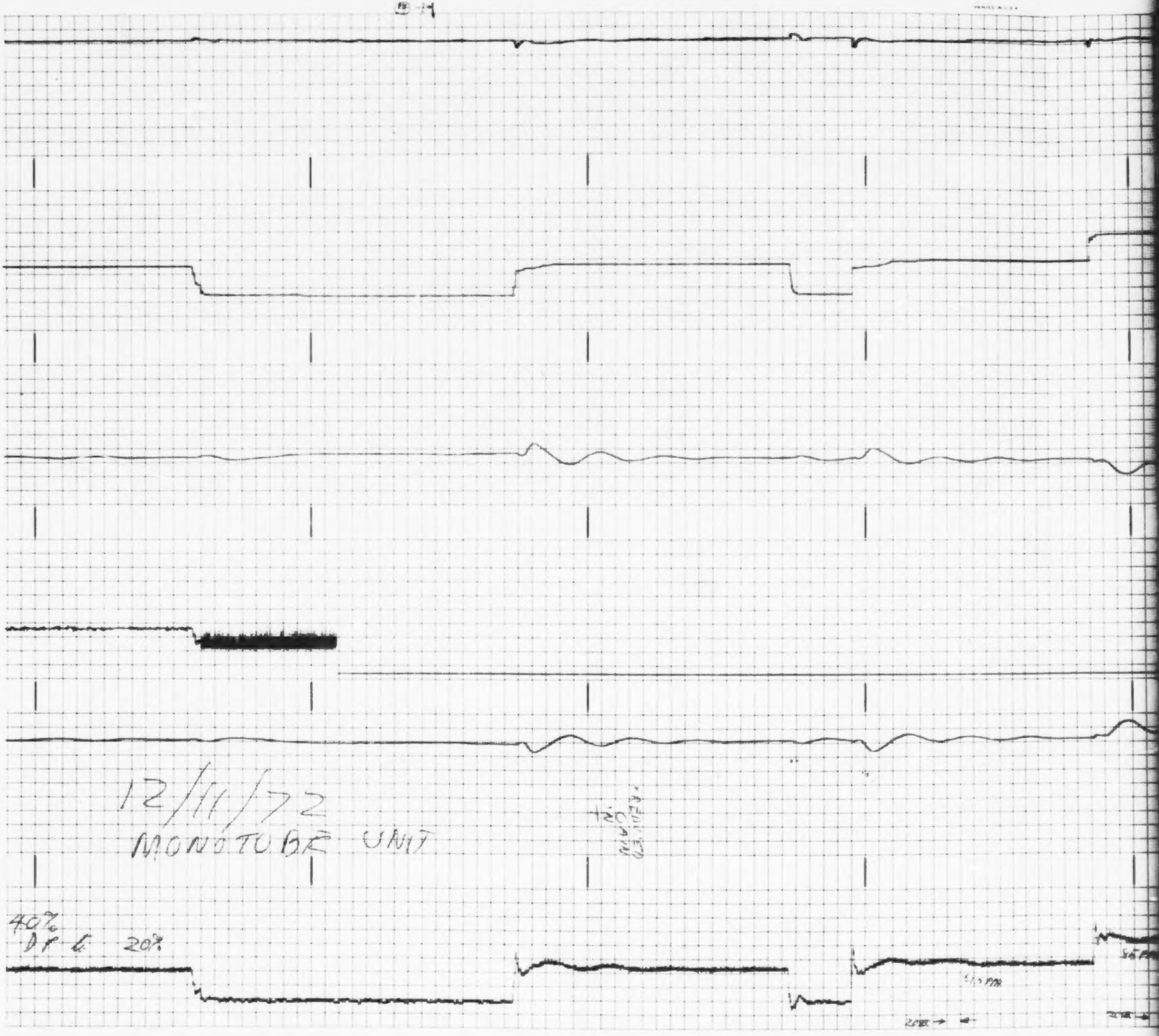

TIME IN SECONDS PER MARK

Preceding page blank

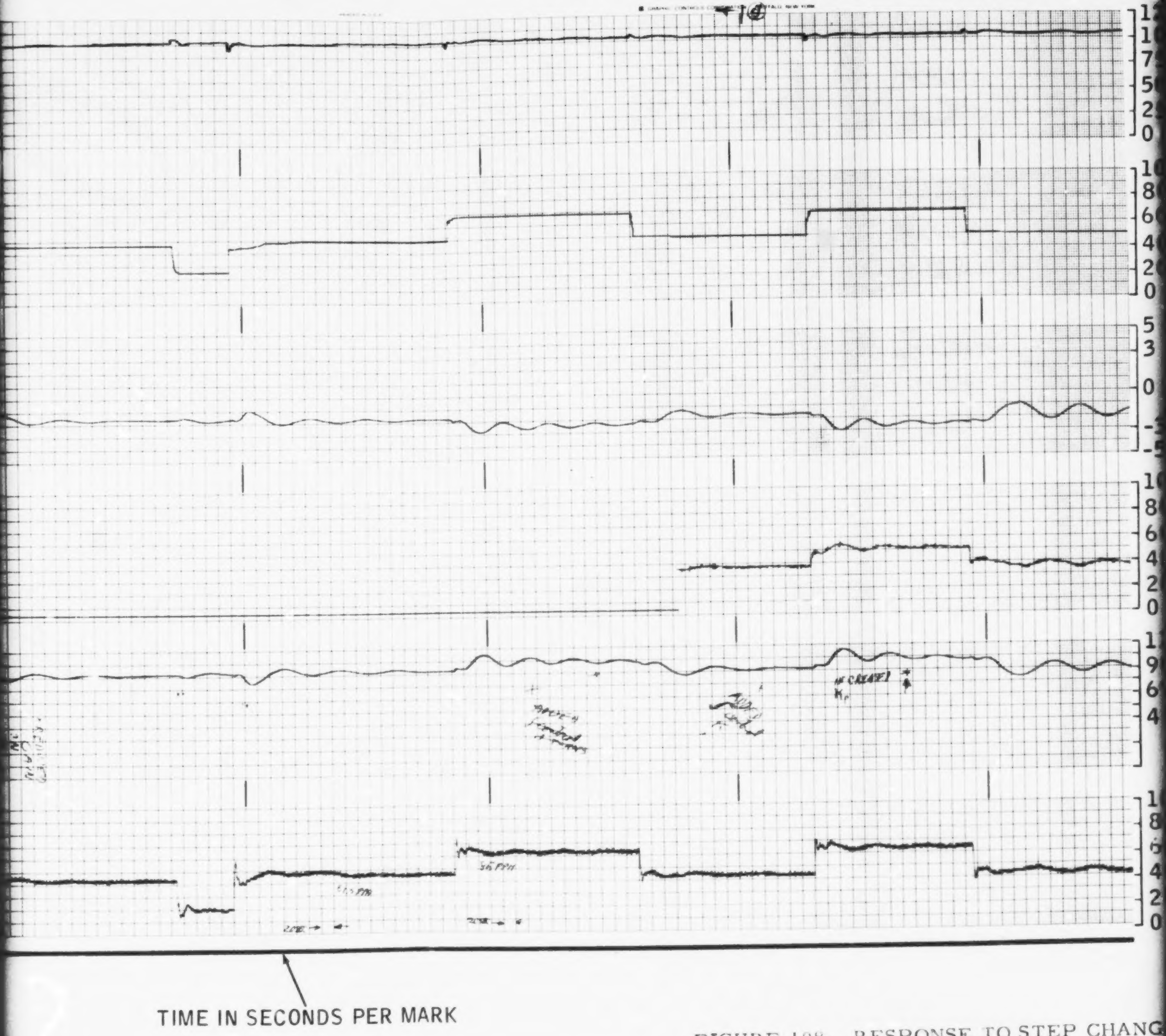

FIGURE 108. RESPONSE TO STEP CHANG

B

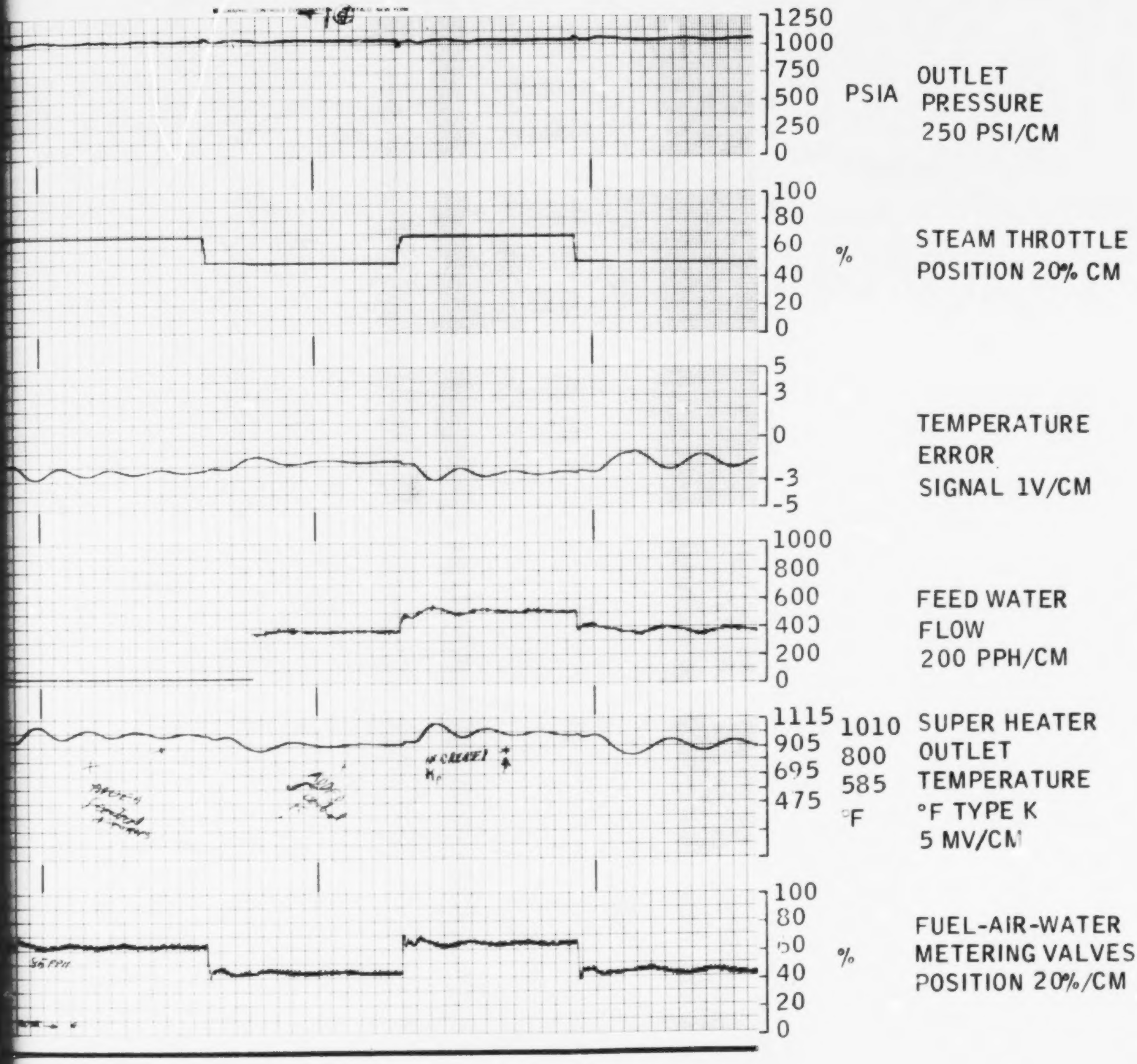

FIGURE 108. RESPONSE TO STEP CHANGES IN STEAM FLOW

B

C

9

ORGANIC SYSTEMS

To provide a possible backup system for the EPA contractors, two organic systems were designed. A Fluorinol-85 system was designed to fit within the packaging constraints of TECO's power plant. AEF-78 was used in the second unit integrated into Aerojet's vehicle constraints. Vapor generator core analysis, combustor design modifications, and detail designs of the steam generators were completed in this portion of the program. Geoscience Limited performed the core analysis for the organic systems (see Appendix VIII). No parts of the system were assembled, only critical long lead time tubing for the core matrix was procured.

9.1 FLUORINOL-85 SYSTEM DESIGN

The general flow arrangement for the vapor generator is shown in the schematic below:

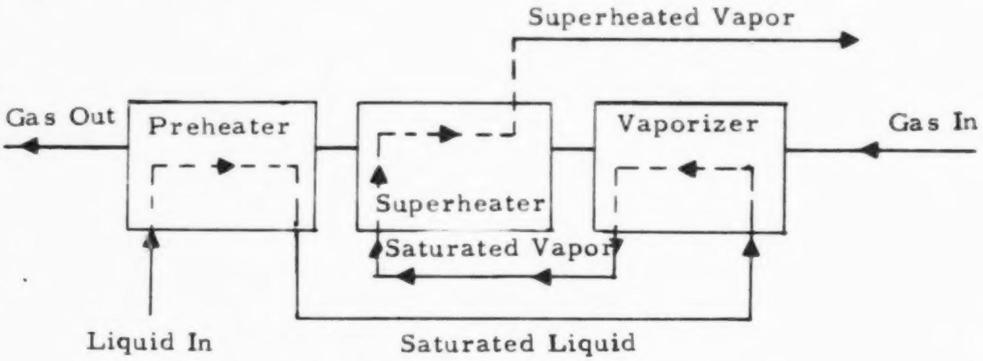

As shown, the working fluid flow arrangement is counterflow in the preheater and the superheater, but is parallel flow in the vaporizer. The superheater is located between the vaporizer and the preheater. This arrangement requires a larger heat transfer area to achieve a given efficiency than a pure counterflow arrangement, but it makes the problem of preventing overheating of the superheater tube walls much more tractable.

Preceding page blank

9.1.1 Design Constraints

The design constraints for this unit were as follows:

F-85 Side

Flow	10,000 lbm/hr
Pressure Drop	130 psia maximum
Outlet pressure	700 psia
Inlet temperature	287°F (at max. power)
Outlet temperature	550°F
Heat transfer rate to organic	2.25×10^6 BTU/hr (reference)

Gas Side

Air-fuel ratio	25:1 (JP-5 fuel)
Flow	3740 lbm/hr
Pressure drop	3.0" H_2O
Outlet pressure	atmospheric
Inlet temperature	2500°F (mean) ±250°F
Efficiency	81% based on HHV 86.5% based on LHV (reference)
Outlet temperature	427°F (reference)

Maximum tube wall temperature was restricted to 575°F. Maximum temperature for all other parts of the core was to be consistent with structural requirements for the materials used. Maximum temperatures were to be based on the assumptions that the gas side inlet temperature is 2750°F, and the velocity at the gas side inlet plane of the vapor generator is 10 percent above the design value.

The vaporizer unit maximum outer dimensions were to be 15 inches width by 25 inches length by 8 inches core depth.

9.1.2 Core

The preheater consists of 10 rows of 45 tubes each. The tubes are 1/4 inch OD by 0.020 wall thickness, and are made of low carbon steel. The tubes centers have their longitudinal and transverse spacing equal to 1.25 tube diameters, or 5/16 inch. The tube rows are staggered, as shown in the sketch below.

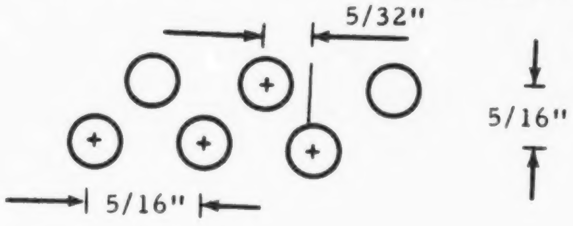

All tubes, in preheater, vaporizer, and superheater, are 22 inches long, leaving approximately 1-1/2 inches on each end for headers and manifolds. The total outside area of the preheater tubes is 53.9 ft^2.

The vaporizer consists of 2 rows of 21 tubes each. The tubes are 1/2 inch OD by 0.030 wall thickness, with 16 internal longitudinal fins 0.030 inch thick by 0.056 inch high. The tube rows are staggered, as in the preheater. The longitudinal and transverse spacings of the tube centers are the same, at 0.675 inch. The tubes are made of low carbon steel. Low carbon steel was chosen as the tube material for three reasons: it improves the heat transfer characteristics of the internal fins, it is possible to fabricate in the internally finned configuration required, and it is amply strong at the low tube wall temperatures required. The internal fins were necessary in order to keep the tube wall temperatures below the specified 575°F maximum. As an additional measure to prevent tube wall overheating, the tubes are protected by a 0.010 inch radial thickness air gap, formed by placing a 0.530 inch OD by 0.005 inch wall thickness AISI type 310 stainless steel tube concentric with the internally finned tube.

The superheater uses three rows of 21 tubes each. The tube spacing, tube material, and internal fin arrangement are the same as for the vaporizer. The superheater tube walls are protected from overheating by a 0.020 inch air gap, formed by placing a 0.550 inch OD by 0.005 inch wall thickness AISI type 321 stainless steel tube concentric with the internally finned tube. The gas side heat transfer area in the vaporizer and superheater, based on the outside area of the 1/2 inch OD tubes, is 25.4 ft^2.

The working fluid side pressure drop is estimated as 89 psi. This includes an allowance for pressure drop in the manifolding. The gas side pressure drop is estimated to be 4.3 inches of water. It appears that the working fluid side pressure drop will be well within 130 psi maximum allowable, while the gas side pressure drop will be in excess of the 3.0 inches of water initially specified.

9.1.3 Manifolds

The manifolds are subject to several conflicting requirements. They must fit within the required envelope, they must be able to withstand the temperatures and pressures to which they will be subjected, and they must direct the flow in the manner required by the core design.

The flow arrangement must satisfy the conflicting requirements that the working fluid velocities be high enough to prevent overheating of the tube walls, but low enough to prevent excessive pressure drop on the working fluid side.

For the first eight rows of its passage through the preheater, the working fluid flows in parallel through the 45 tubes of each row. At the end of each of these rows it passes through a simple return bend manifold, which directs it through the next succeeding row.

For the last two rows of the preheater, local gas temperatures are high enough so that liquid flow velocities must be increased in order to prevent overheating of the tube walls. The flow is redirected so that it passes through only fifteen tubes in parallel, and each tube row consists of three liquid flow passes.

To accomplish the change from 45 to 15 flow tubes in parallel, a simple reducing flow manifold is used. Groups of three adjacent tubes are manifolded across each other and then up to single tube in the next row. Within the row simple return bends then connect each subsequent tube to provide the 15 parallel flow tubes in rows 8, 9, and 10. From 10 the fifteen parallel passages must be connected to the seven parallel flow passages in the vaporization section. The flow from the 15 tubes on the preheater outlet is connected by 6 passages to a common header that feeds the seven vaporization tube inlets. Experience from the test bed system assisted in the decision to place the seven flow restrictors at this point in the manifolding. Liquid phase flow is ensured at this position and thus controllable pressure drops are more likely than the inlet to the superheater (as in the test bed system).

There is no collector manifold at the vaporizer outlet. Instead, the flow is carried in seven parallel passages to seven tubes of the first row of the superheater. (The "first" row is here defined as the first row through which the fluid passes, which here is the row with the coolest local gas temperatures.) The superheater flow is then in seven parallel passages with three passes in each tube row, just as in the vaporizer. As in the vaporizer, this flow is maintained by a complex system of simple return bends.

A collector manifold is provided at the superheater outlet, from which the working fluid is carried to the expander.

9.1.4 Combustor and Air Valve Design

In order to package within the engine compartment of the TECO power plant, it was necessary to redesign the combustor and air valve to fit within a 20 inch diameter envelope. A rectangular 15 by 25 inch vapor generator was also the largest frontal area unit that could be coupled to the 20 inch diameter combustor. Figure 109, 110 and 111 are envelope layouts of the front, side and top view compared to the TECO vapor generator outline drawing. Basic to the approach taken is the goal of obtaining the largest possible diameter for the combustor combined with the largest frontal area

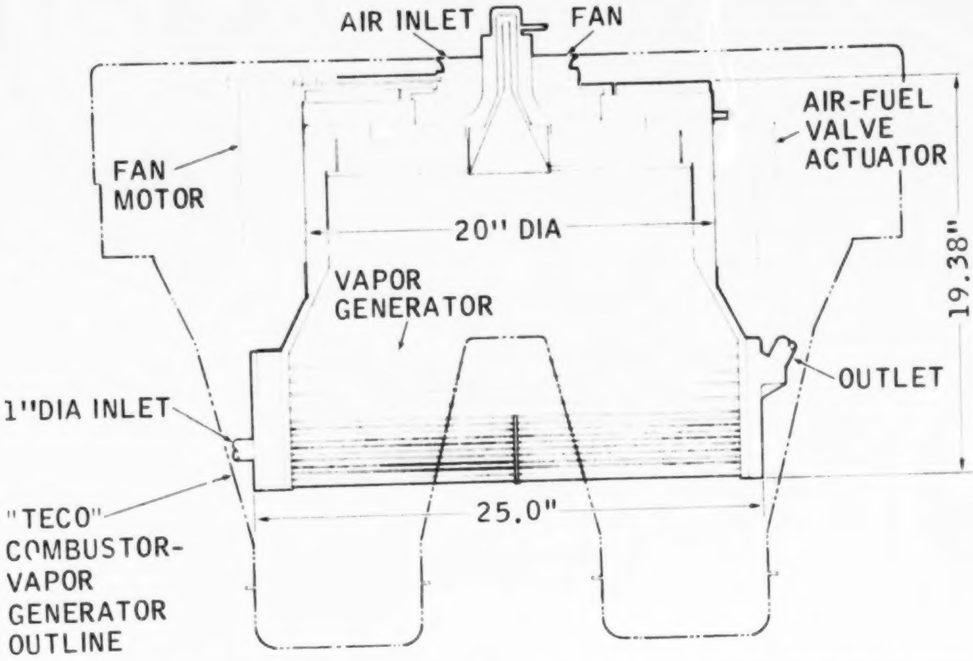
AIR INLET
FAN
AIR-FUEL VALVE ACTUATOR
FAN MOTOR
20" DIA
19.38"
VAPOR GENERATOR
OUTLET
1"DIA INLET
"TECO" COMBUSTOR-VAPOR GENERATOR OUTLINE
25.0"

FIGURE 109. FLUORINOL-85 COMBUSTOR/VAPOR GENERATOR (FRONT VIEW)

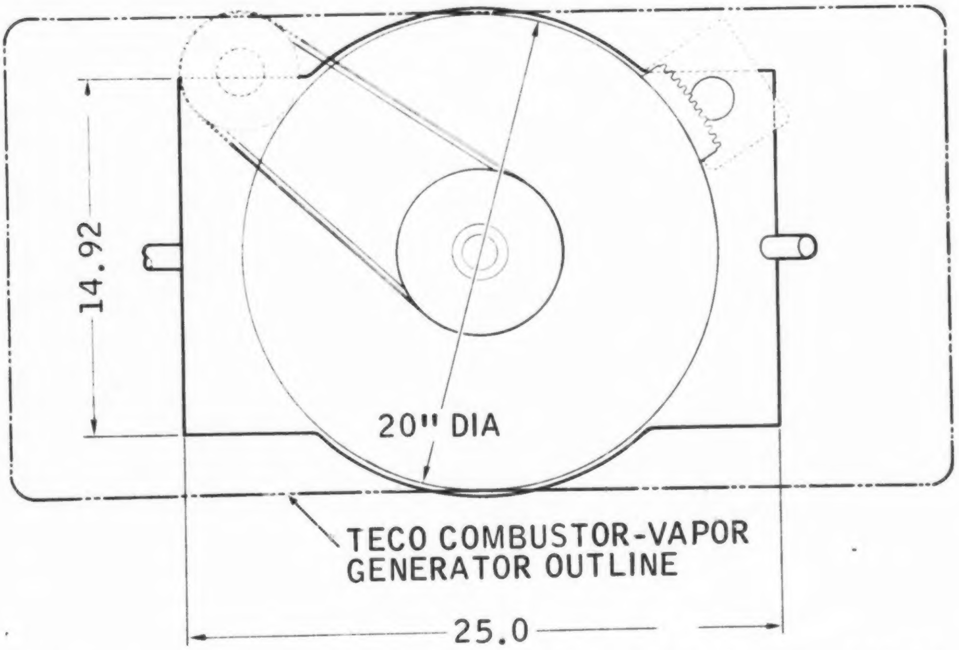
14.92
20" DIA
TECO COMBUSTOR-VAPOR GENERATOR OUTLINE
25.0

FIGURE 110. FLUORINOL-85 COMBUSTOR/VAPOR GENERATOR (TOP VIEW)

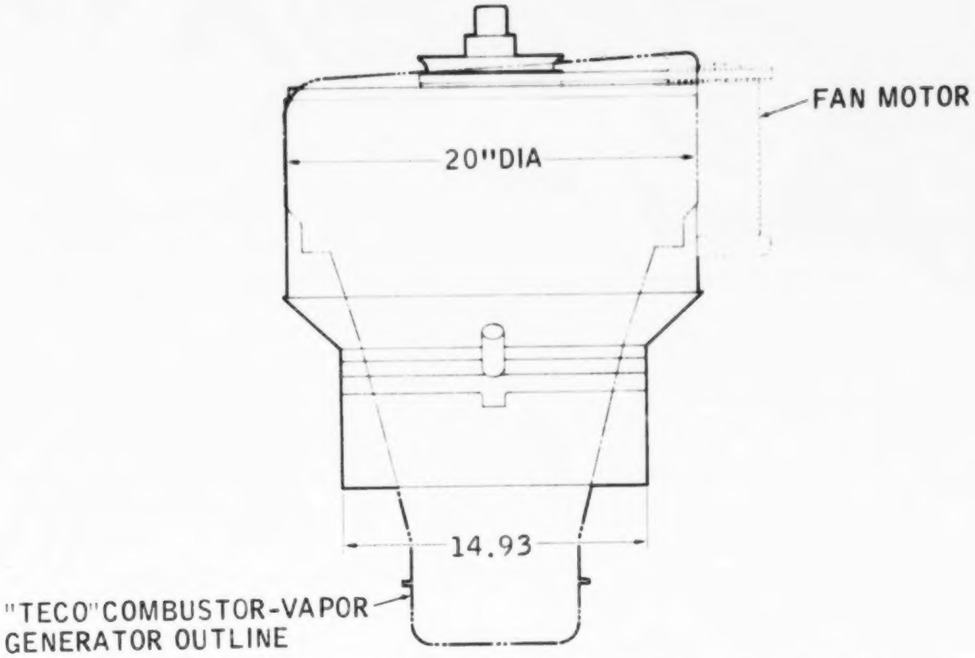

FIGURE 111. FLUORINOL-85 COMBUSTOR/VAPOR GENERATOR (SIDE VIEW)

vapor generator. Symmetrical aerodynamic flow between the combustor and vapor generator with a minimum area transition are design features incorporated to minimize emissions and provide uniform stable air flow. The basic configuration and design approach for the air supply, air metering, atomization and combustion subsystems is the same as tested on the "test bed system" (See Section 5). Air enters at the fan inlet coaxially mounted to the combustor and fuel atomization rotating cup. A symmetrical air valve having 20 ports (10 each for primary and secondary air) controls the air flow circumferentially and axially into the combustor. Immediately before entering the primary zone, combustion air is caused to swirl by ten swirl vanes. A 28 volt DC motor is mounted at any circumferential position around the combustor to assist in packaging or installation. A second electric motor drives the air valve positioning gear to control air and fuel flow into the combustor. In a similar fashion to the fan drive motor the rotary fuel air-valve actuator can be placed in any circumferential position around the combustor to assist with envelope or reduce condenser fan air blockage.
As shown both the fan motor and fuel-air valve actuator would be at the rear of the package thereby reducing their effects on condenser fan air blockage.

Air Metering Valve Design

Because of space limitations with a 20 inch diameter combustor, it was not possible to design a linear air valve. Although several advantages are available with a linear design, one of the most important is a relatively low sensitivity to leakage at the 40 to 1 turndown flow point. The close-off height of the ports in this valve have been made as small as possible to help reduce sensitivity at the low flows. Thus a given angular displacement will produce a relatively small flow change. Since equal flow is essential through each port, this feature is of key importance in the valve's design.

The design parameters are:

- Fan diffuser section remains uninterrupted up to 13.5 inch diameter
- 11.3 inches water pressure is available at fan discharge
- Combined combustor/vapor generator pressure drop (excluding metering orifice) is equal to 9.3 inches of water
- The range 0-56.7% full flow is comprised of primary flow only and primary flow remains constant at 56.7% of full flow at 56.7-100% power setting
- Coefficient of discharge is assumed 0.5 for the entire range
- Full air flow is to be 3740 lb/hr
- At 100% flow, 43% of the air flows through the secondary ports

From these constraints the following was decided upon:

- Primary port height should remain constant for 0-56.7 full flow with the exception of the low end of this range which was modified for more sensitivity
- Secondary port height was made constant in the 56.7-100% full flow range
- Primary port should gain increments of area in the 56.7-100% range to compensate for combustor pressure loss
- Primary port will not close at leading side in range of 56.7-100% flow

- Ten sets of metering ports will be used

- Primary 0-56.7% shall include a travel of 7 degrees and secondary (56.7-100%) valve rotation of 10 degrees

Sample Calculation

The port shape is obtained by an incremental flow area analysis that proportions secondary and primary flow with corresponding pressure drops across air valve and combustor/vapor generator pressure drops.

- Area sizing of 65.6 percent power setting

- Pressure across metering orifice is

$$\Delta P = 11.3 - 9.3 \ \frac{65.6}{100}^{2} = 7.3 \text{ inches water}$$

- Secondary flow is to be:

$$\left(\frac{65.6 - 56.7}{43.3}\right) 1620 \text{ lb/hr} = (0.20)\ 1620 \text{ lb/hr}$$
$$= 5.4 \text{ lb/min}$$

The following flow relationship is used in area calculation

$$Wa = 7.617\ K_{Am} \sqrt{\gamma(P_1 - P_2)} \qquad (66)$$

where

Am = in^2 (area of orifice)
γ = lb/ft^3 (density at standard conditions)
Wa = lbs/min
ΔP = inch of H_2O
K = coefficient of discharge

$$Am_s = \frac{Wa}{7.617\ K\sqrt{\gamma(P_1 - P_2)}} = \frac{5.4}{7.617\ (0.5)\ \ 9.076 \times 7.3}$$

$$= 1.94 \text{ sq. inch}$$

Flow area for each of the secondary ports is 0.194 in^2 in the 65.6 percent valve position. At 65.6 percent port height, h_s, of secondary is 1.125 inch and thus to opening width is 0.172 inch. The corresponding height of the primary port is therefore equal to $h_s(Rs/Rp)(A_{mp}/A_{ms}) = 1.125 \times (9.313/8.00)(0.072/0.19)$ where A_{mp} is incremental area to be added to existing primary area to maintain 35.4 lb/min flow. This is determined through equation (66).

R_s and R_p are effective radii of secondary and primary port areas respectively.

The air metering port configuration determined through this method is shown in Figure 112. The valve is positioned at 56.7 percent full flow.

Exhaust Gas Duct

Since the Solar unit fires down, while the TECO unit fires upward, it was necessary to do some preliminary design work to ensure that Solar's exhaust ducting would be compatible with envelope constraints imposed by the engine compartment and by other components in the system. One of the most severe of these restraints is imposed by the number two cross member, just aft of the vapor generator, and the system components just above it. It appears that the most convenient and acceptable location for the exhaust duct to pass aft is through the shear web of this cross member.

A preliminary calculation was made to determine if it would be possible to turn the exhaust flow aft in the space available between the vaporizer core outlet and the number two cross member. In addition to space constraints, the exhaust duct must satisfy the requirements that it produces low pressure losses and causes no serious gas flow maldistributions in the vaporizer core.

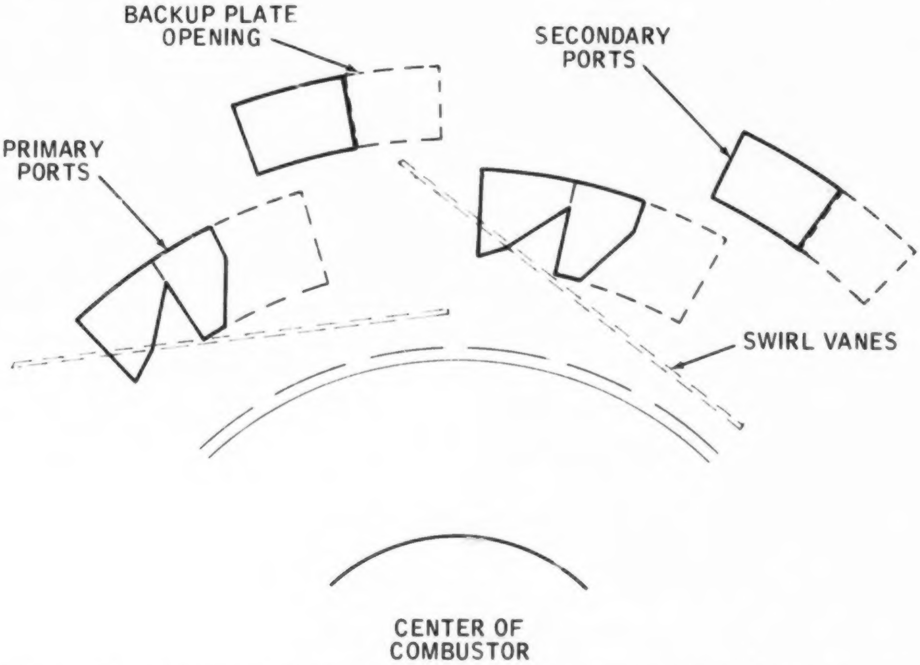

FIGURE 112. FLUORINOL-85 SYSTEM AIR METERING VALVE SHOWN IN 56.7 PERCENT POSITION

It was found that the maximum dynamic head to which the flow could be accelerated without a danger of flow maldistribution in the core was 0.43 in. H_2O. This corresponds to a duct area of 45.1 in^2, or 22 in x 2.05 in inside dimensions. It appears that a duct of these dimensions could easily pass through the shear web of the number two cross member. The minimum bend dimensions necessary for such a duct to achieve low losses are shown below:

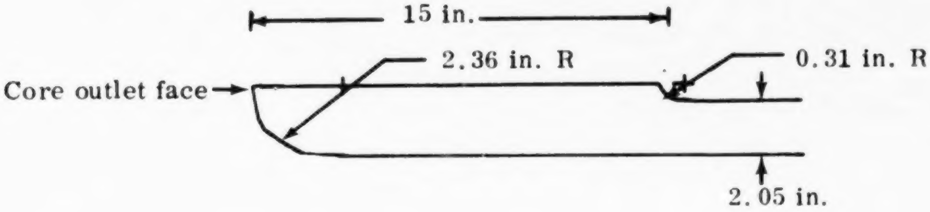

The duct is a constant, 22 in wide. It is seen that, because of the accelerating flow, very little turning space is required in order to achieve low losses.

9.2 AEF-78 SYSTEM DESIGN

Aerojet's engine compartment envelope constraints allow the use of a combustor configuration of 26 inches outside diameter. Operation of the test bed system's combustor at fuel flows up to 140 pph indicated the unit was adequate for the 135 pph fuel flow required by Aerojet's AEF-78 combustor and air supply control system. Figures 113, 114 and 115 show the integration of the 23 inch combustion system with the rectangular vapor generator. A simple aerodynamic flow system has been emphasized with a minimum of flow area changes and no bends or turns in the combustor or vapor generator. As in all of the designs, aerodynamic symmetry is emphasized to the greatest extent possible, while using the largest possible face area for the vapor generator.

Solar completed a detailed design of the heat exchanger incorporating a core matrix established through a subcontract to Geoscience Ltd (see Appendix VIII). The heat exchanger tube arrangement is a simple cross counter flow with all plain tubes on the gas side (no insulation or extended surfaces are used). From inlet to outlet the matrix consists of seven rows of plain 0.25 inch diameter, 0.02 inch wall, carbon steel tubes. These tubes are arranged in a staggered array with an axial and transverse pitch of 1.25 times the diameter of the tube. Sixty tubes are in each row for a total of 420, quarter inch tubes. All tubes in each row are manifolded together by simple return bends to provide sixty parallel flow passages. The remainder of the matrix consists of four rows of internally finned 0.5 diameter tubes, 30 to a row. Each row is manifolded in a manner to provide three sets of ten

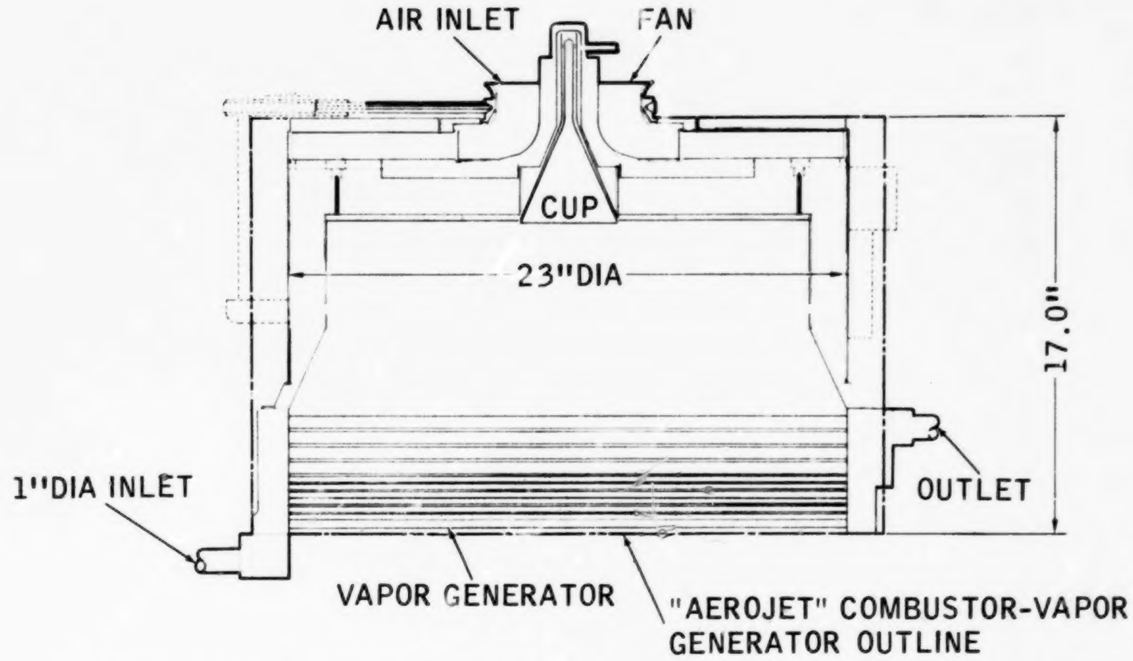
AIR INLET
FAN
CUP
23"DIA
17.0"
1"DIA INLET
OUTLET
VAPOR GENERATOR
"AEROJET" COMBUSTOR-VAPOR GENERATOR OUTLINE

FIGURE 113. AEF-78 COMBUSTOR/VAPOR GENERATOR (FRONT VIEW)

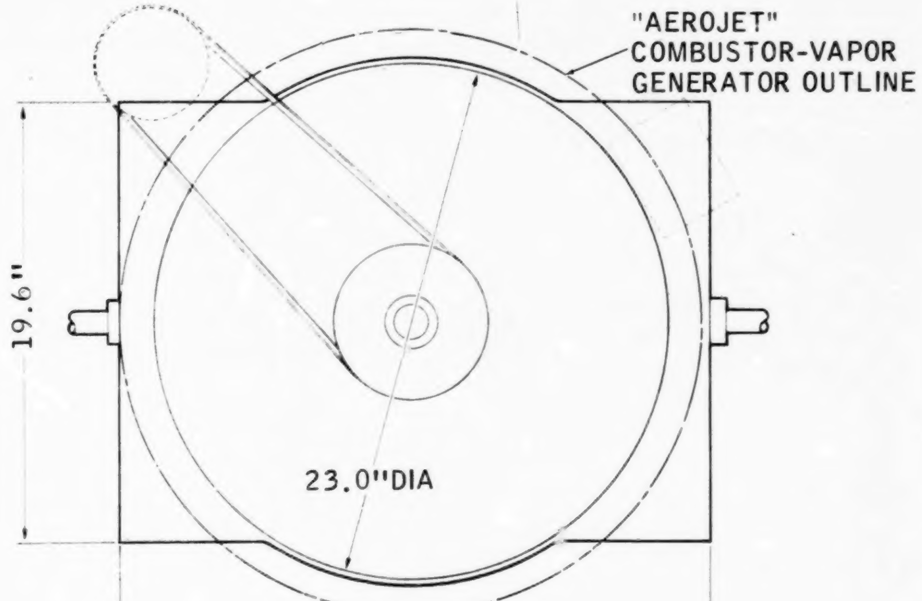
"AEROJET" COMBUSTOR-VAPOR GENERATOR OUTLINE
19.6"
23.0"DIA
26.4"

FIGURE 114. AEF-78 COMBUSTOR/VAPOR GENERATOR (TOP VIEW)

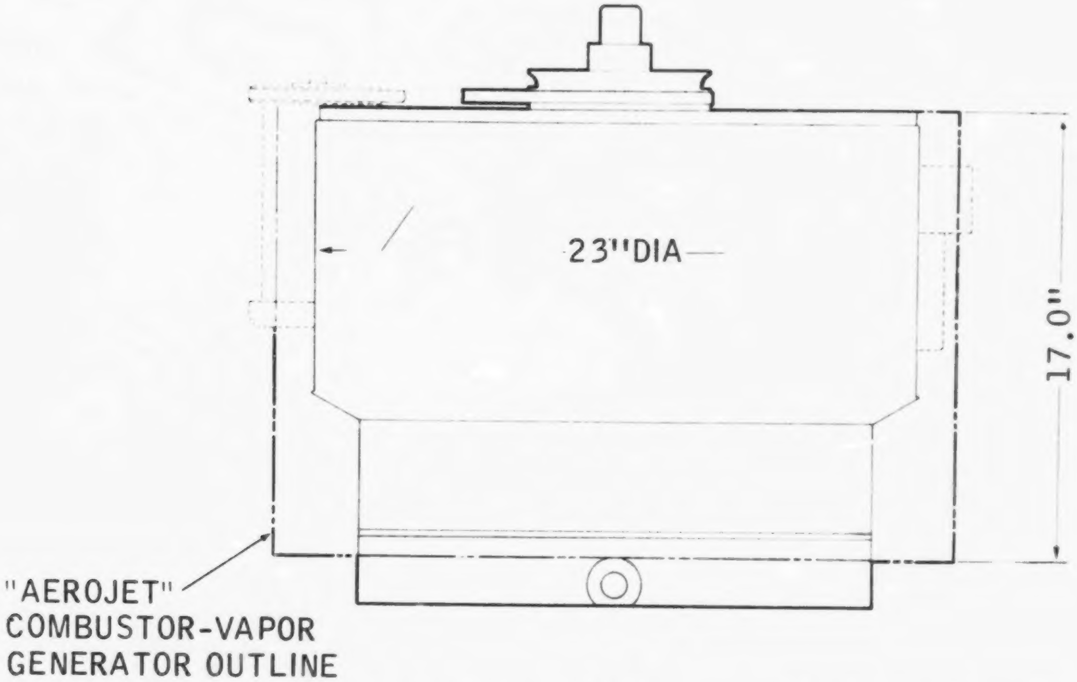

FIGURE 115. AEF-78 COMBUSTOR/VAPOR GENERATOR (SIDE VIEW)

parallel flow paths per row. Fins on the inside of the tubes are straight and parallel to the axis. Sixteen fins are equally spaced inside the tube. Fin height is 0.056 inch by 0.03 inch thick. These fins and the higher velocity fluid flow ensure that the tube wall temperature at the outlet row (adjacent to the combustor) will not exceed 720°F. Other characteristics of the unit are:

AEF-78 Side

Flow	19,300 lb/hr
Outlet pressure	1000 psi
Pressure drop	20 psi
Inlet temperature	396°F
Outlet temperature	650°F
Heat transferred to AEF-78	2.02×10^6 BTU/hr
Efficiency (based on LHV)	82.2%

Gas Side

Outlet temperature	550°F
Flow	3500 lb/hr
Pressure drop	2.9 inches of water
Inlet temperature	2500°F

9.3 INTERNALLY FINNED TUBING

The French Tube Division of Noranda Metal Industries has produced samples of internally finned tubing which appear to be satisfactory. These tubes are necessary in the design of the Fluorinol-85 and AEF-78 unit. These tubes required a special fabrication development effort since they are unique in design.

Tubing samples were examined under magnification. Some small cracks were found, but they did not appear severe enough to affect either the rupture strength or the low cycle fatigue life of the tubing. Photographs of some of the worst cracks are shown under 50X and 500X magnification in Figures 116 and 117.

Three samples of the internally finned tubing were heated to 900°F for 10 minutes and then quenched in water repeatedly for a total of 18 cycles, then pressurized at room temperature until they burst. The bursting pressures were 8,000 psi for two of the samples, and 7,500 psi for the third. Based on nominal wall thickness and typical room temperature properties for low carbon steel, the samples should have burst at 7,020 psi. All samples showed considerable gross yielding before they burst.

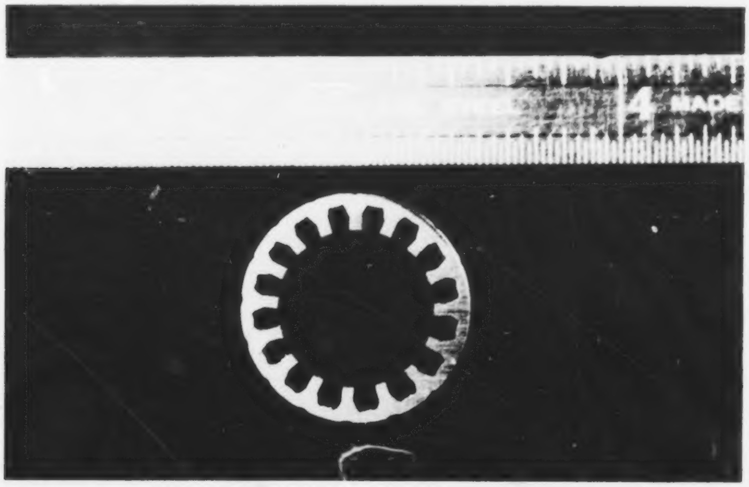

FIGURE 116. TUBE CROSS SECTION

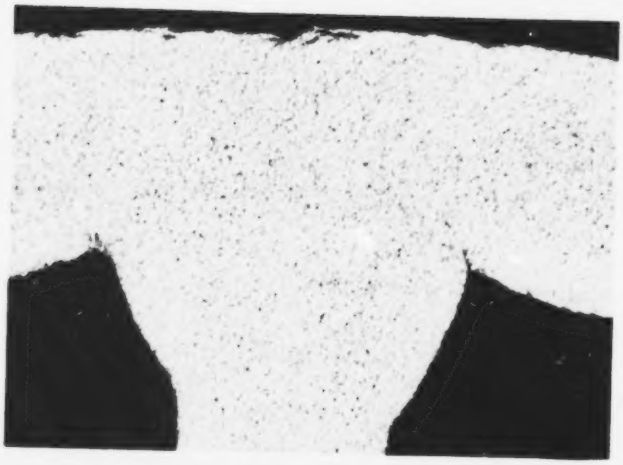

A.

Magnification: 50X
Etchant: Nital

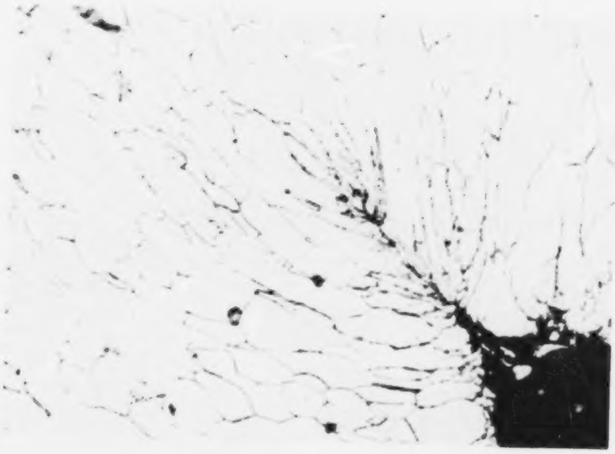

B.

Magnification: 500X
Etchant: Nital

FIGURE 117. PHOTOMICROGRAPHS OF TUBE-FIN WALL (page 1 of 2)

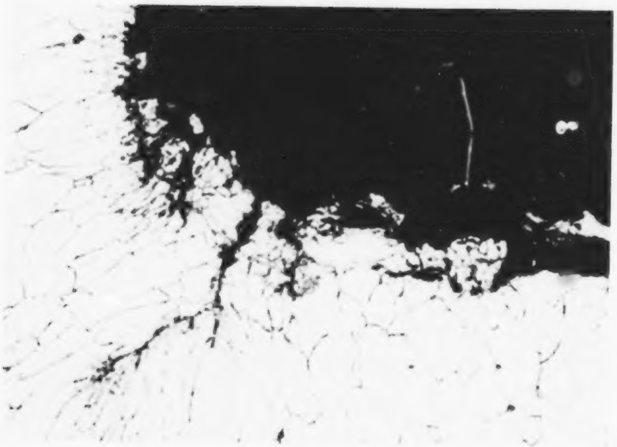

C.

Magnification: 500X
Etchant: Nital

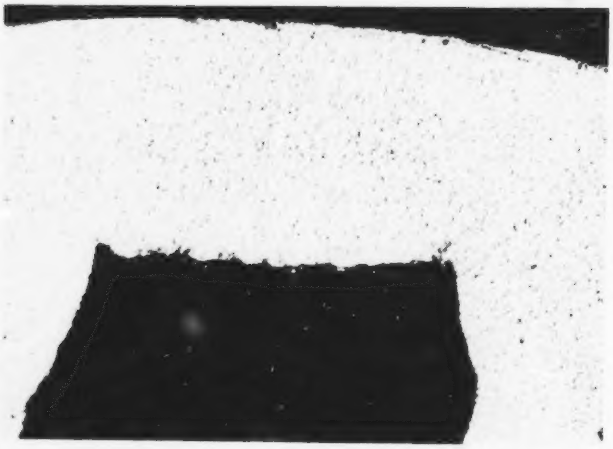

D.

Magnification: 50X
Etchant: Nital

FIGURE 117. PHOTOMICROGRAPHS OF TUBE-FIN WALL
(page 2 of 2)

10

SYSTEM NOISE

Table IX lists overall dB(A)* noise levels of the Rankine system with various components operational and different power settings. The data was taken in an enclosed test cell with equipment positioned as shown in Figure 118.

An estimation of semi-free field levels can be made by assuming the room to be constructed with 100 percent absorbing material on all walls and ceiling (but not floor) and use of the following equation:

$$\text{Noise Level Reduction (db)} = 10 \log_{10} \frac{a_2}{a_1} \quad \text{(Ref. 16)}$$

where a_1 is the actual composite room absorption coefficient given by

$$a_1 = \frac{\sum_{K=1}^{N} (\text{\% area x absorption coefficient})_K}{\text{Total Room Surface Area}}$$

where there are N types of surfaces in the actual test room and a_2 is the composite room absorption coefficient assuming 100 percent absorbing material on all surfaces except the floor. This is determined by a similar expression as used for a_1.

From dimensions and surface materials given in Figure 118, a_1 is found to be 0.0362 and a_2, 0.812. Then the correction factor becomes:

$$10 \log_{10} 22.43 = 13.5 \text{ dB}$$

The resultant dB(A) values are also given in Table IX.

---

* USA Standard for Sound-Level Meters, S1.4, 1961.

Preceding page blank

TABLE IX

OVERALL "A" SCALE WEIGHED SOUND LEVEL FOR STEAM GENERATOR SYSTEM AND COMPONENTS

Operational Components	Percent Air Valve Setting	Fan Speed (rpm)	Steam Flow (lb/hr)	Steam Pressure (psig)	Actual Noise Level [dB(A)]	Approximate "Semi-Free Field" Corrected Noise Level [dB(A)]
Water Pump (Outlet pressure 600 psi)	-	0	-	-	88	75
Fan	30	5700	-	-	92	79
Water Pump, Fan Combustor and Steam Generator	20	5780	380	900	96	83
	20	5780	steam generator flooded	-	94	81
	50	5500	780	900	101	88
	50	5500	steam generator flooded	400	96	83
	77	5300	1200	900	108	95

In order to extrapolate these sound measurements to that expected at 50 feet, six decibels should be substracted for each doubling of distance from actual microphone position. However, this rule applies only if the position was in the "far field" from the sound source. The semi-reverberent surroundings used in this test do not allow for determination of a far-field reference required in this sort of correction. All that can be said is that the 50-foot level could be less than indicated in the "semi-free field" column of Table IX. Installation in an engine compartment with normal noise suppression and treatment would produce further significant reductions of noise.

A sound level versus frequence trace (1/10 octave bandwidth) was made for each of the conditions listed in Table IX. They are shown in Figures 119 through 125. All of these figures use the dB(A) frequency weighting.

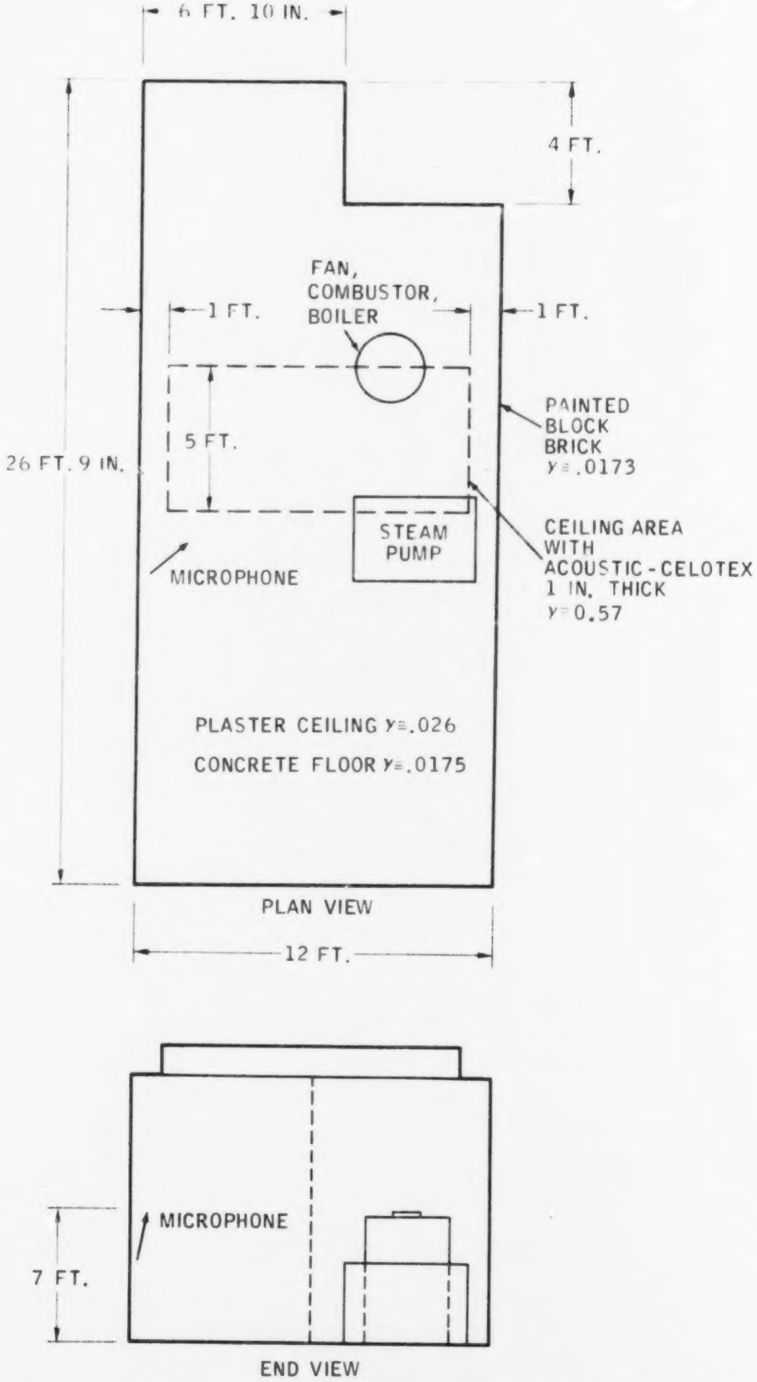
6 FT. 10 IN.
4 FT.
FAN, COMBUSTOR, BOILER
1 FT.
1 FT.
PAINTED BLOCK BRICK $\gamma \equiv .0173$
5 FT.
26 FT. 9 IN.
CEILING AREA WITH ACOUSTIC-CELOTEX 1 IN. THICK $\gamma = 0.57$
STEAM PUMP
MICROPHONE
PLASTER CEILING $\gamma \equiv .026$
CONCRETE FLOOR $\gamma \equiv .0175$
PLAN VIEW
12 FT.
MICROPHONE
7 FT.
END VIEW

FIGURE 118. NOISE EMISSION MICROPHONE LOCATION IN TEST CELL

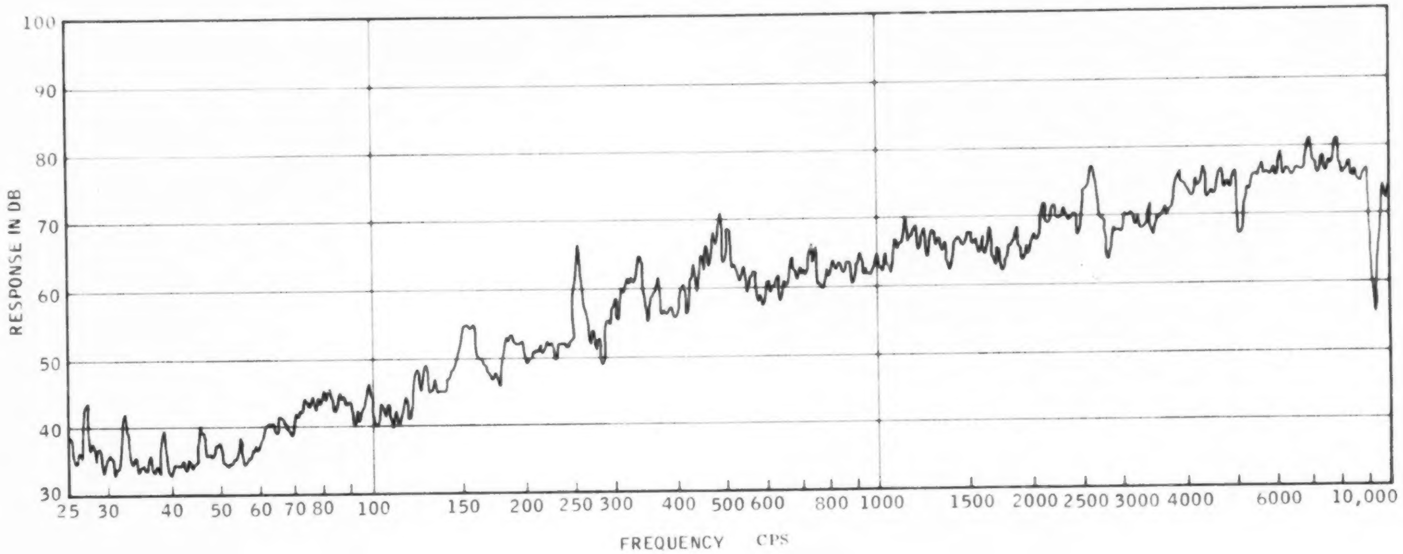

FIGURE 119. SOUND LEVEL, dB(A), VERSUS 1/10 OCTAVE FREQUENCY, WATER PUMP ONLY - 600 PSI OUTLET PRESSURE - 88 dB(A) OVERALL

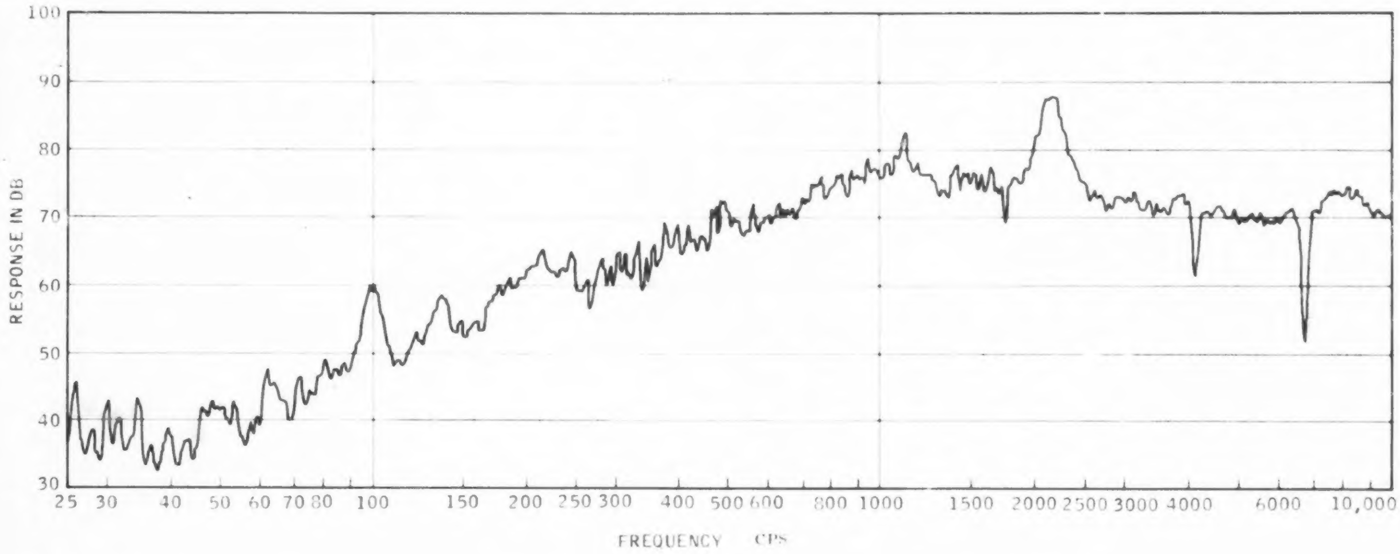

FIGURE 120. SOUND LEVEL, dB(A), VERSUS 1/10 OCTAVE FREQUENCY FAN ONLY - 5700 RPM - 30 PERCENT, 92 dB(A) OVERALL

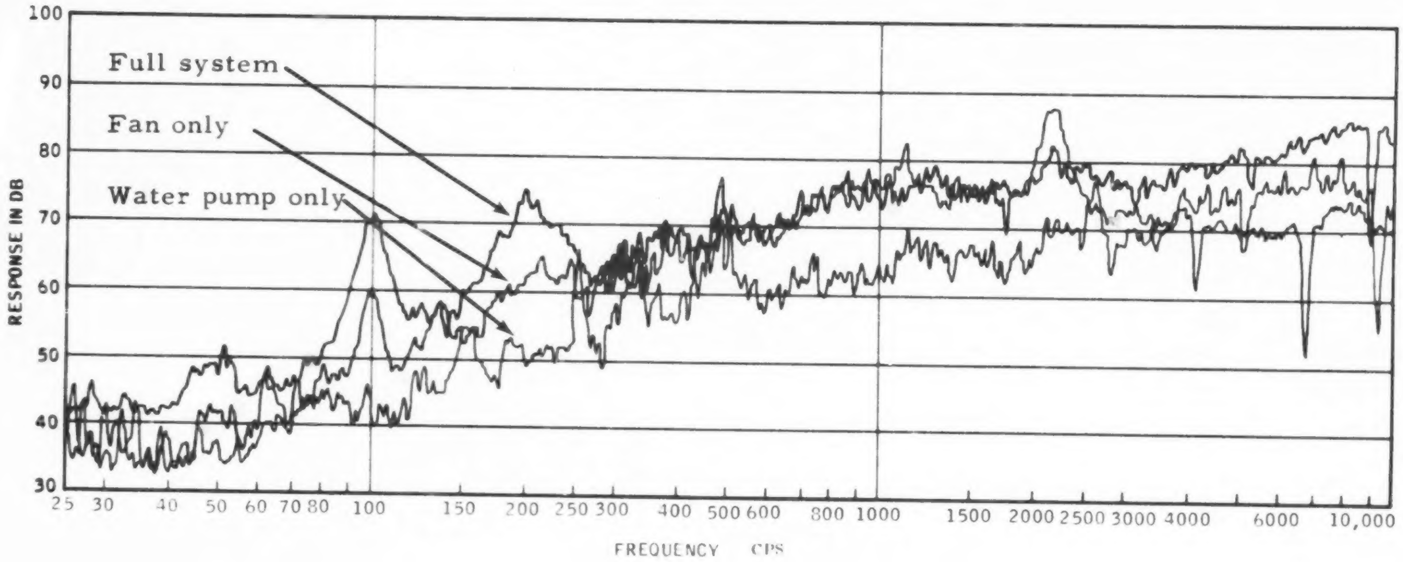

FIGURE 121. SOUND LEVEL, dB(A), VERSUS 1/10 OCTAVE BAND FREQUENCY. FULL SYSTEM, 20 PERCENT FAN, 380 LB/HR STEAM, 96 dB(A) OVERALL (BACKGROUND INCLUDED)

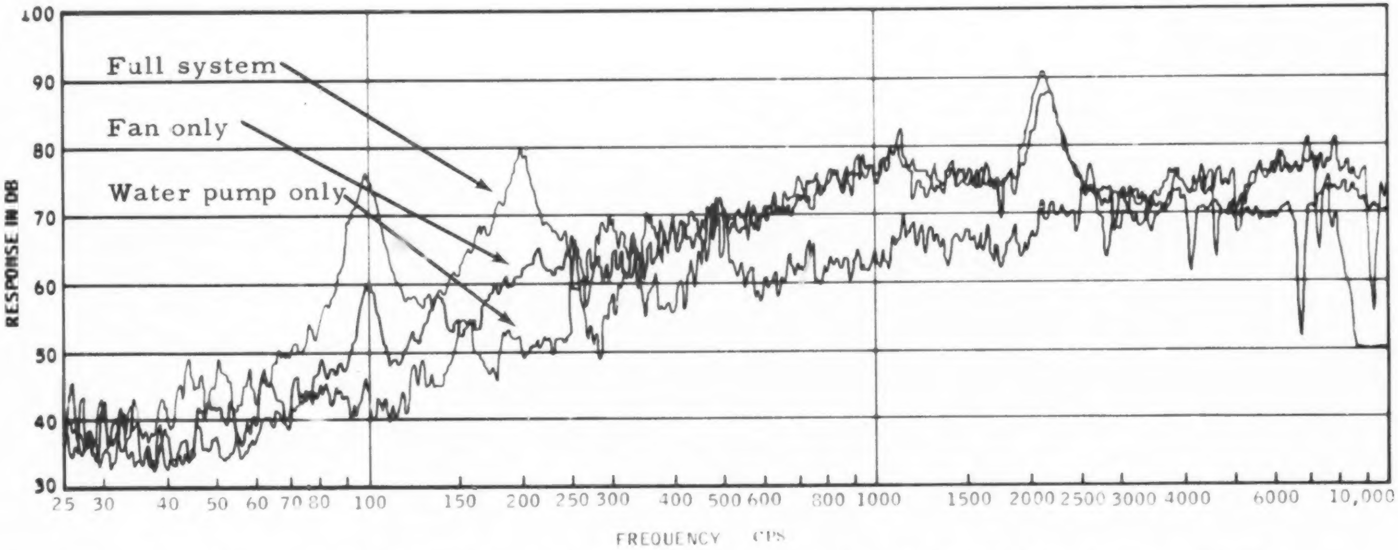

FIGURE 122. SOUND LEVEL, dB(A), VERSUS 1/10 OCTAVE FREQUENCY. FULL SYSTEM, 20 PERCENT FAN, BOILER FLOODED, 94 dB(A) OVERALL (BACKGROUND INCLUDED)

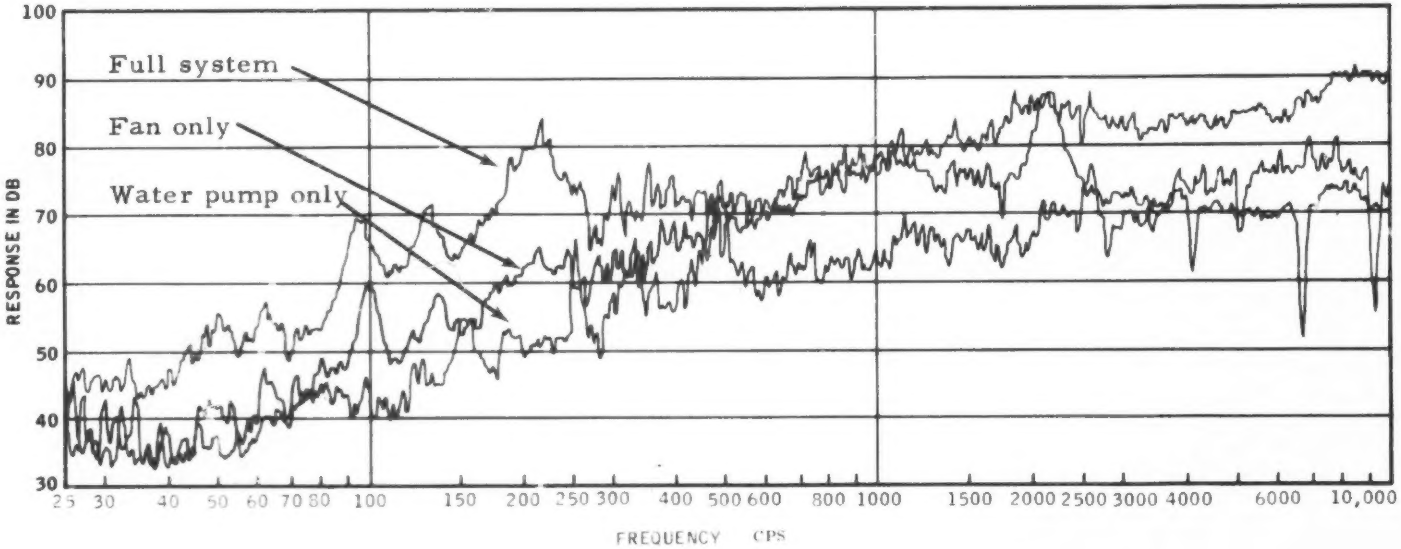

FIGURE 123. SOUND LEVEL, dB(A), VERSUS 1/10 OCTAVE FREQUENCY. FULL SYSTEM, 50 PERCENT AIR VALVE, 780 LB/HR STEAM, 101 dB(A) OVERALL (BACKGROUND INCLUDED)

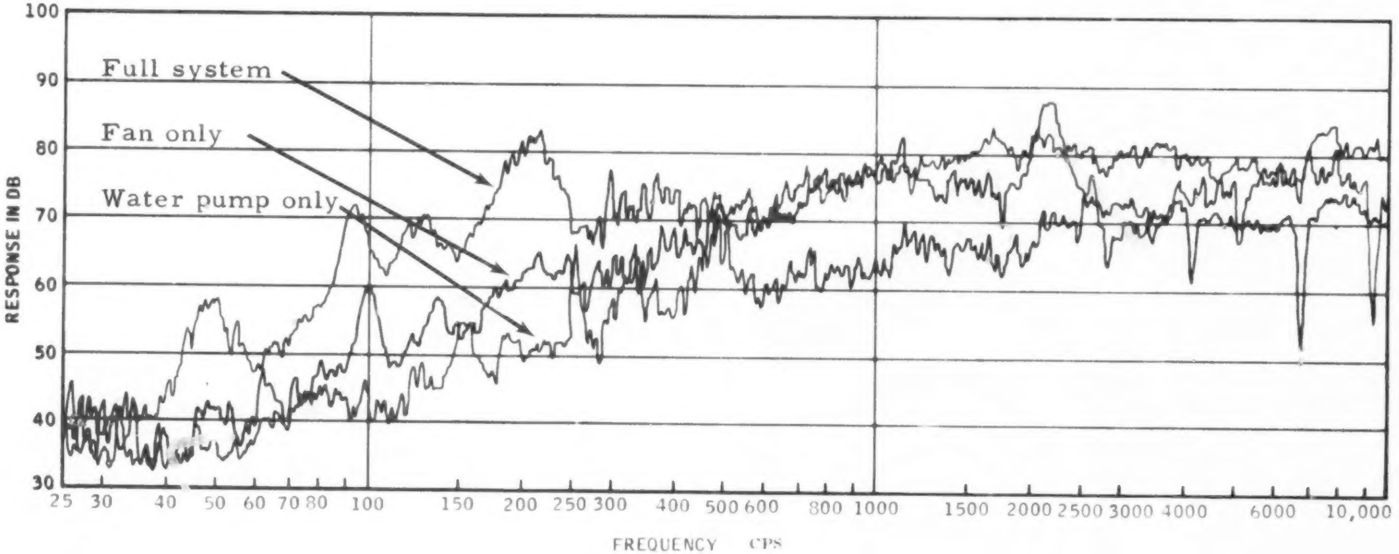

FIGURE 124. SOUND LEVEL, dB(A), VERSUS 1/10 OCTAVE FREQUENCY. FULL SYSTEM 50 PERCENT FAN, BOILER FLOODED, 96 dB(A) OVERALL (BACKGROUND INCLUDED)

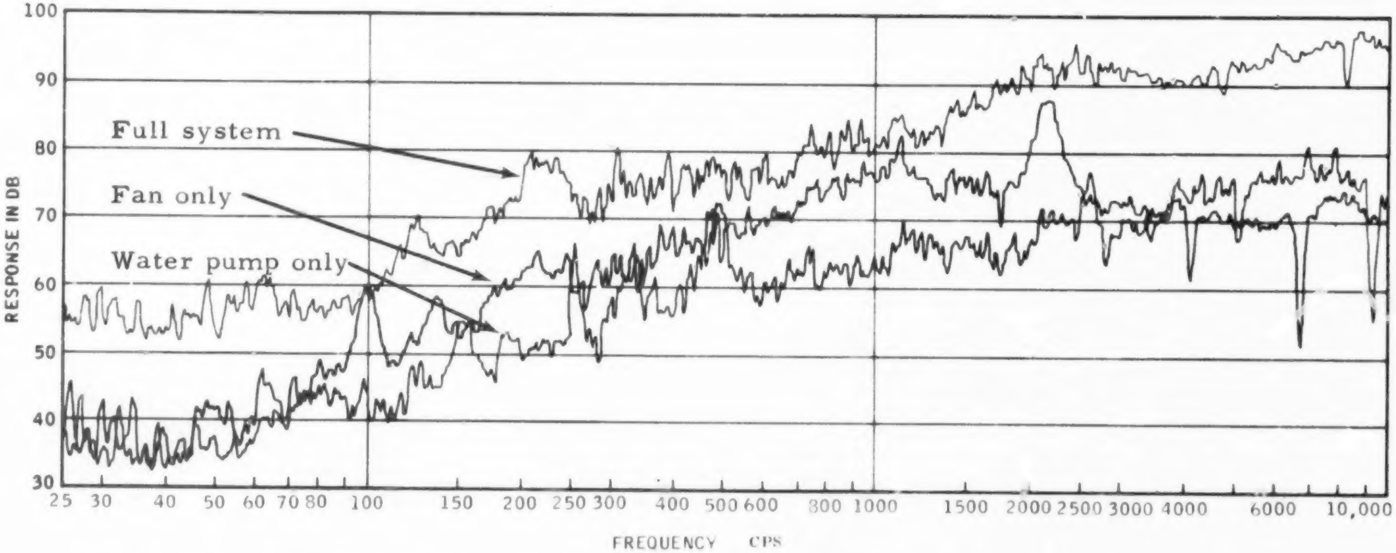

FIGURE 125. SOUND LEVEL, dB(A), VERSUS 1/10 OCTAVE FREQUENCY. FULL SYSTEM, 77 PERCENT FAN, 1200 LB/HR STEAM, 108 dB(A) OVERALL (BACKGROUND INCLUDED)

The fan and its drive motor appear to be a dominant noise source only at the 20 percent air valve setting and no steam (frequency = 2200 cps). The water pump is sufficiently low in noise level that it contributes no more than 1.1 decibel to any of the full system measurements. The maximum levels are due to changing from flooded to steam flow operation. This noise is very broad-band with no specific peaks and occurs between 2,000 and 10,000 cps. Noise contributions during steam flow operation included throttle valve sonic flow and high velocity venting into the test cell light gage metal exhaust ducting. Elimination of this noise source would lower maximum system power noise by approximately 16 db. By flooding the steam generator at a fixed firing rate the noise contribution of the sonic flow throttle valve could be eliminated. In an automotive system, a throttle valve would not normally be used, and thus this contribution would be reduced. For normal driving power the noise from the unit would be estimated to be 81 dB(A) based on a free field correction. Installation in a properly treated enclosed engine compartment would significantly reduce this level in a vehicle.

APPENDIX I

Preceding page blank

APPENDIX I

EMISSIONS SAMPLING EQUIPMENT AND DATA REDUCTION

The emissions analysis is based principally on four pieces of equipment; namely, the Beckman Nondispersive Infrared Analyzer Model 315A for the analysis of CO_2, CO and NO; the Beckman Flame Ionization Detector Model 402 for the analysis of unburnt hydrocarbons, the Thermo Electron Company Chemiluminescent Detector Model 10A for NO_x and a Von Brand Smokemeter in conjunction with a Photovolt Model 610 reflectometer for particulates (smoke).

A schematic of the equipment is shown in Figure 197.

1. The Nondispersive Infrared (NDIR) Analyzer

The Beckman NDIR Analyzer Model 315A shown in Figure 198 consists of a group of three separate instruments for the analysis of CO, CO_2 and NO in parallel through which the sample flows concurrently.

Each of the instruments consists of a reference cell, which is mechanically chopped to a frequency of 10 Hz and directed into the cells. At the bottom of the cells is a detecting chamber subdivided into two separate sections by a moveable metal diaphragm. Both sides of the detecting chamber are fitted with the gaseous constituent to be measured.

As a result of the absorption of the infrared radiation in the sample cell, more radiation reaches the reference side of the detecting chamber than on the sample side hence the gas in the reference chamber expands and distends the diaphragm. Positioned next to the diaphragm is a stationary metal button which, together with the diaphragm, constitutes a variable capacitor.

When the chopper blocks the radiant beam, the gas cools and the diaphragm returns to the neutral position. Thus the detector emits a variable capacitive signal, which is superimposed on a high frequency carrier wave. This latter wave is then modulated, rectified, and filtered to remove the radio frequency. After the signal is amplified, it is again modulated, rectified and filtered. A DC signal results, which is directly proportional to the concentration of the gas to be analyzed in the sample. In this fashion, each of the three components, namely CO_2, CO and NO is analyzed

Preceding page blank

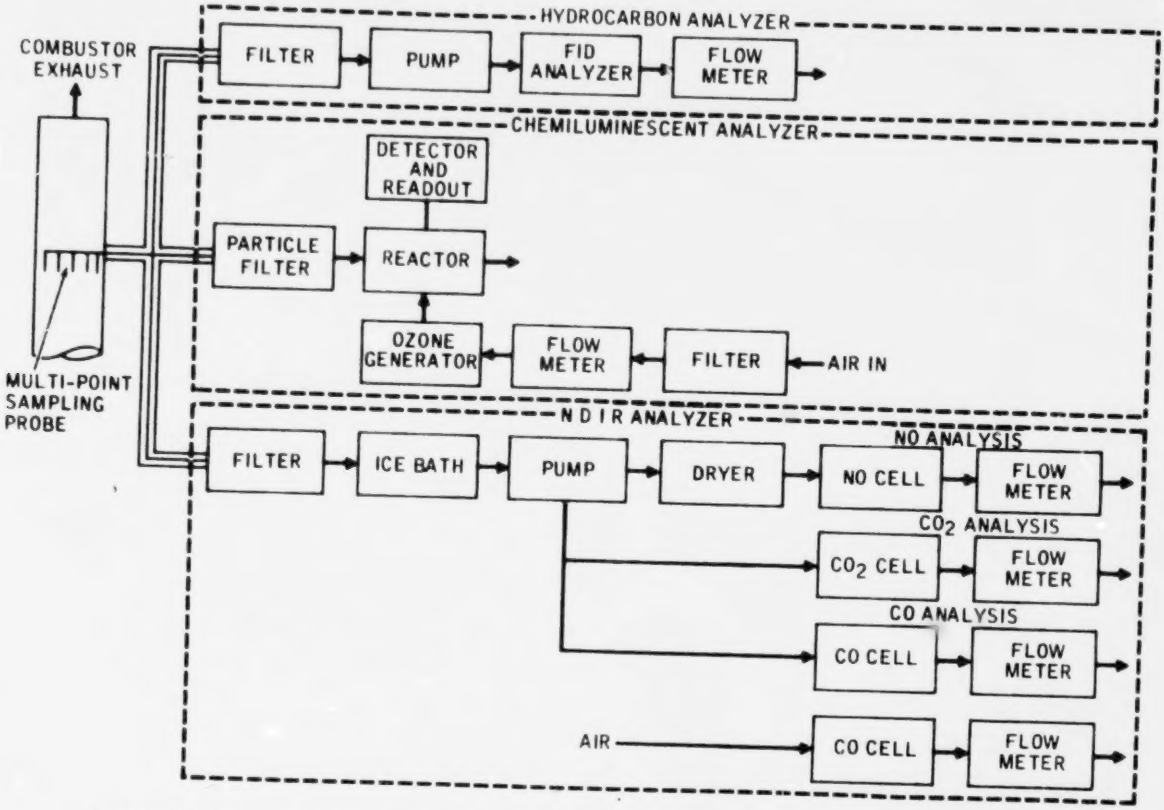
HYDROCARBON ANALYZER
COMBUSTOR EXHAUST
FILTER
PUMP
FID ANALYZER
FLOW METER
CHEMILUMINESCENT ANALYZER
DETECTOR AND READOUT
PARTICLE FILTER
REACTOR
OZONE GENERATOR
FLOW METER
FILTER
AIR IN
MULTI-POINT SAMPLING PROBE
N D I R ANALYZER
NO ANALYSIS
FILTER
ICE BATH
PUMP
DRYER
NO CELL
FLOW METER
CO2 ANALYSIS
CO2 CELL
FLOW METER
CO ANALYSIS
CO CELL
FLOW METER
AIR
CO CELL
FLOW METER

FIGURE 197. SCHEMATIC OF SOLAR RESEARCH EMISSION ANALYSIS EQUIPMENT

in their respective instruments. The capability of the equipment includes the measurement of NO from a few parts per million up to about 1 percent; CO and CO_2 are measured up into the percent range.

2. The Beckman Model 402 Flame Ionization Detector (FID)

In this equipment, shown in Figure 199, the sensor is a burner where a regulated flow of sample gas passes through a flame sustained by a metered flow of hydrogen and air. Within the flame, the hydrocarbon components of the sample gas undergo a complex ionization that produces electrons and positive ions. Polarized electrodes collect these ions, causing a current to flow through an electronic measuring circuit. This ionization current is proportional to the rate at which carbon atoms enter the burner, and is therefore a measure of the concentration of hydrocarbons in the sample stream. The range of this equipment is linear from 5 ppm up to 5 percent. It operates at an oven temperature of approximately 375° F.

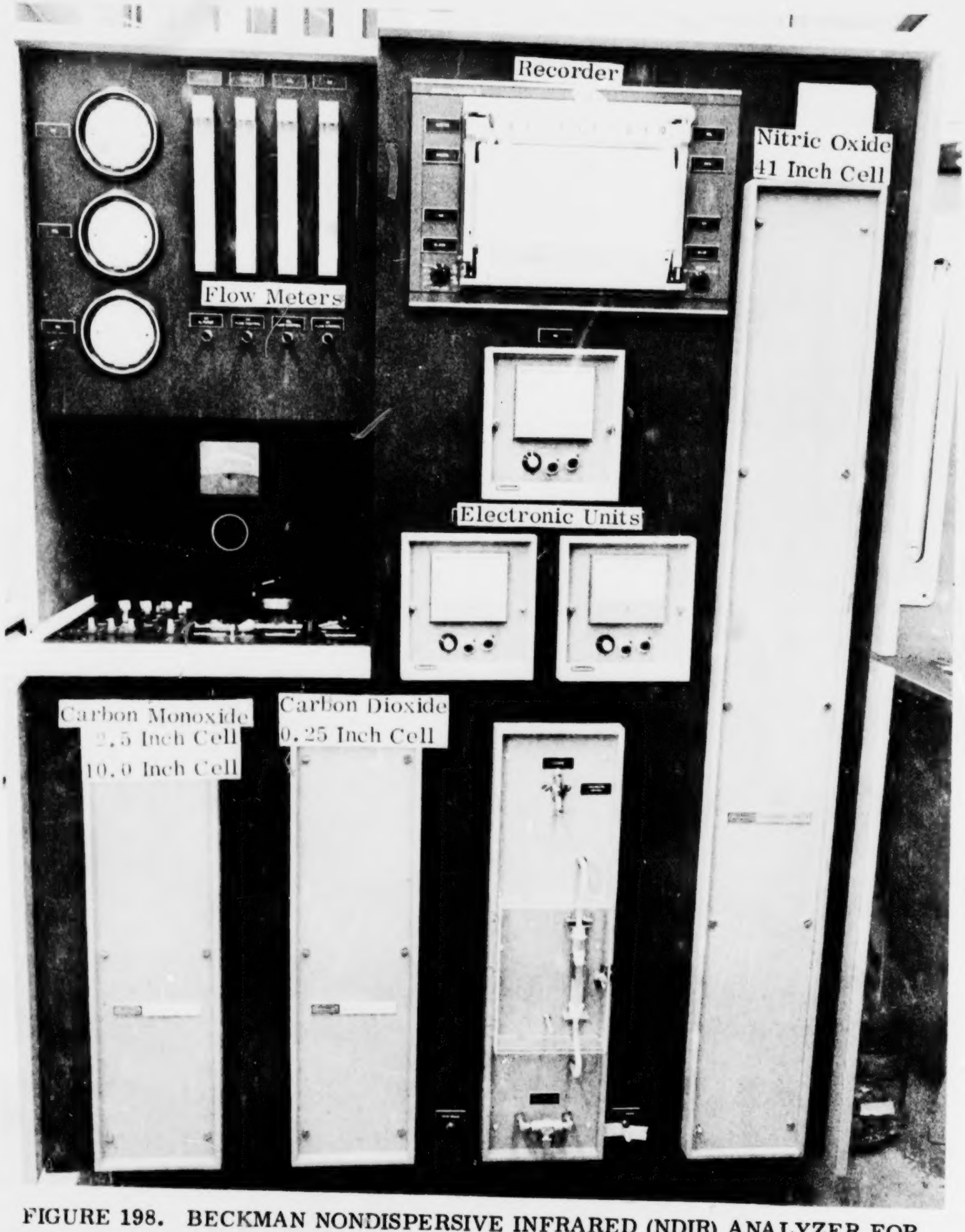
Recorder
Nitric Oxide
41 Inch Cell
Flow Meters
Electronic Units
Carbon Monoxide
2.5 Inch Cell
10.0 Inch Cell
Carbon Dioxide
0.25 Inch Cell

FIGURE 198. BECKMAN NONDISPERSIVE INFRARED (NDIR) ANALYZER FOR MONITORING CO, CO_2, AND NO

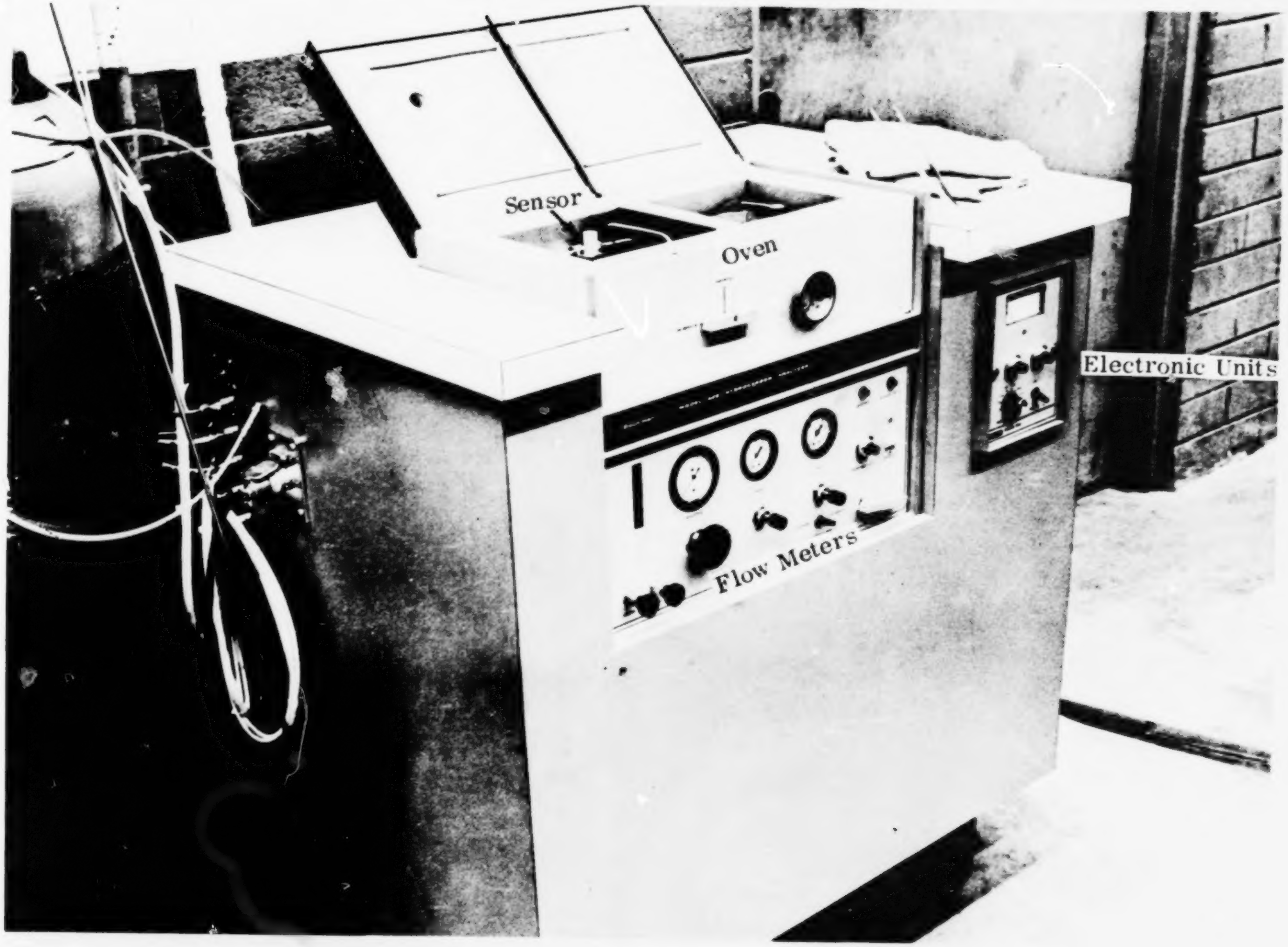
Sensor
Oven
Electronic Units
Flow Meters

FIGURE 199. BECKMAN MODEL 402 HYDROCARBON ANALYZER

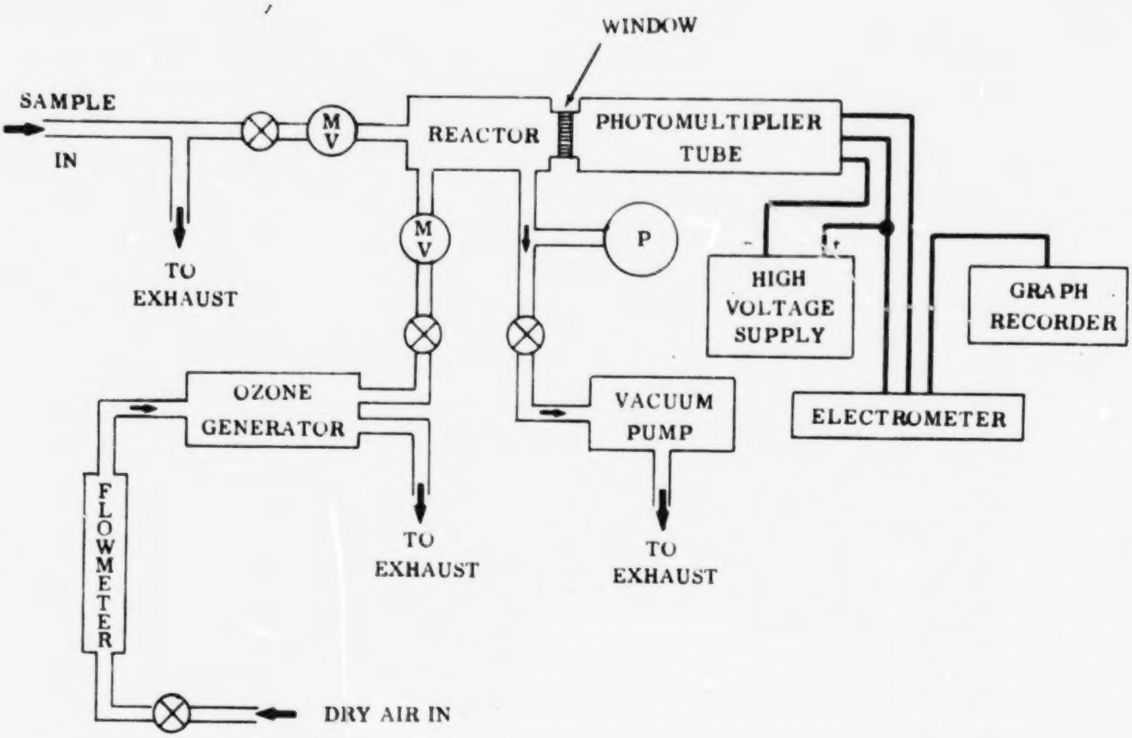
WINDOW
SAMPLE
IN
M
V
REACTOR
PHOTOMULTIPLIER
TUBE
TO
EXHAUST
M
V
P
HIGH
VOLTAGE
SUPPLY
GRAPH
RECORDER
OZONE
GENERATOR
VACUUM
PUMP
ELECTROMETER
FLOWMETER
TO
EXHAUST
TO
EXHAUST
DRY AIR IN

FIGURE 200. SCHEMATIC OF NO CHEMILUMINESCENT DETECTOR

3. The Thermo Electron Model 10A Chemiluminescent NO_x Detector

The Chemiluminescent Detector which is shown schematically in Figure 200 operates on the basis of the reaction: $NO + O_3 \rightarrow NO_2 + NO_2^* + O_2$ whereby about 10 percent of the NO_2 formed is at a higher than base energy level. As this excited NO_2 decays in the ground state energy on the form of photons is emitted.

The sample gas and an excess of ozone are reacted in a low pressure reaction chamber. A photomultiplier tube measures the resultant emissions of chemiluminescent radiation through a window and provides an electrical signal which is proportional to the NO concentration on the sample gas.

The instrument (see Fig. 201) is equipped with a converter which when operated at a temperature of about 1200° F reduces any NO_2 present on the sample gas to NO hence NO_2 can be monitored using a different method.

4. The Von Brand Smokemeter

Exhaust smoke is sampled with a Von Brand Smokemeter (Fig. 202). This meters a quantity of the exhaust, set at 0.108 cubic feet per square inch of filter

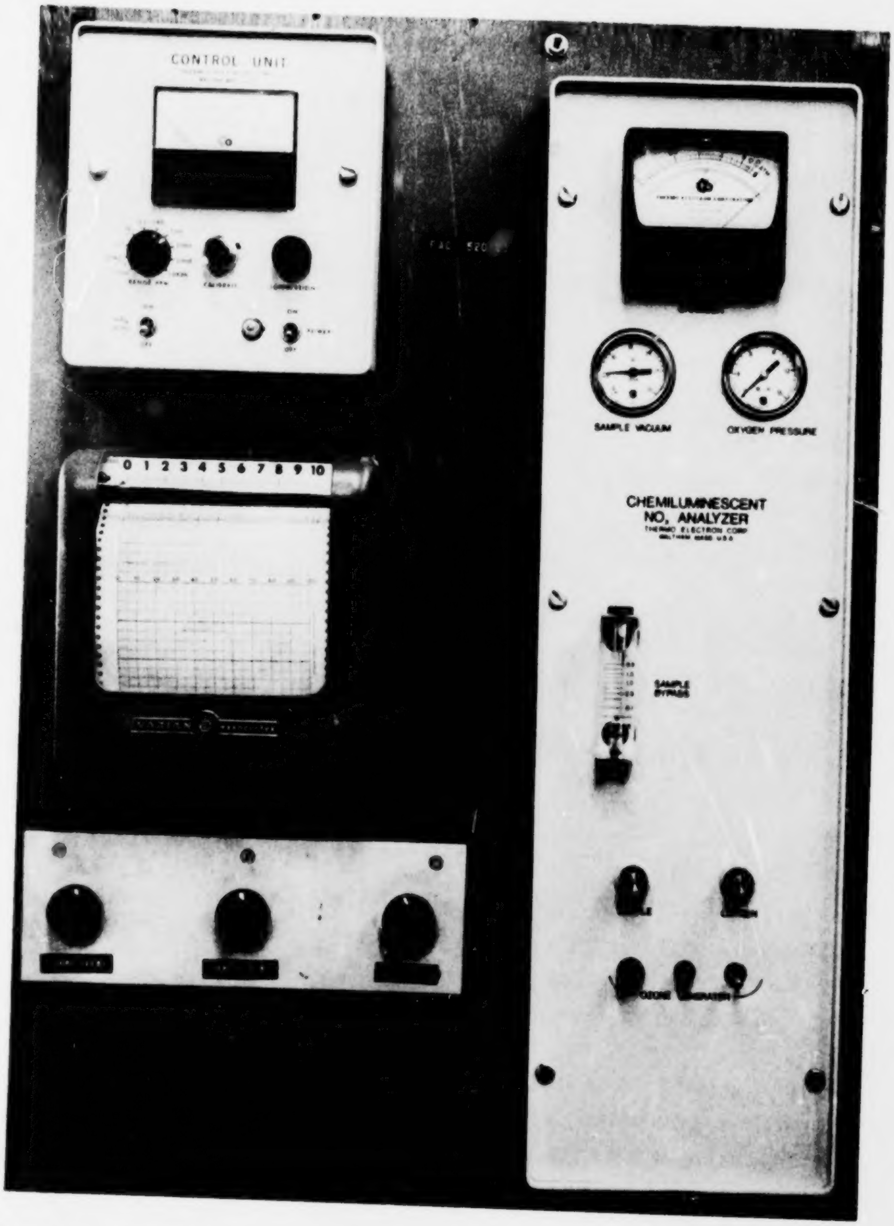
CONTROL UNIT
0 1 2 3 4 5 6 7 8 9 10
SAMPLE VACUUM
OXYGEN PRESSURE
CHEMILUMINESCENT
NOx ANALYZER
THERMO ELECTRON CORP
SAMPLE BYPASS
OZONE GENERATOR

FIGURE 201. THERMO ELECTRON CORP. CHEMILUMINESCENT ANALYZER MODEL 10A

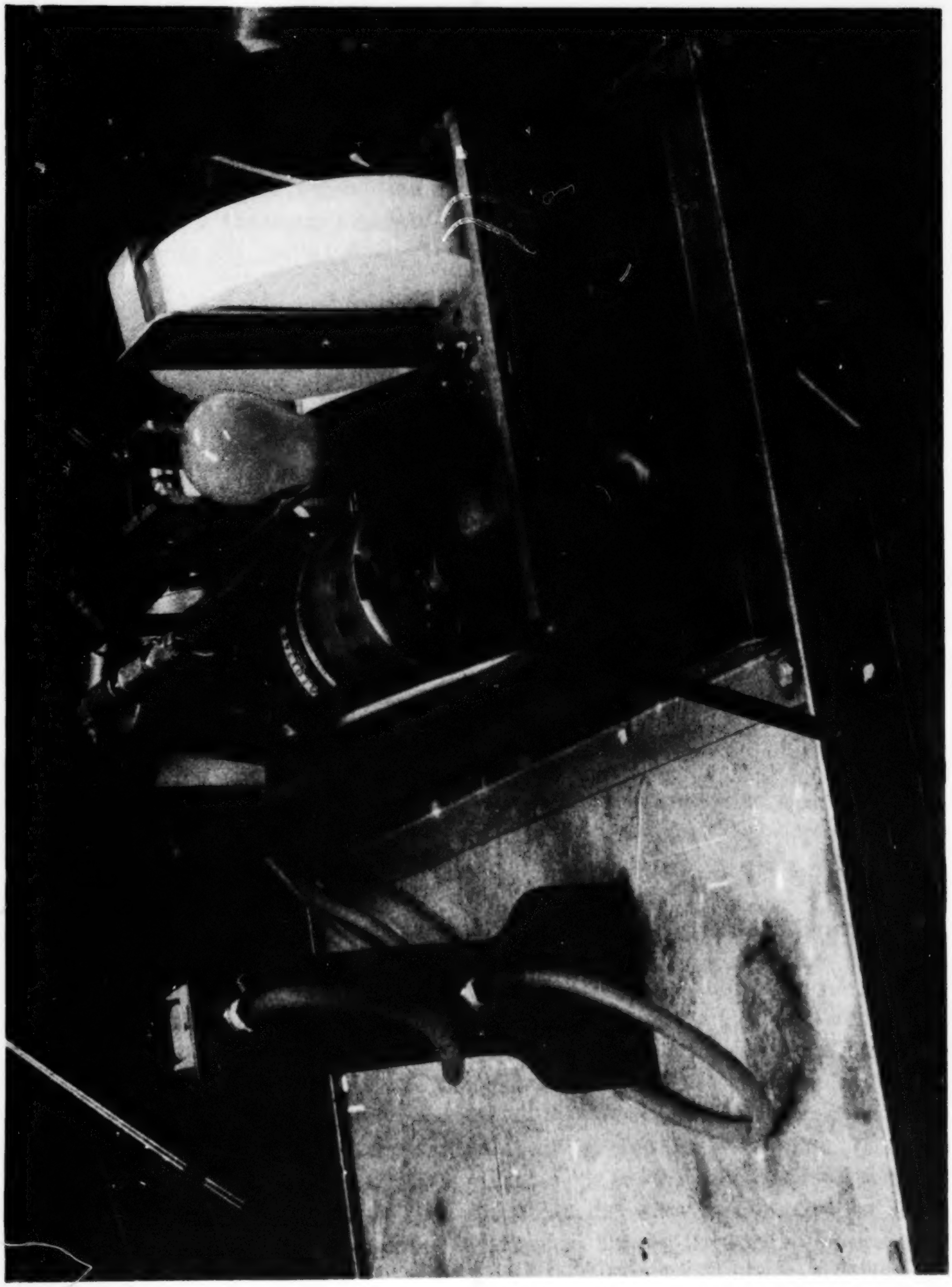

FIGURE 202. VAN BRAND SMOKEMETER

paper, through a Whatman #4 filter paper tape which moves at a constant speed of 4 inches per minute under the sample head. A small vacuum pump draws the sample through the sample head and filter paper. The instrument enables traces to be made during steady state and transient running conditions with the particulate carbon being retained on the filter paper. The resultant trace is analyzed with a Photovolt 610 Reflectometer. With this instrument the filter paper smoke stain is assigned a reflectance number by adopting a standard of 100 for a clean paper trace and zero for black. The filter tape is positioned under a search head which measures the amount of light reflected from the strained tape when subjected to a standard amount of incident light. The Von Brand Smoke number is defined as 100-% (relative reflectance in %).

The sampling probe is mounted at any convenient station and is uncooled. The probe design is either single or multipoint for averaging. The sample line is generally kept as short as possible with the minimum of bends or kinks.

5. Calibration

The NDIR, FID and CL instruments depend upon calibration gases for their operation. Calibration gases can be divided into two categories:

- Primary standards which have an accuracy of between 0.02 and 1 percent for the component being monitored present in the gas. (The smaller the quantity of the component in the gas, the larger the error becomes.)

- Certified standards in which the error in the component monitored is between 2 and 5 percent. (This is again a function of the quantity of concentration of the monitored component in the gas.)

In practice, certified standard gases are used as span gases and zero gases for the calibration of the emission monitoring equipment noted above.

The certified standard gases were carefully analyzed against the ten standardization procedures of the Environmental Protection Agency at the Mobile Source Pollution Control Lab., Willow Run Airport, Ypsilanti, Michigan. Zero gas is defined as a gas which does not contain the component being monitored and therefore sets the zero point on the analytical equipment. The span gas is defined as a certified standard analyzed against the primary standard which contains a certain concentration level of the component being monitored, to which concentration value the analyzing equipment is set. In the case of the flame ionization detector and the chemiluminescent detector, the relationship between concentration and readouts is linear. When calibrating the NDIR several span gas ranges are necessary since the relationship of signal to concentration is not quite linear.

6. Sample Treatment

From the sampling probe the NDIR gas sample passes through a particulate filter and a water vapor drop which dries the sample by freezing out the water vapor. Additional dehydration filters use chemical adsorbants to remove all traces of water on the sample flowing to the NO cell which is extremely sensitive to water vapor interference. In the drying process the temperature of the sample drops to below 100°F.

The samples to the FID and CLD are routed to the instruments through heated lines maintained at temperatures of about 250 and 350°F respectively after passing through particulate filters.

7. Data Reduction

The data reduction procedure is based on IBM 360-50 Program EP-415; a sample data point is given as Figure 203. The various steps are described below.

Raw Data

The raw data are given in parts per million (ppm) on a dry basis for CO and NO by volume; ppm on a wet basis for hydrocarbons by volume (measured as carbon atoms), and percent on a dry basis for CO_2 by volume. If the NO/NO_x is measured on the chemiluminescent instrument, the reading is ppm wet.

Correction for Interference

The NO and CO observed readings are corrected for interference effects. This does not apply if the NO/NO_x is measured on the chemiluminescent instrument.

- The NO is corrected for the presence of CO, CO_2 and HC in the sample.
- The CO is converted for the presence of CO_2 in the sample.
- No corrections are required to the CO_2 and HC observed values.

Conversion to "Dry" Volumetric Concentrations

This is required for the HC and NO/NO_x if measured on the chemiluminescent instrument. The correction factor is a function of the air-fuel ratio (as measured or calculated from a carbon balance) and ultimate analyses of the fuel (5C, $\%H_2$).

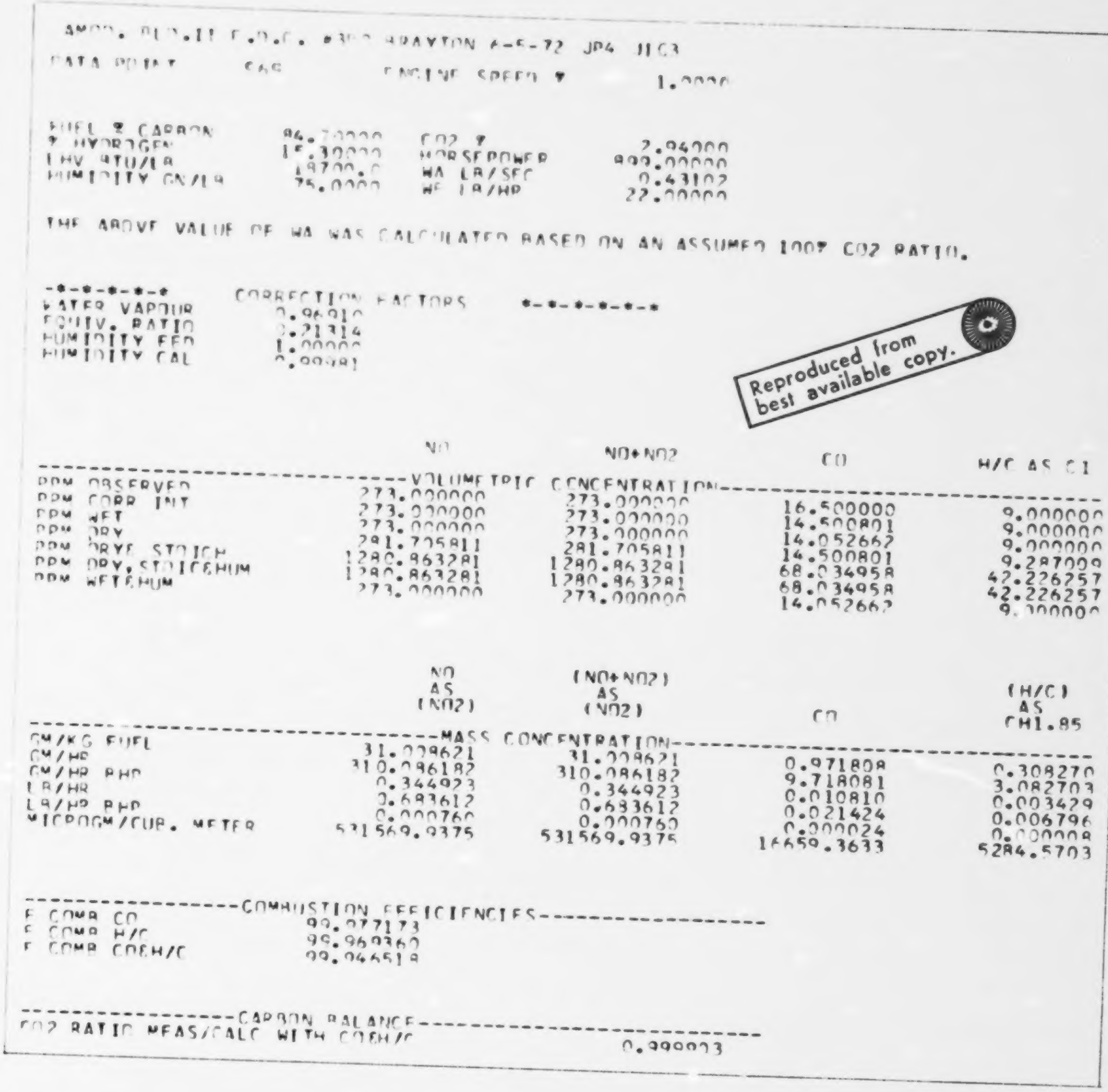

```
 AMOCO. BLD.II F.D.C. #3[illegible] BRAYTON 6-5-72 JP4 JIC3
DATA POINT      668          ENGINE SPEED %          1.0000


FUEL % CARBON          84.70000   CO2 %                 2.94000
% HYDROGEN             15.30000   HORSEPOWER          999.00000
LHV BTU/LB             18700.0    WA LB/SEC             0.43102
HUMIDITY GN/LB         75.0000    WF LB/HP             22.00000

THE ABOVE VALUE OF WA WAS CALCULATED BASED ON AN ASSUMED 100% CO2 RATIO.

-*-*-*-*-*      CORRECTION FACTORS      *-*-*-*-*-*
WATER VAPOUR      0.96910
EQUIV. RATIO      0.21314
HUMIDITY FED      1.00000
HUMIDITY CAL      0.99981



                                 NO              NO+NO2               CO             H/C AS C1
-----------------------------VOLUMETRIC CONCENTRATION----------------------------------------
PPM OBSERVED                 273.000000       273.000000
PPM CORR INT                 273.000000       273.000000        16.500000          9.000000
PPM WET                      273.000000       273.000000        14.500801          9.000000
PPM DRY                      281.705811       281.705811        14.052662          9.000000
PPM DRYE STOICH             1280.863281      1280.863291        14.500801          9.287009
PPM DRY,STOICEHUM           1280.863281      1280.863281        68.034958         42.226257
PPM WETEHUM                  273.000000       273.000000        68.034958         42.226257
                                                                14.052662          9.000000


                                 NO            (NO+NO2)                              (H/C)
                                 AS               AS                                  AS
                               (NO2)            (NO2)                CO              CH1.85
-----------------------------MASS CONCENTRATION----------------------------------------------
GM/KG FUEL                    31.029621        31.029621
GM/HR                        310.086182       310.086182         0.971808          0.308270
GM/HR BHP                      0.344923         0.344923         9.718081          3.082703
LB/HR                          0.683612         0.683612         0.010810          0.003429
LB/HR BHP                      0.000760         0.000760         0.021424          0.006796
MICROGM/CUB. METER        531569.9375      531569.9375           0.000024          0.000008
                                                             16659.3633        5284.5703


----------------COMBUSTION EFFICIENCIES-------------------
E COMB CO           99.977173
E COMB H/C          99.969360
E COMB COEH/C       99.946518


----------------CARBON BALANCE----------------------------
CO2 RATIO MEAS/CALC WITH COEH/C                 0.999993
```

Reproduced from
best available copy.

FIGURE 203. DATA REDUCTION

Conversion to "Equivalent Stoichiometric" Volumetric Concentrations

This step involves a multiplication by the ratio

$$\frac{\text{Actual A/F ratio}}{\text{Stoichiometric A/F ratio}}$$

which is the inverse of the equivalence ratio. The numerator is either obtained from direct measurements of the air and fuel flows or a carbon balance. The demoninator is calculated from the ultimate analysis of the fuel.

Correction of NO/NO_x for Ambient Humidity Effects

The formation rate of NO is sensitive to the humidity of the test air supply. The NO results are therefore normalized to a standard humidity condition of 75 grains/pound dry air in line with the correction formula laid down in the Federal Register of July 2, 1971, Vol. 35, No. 128, Part II, EPA "Exhaust Emission Standards and Test Procedures".

Mass Concentrations

From the wet basis, volumetric concentrations (corrected for humidity in the case of NO/NO_x), and the mass concentrations are calculated using the densities of the various species as laid down in the Federal Register of July 2, 1971, Vol. 35, No. 128, Part II, EPA "Exhaust Emission Standards and Test Procedures". The NO_x is expressed as NO_2 and the HC is assumed to be $CH_{1.85}$.

Combustion Efficiency and Carbon Balance

Combustion efficiencies are extracted from the amounts of CO and HC. (The HC in this case is assumed to be completely unburnt fuel.) A carbon balance is made on the air and fuel flows into the combustor with the CO, CO_2 and HC flows out of the combustor to check on the measurement accuracies. This can only be carried out of the air, and fuel flows are measured directly; otherwise the carbon balance must be assumed to obtain a test air-fuel ratio.

SOLAR RESEARCH MEMORANDUM

R73J-3441

January 11, 1973

To: T. E. Duffy, Research Staff Engineer

cc:
W. A. Compton
J. V. Long
D. J. White
J. Stice
J. Urick, Eng.
File (PBR)
Ref. File

From: P. B. Roberts
Senior Analytical Engineer

Subject: ANALYSIS OF EPA GAS SAMPLES. S.O. 6-3827-7, EWO 6033425

I. BACKGROUND

As part of a continuing effort to ensure the use of uniform gas analysis instrumentation, calibration and sampling methods among its contractors working on low emission programs, the Environmental Protection Agency delivered to Solar last November a number of cylinders containing gaseous constituents of unreported concentration for our analysis.

The objective of the exercise was for Solar Research to label the concentrations of the various cylinders and to then return the cylinders to the EPA for presumably subsequent analysis by other contractors. A listing of the cylinder constituents and their approximate ranges of concentration was supplied by the EPA.

As a secondary effort during this investigation, the cylinders were analyzed by Engineering on their own separate instrumentation for comparison purposes (using their own charge number).

The work was carried out during the month of December 1972.

II. INSTRUMENTATION

The Research instrumentation comprises:

- Beckman 315-A NDIR for CO_2 and CO
- Beckman 402 FID for UHC

Preceding page blank

- Thermo Electron 10A CLD for NO/NO_x with molybdenum coil converter for NO_2 reduction

The Engineering instrumentation is essentially identical to the above with the exception that the NDIR instrument is the Model 315-B which incorporates solid state electronics and has different CO and CO_2 ranges.

The NO_2 converter is of the standard stainless steel coil type.

III. PROCEDURE

The procedure adopted was for Research to initially calibrate the instrumentation with its available Gold Standard gases. These have been labeled by the EPA and are normally retained for use in labeling secondary standards only. The NDIR curves were checked at four points on each range.

The EPA samples were then analyzed by introducing them into the instrumentation through the calibration gas input points rather than through the various heated sample lines. As it was know that the diluent of each sample was either dry air or nitrogen, either method would give identical results with clean sample lines.

Engineering's results were obtained after only preliminary calibration with their normal (secondary standard) gases and a one point span check on the NDIR ranges. It should be understood that Engineering utilizes the Research Golden Standard gases for initial labeling of calibration gases (secondary standards) upon delivery.

IV. RESULTS

The results are shown in tabular form in Table I. Column #1 lists the approximate ranges as reported by the EPA, #2 shows the Research results and #3 gives the Engineering results.

Total time charged for Research to complete the analysis, including reporting is 35 hours.

In comparison, Engineering with its reduced calibration effort completed the analysis within 8 hours.

The expected level of accuracy for the Research results is high except for the three low concentration CO samples. Due to an absence of suitable gold standards for this instrument range only a single point calibration could be made with a secondary standard. Any error however is unlikely to be more than ±10 percent.

TABLE I

ANALYSIS RESULTS

Cylinder No.	Gas	Diluent	#1 EPA Reported Concentration Range	#2 Research Results	#3 Engineering Results
B-1094	NO	N_2	0-100 ppm	96.5 (3)	94.0
B739	NO	N_2	0-50 ppm	47.1	47.0
37562	C_3H_8	Air	0-50 ppm	33.3 (1)	30.7 (1)
37853	C_3H_8	Air	0-200 ppm	150.7 (1)	127.5 (1)
37730	CO	N_2	0-100 ppm	21.0	21.0
37758	CO	N_2	0-100 ppm	46.5	49.0
37769	CO	N_2	0-100 ppm	78.0	82.0
37793	CO	N_2	0-500 ppm	271.0	279.0
37699	CO	N_2	0-500 ppm	447.0	463.0
37749	CO	N_2	0-2000 ppm	- (4)	>1000.0 (2)
B-880	CO_2	N_2	0-5%	2.07	2.0
37768	CO_2	N_2	0-5%	4.28	4.2
37581	CO_2	N_2	0-15%	8.82	8.6
37723	CO_2	N_2	0-15%	13.60	13.4
37847	-	N_2 zero gas	<0.1 ppm HC	0.0	0.1
37764	-	N_2 zero	<0.1 ppm HC	0.0	0.0

(1) measured as methane - CH_4
(2) Engineering instrumentation has maximum CO scale 0-1000 ppm
(3) 2.0 ppm NO_2 analyzed in addition
(4) Not analyzed. Available scales are 0-1000 ppm and 0-2.5%

V. RECOMMENDATIONS

- Obtain sufficient gold standard gases to adequately calibrate every range of each instrument
- Attempt to fall into line more with previous informal EPA recommendations as to procedures, materials, calibration gases, etc. Ref.: S.I.C. "Trip Report, EPA Ann Arbor, Michigan", P. B. Roberts to J. Watkins, 31 Jan. 1972
- Adopt the procedure of regular cross checks between the Engineering and Research instrumentation.

PBR:st

APPENDIX II

Preceding page blank

EFFECT OF SCALING ON MATRIX METAL WEIGHT AND WATER HOLD UP

Kays and London (Ref. 5), on page 10 of their book, show that for a heat exchanger with the gas side resistance dominating,

$$NTU = No_g \left(\frac{4L}{DH}\right)_g \left(\frac{C_g}{C_{min}}\right) St_g \tag{1}$$

If No_g and C_g/C_{min} remain constant,

$$NTU \propto \left(\frac{L}{DH}\right)_g St_g \tag{2}$$

Ordinarily, St can be described by an equation of the form

$$St = KRe^{-a} \tag{3}$$

so

$$St \propto \left(\frac{W}{AF}\right)^{-a} DH^{-a} \tag{4}$$

so

$$NTU \propto \left(\frac{L}{DH}\right)\left(\frac{W}{AF}\right)^{-a} DH^{-a} \tag{5}$$

The exponent a is normally in the range $0.4 < a < 0.7$.

Now if tube stress is to remain constant, then tube wall thickness is proportional to tube diameter, which means that for geometrically similar bare tube arrangements, both matrix metal weight and hold up volume are proportional to core volume. The core volume is given by

$$V = AFL = W\left(\frac{W}{AF}\right)^{-1} \left(\frac{L}{DH}\right) DH \tag{6}$$

Preceding page blank

From equation (5), if NTU is maintained constant,

$$\frac{L}{DH} \propto \left(\frac{W}{AF}\right)^{a} DH^{a} \tag{7}$$

Combining equations (6) and (7), one sees that if NTU and W are maintained constant,

$$V \propto \left(\frac{W}{AF}\right)^{-1 + a} DH^{1 + a} \tag{8}$$

So for geometrically similar bare tube matrices, both core weight and hold up volume tend to be proportional to tube diameter to the (1 + a) power.

For a finned tube, the fin thickness must increase more rapidly than the tube diameter, if fin effectiveness is to remain constant. As is shown on page 9 of Kays and London, if fin effectiveness is to remain constant, then, for geometrically similar arrangements,

$$\delta \propto DH^{2} h \tag{9}$$

but

$$h \propto St\left(\frac{W}{AF}\right) \propto \left(\frac{W}{AF}\right)^{1 - a} DH^{-a}. \tag{10}$$

so

$$\delta \propto DH^{2-a}\left(\frac{W}{AF}\right)^{1-a} \tag{11}$$

Since, for a geometrically similar matrix, spacing between the fins is proportional to DH, core weight for the fins is scaled by

$$M \propto \frac{V\delta}{DH} \tag{12}$$

so

$$M \propto DH^{2} \tag{13}$$

From the above, it is seen that it is advantageous from the standpoint of core weight and hold up to keep the tube diameters as small as possible.

APPENDIX III

SIZING ANALYSIS

The method used to size the various parts of the unit was essentially the same in all cases. First, inlet and outlet gas and water conditions were estimated, using the design requirements and an overall heat balance. This fixed the required effectiveness, and the thermal capacitance rate ratio for the two streams. Next, the amount of heat transfer surface needed to produce the required effectiveness was estimated using the NTU-effectiveness approach described in Chapter 2 of Kays and London (Ref. 5). This approach uses the functional relationship

$$\epsilon = f(\mathrm{NTU},\ C_{min}/C_{max},\ \text{flow arrangement}) \tag{1}$$

where

$$\mathrm{NTU} \equiv \frac{AU}{C_{min}} \tag{2}$$

$$C \equiv WC_p \tag{3}$$

$$\epsilon \equiv \frac{\Delta T_{min}}{T_{hi} - T_{ci}} \tag{4}$$

Various gas side surfaces were evaluated on the basis of ease of manufacturing, water hold up volume, gas side pressure drop, and the number of tube rows needed to produce the required NTU. It was known that in all areas the dominant film resistance would be on the gas side, so the actual configuration of the water side was relatively unimportant from a heat transfer viewpoint.

With the gas side surface chosen, the number of parallel passages on the water side could be determined on the basis of water side pressure drop considerations. With the water side flow arrangement known, a check was made to ensure that the water side thermal resistance did not reduce the NTU below the required limits.

Preheater

The fluid stream temperature estimates used to size the preheater are tabulated below.

	Gas Side	Water Side
Inlet	1090°F	160°F
Outlet	306°F	561°F (saturated)

Preceding page blank

These conditions required

$\epsilon = 0.851$ $\qquad$ $C_{min}/C_{max} = 0.537$

Since most of the actual water hold up in the vaporizer is in the preheater, it is important to minimize the tube volume in this section. For this reason, a finned tube configuration was chosen for the preheater. The preheater is in a cold part of the exchanger, so copper fins were chosen because of their high fin effectiveness and the ease with which they are manufactured. It was decided to use a monotube arrangement if pressure drops permitted, since this would tend toward simplicity in the manifolding arrangements and easy, low-cost assembly of the unit.

The final configuration was three rows of 3/8 OD 321 stainless steel tubing, with 1.8 inch high by 0.012 inch thick copper fins, with 15 fins per inch. Pertinent data for this surface are shown in the table below.

$S = 0.717$ inch	$D = 0.784$ inch
$\sigma = 0.297$	$\alpha = 151.1\ ft^2/ft^3$
$D_H = 0.00785$ ft	fin area/total area = 0.859

This surface is quite similar to the surface of Figure 96 in Kays and London (Ref. 5).

Gas side heat transfer was evaluated using the data provided in Figure 96 of Kays and London. Pertinent results were:

$R_e = 404$
$h = 32.4\ BTU/ft^2{}^\circ F$
tube length/row = 39.0 ft
area/row = 22.3 ft^2
fin effectiveness = 0.98
gas side AU/row = 710 BTU/hr°F

Water side friction factor and pressure drop were evaluated using the standard Darcy-Weisbach friction factor. It was found that a monotube arrangement would allow the pressure drop to be held down to a reasonable level. The water side pressure drop results were:

$R_e = 1.329 \times 10^5$
$f = 0.01804$
$\Delta_p = 45.3$ psi

Heat transfer coefficient on the water side was estimated using the correlation on page 399 of Bird, Stewart, and Lightfoot (Ref. 6).

$$(St)\,(Pr)_b^{2/3} = \frac{0.026}{(R_e)_b^{1/5}} \cdot \left(\frac{\mu_b}{\mu_w}\right)^{0.14} \qquad (5)$$

The following results were obtained for the water side heat transfer.

h = 5070 BTU/hr ft^2°F
water side AU/row = 17,120 BTU/hr°F
area/row = 3.38 ft^2

With the above results for the gas and water side, the results for overall heat transfer were as shown below.

AU/row = 682 BTU/hr°F
C_{min} = 705 BTU/hr°F
NTU/row = 0.967

The effectiveness for each row of tube was estimated using equation 15 on page 12 of Kays and London for the crossflow arrangement with the maximum capacitance side mixed and the minimum side (in this case, the gas side), unmixed.

$$\Gamma' \equiv 1 - e^{-NTU} \qquad (6)$$

$$\epsilon_p = \frac{C_{max}}{C_{min}} \left[1 - e^{-\Gamma' C_{min}/C_{max}}\right] \qquad (7)$$

The number of rows necessary to achieve the required effectiveness was determined from equation 17b on page 13 of Kays and London, which applies to multipass cross counterflow exchangers with each fluid mixed after each pass.

$$\epsilon = \frac{\left[\dfrac{1 - \epsilon_p C_{min}/C_{max}}{1 - \epsilon_p}\right]^n - 1}{\left[\dfrac{1 - \epsilon_p C_{min}/C_{max}}{1 - \epsilon_p}\right]^n - \dfrac{C_{min}}{C_{max}}} \qquad (8)$$

The results obtained for the preheater were:

$\epsilon_p = 0.527$

$\epsilon_3 = 0.843$

$\epsilon_2 = 0.737$

$\epsilon_4 = 0.903$

Although three rows do not quite give the effectiveness of 0.851 which was desired, it was decided that three rows would provide adequate preheating. This was indeed the case, as is shown by Table VI. Water leaves the preheater with only about 5°F of subcooling. Experience with the present test bed unit and the available literature on the subject (discussed in Section 6), indicate that such a small degree of subcooling is unlikely to produce any hydrodynamic stability problems in the vaporizer, especially in the monotube configuration finally chosen for the vaporizer.

Vaporizer

The estimates of inlet fluid conditions shown below were used to size the vaporizer.

Gas Side	Water Side
2500°F	Saturated at 545°F, 1000 psia

It was desired that the vaporizer have an ample safety margin for burnout, and that it produce an outlet steam quality of at least 50 percent. This would allow dryout to take place in a low temperature part of the boiler, at a high quality, so that the reduction in water side heat transfer associated with dryout would not be severe. A wide safety margin for burnout at full load should help keep the safety margin adequate at part load, even when operating at high flame temperatures. As in the preheater, it is desirable that the tube volume be kept down to a minimum, and that the manifolding arrangement be as simple as possible.

It was felt that the best arrangement for satisfying these requirements was two rows of 5/8 OD 321 stainless steel tubing, arranged similar to the surface of Figure 48 of Kays and London. While this is certainly not the most compact possible bare tube arrangement, it was felt that it was the most compact which would allow reasonable ease of manufacturing. It was decided to use a monotube arrangement in the vaporizer for improved stability, if pressure drop and dryout considerations would permit it. Pertinent data for the gas side heat transfer surface are shown below.

S = 0.9375 inch
σ = 0.333
D_H = 0.0496 feet
D = 0.9375 inch
α = 26.9 $\mathrm{ft}^2/\mathrm{ft}^3$

Gas side heat transfer was evaluated by the same method as used in the preheater design. The results were

R_e = 1343
h = 24.2 BTU/hr ft^2°F
tube length/row = 29.8 ft
area/row = 4.88 ft^2
gas side AU/row = 118.1 BTU/hr°F

It was assumed that the water side thermal resistance would be negligible, as long as dryout did not occur.

With the above information for heat transfer, the effectiveness of the vaporizer was determined from

$$\epsilon = 1 - e^{-NTU} \tag{9}$$

This is the relation given on page 12 of Kays and London for heat exchangers with $C_{min}/C_{max} = 0$. The results were

C_{min} = 823 BTU/hr°F
ϵ = 0.249
NTU = 0.287
exit quality = 51.3%

With these results, the probability of dryout in the vaporizer was estimated using the criteria described in Appendix IV. The Baker plot indicates that the flow is indeed in the annular flow regime. The Westinghouse Atomic Power Division correlation, presented as equation (4) in Appendix IV,

$$x_{crit} = (0.825 + 2.3e^{-17De})\, e^{-1.5G/10^6} - 0.41e^{-0.0048L/De} - \frac{1.12}{(v_v/v_L)} + 0.548 \tag{10}$$

was applied with the input data and results shown below. In equation (10), De must be input in inches, and G in lbm/hr ft^2.

$$De = 0.561 \text{ inch}$$

$$G = 0.750 \times 10^6 \text{ lbm/hr ft}^2$$

$$x_{crit} = 76.1\%$$

$$L = 59.6 \text{ ft (for two monotube rows in series)}$$

$$L/D = 1273$$

$$(v_v/v_L) = 20.6$$

It is seen that there is amply safety margin for dryout, so a monotube arrangement in the vaporizer is certainly satisfactory from that standpoint.

Using Tippets' correlation, described in equations 5 through 9 of Appendix V,

$$x = 0.513$$

$$q_{crit} = 2.746 \times 10^5 \text{ BTU/hr ft}^2$$

$$\alpha = 0.808$$

$$q = 4.23 \times 10^4 \text{ BTU/hr ft}^2$$

The margin of safety indicated by Tippets' correlation is not so large as it seems. An increase in flux increases the exit quality, which in turn, sharply reduces the critical heat flux predicted by Tippets' correlation.

Using the values of quality and void fraction shown above, the vapor velocity can be calculated from

$$V_v = \frac{G_x v_v}{\alpha} \tag{11}$$

with $v_v = 0.445 \text{ ft}^3/\text{lbm}$

$$V_v = 59.1 \text{ ft/sec}$$

This is about the maximum velocity which Bennet and his co-workers (Ref. 7) found could be tolerated without danger that the liquid film would be blown off the wall.

After considering the results of all of the above correlations, it was decided that the vaporizer would almost certainly have an ample margin of safety for dryout at full load, and that a monotube arrangement would not produce high enough vapor velocities to cause premature dryout.

Pressure drop in the vaporizer was estimated by the method presented by Martinelli and Nelson (Ref. 8). Their correlation is

$$\frac{\Delta p_{TPF}}{\Delta p_{LO}} = f_1 (p, x_e) \tag{12}$$

$$\Delta p = \Delta p_{TPF} + \frac{r G^2}{gc} \tag{13}$$

and $$r = r(p, x_e) \tag{14}$$

The functions f_1 and r are tabulated in Reference 8. Applying the method of Reference 8 to the vaporizer tube rows, the following results were obtained:

$G = 0.750 \times 10^6$ lbm/hr ft^2

$f_{LO} = 0.01734$

$p = 1000$ psia

$f = 9.13$

$Re_{LO} = 1.452 \times 10^5$

$\Delta p_{LO} = 1.118$ psi/row

$x_e = 0.513$

$r = 0.155$

$\Delta p = 21.9$ psi

For automotive boilers, it appears that vaporizer velocities low enough to prevent premature dryout will almost always ensure that the pressure drop in the vaporizer will be quite acceptable low.

Dryer

It is in the dryer that the working fluid is changed from saturated vapor to superheated steam. Since this is the case, the liquid film on the wall must at some point become so thin that it breaks up, with a consequent reduction in the water side heat transfer coefficient. The dryer tube is placed in a relatively cool part of the exchanger, so that a decrease in water side heat transfer coefficient will not produce excessive increases in tube wall temperatures. The tube mass flow rates are such that wall dryout will occur at relatively high quality. When this is the case, fairly high heat transfer coefficients are maintained on the water side even after dryout, thus keeping tube wall temperatures within reasonable limits.

In order to keep the dryer tube pressure drops within reasonable limits, it was necessary to use either two parallel passages of 3/8 OD tube, or a 5/8 OD monotube. In order to achieve reasonable compactness, a finned tube arrangement was desired. Because of the high fin tip temperatures expected in the dryer, it was felt that the fins should be stainless steel rather than copper. In order to achieve reasonably high fin effectiveness with stainless steel fins, short fins were necessary. In order to get high fin area/total area with short fins, tube diameters must be small. For this reason, the parallel flow 3/8 OD finned tube arrangement was chosen.

The dryer therefore consists of one row of 3/8 OD finned tube, arranged in two parallel flow passages. The tube spacing and fin arrangement are exactly the same as for the preheater, but the fins are 304 stainless steel rather than copper.

For one row of 3/8 OD tube with stainless steel fins, the gas side heat transfer results were:

$R_e = 296$

$h = 42.0$ BTU/hr ft^2°F

tube length/row = 19.5 ft

area/row = 22.3 ft^2

fin effectiveness = 0.76

gas side AU/row = 743 BTU/hr°F

As a preliminary estimate, it was assumed that the gas side heat transfer would be the dominating resistance. An initial guess of both gas and water side entrance and exit temperatures was made, as shown below.

	Gas Side	Water Side
Inlet	1768°F	545 F, 1000 psia, 51.3% quality
Exit	1061°F	707 F, 1000 psia

With these assumed conditions,

$$C_{min} = 760 \text{ BTU/hr°F}$$

$$C_{min}/C_{max} = 0.229$$

$$NTU/row = 0.966$$

Putting these values into equation (7),

$$\epsilon = 0.576$$

When this value for the effectiveness of the dryer was factored into a more precise heat balance for the overall exchanger, the values shown in Table VII resulted.

Pressure drop in the dryer was estimated by the method of Reference 8 for the two phase flow part of the dryer (also see Appendix VI).

The functions f_1 and r of Reference 8 allow the calculation of two phase pressure drop when the heat input to the water is uniform with length and the water is saturated at inlet. It follows, then, that if the heat input is uniform but the water has some quality at inlet, equation (12) and (13) can be generalized to

$$\Delta p = \Delta p_{TPF} + \frac{G^2}{gc}\left[r_e\,(p,\,x)_e - r_i\,(p,\,x)_i\right] \qquad (15)$$

Friction pressure drop in the superheated regime was estimated using the standard Darcy-Weisbach friction factor approach. Acceleration pressure drop in the superheated regime was estimated from the assumed saturation and exit conditions. The results were:

Two Phase Flow

$G = 1.004 \times 10^6$ lbm/hr ft^2

$R_{eLO} = 1.145 \times 10^5$

$f_{LO} = 0.01848$

$\Delta p_{LO} = 1.648$ psi

$p = 1000$ psia

$x_i = 0.513$

$x_e = 1.00$

$f_i = 9.13$

$f_e = 14.9$

$r_i = 0.155$

$r_e = 0.424$

$\Delta p = 14.03$ psi

Superheated

$R_e = 4.41 \times 10^5$

$f = 0.01544$

$\Delta p_f = 20.3$ psi

$\Delta p_{acc} = 2.8$ psi

$\Delta p = 23.1$ psi

Stability of the parallel flow paths was investigated using Quandt's (Ref. 4) approach. The approach to designing for stability in the dryer has been extremely conservative. Quality is quite high at entrance to the dryer at 57.3 percent. As mentioned in Section 6, this should have a strongly stabilizing effect on the flow. There are only two parallel passages in the dryer. The dryer tube material has been selected as Hastelloy X, as alloy with excellent strength at temperatures much higher than those anticipated for the dryer tube walls. To prevent possible development test burnout failures the dryer material and wall thickness selected allows operation at the maximum flow distortion. Even with no flow through one of the passages the tube wall would not fail at maximum system pressure and the wall in equilibrium temperature with the combustion gases. This precaution was necessary as demonstrated by the test results. No serious maldistributions of flow occurred in the dryer during steady state or transient tests. Detailed analysis of the stability of the dryer also confirmed the high degree of stability (see page 226).

Superheater

The fluid temperature estimates used to size the superheater are shown below.

	Gas Side	Water Side
Inlet	2030°F	707 F, 1000 psia
Outlet	1768°F	1000 F, 1000 psia

These conditions required

$$\epsilon = 0.221$$

$$C_{min}/C_{max} = 0.894$$

Unlike the rest of the unit, the maximum capacitance side in the superheater is the gas side, not the water side.

In keeping with a conservative approach to the problem of parallel flow stability, and in order to simplify the manifolding as much as possible, a monotube arrangement was chosen for the superheater. The surface used was the same as for the vaporizer, a 5/8 OD 321 stainless steel monotube with the tube lateral and depth spacing equal to 1.5 times the tube OD. The pertinent data for this surface are presented in the vaporizer section.

Gas side heat transfer results for this surface were

R_e = 1448
h = 23.2 BTU/hr ft^2°F
tube length/row = 29.8 ft/row
area/row = 4.88 ft^2/row
gas side AU/row = 113.1 BTU/hr°F

Water side friction factor and pressure drop were evaluated using the Darcy-Wiesbach friction factor. Acceleration pressure drop was estimated from the assumed inlet and exit conditions. The results were:

R_e = 5.58 x 10^5
Δpf = 62.2 psi
Δp = 64.2 psi
f = 0.01433
Δp_{acc} = 2.0 psi

Heat transfer coefficient on the water side was estimated from a modified form of the MacAdams equation

$$St = \frac{0.023}{(R_e)_f^{1/5} (P_r)_f^{2/3}} \tag{16}$$

The results were

h = 727 BTU/hr ft^2°F
area/row = 4.22 ft^2/row
water side AU/row = 3070 BTU/hr°F

Even in the superheater the gas side thermal resistance greatly dominates that on the water side. This means that the superheater tube temperatures will be quite close to the steam outlet temperature. A pure counterflow unit would probably have been feasible, although slightly less conservative, for this unit.

With the above results for the gas and water sides, the results for overall heat transfer were

$$AU/\text{row} = 109.1 \text{ BTU/hr°F}$$

$$C_{min} = 718 \text{ BTU/hr°F}$$

$$NTU/\text{row} = 0.1519$$

The effectiveness for each row of tube was estimated using the same method as described for the preheater. The minimum capacitance side is now the water side, (the mixed side), so that the pertinent equations become

$$\Gamma = 1 - e^{-NTU(C_{min}/C_{max})} \tag{17}$$

$$\epsilon_p = 1 - e^{-\Gamma/C_{min}/C_{max})} \tag{18}$$

The number of rows necessary to achieve the required effectiveness was then determined from equation (8) of this report.

The results obtained for the superheater were

$\epsilon_p = 0.1324$ $\quad\quad$ $\epsilon_2 = 0.235$

$\epsilon_3 = 0.318$

It appeared that two tube rows would be just barely adequate for the superheater, since the required effectiveness was 0.221.

HEAT BALANCE

As has been pointed out, sizing of the various parts of the unit required that assumptions be made about entering and leaving gas and water side conditions. In order to check these assumptions, a heat balance was made for the whole exchanger. By assuming constant heat capacities and heat transfer coefficients, it was possible to write this heat balance in the form of 12 linear equations in 12 unknowns. These equations and their derivations are presented below. The numerical subscripts refer to the numbered stations shown in Table VII.

Preheater

From the definition of effectiveness, and the calculated value of the preheater effectiveness,

$$\frac{T_5 - T_6}{T_5 - 160} = 0.8431 \tag{19}$$

A second preheater equation if formed from a heat balance on the preheater. The gas side specific heat is assumed to be 0.264 BTU/lbm. The water inlet enthalpy at 160°F is 127.9 BTU/lbm. The ratio of gas side to water side flow rate is 2.225. The energy balance equation for the preheater is then

$$h_8 = 127.9 + (T_5 - T_6) \times 0.264 \times 2.225 \tag{20}$$

A third preheater equation is written to determine the state of the water leaving the preheater. At the calculated preheater exit pressure of 1124 psia,

$$h_{sat} = 560.9 \text{ BTU/lbm} \qquad \Delta h_{fg} = 625.9 \text{ BTU/lbm}$$

so
$$x_8 = \frac{(h_8 - 560.9)}{625.9} \tag{21}$$

Vaporizer

The water in the vaporizer is assumed to be in equilibrium with its vapor at the vaporizer pressure. The average temperature of the water in the vaporizer is therefore 558°F. The effectiveness equation for the vaporizer then becomes

$$\frac{2500 - T_2}{2500 - 558} = 0.249 \tag{22}$$

The average gas side specific heat for the vaporizer was taken as 0.308 BTU/lbm°F. The heat balance equation for the vaporizer is then

$$h_9 = h_8 + (2500 - T_2) \times 0.308 \times 2.225 \tag{23}$$

The outlet pressure from the vaporizer was calculated as 1103 psia. At this pressure,

$$h_{sat} = 557.8 \text{ BTU/lbm} \qquad \Delta h_{fg} = 629.8 \text{ BTU/lbm}$$

The state equation is then

$$x_9 = \frac{(h_9 - 557.8)}{629.8} \tag{24}$$

Dryer

The water entering the dryer is assumed to be in equilibrium with its vapor at the dryer entrance pressure of 1103 psia. At this pressure,

$$T_{sat} = 557°F$$

The effectiveness equation is then

$$\frac{T_4 - T_5}{T_4 - 557} = 0.576 \tag{25}$$

The mean gas side specific heat for the dryer was taken as 0.289. The heat balance equation for the dryer is then

$$h_{10} = h_9 + (T_4 - T_5) \times 0.280 \times 2.225 \tag{26}$$

In calculating the outlet temperature of the dryer, the dryer pressure was taken as 1000 psia, and an average specific heat of 0.851 BTU/lbm°F was assumed for the superheated vapor. At 1000 psia,

$$h_v = 1191.8 \text{ BTU/lbm} \qquad T_{sat} = 545°F$$

The state equation for the dryer is then

$$T_{10} = 545 + \frac{(h_{10} - 1191.8)}{0.851} \tag{27}$$

Superheater

The effectiveness equation for the superheater is

$$\frac{T_{11} - T_{10}}{T_3 - T_{10}} = 0.235 \tag{28}$$

With $C_{min}/C_{max} = 0.894$, and the water side as the minimum capacitance rate side, the heat balance equation for the superheater is

$$\frac{T_3 - T_4}{T_{11} - T_{10}} = 0.894 \qquad (29)$$

An additional heat balance equation was written in order to allow for some heat loss from the unit to ambient. This heat loss was idealized as a drop in gas temperature taking place between the vaporizer and the superheater. The temperature drop used was consistant with heat loss observations on the test bed unit now in operation. The temperature drop used was 32°F, so the heat loss equation is

$$T_2 - T_3 = 32$$

The solution to these equations is shown in Table VII. The values shown in Table VII agree reasonably close with those assumed in the design.

An approach similar to that presented above is used to investigate off-design performance of the unit in the next section.

PART LOAD PERFORMANCE

Part load performance of the single flow path steam generator has been estimated at 5 percent of the rated air flow and 2500°F flame temperature. The results of the part load performance estimation are shown in Table X.

It is evident that as load is reduced, a larger proportion of the total heat transfer takes place in the vaporizer tubes. This causes the quality at exit from the vaporizer to increase as load is reduced. The ratio of water flow to gas flow remains nearly constant as load is reduced. This is because the effectiveness of the unit is quite high, even at full load. Reduction in load therefore produces only a very slight increase in effectiveness, hence only a very slight increase in the ratio of water flow to gas flow.

In general, the method used to estimate part load performance was to assume that the gas side was the dominating heat transfer resistance. If this is the case, and if the gas side is the minimum capitance rate side, as is usually the case for the unit being considered here, then NTU is proportional to the Stanton number, which in turn can usually be considered to be inversely proportional to Reynolds number to some power, depending on the flow regime and heat transfer matrix geometry. In equation form,

$$NTU \propto St \propto Re^{-x} \propto W^{-x} \qquad (30)$$

TABLE X

CONDITIONS AT 138 lbm/hr GAS FLOW AND 66.4 lbm/hr WATER FLOW

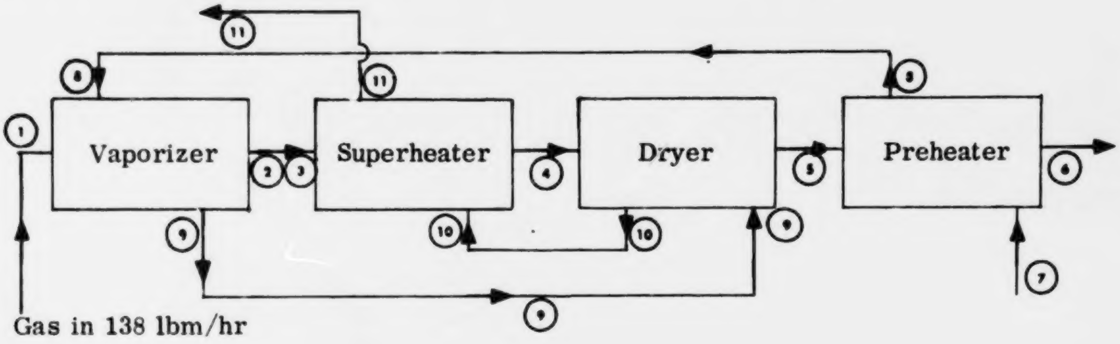

Station	Temperature (°F)	Pressure
1	2500	Atmospheric
2	1281	
3	1249	
4	990	
5	693	
6	172	Atmospheric
7	160	1000 psia
8	418	
9	545 (90.6% quality)	
10	700	
11	962	1000 psia

For the finned tubes of the preheater, the exponent x is 0.624. The full load NTU per row is 0.967, so at five percent of the rated gas flow,

$$\text{NTU/row} = 20^{0.624} \times 0.967 = 6.27$$

For the three cross counterflow passes of the preheater, with an NTU of 6.27 per row, the overall preheater effectiveness is 0.978. The full load preheater effectiveness was 0.843. As was expected, the very large increase in NTU at part load has produced only a slight increase in effectiveness.

For the bare tubes of the vaporizer, the exponent x is 0.409. The full load NTU is 0.287, so at five percent gas flow,

$$\text{NTU} = 20^{0.409} \times 0.287 = 0.977$$

For a heat exchanger with the minimum to maximum capacitance rate ratio equal to zero, this NTU produces an effectiveness of 0.624. This effectiveness compares to an effectiveness of 0.249 at full load. It is this increase in effectiveness with reducing load which causes a larger proportion of the total heat transfer to occur in the vaporizer at part load.

In the dryer, it is not valid to assume that the gas side resistance will still dominate the heat transfer process even at low load. The large proportion of fin area/total area on the gas side, the rather low fin effectiveness at full load, the very large ratio of gas side area to water side area, and the fact that for the finned tubes of the dryer, the gas side exponent x is much larger than it is on the water side, all combine to make the heat transfer resistance on the water side increase much more rapidly than it does on the gas side as load is reduced. At five percent of rated gas flow, the gas side and water side resistances are of the same order of magnitude.

Heat transfer coefficient on the gas side can be estimated by an equation very similar in form to equation (30)

$$h \propto W^{(1 - x)} \tag{31}$$

where the exponent x has the same value as it does in equation (30). Equation (31) implies that thermal transport properties undergo negligible changes as the flow rate is changed. This is an adequate assumption for initial performance estimates.

At full load, the gas side heat transfer coefficient was 42.0 BTU/hr ft^2°F. At five percent of the rated gas flow, with x equal to 0.624 as in the preheater,

$$h = (0.05)^{0.376} \times 42.0 = 13.62 \text{ BTU/hr ft}^2$$

With this h, the fin effectiveness increases to 0.90, which is considerably above its full load value of 0.76. The hA/row at five percent load then becomes 278 BTU/hr°F. The full load gas side hA/row was 743 BTU/hr°F. The gas side hA decreases much more slowly than the flow rate.

It was expected that at part load, dryout on the water side would occur quite close to the entrance of the dryer tube row. Part load heat transfer estimates in the dryer were therefore based on the assumption that the entire length of the dryer was filled with superheated steam. At full load, the water side heat transfer coefficient in the superheated regime was 1080.5 BTU/hr ft^2°F. For turbulent flow inside tubes, x is 0.2, so at five percent flow,

$$h = (0.05)^{0.8} \times 1080.5 = 98.4 \text{ BTU/hr ft}^2\text{°F}$$

With this h, the water side hA/row becomes 332 BTU/hr°F, which is only slightly larger than the gas side hA/row. The overall hA/row for the dryer then becomes 151.3 BTU/hr°F, giving an NTU for the dryer of 3.93. Since at part load the dryer operates almost entirely in the superheated regime, C_{min}/C_{max} is much higher than it is at full load. After a few iterations, the final value of C_{min}/C_{max} used was 0.844, which gave an effectiveness of 0.667.

NTU in the superheater was estimated by the same method used for the preheater and vaporizer, except that allowance must be made for the fact that, in the superheater, while the dominant thermal resistance is on the gas side, the minimum capacitance side is the water side. The exponent x for the superheater tubes is 0.409, as it is for the vaporizer. The full load NTU/row for the superheater was 0.1519. The gas flow is at five percent of rated flow, but the water flow is 5.53 percent of the rated flow. The NTU/row therefore becomes

$$\text{NTU/row} = 20^{0.409} \times 0.1519 \times (0.05/0.0553) = 0.468$$

With this NTU/row, the effectiveness for the superheater becomes 0.477.

With effectiveness for each of the components in the exchanger estimated, linearized effectiveness, state, and energy balance equations were written for each of the components, just as was done for the full load performance estimation, with the results shown in Table X.

DRYER HEAT TRANSFER

The location of the dryout point in the dryer at full load was estimated, and water side heat transfer coefficients were estimated for the dryer both at the dryout point and in the superheated region.

The method presented by Tippets (Ref. 10) was used to estimate the location of the dryout point. The results were:

$$Z_{crit} = 6.44 \text{ ft}/(L = 19.5 \text{ ft - total})$$

$$x = 0.745$$

$$q_{crit} = 1.651 \times 10^5 \text{ BTU/hr ft}^2$$

where Z_{crit} is the flow path distance into the tube at which dryout occurs, x is the quality at the dryout point, and q_{crit} is the critical heat flux.

The heat transfer coefficient at the dryout point was estimated from the correlation of Bishop, Sandberg, and Tong (Ref. 9). Their correlation is

$$h = \frac{0.0193\, G C_{pf} \left(\rho_G/\rho_b\right)^{0.68} \left(P_r\right)_f^{0.23}}{(Re)^{0.2} \left(v_G/v_L\right)^{0.068}} \tag{32}$$

They recommended using a homogeneous flow model for the estimation of the ratio (ρ_G/ρ_b). For homogeneous flow,

$$\frac{\rho_G}{\rho_b} = \frac{x((v_G/v_L) - 1) + 1}{(v_G/v_L)} \tag{33}$$

In equation (32) the transport properties, such as viscosity, thermal conductivity, specific heat, and Prandtl number, are evaluated for the gas phase. Mass flux is evaluated for the entire flow, both liquid and gas. The input quantities and results for equations (32) and (33) were:

C_p = 1.162 BTU/lbm°F k = 0.031 BTU/hr ft°F

μ = 0.0481 lbm/hr ft $Re = 5.76 \times 10^5$

P_r = 1.803 ρ_G/ρ_b = 0.757

v_G/v_L = 20.6 h = 1224 BTU/hr ft^2°F

It appears that dryout occurs at a sufficiently high quality and at sufficiently high mass fluxes to prevent any drastic overheating of the dryer tube wall.

The heat transfer coefficient in the superheated regime of the dryer was estimated using a modified form of the MacAdams equation.

$$h = \frac{0.023\, G\, C_p}{(Re)_f^{0.2} \, (P_r)_f^{2/3}} \tag{34}$$

The input quantities and results for equation (34) were

C_p = 0.851 BTU/lbm°F P_r = 1.486

μ = 0.0521 lbm/hr ft h = 1080 BTU/hr ft^2°F

k = 0.0298 BTU/hr ft°F

It is interesting to see that the average heat transfer coefficient in the superheated regime is slightly lower than that at the dryout point. This is because of the high quality at dryout, and also because the non-ideality of the vapor phase at saturation at the dryer pressure produces quite high specific heat and Prandtl number at the dryout point.

With the heat transfer coefficients on the water side known, the overall dryer heat transfer was re-established. The results were:

Gas Side AU/row = 743 BTU/hr°F

Overall AU/row = 659 BTU/hr°F

NTU/row = 0.857

C_{min}/C_{max} = 0.222

ϵ = 0.540

The ϵ computed with the water side thermal resistance factored in was only very slightly less than the 0.576 estimated without it.

BURNOUT

The high quality calculated at exit from the vaporizer at five percent gas flow indicated that as load is reduced, a point must be reached where dryout occurs in the vaporizer tubes rather than the dryer. In such a case, tube wall temperatures in the vaporizer are subject to two conflicting tendencies. The reduction in water side heat transfer coefficient as dryout occurs tends to increase the tube wall temperature. On the other hand, especially in the second row of the vaporizer, the gas temperature seen by the tubes becomes lower as load is reduced, tending to reduce the tube wall temperature. If dryout can be delayed to a sufficiently high quality, so that post-dryout heat transfer coefficients are high, and if dryout in the vaporizer can be delayed until load is so low that gas temperatures seen by the vaporizer tubes are low, then dryout in the vaporizer will not produce excessive tube wall temperatures.

The possibility of excessive vaporizer tube wall temperatures at low load was checked by investigating the probability and consequences of dryout in the vaporizer tubes at five percent of rated gas flow. It was found that at this load, the water flow rate was so low that it was outside the range of all of the correlations used for investigating burnout at full load. The Westinghouse APD correlation for example, predicted a dryout quality in excess of 100 percent. The Baker plot shows that the water flow rate is so low that even at the vaporizer exit, the flow is probably in the stratified flow or possibly the wave flow regime, rather than the annular flow regime. In any case, it appears that at this low flow rate, dryout is likely to be delayed to a very high quality.

In the full load dryout investigations, it was found that when dryout occurs at high quality, post dryout heat transfer coefficients could be fairly well estimated by simply using the modified MacAdams pipe flow equation used to estimate heat transfer coefficient in the superheated regime. This approach was used for the vaporizer tubes, using thermal transport properties for saturated steam at 1000 psia. Gas side heat transfer coefficient was estimated using the same approach as was used for the dryer tubes, with exponent x equal to 0.409 for the bare tubes of the vaporizer. The results for heat transfer coefficient were 90.4 BTU/hr ft^2°F on the water side, and 4.12 BTU/hr ft^2°F on the gas side.

At five percent of rated gas flow, the gas temperature at exit from the first row of vaporizer tubes is already down to 1744°F. An effective gas source temperature for any point along a tube row can be determined from the following equation, which is derived by considering an elemental slice of tube as a miniature heat exchanger with the gas side capacitance rate negligibly small compared to the water side capacitance rate.

$$T_{source} = T_w + \frac{\left(T_{gi} - T_w\right)\left(1 - e^{-NTU\, C_{min}/C_g}\right)}{NTU} \qquad (35)$$

From equation (35) the effective source temperature for the second row of vaporizer tubes is only 1494°F.

Since gas side and water side heat transfer areas are nearly equal, the tube wall temperature in the vaporizer was estimated from

$$T_W = h_w T_w + h_g T_{source} \qquad (36)$$

It was found that even if dryout did occur in the second row of the vaporizer, the maximum tube wall temperature would be only 586°F.

From the above investigation the following conclusions were drawn.

1. At some part load condition, probably less than five percent load, the dryout zone will move into the vaporizer tubes.

2. When this occurs, water side heat transfer coefficients in the dried out zone will be high enough, and effective source temperatures will be low enough, so that excessive tube wall temperatures will not result.

AIR SIDE PRESSURE DROP

Air side pressure drop at full load has been estimated, using a slightly mofified form of Kays and London (Ref. 5) equation (24b) presented on page 21 of their book.

$$\Delta P = \frac{G^2 v_i}{{}^{2}gc} \left[(1 + \sigma^2)\left(\frac{v_e}{v_i} - 1\right) + \frac{4fL}{DH} \; \frac{v_m}{v_i} \right] \tag{37}$$

The results of the pressure drop analysis are summarized below:

Component	ΔP (in. H_2O)
Vaporizer	0.151
Superheater	0.138
Dryer	0.387
Preheater	0.642
Total	1.318

The pressure drop is quite low, considering the high effectiveness of the unit.

PARALLEL FLOW PASSAGE STABILITY

Theory

A computer program for preducting the hydrodynamic stability of flow in parallel passages was written. The program has been used to investigate the hydrodynamic stability of the two parallel flow tubes in the dryer section of the steam generator. It was found that these passages should be quite stable, with a damping coefficient in excess of one.

The program uses the method of Quandt (Ref. 4) which is essentially a perturbation analysis used to find the transfer function for the perturbation in the water rate as a response to an input perturbation in the heating rate. Quandt's result for the transfer function is:

$$\frac{(\Delta W_i / W_i)}{(\Delta \bar{\Theta} / \bar{\Theta})} = \frac{-H(Ds^2 + Es + C)}{\left\{ \begin{array}{l} s^2\,[\beta(A + D) - \;\; HD] + s[\alpha(A + D) + \beta(B + E) - \;\; HE] \\ + [\alpha(B + E) - \;\; HC] \end{array} \right\}} \qquad (38)$$

where

W = water rate, or its La Place transform

$\bar{\Theta}$ = average surface heat flux for the entire channel, or its La Place transform

H = steady state change in coolant enthalpy as it flows through the channel

A, B, C, D E, α, β = parameters which depend on the unperturbed conditions in the channel. One of the main functions of the program is to evaluate these parameters

i = at the inlet to the heated passage

Each parallel flow path is idealized as shown below

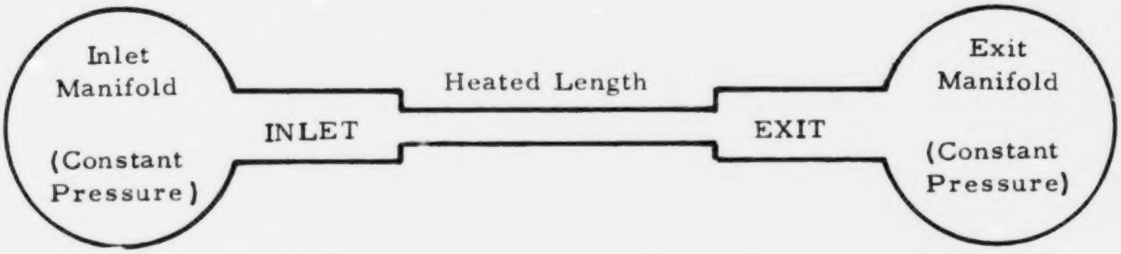

The heated passage is connected at both ends to manifolds which are maintained at constant pressure. There are unheated inlet and exit lengths connecting the heated passages with the manifolds. Quandt indicates that fluid friction, entrance losses to the heated channel, and mass inertia of the fluid are important terms in the entrance length pressure drop. However, exit losses from the heated channel are important in the exit length pressure drop. The exit pressure drop is a function of exit losses only because in many cases the flow either discharges directly into a plenum or into a large diameter pipe which later joins the effective exit plenum. Exit friction, elevation, and time acceleration losses are not included since these are usually very small and the time lags associated with large steam volumes are usually much longer than the transients which are of interest in the stability analysis.

Although the inlet enthalpy is considered to be constant, the flow is assumed to be perturbed in such a way that the resistance time of the flow in the channel is very small when compared to the time scale of the transients considered. If this is the case, then

$$\Delta W = \Delta W_i + (\Delta W_e - \Delta W_i)\frac{z}{L} \tag{39}$$

$$\Delta h = \Delta h_e \frac{z'}{L} \tag{40}$$

$$z' = L(h - h_i)/H \tag{41}$$

where z = distance from the inlet of the heated channel

L = length of heated channel

z' = a weighted distance through the heated channel

e = at the exit of the heated passage

i = at the inlet of the heated passage

With the assumptions described above, it is possible to make a linearized perturbation analysis, with the end result as shown in equation (38).

The computer program input consists of sufficient information to completely define the flow passage geometry, the state of the fluid within the passage, and the friction loss pressure gradient within the passage. This information consists of specific volume as a function of enthalpy, in the form of a table consisting of two corresponding vectors $[(v_1, h_1), (v_2, h_2), (v_3, h_3) \ldots (v_m, h_m)]$, enthalpy as a function of distance through the heated channel in the form of two corresponding vectors, loss factors at inlet and exit, channel areas, friction loss factors for the heated channel, areas for the inlet, main, and exit channels, lengths for the inlet and the heated channels, and the steady state flow rate. The program incorporates an interpolation subroutine which allows functional values to be determined given a value of the independent variable and its functional dependence expressed in the form of two corresponding vectors. For instance, for a value of v between v_2 and v_3 above, the subroutine will interpolate the value of h which is between h_2 and h_3.

The program assumes that in the liquid and vapor phases, friction pressure drop can be described by the usual Darcy-Weisbach relation, while in the two phase regime it can be described by the method described in Appendix VI. The function f_1 of Appendix VI is input as a function of quality in the form of two corresponding vectors.

In the liquid and vapor phases, the interpolation of specific volume as a function of enthalpy is quite straightforward. In the two phase regime, Quandt recommends the following "fog flow" model for calculating specific volume and the partial derivative of density with respect to enthalpy.

$$v = v_L + xv_{LG} \tag{42}$$

where

v = specific volume ($\equiv 1/\rho$)

x = quality

L = liquid phase

LG = change associated with change from liquid to vapor phase

$$\bar{\rho} \equiv \frac{R_G}{v_G} + \frac{(1 - R_G)}{v_L} \tag{43}$$

where

$\bar{\rho}$ = average static density

R_G = void fraction

G = gas phase

$$\frac{\partial \rho}{\partial h} = -\bar{\rho}^2 \frac{v_{LG}}{h_{LG}} \tag{44}$$

The void fraction, R_G, is determined from the method suggested by Yamazaki and Shiba (Ref. 11) where

$$\lambda \equiv \frac{(1 - x)}{x} \frac{v_L}{v_G} \tag{45}$$

$$R_G = \frac{1}{2} [(2 + \lambda) - \sqrt{\lambda(4 + \lambda)}] \tag{46}$$

where λ = liquid-vapor volume flow rate ratio

The program itself is primarily a straightforward evaluation of the parameters A, B, C, D, E, α, and β, as shown in Equation (38) and in Quandt. These parameters in turn depend on the channel geometry and loss factors and on six integrals of fluid properties and pressure gradients, as shown below:

$$D \equiv L/2g_c A_f \tag{47}$$

$$A \equiv D + L_i/g_c A_{fi} \tag{48}$$

$$B \equiv \frac{Wv_i}{g_c A_f^2}\left(\left(\frac{FL}{DH}\right)_i \left(\frac{A_f}{A_{fi}}\right)^2 - 1 + K_i - \left(\frac{A_f}{A_{fi}}\right)^2\right) - I_1 \tag{49}$$

$$M \equiv Ke + \left(\frac{A_f}{A_{fe}}\right)^2 + 1 \tag{50}$$

$$C \equiv -\left|\frac{(W/A_f)^2 M}{2g_c}\left(\frac{\partial v}{\partial h}\right)_e - I_2 + \frac{g}{g_c} I_3\right| \Big/ A_f I_3 \tag{51}$$

$$E \equiv \frac{Wv_e M}{g_c A_f^2} - I_4 \tag{52}$$

$$\alpha \equiv -\frac{W}{A_f I_3} \tag{53}$$

$$\beta \equiv \frac{-I_5}{I_3} + I_6 \tag{54}$$

$$I_1 \equiv \int_0^L \frac{\partial}{\partial w}\left(\frac{\partial P_f}{\partial z}\right)\left(1 - \frac{z}{L}\right) dz \tag{55}$$

$$I_2 \equiv \int_0^L \left[\frac{\partial}{\partial \rho}\left(\frac{\partial P_f}{\partial z}\right)\right] \frac{\partial \rho}{\partial h} \frac{z'}{L} \, dz \tag{56}$$

$$I_3 \equiv \int_0^L \frac{\partial \rho}{\partial h} \frac{z'}{L} \, dz \tag{57}$$

$$I_4 \equiv \int_0^L \frac{\partial}{\partial w}\left(\frac{\partial P_f}{\partial z}\right)\frac{z}{L}\;dz \tag{58}$$

$$I_5 \equiv \int_0^L \rho\,\frac{z'}{L}\;dz \tag{59}$$

$$I_6 \equiv \int_0^L \frac{\partial h}{\partial z}\,\frac{z}{L}\;dz \tag{60}$$

where

g = acceleration due to gravity, 32.2 ft/sec^2

g_c = gravitational mass-force-time conversion constant, 32.2 ft lbm/sec^2 lb

A_f = flow area of heated channel

L_i = inlet channel length

A_{fi} = flow area of inlet channel

A_{fe} = flow area of exit channel

F = Darcy-Weisbach friction factor

K_i = entrance loss factor for heated channel

K_ϵ = exit loss factor for heated channel

$\partial P_f/\partial_z$ = pressure gradient due to friction losses

ρ = density

All of the integrands in I_1 through I_6 can be determined as a function of z, the position in the channel, so the numerical evaluation of the integrals is quite straightforward. The program uses Simpson's rule.

With the integrals I_1 through I_6 and the parameters A, B, C, D, E, α, and β determined, it is possible, through examination of equation (38) to determine any of the properties of interest which are usually considered in the study of a second order system, such as frequency response, steady state gain, step function response, natural frequency, and system damping. A study of these factors and how they change with changes in the system geometrical and thermodynamic inputs is often much more informative than any number of particular solutions could be. The program determines steady state gain, undamped natural frequency, and the system damping coefficient.

From a knowledge of La Place transforms, the transfer function can be written in the generalized form as:

$$\frac{(\Delta W_i / W_i)}{(\Delta \Phi / \Phi)} = \frac{K}{S^2 + 2\eta\, \omega_o S + \omega_o{}^2}$$

Rearranging Equation (38) into this form gives:

$$\omega_o = \sqrt{\frac{\alpha(B + E) - HC}{\beta(A + D) - HD}} \qquad (61)$$

$$\eta = \frac{\alpha(A + D) + \beta(B + E) - HE}{2\sqrt{[\alpha(B + E) - HC]\,[\beta(A + D) - HD]}} \qquad (62)$$

$$G = \frac{-CH}{\alpha(B + E) - CH} \qquad (63)$$

where

ω_o = undamped natural frequency

η = damping factor

G = steady state gain

Chugging

The phenomenon called "chugging" is associated with a diverging oscillatory response, that is, with the damping coefficient in the range

$$-1 < \eta < 0 \qquad (64)$$

The conditions for which this can occur can be determined from a study of the denominator of equation (38). Beta is always positive for a heated channel, and A and D must always be positive. The first term in the denominator of equation (38) must therefore be positive. The "chugging" stability boundary is therefore defined by the conditions causing the bracket multiplying s in the denominator of equation (38) to become negative.

The second bracket of Equation (39) may be rearranged to the form

$$\alpha(A + D) + \beta B + E(\beta - H) \qquad (65)$$

α is always positive, so the first term is always positive. An examination of equations (49) and (55) shows that high inlet losses tend to make β more positive, thus stabilizing the flow. Friction pressure losses also stabilize the flow. The fact that inlet losses tend to stabilize the flow suggests why orifices at the inlet to parallel flow passages are frequently mentioned as a means of eliminating chugging. An examination of equations (52) and (58) show that E must always be positive, and that high exit losses and high friction pressure losses tend to drive E more positive. This is not necessarily a stabilizing factor, however, since E multiplies the term (β - H).

It seems that in practice, the only way for a chugging response to develop is for β to become small, so that the stabilizing effect of the βB term is minimized while the E(β - H) term may become negative. Equation (54) shows that this can happen if the integral I_3, which is always negative, has a large absolute value. The absolute value of I_3 can become very large if there is a substantial region of flow in which the quality is low, as is shown by equations (57) and (44). This is especially true if the pressure is low, so that v_{LG} is large, as is shown by equation (44). A large degree of subcooling tends to accentuate all the above effects, because it increases the value of the weighting multiplier z'/L in equation (58) for regions of low quality. All of the above trends have been observed in operation of the present test bed boiler, as has been discussed in Section 6 of this report.

As seen from the above discussion, the best way to avoid chugging is to ensure that there is some quality at entrance to the parallel flow passages. If this is not practical, the flow can always be stabilized if the inlet loss factor is made sufficiently high.

The dryer tubes were used as a test case for the stability program. The approach taken was to design for very high quality at entrance to the parallel flow passages of the dryer, as shown in Table XI. The stability results from the computer run are shown in Table XI.

As shown, the value of η is greater than one, that is, the system is critically overdamped. For such a system, dynamic response to any oscillatory input over the entire frequency range is quite poor. Calculations indicated that the dryer tubes in the improved test bed unit would not exhibit any tendency toward chugging.

The reason for the high damping coefficient in the dryer tubes is evident from a study of Table XI. The high value of the quality at inlet to the dryer has kept the absolute value of the integral I_3 quite small, thus allowing β to become large enough so that the damping coefficient becomes strongly positive.

TABLE XI

COMPUTER STABILITY RESULTS - DRYER TUBES

$I_1 = -3.902 \times 10^4$ lb sec/lbm ft^2

$I_2 = -11.579$ lb lbm/ft^2 BTU

$I_3 = -0.12847$ lbm^2/ft^2 BTU

$I_4 = -3.917 \times 10^4$ lb sec/lbm ft^2

$I_5 = 22.17$ lbm/ft^2

$I_6 = 195.63$ BTU/lbm

$A = D = 507.2$ lb sec^2/lbm ft^2

$B = 3.134 \times 10^4$ lb sec/lbm ft^2

$C = 1.8854 \times 10^5$ lb/lbm ft^2

$E = 5.662 \times 10^4$ lb sec/lbm ft^2

$\alpha = 2173$ BTU/lbm sec

$\beta = 368.2$ BTU/lbm

$\omega_o = 26.04$ rad/sec

$\eta = 1.3445$

$G = -0.6511$

$H = 399.8$ BTU/lbm

APPENDIX IV

BURNOUT

The vaporizer is ordinarily required to produce dry working fluid at considerable superheat. This means that at some point in the unit the quality will become so high that there will be a transition from nucleate to film boiling, with its characteristic drastic reduction in fluid side heat transfer coefficient. Flame temperature in the combustor is ordinarily above the melting point of most high temperature alloys. It is obvious that the location of the point of departure from nucleate boiling must be accurately predicted and carefully controlled in order to prevent disastrous failure of the tubes

Design approach used here in the high efficiency steam generator is to place the vaporizer closest to the combustor, using it to substantially cool the combustion gases and thus protect the superheater tubes. Burnout in the vaporizer section is prevented by ensuring that the vapor leaving the vaporizer is quite moist over the entire 40 to 1 turndown ratio. The transition from nucleate to film boiling takes place in the superheater coils, in a region where gas temperatures are quite low.

The departure from nucleate boiling has been estimated by a combination of four different methods.

The first of these was a simple estimation of the changes in types of two phase flow in the vaporizer. According to Tong (Ref. 2), page 147, the departure from nucleate boiling is associated with a "drying out" of the liquid film on the wall. A transition from annular to dispersed flow as the quality increases is therefore likely to cause burnout. Flow rate per unit area should be chosen so that the flow is annular throughout the vaporizer, if at all possible.

The type of two phase flow existing was determined by the method of Baker (Ref. 12). A good description of the various types of flow discussed by Baker is given on page 170 of Reference 13.

The second method was to simply estimate the vapor velocity. Bennett, et al. (Ref. 7) found that steam velocities in excess of 50 to 60 ft/sec tended to create sufficient splash and wave action to literally blow the liquid film off the wall. Mean vapor velocity is estimated from:

Preceding page blank

$$V_v = \frac{G x v_v}{\alpha} \tag{1}$$

Where G is the total mass flow rate per unit area, x is the quality, V_v is the specific volume of the vapor phase, and α is the void fraction. The void fraction was estimated from equation (4) of Yamazaki and Shiba (Ref.11),

$$\alpha = \frac{1}{2}\left[\left(2 + \frac{1}{Rv}\right) - \sqrt{\frac{1}{Rv}\left(4 + \frac{1}{Rv}\right)}\right] \tag{2}$$

where Rv is the volumetric flow ratio, given by

$$Rv = \frac{x}{1 - x}\left(\frac{v_v}{v_L}\right) \tag{3}$$

The third method was the Westinghouse Atomic Power Division Correlation for critical enthalpy rise presented by Tong, et al. (Ref.14). If the water is assumed to enter the vaporizer as saturated liquid, this correlation gives the critical quality as:

$$\begin{aligned} x_{crit} = {} & (0.825 + 2.3e^{-17De})e^{-1.5G/10^6} \\ & -0.41e^{-0.0048L/De} - \frac{1.12}{(v_v/v_L)} + 0.548 \end{aligned} \tag{4}$$

Where De is the tube diameter in inches L is the tube heated length, and G is in units of lbm/hr ft^2.

The fourth method was correlation presented by Tippets (Ref.10). This method has a solid theoretical basis and is probably the most reliable of the four. When Tippets' equations (35a) and (35b) are combined with information about the two phase friction factor presented on page 81 of Tong (Ref. 2) and in Yamazaki and Shiba (Ref.11), there results

$$q_c = \frac{C''\psi^m}{\epsilon} \tag{5}$$

$$\psi = B_1 \div \left(\frac{1 - x}{1 - \alpha}\right)^{7/4} \tag{6}$$

$$B_1 = \frac{0.667\,\sigma\,(1 + (v_v/v_L))}{flo\ (G^2/gcPL)\ De\ (1 + \sqrt{(v_v/v_L)})^2} \qquad (7)$$

$$\epsilon = \frac{1 + \left(1 + \frac{C'x}{1 - x}\right)\left(\frac{v_v}{v_L}\right)}{B_2\left(\frac{1 - x}{1 - \alpha}\right)^{7/8}} \qquad (8)$$

$$B_2 = \left(\left(\frac{v_v}{v_L}\right)\left(\frac{flo}{4}\right)\right)^{1/2} G\ Hfg \qquad (9)$$

In these equations, σ is the surface tension, flo is the Darcy-Weisbach friction factor computed assuming the entire flow is in the liquid phase, PL is the density of the liquid phase, C', C" and m are empirically determined constants, and Hfg is the latent heat of vaporization. The units of $G^2/gcPL$ are pounds per square inch. B_1 is a pure number, as is ψ. The units of ϵ are reciprocal heat flow per unit area, that is, hr ft^2/BTU. Tippets used m = 0.75, C" = 0.53, and C' = 1.0 for his empirical constants. Peterson (Ref.15) recommends C' = 2.5 as a more conservative value. A more detailed discussion of how equations (5) through (9) were obtained is presented in Appendix V.

It can be seen that the critical heat flux is approximately inversely proportional to the square root of the mass flow per unit area. Preliminary calculations indicate that mass flow rate per unit area in the vaporizer is more likely to be determined by burnout considerations than by any need to limit the pressure drop.

In summary, four different criteria are used to determine whether or not burnout is likely to occur in the vaporizer tubes. If the Baker plot indicates that flow is in the annular regime, if Bennett's criterion of steam velocity not in excess of 50-60 ft/sec is not greatly exceeded, if the Westinghouse APD critical exit quality is well in excess of the computed exit quality, and if Tippett's critical heat flux is well in excess of the calculated heat flux, and all of these criteria are satisfied over the entire forty to one load range, then the design of the vaporizer section is assumed to be satisfactory.

APPENDIX V

Preceding page blank

A MODIFIED VERSION OF THE TIPPETS BURNOUT CORRELATION

The original correlation presented by Tippets is

$$qc = \frac{C''\psi^m}{\epsilon} \tag{I-1}$$

with

$$\psi = \frac{\sigma \rho_L (1 + \rho_L/\rho_v)}{\phi_{TPF} f_F G^2 b (1 + \sqrt{\rho_L/\rho_v})^2} \tag{I-2}$$

and

$$\epsilon = \frac{1 + \left(1 + \frac{C' x}{1 - x}\right) \frac{\rho_L}{\rho_v}}{\left(\left(\frac{\rho_L}{\rho_v}\right) \phi_{TPF} f_F G H_{fg}\right)} \tag{I-3}$$

The two phase flow friction multiplier, ϕ_{TPF}, and the two phase flow friction factor, f_F, are related to the two phase pressure drop by

$$\left(\frac{dp}{dL}\right)_{TPF} = \frac{\phi_{TPF} f_F G^2}{2 \rho_L b} \tag{I-4}$$

Tippets determined the constants in his correlation by using the method of Martinelli and Nelson (Ref. 8). Their equation is

$$\left(\frac{dp}{dL}\right)_{TPF} = \left(\frac{dp}{dL}\right)_{LO} (1 - x)^{1.75} \phi_L{}^2 \tag{I-5}$$

where ϕ_L is defined by

$$\phi_L{}^2 \equiv \left(\frac{dp}{dL}\right)_{TPF} \div \left(\frac{dp}{dL}\right)_{LPF} \tag{I-6}$$

Preceding page blank

Yamazaki and Shiba (Ref.11) present a very useful empirical relation for ϕ_L,

$$\phi_L = (1 - \alpha)^{-7/8} \qquad \text{(I-7)}$$

But,
$$\left(\frac{dp}{dL}\right)_{LO} = \frac{G^2}{g_c \rho_L} \frac{f_{LO}}{4b} \qquad \text{(I-8)}$$

Combining equations I-4 through I-8 gives

$$\phi_{TPF} f_F = \frac{f_{LO}}{4} \left(\frac{1 - x}{1 - \alpha}\right)^{7/4} \qquad \text{(I-9)}$$

When this is substituted into (I-2) there results

$$\psi = B_1 + \left(\frac{1 - x}{1 - \alpha}\right)^{7/4} \qquad \text{(I-10)}$$

$$B_1 = \frac{0.667\ \sigma\ (1 + (v_v/v_L))}{f_{LO}\ (G^2/g_c \rho_L)\ D\ (1 + \sqrt{(v_v/v_L)}\ )^2} \qquad \text{(I-11)}$$

when σ is in lb/ft, $G^2/g_c\rho_L$ is in psi, and D is in inches. Equations (I-10) and (I-11) are equations (6) and (7) of the main body of this report.

Substituting equation (I-9) into equation (I-3) yields

$$\epsilon = \frac{1 + \left(1 + \frac{C' x}{1 - x}\right)\left(\frac{v_v}{v_L}\right)}{B_2 \left(\frac{1 - x}{1 - \alpha}\right)^{7/8}} \qquad \text{(I-12)}$$

with
$$B_2 \equiv \left(\left(\frac{v_v}{v_L}\right)\left(\frac{f_{LO}}{4}\right)\right)^{1/2} G\ H_{fg} \qquad \text{(I-13)}$$

Equations (I-12) and (I-13) are equations (8) and (9) of the main body of this report.

APPENDIX VI

GENERALIZATION OF THE MARTINELLI-NELSON METHOD FOR ESTIMATING TWO PHASE PRESSURE DROPS

Martinelli and Nelson' (Ref. 8) method for two phase pressure drop depends on their observation that the friction pressure drop can be described by the following equation.

$$\left(\frac{\partial P}{\partial Z}\right)_{TPF} = \left(\frac{\partial P}{\partial Z}\right)_{LO} \cdot J\,(x, P) \tag{1}$$

Integrating equation (1) from inlet to exit

$$\int_{Z_i}^{Z_e} \left(\frac{\partial P}{\partial Z}\right)_{TPF} dZ = \Delta P_{TPF} = \left(\frac{\partial P}{\partial Z}\right)_{LO} \int_{Z_i}^{Z_e} J(x, P)dZ \tag{2}$$

If the absolute pressure is nearly constant, and the heating is uniform,

$$x = A + K(Z_e - Z_i) \tag{3}$$

where

$$K = \frac{x_e - x_i}{Z_e - Z_i} \tag{4}$$

then

$$dZ = \frac{dx}{K} = dx\,\frac{(Z_e - Z_i)}{(x_e - x_i)} \tag{5}$$

Substituting equation (5) into equation (2)

$$\Delta P_{TPF} = \left(\frac{\partial P}{\partial Z}\right)_{LO} \frac{(Z_e - Z_i)}{(x_e - x_i)} \int_{x_i}^{x_e} \underset{P = \text{const}}{J(x, P)\,dx} = \frac{\Delta P_{LO}}{x_e - x_i} \int_{x_i}^{x_e} \underset{P = \text{const}}{J(x, P)\,dx} \tag{6}$$

Preceding page blank

If $$Z_i = 0 = x_i \tag{7}$$

then equation (6) reduces to

$$f_1 \equiv \left(\frac{\Delta P_{TPF}}{\Delta P_{LO}}\right)_{x_i = 0} = \frac{1}{x_e} \int_0^{x_e} \begin{matrix} J(x,\ P)dx \\ P = \text{const} \end{matrix} \tag{8}$$

The function f_1 is presented in tabular form by Martinelli and Nelson (Ref. 8).

Rearranging equation (8)

$$\int_0^x J(x,\ P)\, dx = x\, f_1 \tag{9}$$

Now

$$\int_a^b f(x)dx = \int_0^b f(x)dx - \int_0^a f(x)\, dx \tag{10}$$

Substituting equations (9) and (10) into equation (6) gives

$$\frac{\Delta P_{TPF}}{\Delta P_{LO}} = \frac{\left[x_e\, f_1\, (x_e, P)\ -\ x_i\, f_1\, (x_i, P)\right]}{x_e - x_i} \tag{11}$$

Equation (11) was used to predict two phase pressure drop in the dryer.

APPENDIX VII

TEST BED STEAM GENERATOR CORE ANALYSIS

Appendix VII was prepared for Solar by Geoscience Ltd. to provide a core analysis of the parallel flow steam generator (test bed unit) described in Section 6.

GLR-95

VAPOR GENERATOR TECHNOLOGY SUPPORT FOR SOLAR DIVISION OF INTERNATIONAL HARVESTER

(PO 3739-32134-FO3)

C. M. Sabin
H. F. Poppendiek
G. Mouritzen
R. K. Fergin

GEOSCIENCE LTD
410 S. Cedros Avenue
Solana Beach, California 92075

Preceding page blank

INTRODUCTION

All of the vapor generators presently under development or being proposed for use in mobile Rankine cycle engines are of the forced-convection once-through type. Such vaporizers receive subcooled or saturated liquid at the inlet of a continuous tube, and discharge dry, superheated vapor from the outlet. In steady state operation, the flow past each point in the vaporizer is described by a fixed vapor quality. Typical flow regimes in such a vaporizer can be (in order, from inlet to outlet); (1) all liquid; (2) a foamy, quasi-homogeneous mixture of liquid and vapor; (3) separated annular flow with liquid on the wall and vapor in the core; (4) wetted liquid rivulets or droplets on the wall, wet or dry vapor in the core; (5) film boiling droplets; (6) fog flow; (7) vapor superheating.

This sequence of processes does not appear in every vaporizer. In some cases, flow regimes listed do not occur, or are replaced by others. A number of transition processes can occur which fall in between the flow regimes listed above.

The preheater-vaporizer-superheaters to be designed for the low emission burner are intended to accommodate three distinctly different fluids; pure water; Fluorinol-85, an organic-water mixture; and PID Fluorocarbon*, a pure organic. The first two of these liquids are to be vaporized and superheated, while the third will be exited from the heat exchanger in a super-critical condition, so that no change of phase takes place.

The two fluids containing organics are, of course, restricted in their temperature, so that careful control of the interior wall temperature and heat flux distribution throughout the heat exchanger must be maintained to prevent fluid damage.

The heat exchanger units are subject to a number of design constraints other than those imposed by fluid properties. There are restrictions on total heat exchanger volume, and on the shape of this volume, on pressure drop, and on weight.

In order to originate the most optimum vapor generator designs, and in order to verify predicted performance in the laboratory, certain support studies must be performed. Those being investigated are briefly summarized below:

1. Test and prototype instrumentation for vaporizer temperature and pressure control.

2. Flow changes during power level transients.

---

*PID was the original working fluid in the Aerojet system. This was replaced by AEF-78 at a later date.

3. Radiation transfer between combustor, vaporizer and gases.

4. The effects of nonuniform gas temperature distribution on the vaporizer performance.

5. Performance of the vaporizer at reduced power levels.

6. Influence of duct geometry and possible inserts on working fluid heat transfer.

7. Prevention of vaporizer tube overheating by temperature monitoring.

SUMMARY

Geoscience's support role in the subject program consists of two study areas, (1) vapor generator design, and (2) heat transfer and fluid flow support for the vapor generator-combustor system. The vapor generator design work consists of parameter investigations of the relationships between the fluid properties and the requirements imposed on the vaporizer by other components of the power system. Three different working fluid types and a wide power level range are specified. The support studies are principally concerned with the coupling between the combustor and vapor generator; questions involving instrumentation, power transients, radiation transfer, nonuniform gas temperature distribution, vaporizer performance variation with power level, tube geometry effects, and working fluid overheating are being considered.

During the last quarter, Geoscience's work related to five different tasks: (1) the design of the test bed vapor generator to be used with water as a working fluid; (2) the prediction of part load performance of the test bed water vapor generator, (3) the parametric design study of a Fluorinol-85 vapor generator; (4) the analysis of peripheral heat flux in vaporizer tubes; and (5) radiant heat exchange analyses. The results of these studies are presented in this report.

DESIGN STUDIES

Test Bed Water Vapor Generator Design

A test bed water vapor generator has been designed for use with the Solar combustor. The conditions and constraints to which this design was subjected in order to meet the objectives of Solar's combustor development program are presented in Tables I and II.

Because of the lack of space in which to install flow transition sections, the vapor generator cross-section should match the size and shape of the

TABLE I

OPERATING CONDITIONS

Combustion Side:	
Air flow	1.0 lb/sec
Air-fuel ratio	26 to 1
Combustor outlet temperature	2500°F ± 250°F
Heat release in combustor	2.5×10^6 Btu/hr
Water Side:	
Inlet temperature	250°F
Outlet temperature	1000°F
Outlet pressure	1000 psia

TABLE II

WATER TEST BED VAPOR GENERATOR DESIGN CONSTRAINTS

Physical Maximums:	
Core diameter	21.5 inches
Core length	Unspecified, preferably less than 8 inches
Tubing weight	110 lbs
Tube wall temperature	1200°F
Water side pressure drop	250 psig
Air side pressure drop	3 inches of H_2O
Other Constraints:	
Plain tubing without extended fins	
Essentially the same air side pressure drop and flow distribution as an optimum system	
Thermal efficiency 80 percent or greater based on fuel HHV	

combustor outlet as closely as possible and, since the combustor outlet is circular, this cross section was chosen for the heat transfer matrix. The vapor generator diameter was enlarged from the 18-inch diameter of the combustor to the maximum allowable 21.5 inches, however, so that a short adaptor will be required. The gas side pressure drop is a strong function of frontal area and the pressure drop requirement could not be met with an 18-inch diameter matrix. A matrix made up of a stack of flat-wound spirals was chosen, with the combustion products flow parallel to the spiral axis.

The water-steam side heat transfer conductances in a unit of this type are relatively high, and the controlling heat transfer resistance is on the gas side.

Plain, unfinned tubing was a necessary choice for this heat exchanger in order to avoid the delays associated with special procurements and, since the pressure drop associated with a given heat transfer rate is usually higher for bare tube banks than for extended surfaces, a careful consideration of the heat exchange matrix geometry must be made.

There are a number of criteria by which a candidate heat exchanger surface configuration can be judged for a particular service. For the present purpose, where volume and pressure drop constraints are both important, the configuration must, when compared to others, have a high heat transfer conductance, a high heat transfer area per unit of volume, and relatively low fluid friction. A figure of merit for comparison of heat transfer configurations is the ratio of friction factor to Stanton number. This ratio, which related the momentum transfer to the heat transfer for a given heat transfer rate. The lower is this ratio, the more effective is the configuration in utilizing momentum losses to enhance heat exchange.

Data for several staggered tube arrays in cross flow are presented in Table III , based on data taken from Reference 17. It may be seen that configurations 2 and 3 are the most compact, and that number 2 has the highest conductance and lowest friction factor. The friction factor-Colburn modulus ratio is by far the lowest of the six configurations listed. Configuration 2 appears to be the most attractive for the present purpose.

The tube diameter has a strong effect upon the heat transfer area per unit of volume, and in the heat transfer conductance. For the configuration 2 of Table III, which has tubing on a 1.25 diameter spacing in both the transverse and longitudinal direction, calculations have been made for the change in these parameters as functions of tube size. These data are presented in Table IV. Since a circular cross section arrangement adapts most easily to the combustor, a staggered tube matrix made up of flat spiral coils is the geometry of choice. Therefore, the length of tubing in a flat coil of each tubing diameter is also shown in Table IV. It is clear that from considerations

TABLE III

SOME CHARACTERISTICS OF PLAIN TUBE ARRAYS OF STAGGERED TUBES

(Data Taken From Selected Figures in Reference 17)

Configuration Number	Spacing Longitudinal Inches	 Transverse Inches	Heat Exchange Area Per Cubic Foot of Volume ft^2	Heat Transfer Conductance $Btu/ft^2\,°F$	Friction Factor	$\frac{f}{(h/Gc_p)Pr^{2/3}}$
1	.468	.563	53.6	34.6	.080	4.5
2	.468	.468	64.4	46.1	.051	3.5
3	.375	.563	67.1	36.2	.082	4.3
4	.563	.563	44.8	32.4	.079	4.7
5	.375	.750	50.3	35.3	.140	6.1
6	.282	.938	53.6	38.2	.124	5.7

TABLE IV

EFFECT OF TUBE DIAMETER UPON MATRIX PARAMETERS FOR A STAGGERED TUBE ARRAY WITH A 1.25 DIAMETER GRID

Tube Diameter Inches	Minimum Flow Area Frontal Area	Heat Transfer Area Per Unit Volume ft^2/ft^3	Heat Transfer Conductance Btu/ft^2 hr °F	Tubing Spacing Inches	Turns in Spiral Coil 21.5 in. O.D.	Length of Spiral 21.5 in. O.D. Inches
1/4	0.2	96.6	5[illegible]	.312	29.6	1162
3/8	0.2	64.4	4[illegible]	.468	19.8	775
1/2	0.2	48.3	41	.625	14.8	580
5/8	0.2	38.6	38	.781	11.9	464
3/4	0.2	32.2	36	.937	9.9	387

of overall heat exchanger volume, the smallest possible tubes are the best choice, since the product of heat transfer area and conductance is maximized by the small diameters. However, the internal pressure drop also must be considered, and to a first approximation it changes inversely as the fifth power of the tube diameter.

The choice of one-half inch diameter tubing allows the heat exchanger to fit into the required volume, and the water-side pressure drop can be brought within the required limit with a reasonable number of parallel passages in the vapor phase and two-phase regions of the vapor generator. A choice of smaller tubing would require such a large number of parallel passages, that the flat spiral coil arrangement would have to be abandoned in favor of the more easily manifolded rectangular cross section arrangement, with tube sheets. A choice of larger tubing would decrease the number of flow passages somewhat, but could not reduce the system to a single flow channel within the desired total volume, because the amount of heat transfer area per unit volume decreases rapidly with larger diameter tubing.

The simplest arrangement of flat coils from the point of view of flow passage interconnections is the counterflow arrangement, in which the combustion products enter the matrix from the same end the superheated steam exits. This is however, an intolerable geometry, since superheater wall temperatures would exceed 1200°F by a significant margin even in steady state.

The internal flow passage must, therefore, be modified to reduce tube wall temperatures. A more satisfactory geometry has the vaporizer first, the superheater next, and the preheater last, when listed in the direction of combustion products flow. With this arrangement, the first rows of the matrix, which are immersed in gases near 2500°F, then contain boiling water at a relatively low temperature (~550°F) and very high internal heat transfer conductances, so that the wall temperatures are far below 1200°F, and the last tubing in the superheater, which contains 1000°F vapor with relatively low heat transfer conductances (compared to boiling) is immersed in much lower temperature combustion gases. This water flow path, which places the superheater section between the vapor section and preheater section, is the arrangement of choice.

Forced convection boiling systems, which receive saturated liquid at one end of a passage and discharge dry or superheated vapor at the other all have some location along the passage at which the wall is no longer covered by a liquid film. At this location the conductances on the vaporizing surface change from those characteristic of boiling to those characteristic of gaseous heat transfer, a decrease which can be several orders of magnitude. For fixed conditions the location of this point can be established with tolerable precision. However, in a boiler which will be subjected to sudden and rather large changes in operating power level, the location of the end of the liquid film can be expected to move significant distances upstream or downstream, and the abrupt change in wall temperature associated with the conductance change will also move. In order to avoid potential problems, the expected location at which the liquid film ends has been placed in a location of relatively low heat flux. This is insured by two means. First, the vaporizer coils have been arranged so that the flow from the preheater enters the coil adjacent to the combustor, and the vaporizer is operated in cross-parallel flow. Second, the vapor exits the vaporizer and enters the superheater with a significant amount of moisture, so that vaporization takes place in the superheater under design full load conditions.

Based on the considerations given and detailed calculations of the requirements for each of the three sections (preheater, vaporizer, superheater), the water test bed vapor generator thermal and hydrodynamic design was established.

The physical description is given in Table V. A schematic diagram of the flow paths is shown in Figure 1.

TABLE V

PHYSICAL CHARACTERISTICS OF THE WATER TEST BED VAPOR GENERATOR

Dimensions Overall:	
Matrix diameter	21.5 inches
Matrix thickness	6.25 inches
Heat transfer area (outside)	62 ft^2
Geometry:	
Flat spiral coils arranged with axes parallel to combustion products flow direction	
10 flat coils; 2 in vaporizer, 3 in superheater, 5 in preheater	
Preheater and superheater, cross-counterflow; vaporizer, cross-parallel flow	
Tubing arranged on a 1.25 tube diameter staggered grid when viewed on a radial cut through core	
Tubing 1/2-inch outside diameter by 0.035-inch wall thickness	
6 parallel passages in vaporizer and superheater; one passage in preheater	
Pressure Drops	
Combustion products 2.8 inches of water	
Water	175 psi
Water Design Flow Rate:	1525 lbs/hr
Weight of Tubing:	106 lbs
Weight of Water Hold Up:	30 lbs.
Design Power Output:	2 x 10^6 Btu/hr

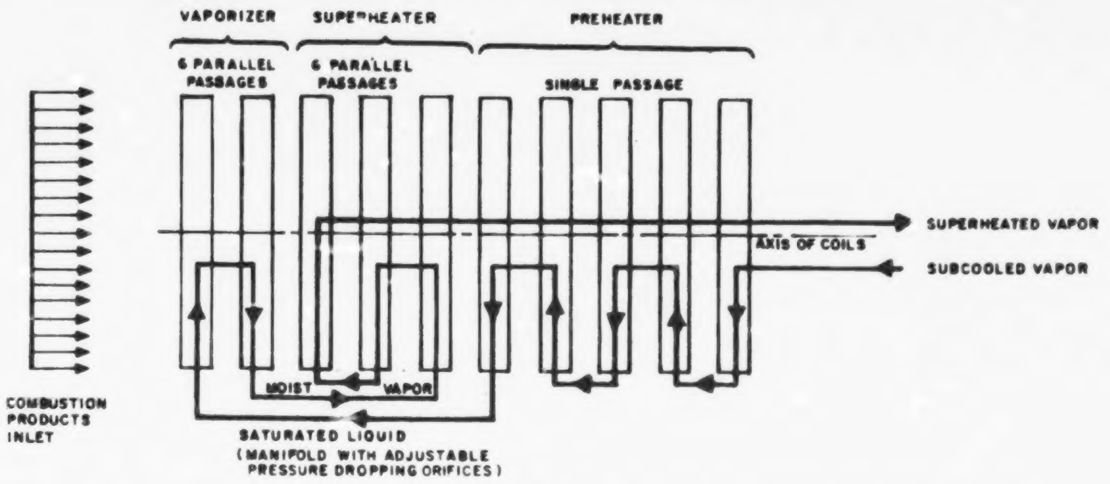
VAPORIZER
SUPERHEATER
PREHEATER
6 PARALLEL PASSAGES
6 PARALLEL PASSAGES
SINGLE PASSAGE
SUPERHEATED VAPOR
AXIS OF COILS
SUBCOOLED VAPOR
MOIST VAPOR
COMBUSTION PRODUCTS INLET
SATURATED LIQUID
(MANIFOLD WITH ADJUSTABLE PRESSURE DROPPING ORIFICES)

FIGURE 1. SCHEMATIC DIAGRAM OF WATER FLOW PATH THROUGH VAPOR GENERATOR

This design could be improved significantly (although not necessarily optimized), by the use of extended surfaces in the preheater. The total length of tubing in the exchanger could be reduced by at least one third, so that water hold-up volume, water-side pressure drop, and possible gas-side pressure drop could be reduced. There would probably not be a great reduction in metal weight, however, since high temperature resistant materials would have to be used for the fin material.

Part Load Performance of the Test Bed Water Vapor Generator

The part load performance of the test bed water vapor generator has been computed for the range of operating levels between full load and idle (2.5 percent of full load). The calculations were performed with the idealizations that neither the water inlet and outlet conditions, nor the combustion products inlet temperature change over this range.

As the power level is decreased, a larger portion of the total heat is transferred in the first two coils (the "vaporizer section") of the matrix. As a result, there are significant shifts in the location of the vaporization process over the power range. However, no operational difficulty should be encountered because of these shifts.

The heat exchanger effectiveness of the water vaporizer as a function of combustor load is shown in Figure 2 . As expected, the effectiveness increases rapidly as the power level decreases. The thermal efficiency, based on the lower heating value of the fuel and a 90°F air stream into the combustor is also shown. The efficiency is necessarily lower than the effectiveness because the water inlet temperature is above the assumed

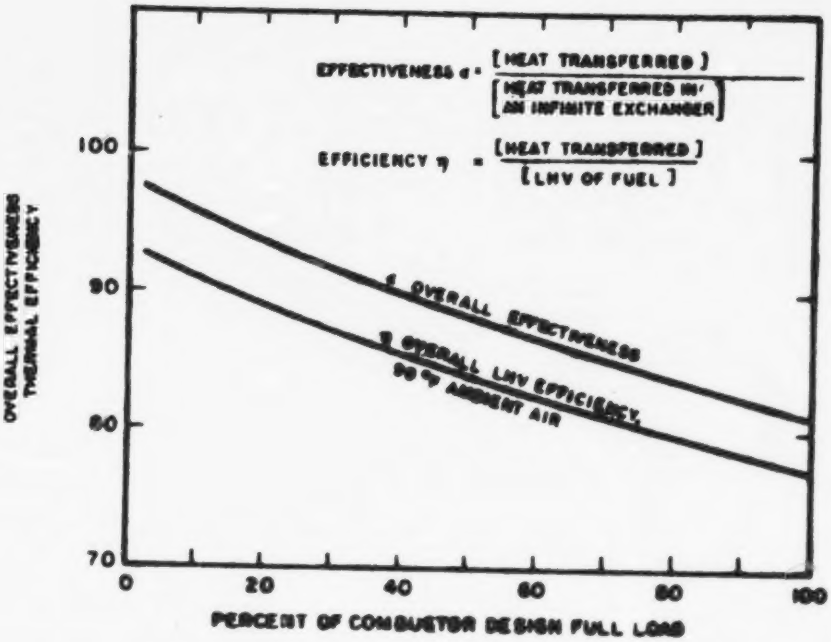

FIGURE 2. TEST BED WATER VAPORIZER PERFORMANCE AT PART LOAD

combustor inlet air temperature. The higher the water inlet temperature, the lower the efficiency will be. At 250°F water inlet, and 90°F air inlet to the combustor, the thermal efficiency of an infinitely large vaporizer would be 94 percent. The two curves in Figure 2 approach 100 percent and 94 percent at zero power level. They are, however, not simple curves in the region below 2.5 percent of full load.

There is a strong influence between the water-stream flow path through the heat exchanger and the performance of the superheater at part load. At the design load, approximately 26 percent of the total heat flow is in the superheater, while at idle load (2.5 percent of full power), the superheater transfers only 3 percent of the total heat. At that low power level, the vapor discharged from the vaporizer is already at 930°F and, therefore, rises only 70°F in its passage through the superheater. If the same vapor generator were arranged in cross-counterflow from preheater through superheater (an intolerable geometry at full load with unprotected tubing), the part load performance would be significantly better.

The temperatures of the two streams at various points in the vapor generator are shown in Figure 3. It may be seen that the steam coming out of the vaporizer (and into the superheater) is saturated from the full load power level down to about 45 percent of full power. From this level on down, the vapor superheats in the vaporizer section. At the design full load,

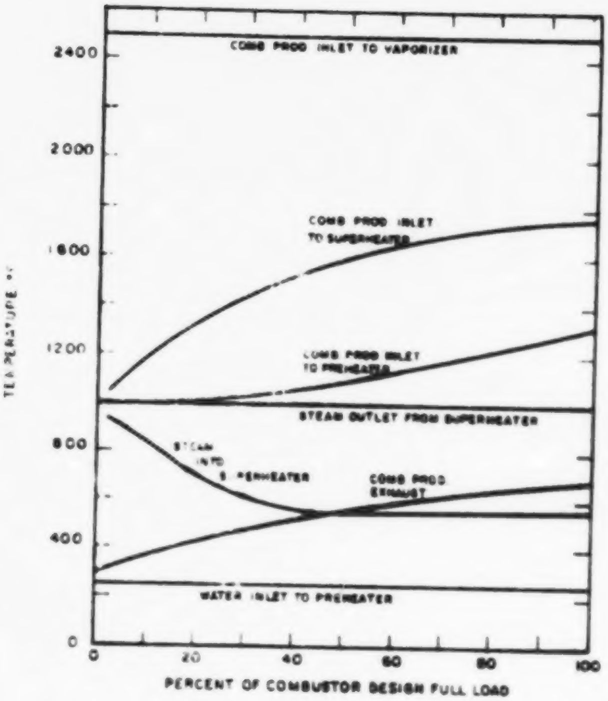

FIGURE 3. TEST BED WATER VAPORIZER TEMPERATURES AT PART LOAD

the steam coming from the vaporizer into the superheater is quite wet, in order to prevent tube wall overheating which can occur at high qualities due to loss of the liquid film on the wall.

The maximum wall temperature under steady operating conditons should always occur at the superheater outlet. This temperature does not change rapidly with power level, but is highest at the design full load. A plot of tube wall temperature is shown in Figure 4.

A Fluorinol-85 Vapor Generator Design

Introduction. A Fluorinol-85 vaporizer, optimized for size and weight, is to be designed for use with the Solar combustor. The design constraints are listed in Table VI. The Fluorinol-85 vapor generator design is designated as Base Design No. 1.

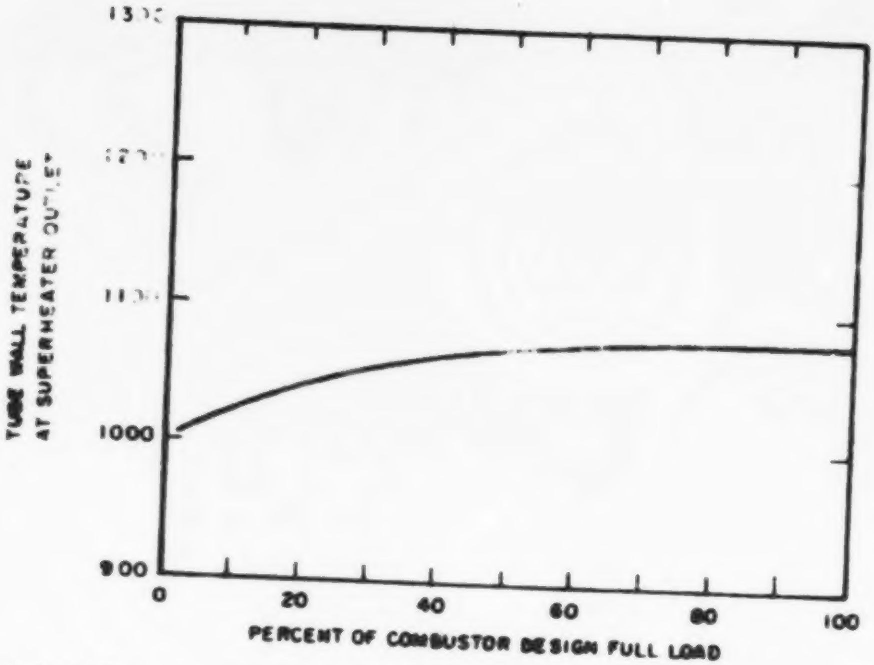

FIGURE 4. TEST BED WATER VAPORIZER TUBE WALL TEMPERATURE

Base Design No. 1 was optimized to obtain the smallest size vapor generator which could be designed to meet the pressure drops and temperature limits specified in the work statement. Base Design No. 1 is not a conservative design and was not recommended for construction. Rather this design serves as a size reference for the smallest obtainable vapor generator, from which the envelope may be expected to expant to meet practical considerations for a manufactured vapor generator, or to meet new limitations for Fluorinol-85.

In the Fluorinol-85 vapor generator extended surfaces may be employed. However, the stringent limitation upon maximum fluid temperature, combined with the relatively poor heat transfer properties of the Fluorinol (compared to water) limit the heat fluxes so that only relatively shallow fins may be utilized, and these only in portions of the heat exchanger. The temperature limit on the internal wall was established at 600°F for Base Design No. 1. Because of the relative magnitudes of the gas side and organic side heat transfer conductances, some sort of heat flux limiting for the inner wall is required. Two means to accomplish this end are to use internal fins in the vaporizer and superheater, which would increase the inside heat transfer area, or to use external insulation. The internal fins used alone would increase the internal pressure drop significantly and would be more costly to manufacture in the spiral coil tube design. To compensate for the increased pressure drop, it would be necessary to use about 12 parallel passages in

TABLE VI

CONDITIONS FOR FLUORINOL-85 VAPOR GENERATOR

Specified Flow Conditions		
Combustion side:	Same as for Test Bed Water Vapor Generator (see Table I)	
Fluorinol-85 side:	Inlet temperature	250°F
	Outlet temperature	550°F
	Outlet pressure	700 psia
Design Constraints		
Physical maximums:	Core diameter	21.5 inches
	Core length	8.0 inches
	Fluorinol-85 pressure drop	100 psi (50 psi preferred)
	Air side pressure drop	3 inches of H_2O
	Tubing weight	110 lbs
	Tube wall temperature	600°F
Other Constraints:		
Full rated output from a cold start in 15 seconds		
Maximum fluid temperature shall be kept sufficiently low during transients to prevent decomposition		

each coil of the vaporizer and superheater. The external insulation requires more coils in order to obtain the same total heat transfer, but is a mechanically-simpler alternative. External insulation must be of fairly low thermal conductivity, two to three orders in magnitude lower than stainless steel. This is clear, since the insulation is added to the outside of the tubes and must be reasonably thin, otherwise the effective diameter of the tubing increases so much as to cause a significant decrease in the inside wall heat transfer area per unit volume.

Design Considerations. Near the outset of the work on Fluorinol-85 Base Design No. 1, a configuration similar to that of the water vaporizer was chosen. It was also decided to use the same combustion side heat transfer configuration wherever external finning was not required.

For a given heat exchanger configuration, pair of fluids and inlet and outlet flow conditions, the amount of heat to be transferred in the exchanger is fixed, and depends only on the product of heat transfer area and overall conductance. The overall conductance, which normally may be computed in a straightforward manner from the properties of the two fluid streams and the wall, is used to establish the required heat transfer area. However, it may be shown that the overall conductances computed in the normal manner for the Fluorinol-85 vapor generator lead to tube wall temperatures which greatly exceed the temperature limit for the fluid throughout a significant portion of the heat exchanger. There is, thus, a heat flux limit imposed by the fluid temperature limit. For example, consider the superheater outlet condition. At this location the bulk vapor temperature is 550°F, and the maximum acceptable wall temperature is 600°F, so that the maximum acceptable temperature difference, from wall to bulk, is only 50°F. This temperature difference, combined with the vapor side heat transfer conductance, yields a maximum acceptable heat flux which is two to three times smaller than that which is computed from the overall heat transfer conductance for a matrix containing plain metal tubing. To avoid fluid overheating, the local overall heat transfer conductance must be decreased to a value which yields a heat flux less than the maximum acceptable value with the existing local temperature difference, i.e., the heat flux must be tailored locally in the heat exchanger.

There are basically three approaches which may be utilized to accomplish this decrease in overall conductance, which are: decrease the outside (combustion products) conductance, decrease the wall conductivity, or increase effective organic side conductance. The decrease in external conductance is probably the simplest, but requires changes in heat transfer configuration which lead to very bulky heat exchangers, and this choice does not appear to be a useful one for the present application. An effective increase in the internal conductance may be accomplished by an unacceptably large increase in pressure drop, or by increasing the internal wall heat transfer area by use of extended surfaces. Extended surfaces on the interior lead to the most compact heat exchangers, but have a significant effect on pressure drop, are very difficult to obtain in materials usable for the present purpose, and may be impossible to form into spirals as required. The third alternative is to decrease the effective thermal conductivity of the tube wall, by the addition of an insulating layer.

In the case of Base Design No. 1, the insulating layer approach to heat flux tailoring was chosen. Although half-inch outside diameter tubing with an 0.020-inch wall was used to perform the calculations involving the organic side, the outside diameter used for the combustion products side calculations was taken to be 5/8-inch. Therefore, a one-sixteenth inch insulating layer on the outside of the tubes was visualized.

With these choices, an insulation conductivity which yielded the maximum acceptable heat flux (or 600°F internal wall temperature) was specified throughout the vaporizer and superheater sections. It was found that insulation was not required on the vaporizer first row (next to the combustor), nor on the superheater first row (farthest from the combustor).

The preheater does not require insulation, but may instead be finned externally to increase the local heat flux (based on the bare tube surface area). However, because of the relatively poor thermal properties of Fluorinol-85 compared to water, only shallow fins may be used. These increase the external surface area by somewhat over a factor of three. This increase yields preheater wall temperatures which are well below the 600 F maximum, so that somewhat larger fins could possibly be used. However, the design is constrained to integral numbers of spiral coils, and a full coil could not be eliminated by increasing the fin area to bring the wall temperature to 600°F.

As stated previously, no insulation was specified for the first vaporizer coil for Base Design No. 1. There are several reasons why a bare coil would probably actually be unacceptable for this application. For one example, at part load, the location at which vapor superheating begins is expected to move from the superheater into the vaporizer. The organic vapor could overheat under this condition.

The Fluorinol-85 is to be vaporized at a pressure quite near the critical point, so that the latent heat of vaporization is a relatively small portion of the total heat added. The density change upon vaporization is also relatively small. It is expected that the forced convection vaporization processes in this heat exchanger will be modified enough from those usually encountered to warrant a rather conservative vaporizing section design.

Base Design No. 1. Some of the physical characteristics of Fluorinol-85 Base Design No. 1 are given in Table VII. A flow diagram is shown in Figure 5. Under design full load condition the vapor exits the vaporizer coil with considerable moisture, and vaporization is completed in the first superheater coil. This feature is similar to that in the water vapor generator.

The preheater is required to have four parallel passages in order to control pressure drop, while the vaporizer and superheater have six.

The size and weight of this vapor generator could be further reduced by extensive use of internally finned tubes but this change would increase the internal pressure drop.

TABLE VII

FLUORINOL-85 BASE DESIGN NO. 1

Vaporizer	1 coil 1/2-inch O.D. x 0.020 wall tubing 6 parallel passages.
Superheater	4 coils in cross-counterflow, 6 parallel passages. First three coils effectively 5/8-inch O.D., built up of 1/2-inch O.D. x 0.020-inch wall tubing. Effective thermal conductivity of insulation in each coil is tailored to bring inside wall temperature to 600°F. The fourth coil is bare 1/2-inch tubing.
Preheater	Two coils in cross-counterflow, 4 parallel passages. The tubes are 1/2-inch O.D. x 0.020 wall with shallow fins on the outside to give an area ratio (based on the bare tube area) of 3.45. Slightly larger fins could be used without exceeding the wall temperature limit. However, a complete coil could not be eliminated, and partial coils are unacceptable.
Pressure drops	Fluorinol-85: 36 psi Combustion products: 3.1 inches of H_2O
Axial length	5.36 inches
Computed thermal efficiency (based on LHV)	80 percent

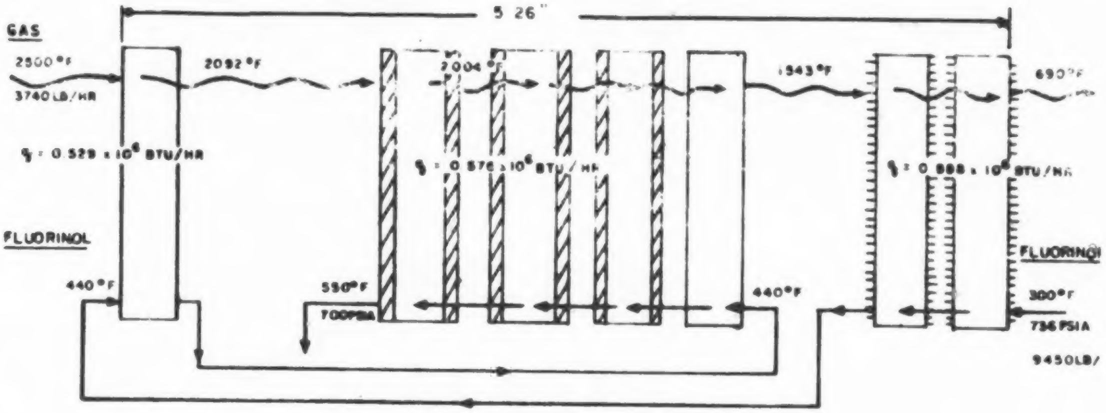
5.26"
GAS
2500 °F
3740 LB/HR
2092 °F
2004 °F
1543 °F
690 °F
q = 0.529 x 10^6 BTU/HR
q = 0.576 x 10^6 BTU/HR
q = 0.888 x 10^6 BTU/HR
FLUORINOL
440 °F
550 °F
700PSIA
440 °F
FLUORINOL
300 °F
736 PSIA
9450LB/

FIGURE 5. . FLOW DIAGRAM OF FLUORINOL-85 BASE DESIGN NO. 1

A significant decrease in structural complexity might be realized by changing from the spiral coil configuration to a conventional rectangular cross section matrix utilizing lengths of straight tubing. Although this alternative would require a transition section between the combustor and vapor generator, the tube interconnections, manifolding for parallel passages, and the construction of the matrix would be greatly simplified. This change might also make the use of internally finned tubing acceptable, since the tubing would not have to be coiled.

APPENDIX VIII

Appendix VIII was prepared for Solar by Geoscience Ltd to provide a core analysis for the organic vapor generators described in Section 9.

Preceding page blank

GLR-95

VAPOR GENERATOR TECHNOLOGY SUPPORT FOR SOLAR DIVISION OF INTERNATIONAL HARVESTER

(PO 3739-32134-FO3)

C. M. Sabin
H. F. Poppendiek
G. Mouritzen
R. K. Fergin

GEOSCIENCE LTD
410 S. Cedros Avenue
Solana Beach, California 92075

Preceding page blank

SUPPORTING STUDIES

Methods of Controlling Wall Temperatures in Vapor Generators

Because organic fluids in both liquid and vapor phases can decompose (thereby adding thermal resistances to vapor generator tubes), the wall temperatures must be controlled. For fixed hot gas and working fluid temperatures, the inner tube wall temperature (maximum working fluid temperature) can be reduced by a number of ways; several being considered are:

1. Increase the working fluid convective conductance
2. Decrease the gas convective conductance
3. Add a thermal resistance on the outer tube surface
4. Combinations of items 1, 2 and 3

An increase in the working fluid conductances can be best achieved by using internal extended surfaces, new boundary layer development, turbulence promotion and rectangular ducts. This method leads to increases in heat flux and thus decreases in heat exchange volume.

A decrease in gas conductances can be obtained by such limited procedures as operating under in-line rather than staggered flow conditions and by increasing the heat exchanger matrix compactness with some gas flow bypass. This method, as well as the subsequent one, yields decreases in heat flux and corresponding increases in heat exchange volumes.

The approach of utilizing added thermal resistance at the outer tube surface for the purpose of reducing inside tube wall and working fluid temperatures has been reviewed.

In specifying insulating layers to be added to the outside of vapor generator tube walls, it is important to consider the relative arrangement of the components involved. Consider a two-component system (one component being a good thermal insulator). Three different models have been considered. One model is based on the postulate that the constituents are positioned in laminae parallel to the heat flow; in the second one the laminae are positioned normal to the heat flow; the third one is based on the postulate that small particles are uniformly distributed in a second component and that the volume of all the particles is small compared to the total (the Eucken model).

The results for the three models are:

Parallel Model: $k = k_1 (1 - \nu_2) + k_2 \nu_2$

Series Model: $\frac{1}{k} = \frac{1 - \nu_2}{k_1} + \frac{\nu_2}{k_2}$

Eucken Model: $\frac{k_2}{k_1} = \frac{2(\frac{k}{k_1} - 1) + \nu_2 (\frac{k}{k_1} + 2)}{\nu_2 (\frac{k}{k_1} + 2) - (\frac{k}{k_1} - 1)}$

where,

k = resulting conductivity of the two-component system

k_1 = conductivity of component 1

k_2 = conductivity of component 2 (the insulator)

ν_2 = volume fraction of component 2

Typical examples for these models are plotted in Figure 1. It is seen in the case of the Series model (stratified arrangement of components) of the insulating material reductions in the mean thermal conductivity of the matrix are relatively large with small additions of the insulating component in comparison to the Parallel and Eucken models. The geometric arrangement of the two materials combined to obtain the insulating structure is, therefore, very important. For example, honeycomb-like structures which are defined by the Parallel model would be the least desirable, whereas a stratified structure, defined by the Series model, would be more desirable.

A thin air gap could be trapped between the tube and a shield by first winding the tube with a low conductivity screen and covering it with a thin metal foil. Another, perhaps more practical method, would be to wrap the tube with a thin foil which has spacer dimples pressed into, say, one percent of the area. These air gap insulators would closely follow the Series model and yield an overall reduction in thermal conductivity by three orders of magnitude, as compared to a bare steel tube of the same thickness as the air gap.

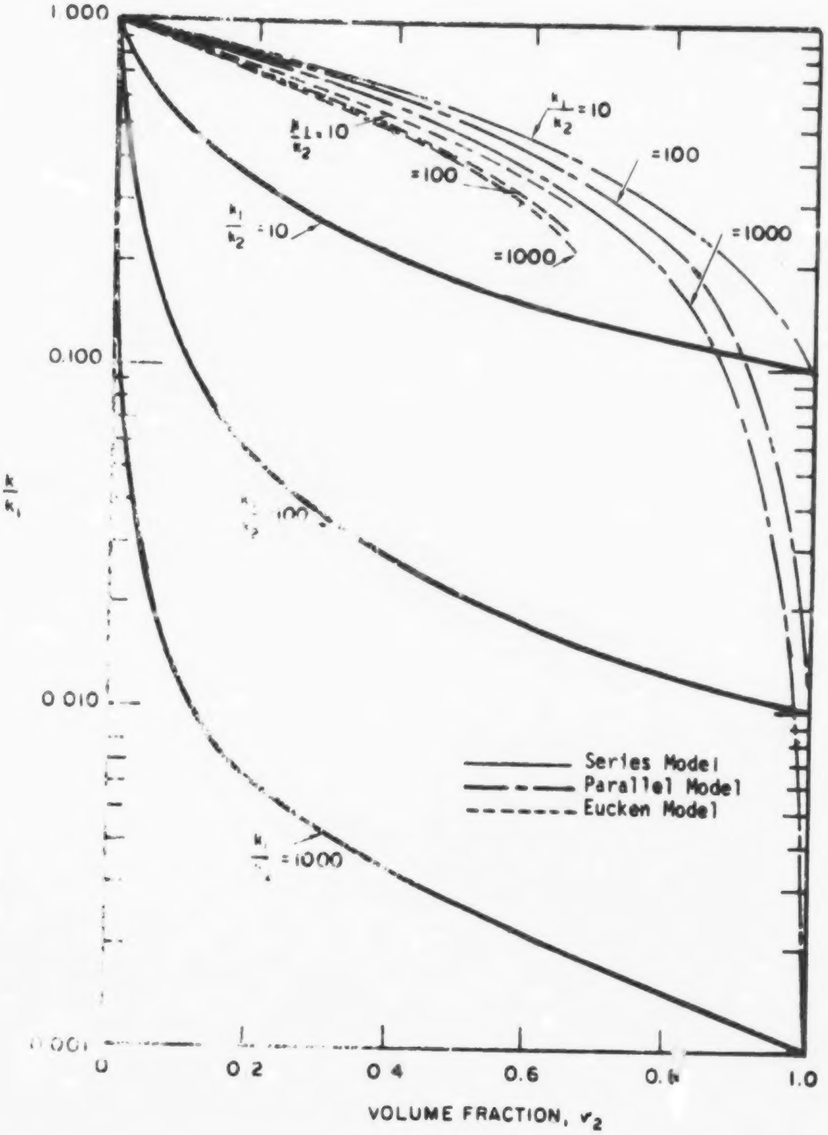

FIGURE 1. COMPARISON OF TRANSFER CONDUCTION MODELS FOR A TWO COMPONENT INSULATOR

Nonuniform Heat Transfer Considerations in a Vapor Generator Matrix

1. Radial and Tangential Gas Temperature Variations

In order to be able to design and fabricate vapor generators that are as compact as possible, uniform combustion gas temperature distributions at the vapor generator inlet must be realized. Otherwise, the design must be based on minimum gas temperatures yielding larger heat exchanger matrices. Nonuniform gas temperature fields can result fron nonuniform air and gas velocity fields or nonuniform fuel droplet addition to the air flow. A number of idealized convection models have been outlined that can be used to bound such temperature differences in the combustion gases at the entrance of the vapor generator. Variations in the velocity fields and the volumetric heat sources are being considered; thermal and fluid flow boundary layer development and jet mixing processes are involved.

2. Peripheral Tube Wall Variations

For the water test bed vapor generator, nonuniform heat rates do not pose a problem as the tube wall temperaturs are well below the material temperature limits and water does not present a decomposition problem. However, for the vaporizer design for Fluorinol-85, nonuniform heat rates require careful consideration as wall temperatures must be controlled to a maximum of about 600°F to prevent decomposition of the Fluorinol-85. The analyses include the review of nonuniform radiation and convective conductances which control peripheral tube wall temperature variations.

Values for the peripheral variation of the convective conductance are available in the literature only for in-line tube banks, single tubes or staggered tube banks with large spacing. However, by considering the probable effects of the closer spacing, based on photographic observations, a close approximation can be made by using stagnation values at the leading edge, based on the maximum velocity through the minimum flow area and then using a flat plate boundary layer convective conductance variation to slightly less than 90 degrees (except for the front row, which can be approximated by using the stagnation value based on the on-flowing stream velocity and then using boundary layer conductance values based upon changing freestream velocity). Convective conductances for the rear half of the tube are approximated by extrapolating from 90 degrees by use of profile geometry for cylinders at the same Reynolds number (based on the maximum velocity and tube diameter).

In view of the above discussion and the geometry of the tube bank, the maximum heat flux is believed to occur at the leading edge of the second row of the tube bank where both the convective conductance and radiation total shape factor are at their maximum values (although the leading edge of the front row in the tube bank has a higher total shape factor for radiation, when considered with the convective conductance, the flux is not as great as in the second row). Figure 2 shows a typical convective conductance distribution for which wall temperature profiles are to be calculated.

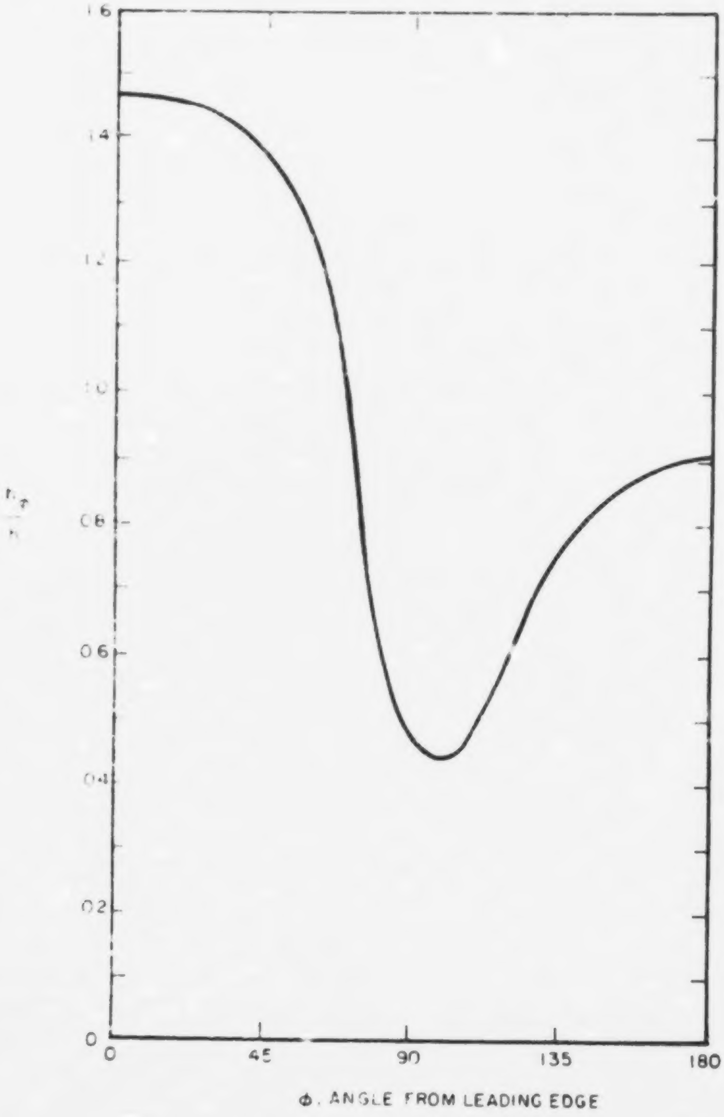

FIGURE 2. TYPICAL TUBE OUTER CONVECTIVE CONDUCTANCE PERIPHERAL VARIATION - TRANSITION REYNOLDS NUMBER RANGE - STAGGERED TUBE BANK - INTERIOR TUBE

The combined effects of nonuniform convective conductance and radiation will be used to provide design criteria for tube insulation or internal finning in those areas where tube wall temperatures could exceed the allowable decomposition limit for Fluorinol-85. Radiation considerations are further discussed in the following section.

Radiant Heat Transfer Considerations in a Combustor-Vaporizer System

A grid plate located between the combustor and the vapor generator entrance has been used at times by Solar in some of its experimental combustor work. One reason for using the grid is that it can act as a fluid flow mixer. With this component, it may be possible to obtain more uniform temperature and velocity fields at the vapor generator entrance. Another reason for considering a grid is that changes in radiant heat transfer within the combustor can be made; such changes in net radiation fluxes can be significant. Therefore, a study of the radiation and convection heat transfer in an idealized perforated radiation shield system was performed.

Consider first only the radiant energy transfer in the system shown in Figure 3 (by two infinite parallel planes separated by a perforated radiation shield). The two parallel planes (which represent the combustor wall and the vaporizer surface at its entrance) are at two different uniform and constant temperatures. The radiation shield is infinite in extent, thin, a gray body, a diffuse reflector, a diffuse emitter, at some uniform and constant temperature, and uniformly perforated. The two parallel planes are gray bodies. Gaseous absorption in this radiation system is small and neglected. The temperatures of the two infinite planes, all gray body absorptivities in the system, and the amount of shield perforation are known; the net radiant heat transferred and the shield temperature are unknown and to be determined.

The net radiant heat transferred at the surface of either of the two parallel planes in the radiation system under consideration is equal to the difference between the emission power of that surface and the absorbed amount of all radiation falling upon it. This incident radiation (irradiation) consists of direct and reflected radiation from the various radiating surfaces of the system. For instance, the net radiation exchange at surface 1 is expressed as follows:

$$\left(\frac{q}{A}\right)_{n_1} = E_1 - \alpha_1 \left(G_{1-1} + G_{2-1} + G_{3L-1} + G_{3R-1}\right) \qquad (1)$$

where,

E_1 = emissive power of surface 1

α_1 = gray body absorptivity or emissivity of plane 1

G_{1-1} = irradiation on surface 1 as a result of all reflected radiation originating at surface 1

G_{2-1} = irradiation on surface 1 as a result of all direct and reflected radiation originating at surface 2

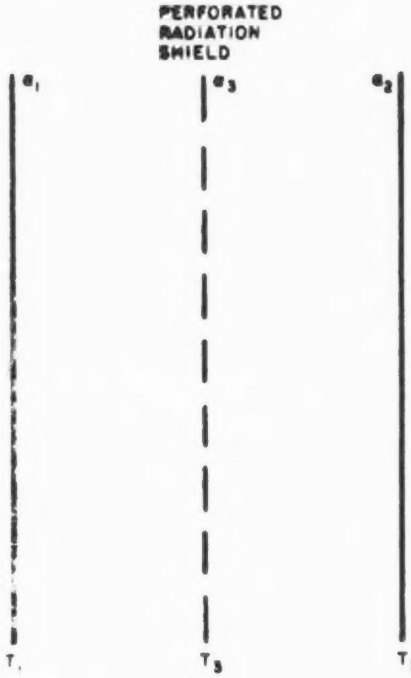

FIGURE 3. PERFORATED RADIATION SHIELD SYSTEM

$G_{3L - 1}$ = irradiation on surface 1 as a result of all direct and reflected radiation originating at the left face of the shield

$G_{3R - 1}$ = irradiation on surface 1 as a result of all reflected radiation originating at the right face of the shield

The irradiation terms indicated in Equation (1) have been evaluated considering the multiple inter-reflection processes involved (details not shown here). These terms are functions of wall and shield temperatures, absorptivities and reflectivities and the shield fraction. Upon making these substitutions, Equation (1) becomes:

$$\left(\frac{q}{A}\right)_{n_1} = \frac{\alpha_1 \sigma}{(1 - \rho_1 C_1)(1 - a\,\rho_2 \rho_3)} \Big[a(T_2^4 - T_3^4) + \Big\{(1 - \rho_2 + a\,\rho_2) (T_1^4 - T_2^4)\Big\} + a(\rho_2 - \rho_3 - \rho_2 - \rho_3 - a\,\rho_2 \rho_3^2)(T_1^4 - T_3^4)\Big] \quad (2)$$

where

$$C_1 = \left[a\,\rho_3 + \frac{(1 - a)^2\,\rho_2}{(1 - a\,\rho_2\,\rho_3)} \right]$$

a = shield fraction equal to the nonperforated shield area per unit area (e.g., a = 1 for a shield with no perforations, and a = 0 for complete perforation (no shield))

$\rho = 1 - \alpha$

Similarily, the net radiation flux at plane 2 can be expressed as,

$$\left(\frac{q}{A}\right)_{n_2} = \frac{\alpha_2\sigma}{(1 - \rho_2 C_3)(1 - a\rho_1\,\rho_3)} \Big[a(T_3^4 - T_1^4) + (1 - \rho_1 + a\,\rho_1)(T_1^4 - T_2^4)$$

$$+ a(\rho_1 - \rho_3 - \rho_1\,\rho_3 - a\,\rho_1 + a\,\rho_1\rho_3^2)(T_3^4 - T_2^4)\Big] \qquad (3)$$

where

$$C_3 = \left[a\,\rho_3 + \frac{(1 - a)^2\,\rho_1}{(1 - a\rho_1\,\rho_3)} \right]$$

For the specific case where no convection exists (a vacuum system), $(q/A)_{n_1} = (q/A)_{n_2}$; the simultaneous solution of Equation (2) and (3) yields the net radiation flux and shield temperature.

For the more general case where hot gases flow through the radiation shield (thereby transferring convective heat to it), the sum of the net radiant heat flow at planes 1 and 2 must be equal to the convective heat flow from the gases to the shield, namely,

$$q_{conv} = q_{n_1} + q_{n_2} \qquad (4)$$

The net radiation flows q_{n_1} and q_{n_2} are defined by Equations (2) and (3) and the convective heat flow term q_{conv}, is given by the defining expression,

$$q_{conv} = h A_s (T_g - T_3) \tag{5}$$

where

h = convective conductance of shield

A_s = total shield surface area

$(T_g - T_3)$ = gas-shield temperature difference

Upon substituting Equations (2), (3), and (5) into Equation (4), one equation in one unknown, T_3, results; its solution yields the shield temperature, with which the net radiation and convection heat flow terms are determined.

Calculations were made for the following representative conditions:

Combustor wall temperatures	1200°F
Vaporizer tube wall temperature	600°F
Gas temperature flowing past shield	2500°F
Solid fraction of radiation shield	0.5
Convective conductance for radiation shield (flow through grid)	53 Btu/hr ft^2 °F
Emissivities of all radiating surfaces	0.8

For the conditions given, the following results were obtained:

t_{shield} = 2350°F

$(q/A)_{n_1}$ = 10,600 Btu/hr ft^2

$(q/A)_{n_2}$ = 22,200 Btu/hr ft^2

This example was representative of some recent experiments performed at Solar. On the basis of temperature measurements made in the experimental system, the predicted shield temperature of 2350°F appears to be reasonable.

The idealized heat transfer model described has been further generalized to include the effect of the radiant energy emitted by the flame within the combustor; although the flame emissivity is low, the inclusion of this term will give a more exact representation of convection and radiation in the combustor-vaporizer system.

GLR-98

VAPOR GENERATOR TECHNOLOGY SUPPORT FOR SOLAR, DIVISION OF INTERNATIONAL HARVESTER

(PO 3739-32134-FO3)

C. M. Sabin
H. F. Poppendiek
G. Mouritzen
R. K. Fergin

GEOSCIENCE LTD
410 S. Cedros Avenue
Solana Beach, California 92075

Preceding page blank

I. SUMMARY

Geoscience's support role in the subject program consists of two study areas, (1) vapor generator design, and (2) heat transfer and fluid flow support for the vapor generator-combustor system. The vapor generator design work involves an investigation of the relationships between the fluid properties and the requirements imposed on the vaporizer by other components of the power system.

During the last quarter, Geoscience performed the following tasks: (1) Fluorinol-85 vapor generator design studies; (2) transient analyses of the water vapor generator; (3) radiant heat transfer analysis for the vapor generator-combustor system; (4) studies involving nonuniform heat transfer in vapor generator matrices; (5) investigation of methods for controlling excessive wall temperatures in vapor generators; and (6) test instrumentation reviews.

II. INTRODUCTION

The vapor generators presently under consideration for use in mobile Rankine-cycle engines are of the forced-convection, once-through type. In such generators, a working fluid in the subcooled or saturated state flows into the generator and is discharged in a dry, superheated vapor state at the outlet. In steady state operation, the flow past each point in the vaporizer is described by a fixed vapor quality. Typical flow regimes in such a vaporizer can be (in order, from inlet to outlet); (1) all liquid; (2) a foamy, quasi-homogeneous mixture of liquid and vapor; (3) separated annular flow with liquid on the wall and vapor in the core; (4) wetted liquid rivulets or droplets on the wall, wet or dry vapor in the core; (5) film boiling droplets; (6) fog flow; (7) vapor superheating. This sequence of processes does not appear in every vaporizer. In some cases, flow regimes listed do not occur, or are replaced by others. A number of transition processes can occur which fall in between the flow regimes listed above.

The preheater-vaporizer-superheater systems being designed for low emission combustors are to service three different Rankine cycle systems. One utilizes water, a second Fluorinol-85, and the third uses AEF-78, a pure organic. The first two liquids are to be vaporized and superheated, while the third will be exited from the heat exchanger in a super-critical conditions, so that no change of phase takes place.

The two organic fluids are, of course, restricted in their temperature, so that careful control of the interior wall temperature and heat flux distribution throughout the heat exchanger must be maintained to prevent fluid damage. The heat exchanger units are subject to a number of design constraints other than those imposed by fluid properties. There are restrictions on total heat exchanger volume, and on the shape of this volume, on pressure drop, and on weight.

A number of heat transfer and fluid flow studies are being performed for the purpose of supporting the design studies noted above. Examples of the main tasks being undertaken are given below:

1. Test and prototype instrumentation for vaporizer temperature and pressure control.
2. Flow changes during power level transients.
3. Radiation transfer between combustor, vaporizer and gases.
4. The effects of nonuniform gas temperature distribution on the vaporizer performance.
5. Performance of the vaporizer at reduced power levels.
6. Influence of duct geometry and possible inserts on working fluid heat transfer.
7. Prevention of vaporizer tube overheating by temperature monitoring.

III. DESIGN STUDIES

A. Fluorinol-85 Vapor Generator Design Considerations

1. Effects of Lowering the Maximum Fluid Temperature Limit on Flourinol Base Design No. 1

The size and characteristics of Fluorinol Base Design No. 1 were established with 600°F as the maximum temperature limit for the working fluid. However, new information on fluid decomposition indicates that this temperature limit of 600°F should be considered as a peak to be reached only during transients, and that the steady state limit should be reduced to 575°F. The desired superheated vapor outlet temperature is 550°F, so that this reduction in maximum fluid temperature (or maximum wall temperature) decreases the available temperature difference, from wall to bulk, in the superheater by a significant amount. The final portions of the superheater, in which the bulk fluid temperature approaches 550°F, must have nearly double the inside surface area.

The overall conductances in Base Design No. 1 have been tailored to bring the inside wall temperature near 600°F throughout the heat exchanger, in order to produce the most compact design possible without internal finning. Some discussion of the changes required to accommodate this new criterion is required.

The design changes which can be made to control the wall temperatures are: (1) addition of internal fins; (2) vary the external fin sizes on the preheater; (3) vary the number of passages in each coil; and (4) vary the insulation on the superheater coils.

a. Preheater

If the internal wall temperature limit is to be lowered to 575°F, it might be necessary to add internal fins to the preheater coils. The number of passages would then have to be increased to compensate for the additional pressure drop as a result of the internal finning. If eight longitudinal fins (height 0.067 inches, thickness 0.020 inches) were equally spaced around the periphery of the half inch tubing, the number of passages required would increase from four to six. The internal finning would make it possible to maintain the two coil preheater arrangement with external finning, as in Base Design No. 1, without exceeding an internal wall temperature of 575 F.

If more than eight internal fins were required, the fluid side pressure drop would exceed the specified limit or the number of passages required would become impractical.

With the addition of internal fins, it would be possible to increase the external finning. However, it does not seem possible to reduce the preheater section from two coils to one coil by this method. From a manufacturing point of view, the combination of internal and external finning would make it more desirable to design a vapor generator with a square cross section.

b. Vaporizer

If the inside wall temperature limit is lowered from 600°F to 575°F, either internal finning or outside insulation would be required on the vaporizer coil, which was previously bare tubing. If outside insulation is chosen, the number of vaporizer coils would have to increase from one to two. Internal finning would require an increase in the number of passages from six to ten in order to compensate for the increased pressure drop.

c. Superheater

Internal fins could be added to the superheater coils for the purpose of lowering the wall temperature. It would then have been possible to reduce the number of superheater coils from four to two for the obsolete 600°F maximum temperature. The overall internal pressure drop could also have been maintained below 50 psig. No external insulation would be necessary with internal finning if the wall temperature limit is 600°F. External insulation would be necessary in addition to the internal finning if the wall temperature limit is 575°F, unless the total pressure drop could be increased to, say, 100 psig. In that case, sixteen diagonal fins across the entire tube cross section would lower the temperature to nearly 575°F. The pressure drop in two superheater coils would be 68 psi using six passages in each coil.

Base Design No. 1 has not been analyzed for part load operations or overload operation. The latter would result in excessive wall temperatures. It is possible that certain part load operations could also result in excessive temperatures because the liquid-vapor distribution would be different from the design point operation. However, since other changes in the operating characteristics are sure to take place before the Flourinol design is frozen, it is felt that these changes should be established before further detailed analysis is performed.

2. Special Fluorinol-85 Vapor Generator Problems

The Fluorinol vapor generator operates at a high pressure so that vaporization occurs near the critical point. The latent heat of vaporization is, therefore, a relatively small portion of the total heat added, as seen in Figure 4. The vaporizer is, therefore, the least bulky portion of the vapor generator, in contrast to a water system. The largest heat addition occurs in the preheater where the temperature difference is smallest. Furthermore, the thermal conductivity of Fluorinol liquid is relatively low so that external as well as internal finning is desirable in order to obtain a compact design.

Because the operating temperature of the superheater (550°F) is very close to the allowable limit for the Fluorinol (575°F to 600°F), it is the most difficult and most critical component to design.

Because of the low temperature limit, it is also necessary to control the liquid-vapor cycle so that no superheating occurs in the vaporizer at part load operating conditions. In Base Design No. 1, only the superheater would provide the temperature protection required. In a practical design such protection will have to be provided in the vaporizer as well.

A few observations may be made concerning the vaporization process in Fluorinol. As the critical point is approached, the change in fluid volume with a change of phase approaches zero, and for Fluorinol vaporizing at 700 psia, the volume change is approximately five times. The familiar energetic bubble action in nucleat boiling, which is frequently visualized, is associated with density changes of several orders of magnitude, and one may expect this process to be suppressed with small density change. For vaporization under

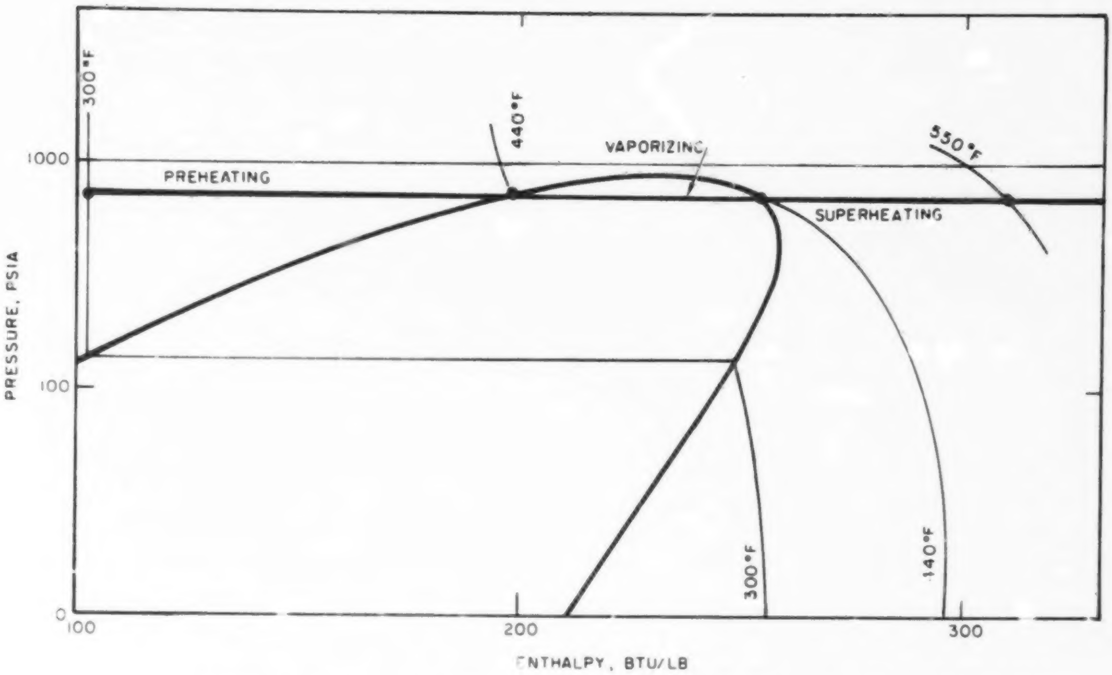

FIGURE 4. ENTHALPY, PRESSURE AND TEMPERATURE CHART FOR FLUORINOL

forced convection conditions in tubes, the flow through a large portion of the vapor quality range is annular, with the vapor flowing down the core. The thickness of the liquid layer on the wall is inversely related to the ratio of vapor velocity to liquid velocity, a ratio which is, in turn, related to the density ratio. In the case of vaporization near the critical point, thick liquid layers with small mixing due to bubble generation may very well occur, and under such conditions heat transfer conductances may not be particularly high. In the complete absence of bubble generation at the wall, one model of the vaporization heat transfer process visualizes the heat as being convected across a superheated liquid layer to vaporize liquid at the interface with the vapor. Such a process may very well be the dominant heat transfer mechanism in the vaporizer.

It is well established that vapor bubble generation next to liquid-solid interfaces in boiling occurs at particular nucleation sites, which are surface cavities and crevices containing inert gas or vapor. In the absence of suitable cavities or in the absence of inert gases to render the cavities active, many liquids can superheat without phase change far above their equilibrium saturation temperature. Metallic tubing is usually adequately provided with potential nucleation cavities, because the manufacturing processes enhance their formation. However, in sealed, carefully cleaned and evacuated systems, these potential sites may not be active.

The preceding considerations indicate that for a conservative design for organic vaporization, it would be appropriate to use a relatively low heat transfer conductance, based on an annular flow model without bubble generation.

3. Alternative Geometries

External insulation and external and internal fins will be required for the Fluorinol vapor generator. A conventional rectangular array substituted for the spiral coils, would simplify the installation of insulation and eliminate the possibility of collapse of internal longitudinal fins during coiling. In addition, a rectangular array is much easier to manifold, so that the use of many parallel channels to control pressure drop would not present serious difficulties. A short flow transition section would be required between the combustor and vapor generator to adapt the change in cross section, but if the actual flow area change were not large, this adaptor could probably be simple in form.

B. Transient Behavior of the Water Vapor Generator

There are two distinct transient operations of major importance in the operations of the water vapor generator. These are; the startup process, and varying load during operation. In the former case, the heat exchanger is initially full of water, and the liquid must be cleared from the vaporizer and superheater coils during the startup. In the latter case, the heat exchanger responds to changes in combustor output, steam demand at the outlet, and water flow at the inlet. Since these two transient operations are very difficult in nature, they can be discussed independently.

1. Vapor Generator Startup

The idealized startup process proceeds in the following manner. With the heat exchanger completely full of liquid at ambient air temperature, the combustor is impulsively brought to full rated output and maintained at that level until the superheater outlet conditions are at the design point, 1000 psia and 1000°F. During this process, the boiler tube may be dry, filled with stagnant or flowing fluid.

a. Dry Tube

In the case of the dry tube, the temperature history of the first coil wall is similar to that of the voltage on the capacitor in a series resistance-capacitor circuit impulsively subjected to a steady voltage at time equal to zero.

The governing equation is

$$\bar{T}_m = 1 - e^{-\bar{t}} \tag{1}$$

where

$$\bar{T}_m = \frac{T_m - T_i}{T_g - T_i}$$

$$\bar{t} = \frac{t}{R_g C_m}$$

values of the constants appropriate to the vapor generator are as follows

T_m = metal wall temperature

T_i = initial temperature (a constant), 70°F

T_g = gas temperature (a constant after $t = 0$), 2500°F

t = time

C_m = metal wall heat capacity Mc_{pm} = 1.2 Btu/°F for the first coil

M = metal mass, 11 lbs

c_{pm} = metal specific heat, 0.11 Btu

R_g = $1/h_gA$, the heat transfer resistance on the gas side

h_g = gas side heat transfer conductance, 43 Btu/ft^2 hr°F

A = gas side heat transfer area, 6.2 ft^2

The time constant R_gC_m has the value 16.1 seconds. In the absence of cooling, the metal temperature will go to the gas temperature. However, at some time after combustor startup the water flow would presumably begin. The time taken for the wall of the first coil to reach the saturation temperature of water at 1000 psi, 545°F, is, from Equation (1).

$$t = 3.52 \text{ seconds}$$

The test bed water vapor generator contains six coils between the preheater inlet and the end of the first vaporizer coil, representing a length of 280 feet of tubing. The design liquid velocity is approximately eight feet per second, so that the transit time from the inlet of the preheater to the outlet of the first vaporizer coil is about 35 seconds. It seems clear that a startup process with the vapor generator dry would have to have significant operational advantages to justify the necessary careful timing.

b. Tube Filled With Stationary Fluid

In the case of startup of the boiler containing stationary liquid, the temperature history of the first coil wall is similar to that of the voltage on the first capacitor in a series arrangement of resistor-capacitor and resistor-capacitor. The temperature history of the liquid mixed mean is similar to that of the voltage on the second capacitor. The governing equations are

$$\bar{T}_m = 1 + \frac{1 + r_2}{r_1 - r_2} e^{r_1 \bar{t}} - \frac{1 + r_1}{r_1 - r_2} e^{r_2 \bar{t}} \qquad (2)$$

and

$$\bar{T}_\ell = \frac{(1 - K) - e^{-K\bar{t}} + Ke^{-\bar{t}}}{1 - K} \qquad (3)$$

where

$$\bar{T}_\ell = \frac{T_\ell - T_i}{T_g - T_i}$$

$$K = \frac{R_g C_m}{R_\ell C_\ell}$$

$$r_1, r_2 = \frac{1}{2}\left(1 + \frac{h_\ell}{h_g}\right) \left\{ - 1 \pm \sqrt{1 - 4K \frac{1}{\left(1 + \frac{h_\ell}{h_g}\right)^2}} \right.$$

T_ℓ = liquid mixed mean temperature

R_ℓ = $1/h_\ell A_\ell$ heat transfer resistance on liquid side

C_ℓ = liquid heat capacity for entire first coil, 3 Btu/°F

R_g = $1/h_g A$, the heat transfer resistance on the gas side

A_ℓ = heat transfer area on liquid side of first coil, 5.4 ft^2

h_ℓ = liquid side heat transfer conductance

Evaluation of these solutions depends upon the establishment of a conductance for the liquid side. For a stationary liquid, the classical solution for the flow of heat in a cylinder subjected to a uniform external heat flux may be used. The appropriate solution may be found on page 203 of Reference 18, and elsewhere. The conductance extracted from this solution is a function of time, but may be approximated by a constant for the early part of the heating process. For the thermal properties of water and the dimensions of the water vapor generator, the water side conductance may be computed to be approximately

$$U_\ell = 128 \text{ Btu/ft}^2 \text{ hr F}$$

Based on the indicated constants, Equation (2) for the vaporizer tube wall becomes

$$\bar{T}_m = 1 - 0.765\, e^{-0.31\bar{t}} - 0.235\, e^{-3.24\bar{t}} \qquad (4)$$

The composite ime constants for the two terms are 52.0 seconds and 4.98 seconds, respectively. The vaporizer tube wall reaches the temperature of 545°F when $\bar{T}_m = 0.196$, $\bar{t} = 0.263$, and $t = 4.23$ seconds.

Equation (3) for the mixed mean liquid temperature becomes, with introduction of the indicated constants,

$$\bar{T}_\ell = 1.0 + 40\, e^{-1.025\bar{t}} - 41\, e^{-\bar{t}} \qquad (5)$$

The time constants for the two terms are 15.7 seconds and 16.1 seconds, respectively. At $t = 4.23$ seconds, when the tube wall has come to the boiling point, the liquid mixed mean temperature is 187°F.

The idealizations upon which Equation (4) and (5) are based become invalid after subcooled boiling begins at the wall. At this time, the effective inside conductances and the mixing of the liquid increase to fairly high values. However, the possibility of film boiling, with a consequent decrease in the inside wall conductance to a very low value is a distinct possibility if boiling continues without forced convection. It, therefore, appears that the water flow will have to be established soon after the wall reaches the water boiling point in order to insure that film boiling does not occur. With this constraint, it appears unlikely that there will be any net vapor generation possible before water flow must be started.

c. Tube Filled With Moving Fluid

These cases are more complex than the preceding two. The analyses presented below strictly apply only to such short lengths of tubing that the average temperature for heat transfer from the gas may be taken as the arithmetic mean temperature between inlet and outlet liquid flows. They are further restricted to water flows large enough that the liquid side heat transfer resistance is negligible compared to that on the gas side.

Other restrictions consistent with the above qualifications are:

1. Water and metal temperatures are identical
2. Conductances are invariant
3. Gas temperature is invariant
4. Water flow in invariant

(1) Constant Inlet Water Temperature

The governing differential equation for the water outlet temperature is

$$\hat{T} + \frac{d\hat{T}}{d\hat{t}} = 0 \qquad (6)$$

$$\hat{t} = \frac{t}{\tau_R}$$

$$\hat{T} = \frac{T_{wo}}{T_R} - 1$$

The reference temperature is

$$T_R = \left\{ \frac{2\, h_g\, A_\ell}{C_\ell}\, T_g + T_{wi} \left[\frac{2wc_p}{C_\ell} - \frac{2h_g A_\ell}{C_\ell} \right] \right\} \tau_R$$

The reference time is

$$\tau_R \equiv \frac{C_\ell}{2wc_p + h_g A_\ell}$$

The other new symbols are

A_ℓ = gas side heat transfer area for chosen tube length

C_ℓ = heat capacity of both water and metal for chosen tube length

w = water flow rate

c_p = water heat capacity

T_{wi} = water inlet temperature

T_{wo} = water outlet temperature

The solution to Equation (6) for the appropriate boundary condition $\hat{T} = \hat{T}_1$, $\hat{t} = 0$, is

$$\frac{\hat{T}}{\hat{T}_1} = e^{-t} \tag{7}$$

For conditions appropriate to the entire water vaporizer first coil and full design water flow, the time constant is

$$\tau_R = 4.59 \text{ seconds}$$

The reference temperature is

$$\tau_R = 458°\text{F}$$

The resulting temperature history of the water outlet is, for an initial temperature of 70°F,

$$\frac{458°\text{F} - T_{wo}}{388°\text{F}} = e^{-\hat{t}} \tag{8}$$

After one time constant, 4.59 seconds, the temperature has increased to 316°F.

It may be observed that in this case the time to boiling temperature cannot be computed, since the water will not reach boiling with a 70°F inlet to the first coil. The limit temperature is 458°F.

The restriction of this case to fixed inlet temperature invalidates the solution for times great enough so that the preheater outlet temperature has begun to rise. For cases with significant variation in first vaporizer coil inlet temperature, the following analysis is presented.

(2) For the case of a variable water temperature of the form

$$T_{wi} = \lambda(1 - e^{-\hat{t}}) \tag{9}$$

similar to Equation (8), the differential equation is of the form

$$(k_1 + k_2) - k_2 e^{-\hat{t}} = \frac{d\tilde{T}_{wo}}{d\hat{t}} + \tilde{T}_{wo} \tag{10}$$

where the appropriate temperatures are normalized according to the relationship

$$\tilde{T} = \frac{T - T_{initial}}{T_{boil} - T_{initial}}$$

$$k_1 = \frac{2\, h_g\, A\, \tau_R}{C_\ell}\, \tilde{T}_g$$

$$k_2 = \left[\frac{2wc_p}{C_\ell} - \frac{2h_g A}{C_\ell}\right] \tau_R \lambda$$

Equation (10) has the solution

$$\tilde{T}_{wo} = (k_1 + k_2) - e^{-\hat{t}}\left[C + k_2\hat{t}\right] \tag{11}$$

where C is an arbitrary constant dependent upon the initial conditions.

This equation has not been evaluated in detail. The essential information with regard to the time constant has already been obtained. The time constant for this case is identical to that for the constant water temperature inlet case.

Although the time constants are the same, the actual water flow temperature from the preheater is not described well by the relationship used. The preheater gas side temperature varies during startup. At the initial instant, while the heat exchanger coil is at a uniform temperature, the gas temperature profile is easily computed, and its variation is shown in Figure 5. Also shown in the figure is the gas temperature distribution for the steady state full load condition.

d. Startup of the Test Bed Water Vaporizer Generator as a Whole

The transient behavior of the entire heat exchanger during startup can be computed numerically subject to some simplifications. The early part of this process has been worked out and the calculations indicate that the time constants obtained from Equations (8) and (11) are representative of the behavior of the entire heat exchanger core.

Therefore, one may expect the heat exchanger to be near the design full load output within two to three time constants, or ten to fifteen seconds. However, the design full load conditions have been computed with a liquid flow into the preheater of 250°F, and since after fifteen seconds the preheater inlet flow will probably be still near the initial temperature of the condenser, hot well and pump assemblies, the steam output will probably be somewhat below the full design superheat.

The principal difficulty with this numerical calculation (and the one which makes transient analysis by means of tables available

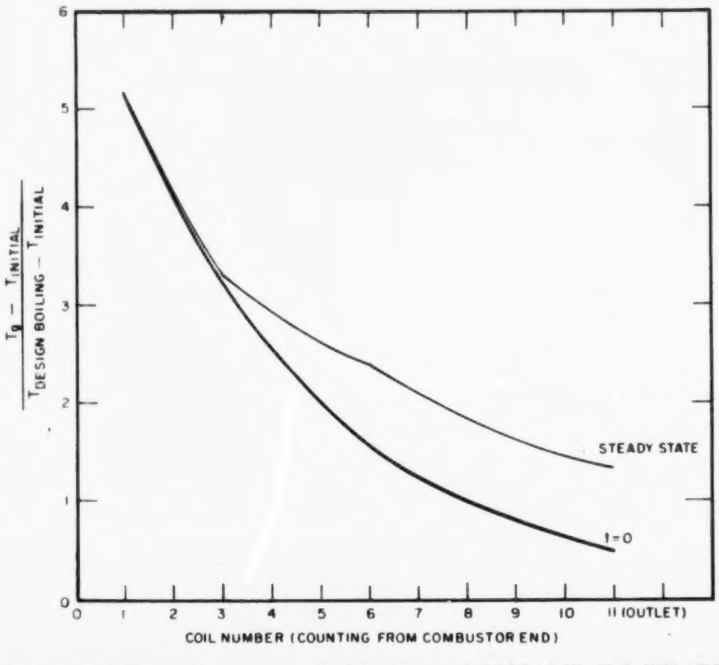

FIGURE 5. GAS TEMPERATURE DISTRIBUTION AT FACE OF EACH COIL AT STARTUP AND STEADY STATE FULL LOAD

in the heat exchanger literature impossible) is caused by the complex water flow path. The flow path is also responsible for the serious problem associated with actual startup of the vapor generator. The onset of boiling will almost certainly occur near the outlet end in the first coil of the vaporizer section (next to the combustor). In order to accommodate the vapor expansion, the liquid will have to be expelled from the superheater coils. This process could be quite violent under some circumstances.

The analyses presented for temperature history of the first coil indicate a temperature rise in the absence of boiling, which is in the order of 25 to 50°F per second. At the temperature level of 545°F (the design boiling point), this temperature rise rate corresponds to a saturation pressure change of in the range of 200 to 500 psi per second. If the pressure in the vapor generator is not to exceed 1200 to 1500 psi, then the superheater must be cleared in a few seconds. Since each of the six passages is some 32 feet long and the design water velocity is of the order of eight feet/second, this clearing process requires some significant changes in flow velocity.

If adequate flow accelerations cannot be attained within the pressure limits of the vapor generator, the combustor heat release would have to be limited to something less than full power on startup. This change would lead to longer startup times.

2. Transient Performance Characteristics

Perturbations around the full load design point have several aspects. At a change in load, the water flow must change as well as the combustor firing rate in order to bring the system into equilibrium at the new demand level.

The transient times for the two streams through the heat exchanger core are very different. At full load, the gas stream transit time is 14 milliseconds. The water stream total transit time is 36.4 seconds, of which 35.0 seconds is required for the water to pass through the preheater, 0.8 seconds for the vaporizer, and 0.6 through the superheater. The long time required for a particle of water to flow through the vapor generator is indicative of the time required for a thermal change in the inlet condition to make itself felt at the steam outlet. However, flow rate accommodation times are much shorter. Since the liquid in the preheater is substantially incompressible, a flow rate change at the inlet to the preheater is instantaneously transmitted to the location of the onset of boiling.

The principal time lags associated with a change in steam demand are probably caused by the inertia of the water in the preheater, which affects the rate of change of flow; the flow response time of the steam vapor space considered as a long, narrow storage reservoir; and the thermal time constant of the wall.

A simple analysis of the vaporizer wall in the first coil can be used to illustrate the magnitude of time lags associated with energy storage in the vaporizer metal. Consider a tube initially in steady state at the design full load conditions, which at time $t = 0$ is subjected to an impulsive change in gas temperature while all other conditions are held constant. This perturbation is approximately that which occurs when the combustor output is suddendly changed to a new level. The governing equation for the tube wall temperature is:

$$\frac{d\bar{T}}{d\bar{t}} = \bar{T}_f - \bar{T} \tag{12}$$

where

$\bar{t} = t/\tau$

$T_f = \dfrac{\left(\frac{1}{2} + \lambda_1\right) T_s + \lambda_2 T_{g1}}{T_{gd}\left(\frac{1}{2} + \lambda_1 + \lambda_2\right)}$ = normalized final tube wall temperature

$\bar{T} = T/T_{gd}$

T = tube wall temperature

T_{g1} = inlet gas temperature

T_{gd} = design inlet gas temperature

T_s = water saturation temperature

t = time

τ = time constant = $\dfrac{C_m}{w_g C_{pg}} \dfrac{\left(\frac{1}{2} + \lambda_1\right)\lambda_2}{\frac{1}{2} + \lambda_1 + \lambda_2}$

C_m = tube wall heat capacity (for entire first coil)

w_g = gas flow rate

c_{pg} = gas heat capacity

λ_1 = $w_g c_{pg}/U_g A$

λ_2 = $w_g c_{pg}/U_b A$

U_g = gas side conductance based on gas side heat transfer area

U_b = boiling side conductance

A = gas side heat transfer area for first coil

This equation is subject to the following idealizations and approximations:

1. Conductances are invariant with time
2. Gas side temperature is always greater than tube wall temperature
3. The mean gas side temperature for heat transfer may be approximated by the average of the incoming and outgoing gas temperatures for the single coil
4. The saturation temperature is constant and the fluid is always boiling

The approximate boundary condition for Equation (12) is

$$\bar{t} = 0, \quad \bar{T} = \bar{T}_d$$

The solution is simply

$$\frac{\bar{T}_f = \bar{T}}{\bar{T}_f - \bar{T}_d} = e^{-\bar{t}} \qquad (13)$$

The time constant, τ, is of particular interest. The following constants are appropriate to the water vapor generator

$w_g c_{pg}$ = 1.2×10^3 Btu/hr°F

U_g = 43 Btu/ft^2 hr°F

C_m = 1.2 Btu/°F

A = 6.2 ft^2

$U_b = 3000 \text{ Btu/ft}^2 \text{ hr}$

$\lambda_1 = 4.5$

$\lambda_2 = 0.0645$

These yield the time constant value

$\tau = 0.23$ seconds

It appears that the wall temperature will have accommodated itself to a new level within one second of onset of a temperature change.

IV. SUPPORT STUDIES

A. Radiant Heat Transfer Considerations for the Combustor-Vapor Generator Design

In the previous quarterly report, an equation set was defined which accounts for thermal radiant heat transfer processes between the combustor and entrance of the vapor generator. The system consisted of two planes separated by a perforated radiation shield. Plane one of this idealized system represented the combustor walls, plane two represented the entrance of the vapor generator, and the perforated radiation shield represented a flow distribution grid for the system. The analysis accounted for radiant exchange from the various surfaces identified, including multiple interreflection as well as convective heat addition to the flow distribution grid from the hot gases. This system has subsequently been extended to include radiant heat transfer from the luminous flame. The luminous radiation was postulated to be absorbed completely at the first impingement on a surface (reasonable approximation). This extension consisted of adding a constant thermal input term to the shield as a result of the absorption of the luminous heat transfer from the flame. The general equation set that defines the thermal radiation, convection and luminous radiation shield absorption for this system follows:

$$q_{conv} + q_{lum} = q_{n_1} + q_{n_2}$$

$$q_{n_1} = f_1(T_1, T_2, a, \alpha\text{'s}, T_3)$$

$$q_{n_2} = f_2(T_1, T_2, a, \alpha\text{'s}, T_3) \qquad (14)$$

$$q_{con} = h\, A_s\, (T_g - T_3)$$

$$q_{lum} = f_3(T_f, \epsilon_f)$$

where

q_{conv}, convective heat transfer to shield

q_{lum}, luminous heat transfer from flame

q_{n_1}, net thermal radiation exchange at plane 1

q_{n_2}, net thermal radiation exchange at plane 2

T_1, known temperature of plane 1

T_2, known temperature of plane 2

T_3, unknown temperature of the shield

T_g, known gas temperature

T_f, known flame temperature

a, solid fraction of shield

α, gray body absorptivity or emissivity of radiation surface

h, convective conductance of shield

A_s, total shield area

ϵ_f, flame emissivity

In order to calculate the total net radiant fluxes at planes 1 and 2, one would add the net thermal flux and the absorbed luminous flux. The net thermal fluxes would be obtained from equation set (14) and the luminous flux from classical procedures; at plane 2, however, only that fraction of the luminous radiation that passes through the perforated radiation shield would be involved.

In order to illustrate the effects of varying the porosity and emissivity of the radiation shield on the net radiation flux at plane 2 (at the first row of tubes in the vapor generator) and on shield temperature, parameter evaluations of the equation set were performed neglecting the effect of flame luminosity. Some of the results are shown in Figure 6 and 7. Note that the net radiant flux at plane 2 (vapor generator entrance) significantly increases as the solid fraction of the shield increases. Also note that it is possible to reduce the net radiant flux at the vapor generator entrance by decreasing the emissivity of the shield.

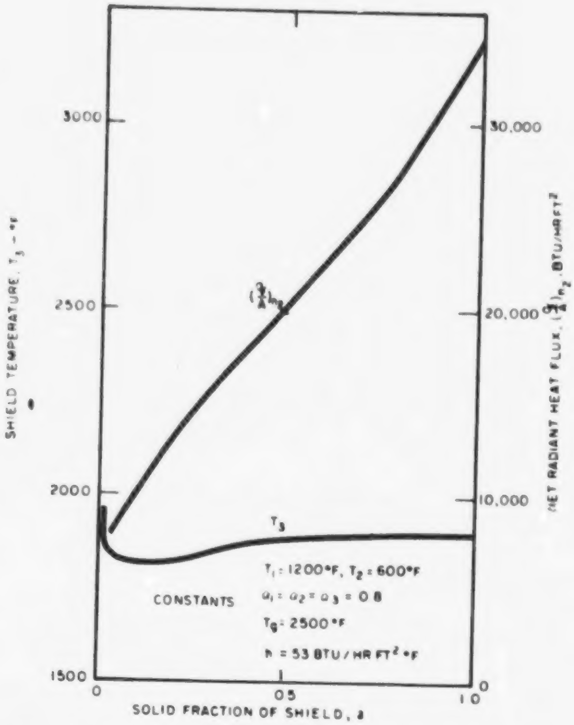

FIGURE 6. $(q/A)_{n_2}$ AND T_3 VERSUS a

B. Nonuniform Heat Transfer in Vapor Generator Matrices

1. Effects of Combustion Gas Velocity and Temperature Variations From Their Mean Values on Tube Wall Temperatures

When dealing with vapor generator systems that utilize organic working fluids such as Fluorinol-85, it is important to be able to define quantitatively the effect of combustion gas velocity and temperature variations (from their mean values) on tube wall hot spots. An elementary analysis has been performed which establishes the criteria for defining the hot spots.

Consider the thermal circuit shown in Figure 8. In this system it is postulated that the convective conductance of the working fluid, h_c, the tube wall thickness, δ_w, the tube wall thermal conductivity, k_w, and the working fluid bulk temperature, τ_c, are all constants. The combustion gas temperature, τ_g, and velocity, u (and, therefore, the convective conductance, h_g), are variable and control the wall temperature, t_w.

A heat flow equation can be written for the thermal circuit in terms of the unknown wall temperature, t_w, namely,

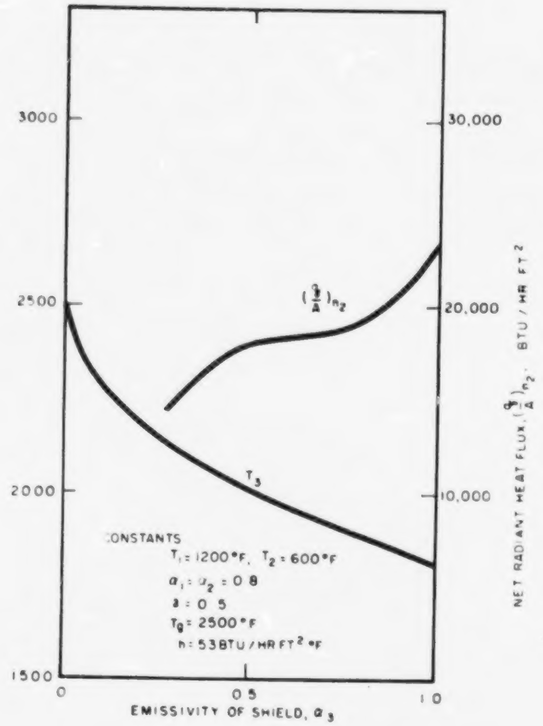

FIGURE 7. $(q/A)_{n_2}$ AND T_3 VERSUS α_3

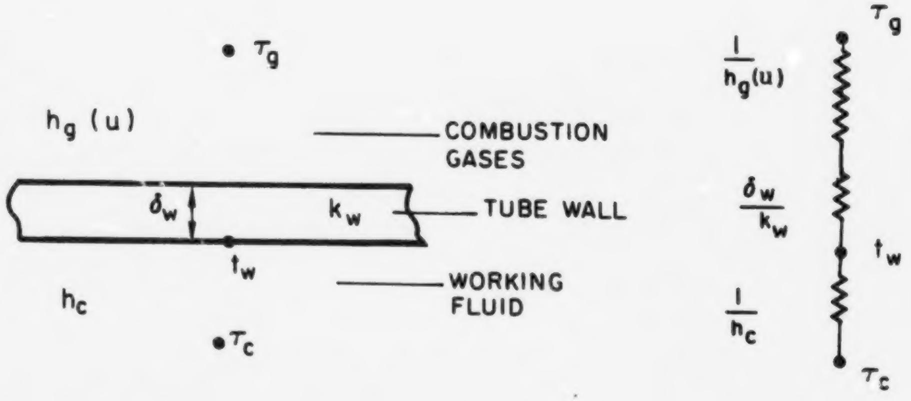
τ_g
$h_g(u)$
COMBUSTION GASES
δ_w
k_w
TUBE WALL
t_w
WORKING FLUID
h_c
τ_c
$\frac{1}{h_g(u)}$
$\frac{\delta_w}{k_w}$
$\frac{1}{h_c}$
τ_g
t_w
τ_c

FIGURE 8. THERMAL CIRCUIT DESCRIBING HEAT FLOW FROM COMBUSTION GASES TO THE WORKING FLUID

A heat flow equation can be written for the thermal circuit in terms of the unknown wall temperature, t_w, namely,

$$\frac{\tau_g - \tau_c}{\frac{1}{h_g} + \frac{\delta_w}{k_w} + \frac{1}{h_c}} = \frac{t_w - \tau_c}{\frac{1}{h_c}} \tag{15}$$

Upon regrouping Equation (14) in a dimensionless form, one obtains

$$\frac{t_w - \tau_c}{\tau_{g_o} - \tau_c} = \frac{\frac{h_{g_o}}{h_c}}{\left(\frac{h_{g_o}}{h_g} + \frac{h_{g_o}\delta_w}{k_w} + \frac{h_{g_o}}{h_c}\right)} \left(\frac{\tau_g - \tau_c}{\tau_{g_o} - \tau_c}\right) \tag{16}$$

where

h_{g_o} , the uniform or design value of h_g

g_o , the uniform or design value of g

The convective conductance on the combustion gas side is a function of the local gas velocity (dependent upon the Nusselt-Reynolds modulus function for flow over tubes). For the systems under consideration, it can be shown that the conductance varies as the 0.6 power of the velocity, namely;

$$\frac{h_g}{h_{g_o}} = \left(\frac{u}{u_o}\right)^{0.6} \tag{17}$$

Therefore, the dimensionless wall temperature can be expressed as

$$\frac{t_w - \tau_c}{\tau_{g_o} - \tau_c} = \frac{c_1}{\frac{1}{\left(\frac{u}{u_o}\right)^{0.6}} + c_2} \quad \frac{\tau_g - \tau_c}{\tau_{g_o} - \tau_c} \tag{18}$$

where

$$c_1 = \frac{h_{g_o}}{h_c}$$

$$c_2 = \frac{h_{g_o} \delta_w}{k_w} + \frac{h_{g_o}}{h_c}$$

Equation (18) has been used to predict mean wall temperature variations in tubes of a typical Fluorinol-85 superheater. The results are shown in Figures 9 and 10 in terms of gas velocity ratio, u/u_o, and temperature ratio, $\tau_g - \tau_c / \tau_{g_o} - \tau_c$, typical of this system.

Some experimental information available from Solar's combustor gas temperature traverses indicate that the temperature ratio might vary from a low value of 1.05 to a high value approaching 1.3. Clearly by good combustor design it is not expected that the high value will be typical, but that the low value can be achieved. No experimental information is available on the velocity ratio, u/u_o.

It was thought appropriate to determine from Figure 10 how large a wall temperature increase would result for the hypothetical condition that both the combustion gas velocity and temperature ratios are equal to 1.2. For this case, the wall temperature increase above the design (uniform) value was $t_w - t_{w_o} = 38°F$. The results indicate that such temperature asymmetries at the hot spots could cause decomposition and deposition problems; thus, lower gas velocity and temperature ratios should be set.

It is believed that it would be fruitful to analyze combustion processes and secondary air addition processes for idealized flow geometries representative of the Solar combustor for the purpose of estimating the limiting gas velocity and temperature ratios that may occur and what can be done about reducing them. Some possible mathematical model studies that would give such information have been outlined for future evaluation.

2. Effects of Peripheral Variations in Heat Transfer Around Vaporizer Tubes

The matter of peripheral variations in heat transfer in vapor generator tubes is also of interest in connection with excessive wall temperatures, if organic working fluids are used.

The peripheral variation in heat flux is composed of convection and radiation terms. The latter mode is only present to any practical extent in the first or second row at the vapor generator entrance, of course.

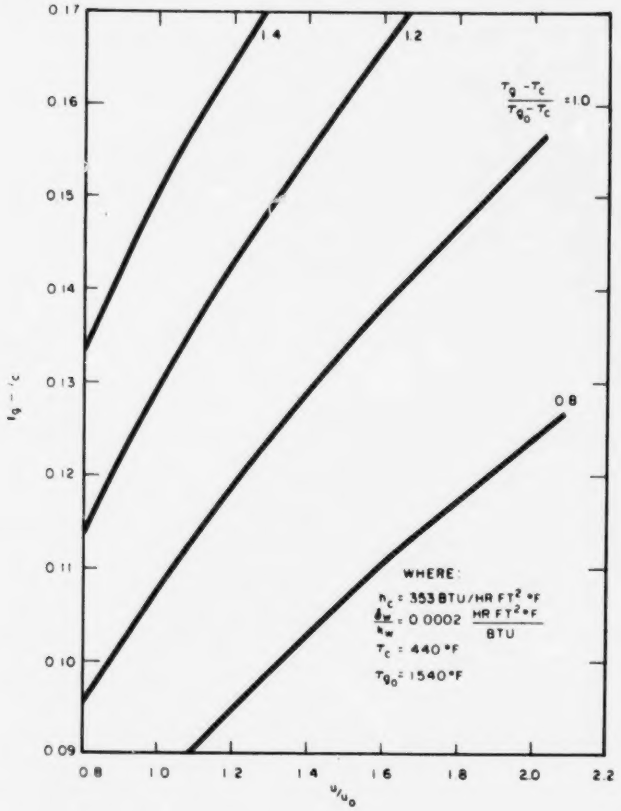

FIGURE 9. DIMENSIONLESS TUBE WALL TEMPERATURE VERSUS GAS VELOCITY AND TEMPERATURE RATIOS

Maximum peripheral wall temperature variations (without considering peripheral tube wall conduction) at the vaporizer inlet of the Fluorinol-85 vapor generator were calculated. At the stagnation point of the first tube, the ratio of the local convective heat flux of the tube is greater than 1.5 (depending on how large the radiation flux is as shown in Figures 6 and 7, for example). This means that the inner tube wall temperature at the stagnation point can be as much as 49°F greater than a mean inner tube wall temperature. Similar calculations have been made for the superheater. In this case, the maximum inner wall temperature excess at the stagnation point is a little higher than the value for the vaporizer tubes, namely, 54°F. Although the radiation flux does not exist and the gas temperature is only 1540°F (rather than 2500°F) for the superheater, the inner wall-working fluid temperature difference is higher in this component because of the relatively low working fluid convective conductance that exists.

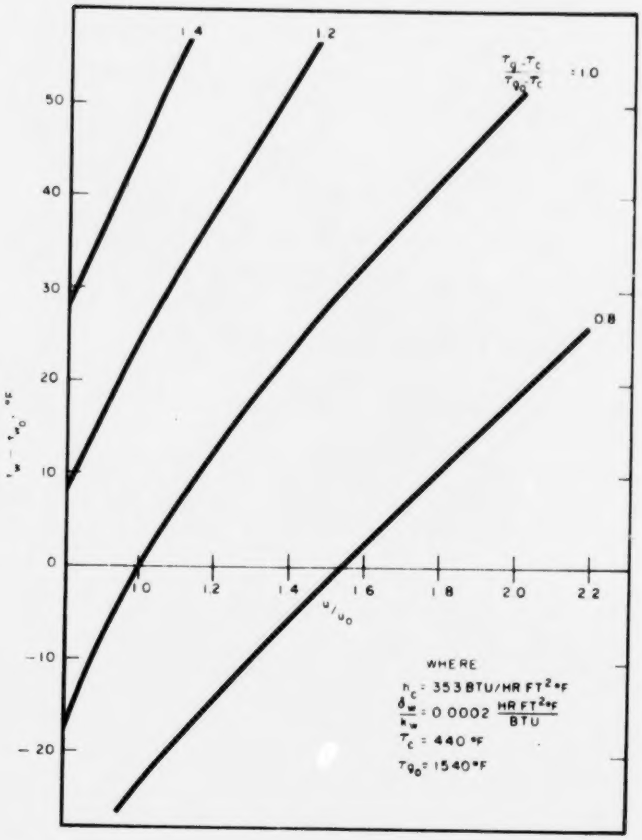

FIGURE 10. TUBE WALL TEMPERATURE VERSUS GAS VELOCITY AND TEMPERATURE RATIOS

Geoscience has previously studied the effects of peripheral heat conduction in tube walls for asymmetrical heat transfer situations. An analytical solution has been developed that can be used to predict the peripheral wall temperature distribution when there is a step function variation in the heat transfer conductance on one side of the wall and a uniform value on the other. The solution also accounts for wall thickness and its thermal conductivity. It is possible to use this work to predict how much the wall temperature hot spots described in the first part of this section will be reduced as a result of tube wall conduction. In addition to this method of analysis, it is also possible to perform two-dimensional flux plots with a thermal analog apparatus, if necessary.

C. Methods for Controlling Excessive Wall Temperatures in Vapor Generators

There are a number of methods by which excessive wall temperatures in vapor generators can be reduced, two of which have been studied by Geoscience to date. They involve rather direct and relatively uncomplicated approaches to the problem. One method involves adding thin thermal resistances to the outside of vapor generator tubes and the second one consists of internal tube finning.

1. External Thermal Resistance

The addition of a thermal resistance to the outer tube surface has the additional advantage that it does not increase the internal fluid pressure drop. Further, if the resistance layer is thin, it does not significantly change gas flow patterns or increase the heat exchanger size.

The overall heat transfer conductance, U, for the insulated tube system is,

$$\frac{1}{U} = \frac{1}{h_o} + \frac{\delta_r}{k_r} + \frac{r_o}{k_w} \ln \frac{r_o}{r_i} + \frac{r_o}{h_i r_i} \qquad (19)$$

where the subscripts o, r, w, and i, refer to outside, added thermal resistance, wall and inside, respectively. The other symbols have been described previously. It is clear that the overall heat transfer coefficient can be reduced by increasing the thickness of the added resistance in addition to decreasing its thermal conductivity. Figure 11 illustrates this feature for typical Fluorinol-85 superheater conditions.

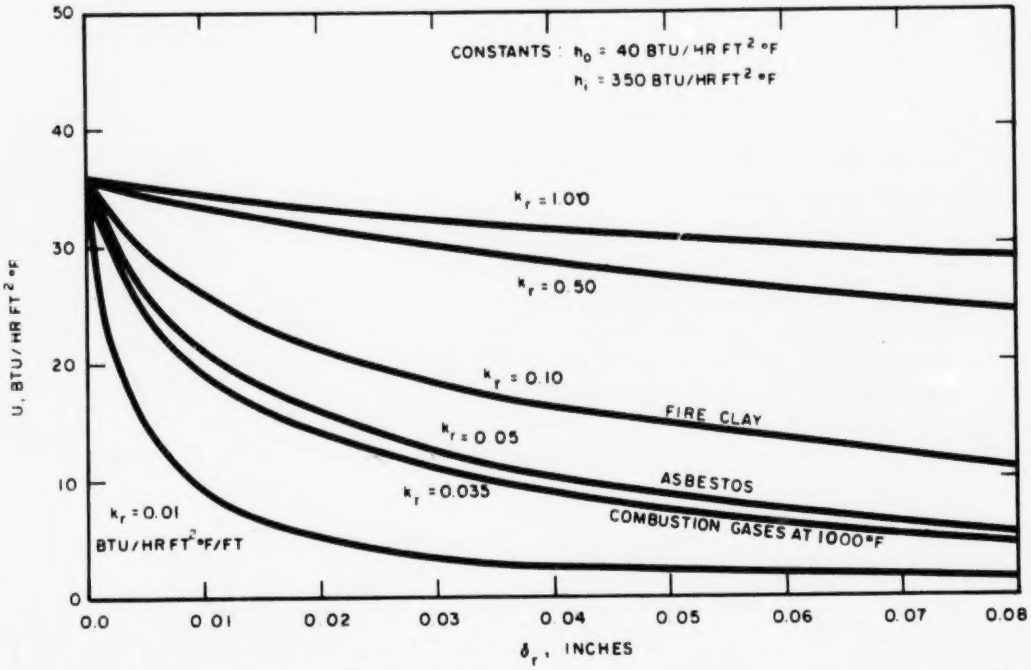

FIGURE 11. THE EFFECTS OF k_r AND δ_r ON THE CONDUCTANCE U

It is seen that a gas layer would provide a high thermal resistance to the wall. In this case, the tube could be wrapped with a thin foil which is spaced by dimples pressed into, say, one percent of the foil area. By varying the depth of the dimples, various thermal resistances can be obtained to satisfy the requirements in each row of tubes. For example, the material gaps required for each row of the superheater in the system illustrated in Figure 12 would be:

Row No.	Overall Heat Transfer Conductance, Btu/hr ft^2°F	Material Having a $k_r = 0.035$ (gas) δ, Inches	Material Having a $k_r = 0.10$ δ, Inches
2	$U_2 = 12$	$\delta_2 = 0.031$	$\delta_2 = 0.075$
3	$U_3 = 17$	$\delta_3 = 0.017$	$\delta_3 = 0.040$
4	$U_4 = 25$	$\delta_4 = 0.006$	$\delta_4 = 0.015$
5	$U_5 = 36$	$\delta_5 = 0.000$	$\delta_5 = 0.000$

The above calculations illustrate that a gas gap would increase the overall tube diameter less than twelve percent for a half inch tube. In comparison, an insulator with $k_r = 0.10$ Btu/hr ft°F would increase the overall tube diameter up to 30 percent.

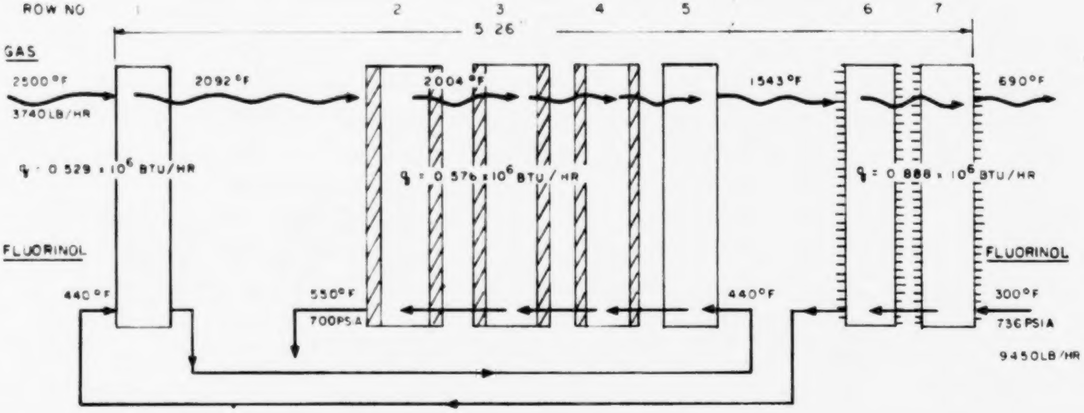
ROW NO
1
2
3
4
5
6
7
5 26"
GAS
2500 °F
3740 LB/HR
2092 °F
2004 °F
1543 °F
690 °F
q = 0 529 x 10^6 BTU/HR
q = 0 576 x 10^6 BTU/HR
q = 0 888 x 10^6 BTU/HR
FLUORINOL
FLUORINOL
440 °F
550 °F
700 PSIA
440 °F
300 °F
736 PSIA
9450 LB/HR

FIGURE 12. FLOW DIAGRAM OF FLUORINOL-85 BASE DESIGN NO. 1

In order to demonstrate the insulating effectiveness of various types of tube insulators, a one-half inch diameter steel pipe, covered with test insulation samples, was heated electrically to a glowing red color. The test samples consisted of:

(1) A dimpled stainless steel foil,

(2) A single stainless steel foil wrapped directly on the pipe,

(3) A stainless steel foil separated from the tube by a fine gauge screen,

(4) A stainless steel foil separated from the tube by a coarse gauge screen,

(5) A ceramic coating.

Except for the ceramic coating, each test sample had a small hole drilled through the foil, through which the pipe wall color-temperature could be estimated. It is noted that the reverse direction of heat flow in these tests in comparison to that to a vapor generator tube is unimportant because one is only interested in the thermal insulating effect. The dimpled foil showed significant insulating characteristics because of the air gap between it and the pipe wall. The thermal insulating effect of the foil wrapped directly on the wall was not very good (as expected because of the thin air gap). Both foil samples separated by the screens demonstrated good insulating characteristics, the one with the coarse screen being somewhat better. The ceramic coating was not as good an insulator as the other test samples because the coating was in direct contact with the wall. These tests verified that gas gaps are very effective as insulators as would be expected from the previous calculations.

2. Internal Finning

Another method of reducing the inner tube wall temperatures in the Fluorinol vapor generator is to increase the internal tube wall area by adding fins. However, increased surface area also means additional pressure losses, particularly in viscous fluids. In order to avoid profile pressure losses, the fins should be longitudinal and with a cross sectional geometry which reduces the equivalent tube diameter the least possible. Ring or spiral fin arrangements are, therefore, undesirable. In order to minimize pressure losses, sudden flow changes should be avoided at the tube inlets and outlets.

In designing internal finning, the pressure losses and the heat transfer effectiveness must be optimized for each component in the vapor generator so that allowable pressure losses are distributed most advantageously for obtaining desired heat fluxes and temperatures in each tube section. The number of flow passages in each section must be large enough, within practical limits, to effectively reduce the pressure drop to a minimum in each section.

In some cases, external finning or external resistance is required together with internal finning in order to control optimum heat fluxes. To do this, it is necessary to optimize the external and internal geometries to obtain the best design.

Design trade-offs using internal finning on the Fluorinol vapor generator for the purpose of lowering wall temperatures are given in the design section of this report.

D. Instrumentation Support

Geoscience has also reviewed the water test bed vapor generator that has been fabricated by Solar and made recommendations concerning primarily thermocouple instrumentation. It is important that the actual steady state and transient performances of the system are determined and compared to design values.

GLR-102

VAPOR GENERATOR TECHNOLOGY SUPPORT FOR SOLAR DIVISION OF INTERNATIONAL HARVESTER

(P03739-32134-F03)

C. M. Sabin
H. F. Poppendiek
G. Mouritzen
R. K. Fergin

GEOSCIENCE LTD
410 South Cedros Avenue
Solana Beach, California 92075

Preceding page blank

I. SUMMARY

Geoscience's support role in the subject program consists of two study areas (1) vapor generator design, and (2) heat transfer and fluid flow support for the vapor generator-combustor system. The vapor generator design work involves an investigation of the relationships between the fluid properties and the requirements imposed on the vaporizer by other components of the power system.

During the last quarter, Geoscience performed the following tasks: (1) final Fluorinol-85 vapor generator design, (2) final AEF-78 vapor generator design, (3) water test bed vapor generator performance experiments, and (4) several support studies. Also there are summarized project meetings and test cell experiments.

II. PROJECT MEETINGS AND TEST CELL EXPERIMENTS

A. Ann Arbor Rankine Cycle Contractor's Meeting (January 20-21, 1972).

Geoscience participated in the Solar presentation by reporting on its vapor generator design and support studies for Solar.

B. Progress Report to S. Luchter, P. Hutchins, H. Naser and A. Kreeger (January 27, 1972)

Geoscience reported progress to date and reviewed questions relative to AEF-78 physical properties and vapor generator design efficiencies.

C. Technical Discussions With Aerojet Staff Members (February 7, 1972)

Solar and Geoscience staff visited Aerojet to review physical properties and thermal stability questions in addition to considering vapor generator efficiency limitations.

D. Progress Report to P. Hutchins (February 23, 1972).

The water test bed vapor generator was operated for Mr. Hutchins at Solar. Geoscience reviewed and interpreted the steady state and transient performance characteristics of the generator. Additional steady state water test bed vapor generator experiments were scheduled to be performed within the next several weeks.

E. Progress Report to G. Thur and W. Mirsky (February 24, 1972).

The water test bed vapor generator was operated for Messrs Thur and Mirsky. Geoscience reviewed and interpreted the steady state and transient performance characteristics of the generator. Additional steady state water test bed vapor generator experiments were scheduled to be performed within the next several weeks.

F. Test Cell Experiments

In this quarterly period, Geoscience staff assisted Solar in the operation of the water test bed vapor generator. During the many tests performed, Geoscience proposed modifications to the test cell equipment to simplify system operation; these modifications were subsequently made. Steady state and startup performance data were obtained during these tests.

III. VAPOR GENERATOR DESIGN STUDIES

Two vapor generator designs have been completed during this quarter. These are for the fluids Fluorinol-85 and AEF-78. Descriptions of these two vapor generatores are given below. The test bed water vapor generator operation has shown that it performs as expected. Some details on the operation are presented in the following paragraphs, also.

A. Fluorinol-85 Vapor Generator Design

A demonstration prototype vapor generator was designed for a Fluorinol-85 Rankine cycle engine system. The resulting design conditions are

Fluorinol-85 Side:

Flow	10,000 lbm/hr
Pressure drop	89 psi
Outlet pressure	700 psia
Inlet temperature	287°F (at max. power)
Outlet temperature	550°F
Heat transfer rate	2.25×10^6 Btu/hr
Efficiency	81% based on HHV of JP-5 (19800 Btu/lb)
Max tube wall temperature	506°F

Gas Side:

Air-fuel ratio	25 to 1 (JP-5 fuel)
Flow (gas)	3740 lbm/hr
Pressure drop	4.3 inches H_2O
Outlet pressure	atmospheric
Inlet temperature	2500°F (mean) ± 250°F

In the direction of the gas flow, the vapor generator consists of a vaporizer, a superheater and preheater. The preheater and superheater are in counterflow to the gas and the vaporizer is parallel.

The preheater consists of ten rows of 45 tubes each (1/4-inch OD tubing with 0.016 inch walls). Longitudinal and transverse spacing is 5/16-inch in a triangular array. Tube heat transfer length is 22 inches with an outside area of 53.9 ft^2.

Material, stainless steel or carbon steel. First eight rows of preheater measured from cold end, are 45 tubes in parallel. Remaining two rows are 15 tubes in parallel.

Flow exiting preheater passes into first vaporizer row adjacent to combustor, then into second vaporizer row, in a cross parallel flow arrangement. From second vaporizer row, saturated vapor flows into 1/2-inch tube row farthest from combustor, passes through two remaining 1/2-inch tube rows in a cross-counterflow arrangement.

All 1/2-inch tubes are arranged seven tubes in parallel, so that each parallel path makes three passes in each row.

The five vaporizer and superheater rows consist of 1/2-inch OD tubing, 0.030-inch wall, 16 internal longitudinal fins 0.030-inch thick by 0.056-inch high. Material is carbon steel, longitudinal and transverse spacing is 0.675-inch. Active heat transfer length is 22 inches with a total outside heat transfer area of 25.4 ft^2.

In order to control the amount of heat transferred through the vaporizer, the tubes are insulated with a foil tube forming a 0.010-inch thick insulating layer of gas around the vaporizer tubes. The combined conduction and radiation effects result in all saturated vapor at the vaporizer outlet.

All three rows of the superheater are, likewise, insulated with a 0.020-inch thick gas layer to obtain superheated vapor of 550°F at the outlet. An experiment was performed at Geoscience to support the analysis of the foil tube.

The maximum tube wall temperature was calculated to occur at the superheater outlet. This temperature is 566°F as compared to the design limit of 575°F. It is not feasible to lower this temperature for safety reasons since the outlet temperature of the Fluorinol is 550°F. Tube wall temperatures at the vaporizer inlet and outlet and at the superheater inlet are about 470°F.

Carbon steel tubing was used in the design in order to obtain minimum peripheral tube wall temperature variations. Also, internal finning was used in designing the vaporizer and superheater in order to obtain minimum tube wall temperature.

B. AEF-78 Vapor Generator Design

An AEF-78 vapor generator designed for 85.5 percent thermal efficiency (based on the LHV) has been completed. This unit is of rectangular cross section, utilizing straight tubes in tube sheets. The heat exchanger is made up of four rows of 15 one-half inch diameter internally finned tubes at the combustor end, followed by ten rows of 60 one-fourth inch diameter plain tubes at the cooler end. The total gas side heat exchange area is approximately 106 square feet. Although the most critical location in the matrix with respect to fluid overheating is at the outlet, the combination of the high temperature tolerance of AEF-78 (the maximum acceptable tube wall temperature is 810°F) and the internally finned tubing allow this heat exchanger to be arranged completely in a cross counterflow arrangement, without the complex paths required in the test bed water vapor generator and the Fluorinol-85 vapor generator. This AEF-78 vapor generator is expected to have a maximum tube wall temperature near 720°F.

Physical characteristics of this design are listed in the table below.

With the specified flow conditions imposed by the other engine components on this design, a thermal efficiency of 85.5 percent based on the lower heating value requires a heat exchanger effectiveness of 0.97. In this range of effectiveness, an increase of only one percent in effectiveness requires a heat transfer area increase of over ten percent. In a joint meeting with Aerojet personnel, it was decided that the decrease in size, complexity, and weight of the vapor generator justified a decrease in the specified thermal efficiency. It was, therefore, decided to decrease the efficiency to 82.2 percent, and thereby eliminate three rows of quarter inch tubing. With this change, the total number of quarter inch tubes decreases from 600 to 420, arranged in seven rows of 60 tubes each.

A change such as this does not affect the vapor flow rate or heat transfer rate. Instead, the combustion products flow rate increases (by some three percent) and the exhaust temperature rises about 100°F. The fuel-air ratio is, of course, held constant, so the combustion products inlet to the vapor generator remains at 2500°F.

C. The Water Test-Bed Vapor Generator Performance

During the past quarterly period, the water test bed vapor generator has been operated with the Solar combustor for the purpose of determining experimental steady state and transient performance characteristics.

A number of experiments have been performed with the vapor generator covering the following ranges of parameters:

TABLE I

Characteristics of AEF-78 Vapor Generator for 85.5 Percent Thermal Efficiency (Based on the Lower Heating Value)

AEF-78 Side:

Flow	19,300 lb/hr
Pressure drop	20 psi
Outlet pressure	1,000 psi
Inlet temperature	396°F
Outlet temperature	650°F
Heat transfer rate to organic	2.02 x 10^6 Btu/hr

Gas Side:

Outlet temperature	455°F
Flow	3,400 lb/hr
Pressure drop	2.9 inches of water
Inlet temperature	2500°F mean

Tube Arrangement:

Four rows of 30 tubes each, internally finned 1/2 inch OD carbon steel tubing at combustor end of heat exchanger. Internal fins identical to those for Fluorinol-85 vapor generator. Exterior of tubes bare.

Ten rows of 60 tubes each, bare 1/4 inch OD tubing at combustion products outlet end.

AEF-78 flow path through exchanger is cross counterflow. Cold fluid enters at combustion products outlet end and passes through 1/4 inch tubing with 60 tubes in each row in parallel. Return bends are manifolded. The half-inch tubing is to be ten parallel paths, so each group of three tubes in each row is in series. Superheated vapor outlet collector manifold is at row next to combustor outlet face.

Physical Characteristics of Tube Bank:

Tubes	23 inches long (heat transfer length)
Face area	23 x 19.1 inches
Total thickness	5.6 inches
Tube bank weight (without tube sheets or headers)	92 lbs
Liquid hold up weight	38 lbs.

(1) Water flow rate range	400-1700 lbs/hr
(2) Percent air	22-51 percent
(3) Fuel rate	40-75 lb/hr
(4) Inlet water pressure	150-1100 psia
(5) Outlet water pressure	15-1100 psia
(6) Exit water temperature	up to 1100°F
(7) Degree of superheat	9-580°F

When operating the system so that the temperature out of the preheater was close to the saturation temperature, the flows and the temperature profiles in the six parallel passages (through the vaporizer and superheater) were satisfactorily balanced.

IV. SUPPORT STUDIES

The vapor generator support activities carried on by Geoscience during this quarter included analysis of two phase flow in parallel channels, some assistance to Solar on fabrication sources, and proposals for the fabrication or mechanical simplification of the vapor generators. Typical examples of this work are given in the following paragraphs.

A. Two Phase Flow in Parallel Channels

Analyses have been made for the differences in mass flow rate through parallel tube vapor generators for the cases of liquid flow in some channels and vapor in others (hypothetical worst case). In particular, one is interested in the difference in maximum wall temperature at the vapor generator exit for the case where half the tubes are filled with vapor and another half liquid. The results of the analyses show that a number of the important system parameters control this process. An important variable is the fluid density. One can show that a water vapor-filled tube can have approximately twice the temperature rise that a liquid-filled tube has for a typical set of design conditions. In an actual situation, however, this temperature difference would be less because the tubes would contain two phases rather than either vapor or liquid alone. It is pointed out that for the Fluorinol-85 case, this hypothetical result would be much smaller. These calculated performance features were noted during the water test bed vapor generator tests. For example, flow asymmetries could be generated by reducing the vapor generator back pressure (to create a large liquid-vapor density ratio). It was also possible to show that flow asymmetries could be created by increasing the water flow rate to such a value that the exit temperature of the preheater was well below the saturation temperature.

When the water test bed vapor generator is operated with very large water flow and low combustor power, the liquid from the preheater passes into the vaporizer rows very much subcooled. Under this condition, the location at which vapor generation begins is not well established, and small variations in flow from one channel to the next can cause chugging and erratic behavior. If in the startup process the combustor power level and water flow rate are reasonably well matched, startup occurs without difficulty, since the first vaporization occurs at nearly the same location in all tubes.

B. Proposals For the Simplification of the Fluorinol-85 Vapor Generator Return Bends

The tube connection arrangement for the Fluorinol-85 vapor generator which was proposed in the sketches submitted with the design utilized manifolded return bends through the preheater. In the preheater rows 9 and 10, where the flow makes three passes instead of one, the manifolded return bends led to a header design which is bulky and expensive to produce. It is, therefore, suggested that an individual return bend arrangement be made for the preheater rows 8, 9, and 10. The three-to-one flow area reduction required in going from row 8 to 9 would then be accomplished locally, with 15 identical reducing return passages, so that these returns need not have a passage depth from the tube sheet greater than that of the manifolded return bends on rows 1 through 7. This arrangement also allows the use of 15 (or less) small tubes as connectors between the preheater outlet and the vaporizer inlet manifold, so that less space is required for this connection.

The construction of the tube bend assembly can be accomplished in several ways. It is possible to machine the assembly from a solid block. It is also possible, however, to braze the assembly from a number of small subassemblies in several stages. This latter approach may decrease the machining costs significantly, so that a net savings is realized in spite of the additional steps in assembly. The individual return bends in preheater rows 8, 9, and 10 and in the vaporizer and superheater sections could, for example, be built up from short pieces of drawn tubing reformed in cross section to provide the required passages. The row-to-row pressure drop is small, so that pressure across these dividers need not be a serious consideration in choice of their wall thickness. They would, however, be loaded in tension, since they would provide the link between the cover plate and the tube sheet. If the manifolds were built up of tubing, there would be voids in the assembly which were not part of the flow passages. However, these would be sealed and need not present a problem.

It is also possible to form the return bend arrangement for the superheater (or vaporizer) from reformed tubing sections. These would have to be in the order of 1/2 to 5/8 of an inch thick to provide adequate flow area. If the preheater return assembly were made up of the same thickness, a continuous cover plate could be used for the entire assembly. This cover plate would be perforated only by inlet, outlet, and section interconnection lines. It appears that a rather large decrease in machine work would be accomplished by this means.

The manifolding could also be made up with return bends, separators machined from a single plate, but using a cover plate rather than machining the cover integral. In this manner, a large portion of the metal removal could be accomplished by through drilling, rather than by use of an end mill. The cover plate would then be brazed on in a separate step.

V. DESIGN PROCEDURES FOR COMBUSTION HEATED FORCED CONVECTION VAPOR GENERATORS

A. Principal Design Steps

The vapor generator has performance criteria specified by requirements of the system. This information usually includes the following items:

Inlet thermodynamic state of both streams

Mass flows of both streams

Outlet vapor thermodynamic state

Minimum acceptable thermal efficiency of burner-vaporizer combination at full load

Maximum acceptable pressure drops in both streams

Matrix volume limits

If these specifications are made arbitrarily, it may be impossible to satisfy them all. More discussion of this aspect appears in Section B.

The first five steps in the design procedure are straighforward thermodynamic calculations. However, it is frequently necessary to use some arrangement for superheater and vaporizer other than counterflow to limit tube wall temperatures so these steps may be done several times.

Step 1 By energy balance and with properties tables for the fluids, establish for the preheater, vaporizer, and superheater sections:

Enthalpy changes in each stream
Heat flow
State points between sections

If pressure drops are expected to alter fluid state points significantly, assume some pressure drop distribution for the above calculations.

The next four steps may be done by several equivalent procedures. The notation used here is from Kays and London, Compact Heat Exchangers, 2nd Edition.

Step 2 For both streams compute the capacity rates for each of the three sections. The capacity rate for a vaporizing fluid is infinite. Compute the capacity rate ratios for each section.

Step 3 Compute heat transfer effectiveness of each section.

Step 4 Compute the NTU requirement for each section, utilizing a reasonable choice for the heat exchanger arrangement, such as multipass counter cross flow.

Step 5 Using the appropriate value of C_{min}, compute the product AU from the NTU values for each section.

The establishment of the overall conductance requires computation of hot and cold side heat transfer conductances. For normal combinations of fluids, the controlling heat transfer resistance will be on the hot, combustion products side. It is at this point in the procedure that the major choices are available to the designer. There are several tradeoffs which must be considered.

a. For most heat exchange surfaces, pressure drop goes up more rapidly with increasing velocity than does heat transfer conductance. If pressure drop is an important criterion, as it is with most automotive power plants, then one wants to use the maximum available frontal area, and in addition consider configurations which have relatively large free flow area.

b. Neither the conductance nor the area per unit of volume of a surface configuration is to be maximized but, instead, the product αh must be maximized for a compact matrix.

c. Extended surfaces on the hot side increase heat fluxes on the vaporizing fluid side. If the vaporizing fluid is an organic and subject to thermal decomposition or if the possibility of film boiling exists, extended surfaces cannot be used without consideration of the cold side conditions.

An example of such a condition occurs in the Fluorinol-85 vapor generator near the preheater outlet. The overall U at this location (which depends only weakly on the internal conductance), together with the local ΔT, specifies a heat flux which could lead to unacceptably high wall temperatures. The internal velocity was tripled at this location in order to raise the internal conductance and bring the wall temperature down. If an extended surface configuration had been used which held the overall αh constant but decreased the internal wall area, the internal velocity would have to be increased still more to control wall temperature. Pressure drop goes up rapidly with velocity increase so such a change would probably make the internal pressure drop too high. An extended surface configuration which had a lesser αh product would, of course, lead to a preheater with larger volume.

Step 6 Choose a hot side heat exchanger surface appropriate to the hot side surface and determine appropriate conductance relationships.

Proper heat transfer relationships for the cold side flows may be chosen with the aid of the following guidelines.

a. For the all-liquid (preheat) and all vapor (superheat) locations use standard single phase relationships. Beware of using relationships for fully established flow for computations involving short runs of tubing.

b. Subcooled boiling may occur near the preheater outlet.

c. The point of the so-called "boiling burnout" or "transition boiling" which corresponds to the end of the wetted wall in the vaporization region, marks the change from boiling or liquid-like conductances to vapor-like conductances. This point is usually found at vapor qualities significantly less than unity. The location depends upon the fluid properties, the mass flux, heat flux, orientation in the gravitational field, etc. A wealth of literature is available which describes this phenomenon with varying degrees of accuracy.

d. The actual boiling conductance depends upon the fluid the local thermodynamic conditions, and the phase distributions.

e. The maximum heat flux which can be applied during boiling without film boiling is limited. If the computed wall temperature under wetted wall boiling is too high, the liquid will not remain in contact with the wall, since the liquid in contact with the wall must clearly be superheated.

Step 8 Compute cold side conductances as functions of pressure drop, number of parallel passages, or tube diameter (in the case of a monotube circuit). Choose particular combinations for each section or subsection which meet the design requirements.

Step 9 Compute overall conductances using proper corrections for fin effectiveness, wall resistance, etc. Beware of fin effectivenesses which are too low. Fin effectiveness relationships are based upon the idealization that the gas side conductances are uniform. Since they are in actuality not uniform, the designer depends upon conduction in the fin to transfer heat from one area of the fin to another. Low fin effectiveness implies that the heat flow into the tube wall from the fin will not be uniform.

Step 10 Compute the required heat transfer area and the heat exchanger volume from the required AU product determined in Step 5. If the volume is too great, choose a more compact surface (larger αh product).

Step 11 Compute the gas side pressure drop.

It may be observed that the frontal area, heat transfer surface type and array, and flow paths have been determined, but that the construction of the matrix is not defined. All of these calculations are equally valid for a round cross section or a tube-in-sheet geometry. If a tube sheet geometry is chosen, it must have a number of tubes in each row which is evenly divisible by the number of parallel flow paths. A nested spiral arrangement may have any number. The tube sheet arrangement has a high cold side pressure loss in tube bends, and this pressure loss does not contribute to the heat transfer performance.

Step 12 Choose configuration, manifolding connections, tube wall thicknesses and other mechanical details. Since an approximate tube wall thickness was necessarily made before internal conductances and pressure drops could be calculated, a large change in tube wall thickness could require recalculation of some of the above steps.

B. Vapor Generator Example Design for AEF-78

Initial Data:

AEF-78

Flow	19,300 lb/hr
Δp	50 psi goal, 100 psi max.
Outlet pressure	1000 psia
Inlet temperature	396°F
Heat transfer rate to organic	2.02×10^6 Btu/hr

Gas Side

Outlet temperature	455°F
Air-fuel ratio	25:1 (JP-5)
Flow	3400 lb/hr
Δp	3.0 inches H_2O
Outlet pressure	atmospheric
Inlet temperature	2500 F (mean) ±250°F

General Constraints

Efficiency based on HHV	80 percent
Efficiency based on LHV	85.5 percent
Maximum tube wall temperature	810°F
Maximum face size	26 in. diameter circle, or 26 in. by 21 in. rectangle
Maximum core thickness	6 inches

Step 1

In this case there is no change of phase, so energy balance specified all information for Step 2.

Step 2

Overall gas capacity rate:

$$C_{min} = \frac{2.02 \times 10^6 \text{ Btu/hr}}{2045°F} = 988 \text{ Btu/hr°F}$$

$$C_{max} = \frac{2.02 \times 10^6 \text{ Btu/hr}}{254°F} = 7950 \text{ Btu/hr°F}$$

$$\frac{C_{min}}{C_{max}} = 0.124$$

Step 3 For the entire matrix:

$$\epsilon = \frac{2000\ F - 455°F}{2500\ F - 396°F} = 0.972$$

Step 4 A reasonable first choice of flow arrangement for this unit is multipass counter cross flow. For the probable number of passes, this arrangement is indistinguishable from counterflow. From the appropriate equation in Kays and London,

$$NTU = \frac{AU}{C_{min}} = 3.9$$

Step 5

$$AU = 3.9\ (988\ Btu/hr°F) = 3870\ Btu/hr°F$$

Step 6 Choose 1/2 inch OD plain tubes in a staggered array, 5/4 diameter on centers. It has been shown that this configuration yields compact vapor generators. For more details on the basis for this choice among other staggered bare tube arrays, see Geoscience Ltd quarterly report to Solar for June to August 1971, GLR-95. The heat transfer and flow friction characteristics of this geometry are to be found in Figure 10-6, page 185 of Kays and London's Compact Heat Exchangers, 2nd Edition.

Choose a rectangular matrix of 10.09 inches by 23 inches.

$$A_f = 3.05\ ft$$

This area corresponds to 30 tubes in each row of one-half inch tubes, each 23 inches long.

For average gas properties,

$$h_g = 31.3\ Btu/ft^2\ hr°F$$

This value ranges from a maximum (at the combustion products inlet) of 38.9 Btu/ft^2 hr°F to a minimum (at the combustion products outlet of 24.8 Btu/ft^2°F.

For one quarter inch tubing in a geometrically similar array, the corresponding values are

$$h_{mean} = 42.9 \text{ Btu/ft}^2 \text{ hr°F}$$

$$h_{inlet} = 51.5 \text{ Btu/ft}^2 \text{ hr°F}$$

$$h_{outlet} = 32.2 \text{ Btu/ft}^2 \text{ hr°F}$$

Step 7 The internal conductances may be computed based on standard correlations. No details can be shown because of the proprietary nature of the fluid AEF-78. The fluid throughout this vapor generator may be treated as single phase. There are, however, some temperature levels at which the transport properties vary rapidly with small temperature changes.

Step 8 For ten parallel paths, the internal conductance at 650°F is

$$h_r = 895 \text{ Btu/ft}^2 \text{ hr°F}$$

This value is based on the Dittus-Boelter correlation for heat transfer to a single phase fluid in a tube. The half inch tubing is internally finned and, including the fin effectiveness, approximately doubles the heat transfer over that of a bare tube.

Step 9 If the gas side conductance is computed for the inlet state of the combustion products (the same location where the vapor exits), the gas side conductance may be determined to be

$$h_g = 38.9 \text{ Btu/ft}^2 \text{ hr°F}$$

The overall conductance, including the wall infludence is,

$$U = 38.0 \text{ Btu/ft}^2 \text{ hr°F}$$

The overall ΔT at this location is 1850°F, so that the local heat flux is (based on the outside wall area)

$$\left(\frac{q}{a}\right)_{outlet} = 70,300 \text{ Btu/ft}^2\text{hr}$$

The inside wall to vapor temperature difference is 43°F. This is, of course, a mean value and does not take into consideration the peripheral variations in heat flux due to radiation from the combustor and circumferential distribution of gas side heat flux. This mean value does not include possible variations in local flux from combustor hot spots or local high velocities. All of these variations have been discussed in previous quarterly reports.

The apparent mean wall temperature at the superheated vapor exit, based on gas convection alone, is 693°F. This value, which is very conservative compared to the 810°F maximum allowable, therefore allows the design to be tolerant of local high fluxes and variations in fluid properties from those so far measured for this fluid.

A typical relationship between number of flow passages, heat transfer, and pressure drop is shown in Table II (for a one-half inch OD by 0.020 wall thickness tube which is internally smooth, and unfinned).

TABLE II

Number of parallel passages	h Btu/hr ft^2 F	P dyn psi	q/A_{max} Based on T_{wall} = 810°F
1	5640	157	0.9×10^6
2	3240	39	0.52×10^6
5	1560	6.3	0.16×10^6
10	895	1.6	0.14×10^6
15	648	0.7	0.10×10^6
20	513	0.4	0.082×10^6
25	434	0.25	0.070×10^6

Step 10 The quantity, α, for this staggered tube configuration and one-half inch tubes is 48.3 ft^2/ft^3, so that

$$U\alpha = 1500 \text{ Btu/ft}^3 \text{ hr F}$$

The total volume available for this vapor generator is 1.53 ft^3, so that based on the above figure, the maximum AU product with this configuration (neglecting wall and liquid heat transfer resistances) is 2290 Btu/hr°F, less than the 3870 Btu/hr°F required to meet the specified performance. Clearly the entire matrix cannot be made up of one half inch plain tubing.

One quarter inch tubing in an array similar to that of the one half inch tubing has an α of 96.6 ft^2/ft^3, so that

$$U\alpha = 3660 \text{ Btu/ft}^3 \text{ hr°F}$$

based on properties at temperatures typical of the cooler end of the exchanger. The matrix may be made up of a combination of one-half inch and quarter-inch tubing. Such a combination is four rows of one-half inch tubing, 30 tubes per row, and ten rows of one-fourth inch tubing, 60 tubes per row.

Step 11 The gas side pressure drop for this configuration may be computed to be 2.9 inches of water. This is within the design maximum limit.

Step 12 It can be shown for this geometry that the inside wall temperature in the last row of the one-fourth inch tubing is not critical with all 60 tubes in parallel, and since this flow path configuration yields a simple manifolded return bend arrangement for the entire small-tube section, it is chosen for the entire quarter inch tube section. At the connection between the one-fourth and one-half inch sections, the flow goes into a 10-tubes-in-parallel arrangement, so that six one-fourth inch tubes feed each of 10 one-half inch tubes. Each of the 10 streams in the one-half inch section therefore makes three passes across the exchanger in each row, for a total of 12 passes between the last one-quarter inch tube row and the superheater vapor outlet.

Commentary on the Design:

The one-fourth inch section of this exchanger contains 60 tubes. Because the effectiveness is very near one, a small decrease in performance yields a large decrease in tube number, and in weight. After consultation with Aerojet, Solar, and EPA personnel, the effectiveness and efficiency were decreased, so that the one-fourth inch tube section was reduced to seven rows. The consequences of this change are discussed in Section C of this report.

Portions of this exchanger could very well be designed with finned tubing as well as plain tubing. Some precautions associated with such a change are noted in the description of the Design Steps. It should be clear that there are many configurations which will satisfy the particular design requirements, and that choices must be made frequently on the basis of cost, materials and component availability, fabrication techniques, and other considerations not related to the heat transfer calculations.

C. Effects of Thermal Efficiency Specification

The usual definition of thermal efficiency of a combustor-vapor generator assembly is the ratio of the heat transferred to the working fluid divided by the heat of combustion of the fuel added. This definition may be formed either with the lower or higher heating value. Therefore,

$$\text{LHV} = \frac{C(T_{in} - T_{out})}{W_F(\text{LHV})} \qquad (20)$$

where

η is the thermal efficiency
C is the combustion products capacity rate
T_{in} is the combustion products temperature into the vapor generator
T_{out} is the combustion products temperature out of the vapor generator
W_F is the flow
LHV is the lower heating value of the fuel

For an efficient combustor with small heat loss, Equation (2) may be written

$$\eta_{\text{LHV}} = \frac{C\,(T_{in} - T_{out})}{C\,(T_{in} - T_{comb})} \qquad (21)$$

where

T_{comb} is the air (and fuel) temperature at the combustor inlet

The heat exchanger effectiveness is defined as the ratio of the heat transferred to that which would be transferred in an infinite counterflow heat exchanger, i.e., for the condition of zero temperature difference between the inlet cold side temperature and the outlet hot side temperature. Therefore,

$$\epsilon = \frac{C(T_{in} - T_{out})}{C(T_{in} - T_{cin})} \qquad (22)$$

where

T_{cin} is the inlet cold side temperature

The quantity ϵ cannot exceed unity.

These two expressions, (21) and (22), can be combined to yield a relationship between ϵ and η.

$$\eta_{\text{LHV}} = \epsilon\,\frac{(T_{in} - T_{cin})}{(T_{in} - T_{comb})} \qquad (23)$$

The efficiency of a boiler-vapor generator combination is limited by the difference between the ambient air and the working fluid inlet, even with very large heat exchangers, where ϵ approaches unity.

A graph of Equation (23) utilizing a 2500°F peak combustion products temperature, a 70°F ambient and using inlet working fluid temperature as a parameter, is shown in Figure 13.

The relationships between effectiveness and heat exchanger size are all exponential in form, so that for effectiveness near unity, a small increase in effectiveness requires a large increase in exchanger size. Figure 14 is a graph of heat exchanger size as a function of inlet liquid temperature and η_{LHV} for a counterflow arrangement.

A detailed analysis of these considerations has been worked out for the AEF-78 vapor generator, which is a cross counterflow tube bank made up partly of one-half inch tubing (in the hot section) and partly of one-fourth inch tubing (in the cool section). Figure 15 shows the percentage change in total gas side heat transfer area as a function of thermal efficiency for the design operating conditions. The design operating liquid inlet temperature is 396°F. It may be seen that the slope of this curve is very steep. At the

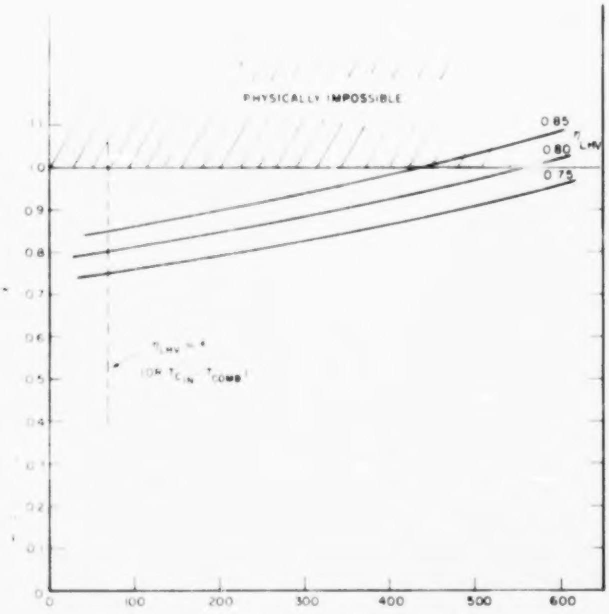

FIGURE 13. RELATIONSHIP BETWEEN THERMAL EFFICIENCY, EFFECTIVENESS, AND INLET LIQUID TEMPERATURE

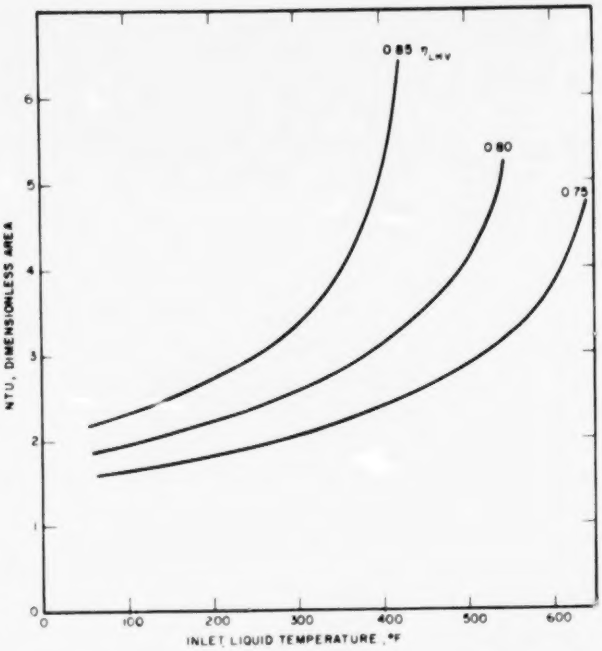

FIGURE 14. VAPOR GENERATOR SIZE AS EFFECTED BY EFFICIENCY AND LIQUID INLET TEMPERATURE 70°F AMBIENT AIR

85 percent efficiency level, a one percent change in thermal efficiency causes a ten percent change in required heat transfer area.

For this particular vapor generator, the design thermal efficiency was very difficult to meet within the required volume, and the one-fourth inch tube section consisted of a rather formidable number of tubes. Discussions between Geoscience, Solar, Aerojet and EPA led to a reduction in the thermal efficiency requirement to simplify the matrix. A graph of the relationship between heat transfer area, thermal efficiency, and number of one-fourth inch tubes is shown in Figure 16.

D. Factors Affecting Gas Side Pressure Drop

Two equations are given by Kays and London for heat exchanger pressure drop. For simplicity, the equation appropriate to tube banks will be used here. The following arguments hold for both.

The pressure drop relationship is

$$\Delta p = \frac{G^2}{2g_c \rho_1} \left[(1 + \sigma^2) \left(\frac{\rho_1}{\rho_2} - 1 \right) + f \frac{A}{A_c} \frac{\rho_1}{\rho_m} \right] \qquad (24)$$

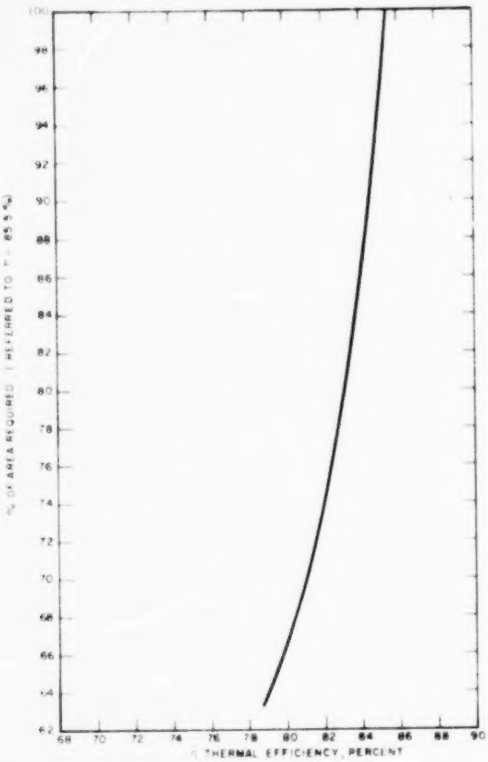

FIGURE 15. EFFECT OF VAPOR GENERATOR THERMAL EFFICIENCY UPON REQUIRED HEAT TRANSFER AREA OF AEF-78 MATRIX

where

Δp	is pressure drop
G	is mass velocity, w/A_c (It is based on minimum free flow area)
ρ_1	is inlet gas density
ρ_2	is outlet gas density
ρ_m	is mean gas density
g_c	is the proportionality constant in Newton's second law
σ	is the ratio between free flow area and frontal area for the matrix
f	is friction factor
A	is heat exchange area
A_c	is minimum free flow area
w	is mass flow rate

For simplicity, density variations are neglected in this discussion (first term in the square brackets). In a real combustion heated vapor generator, flow accelerations and density changes may not be neglected.

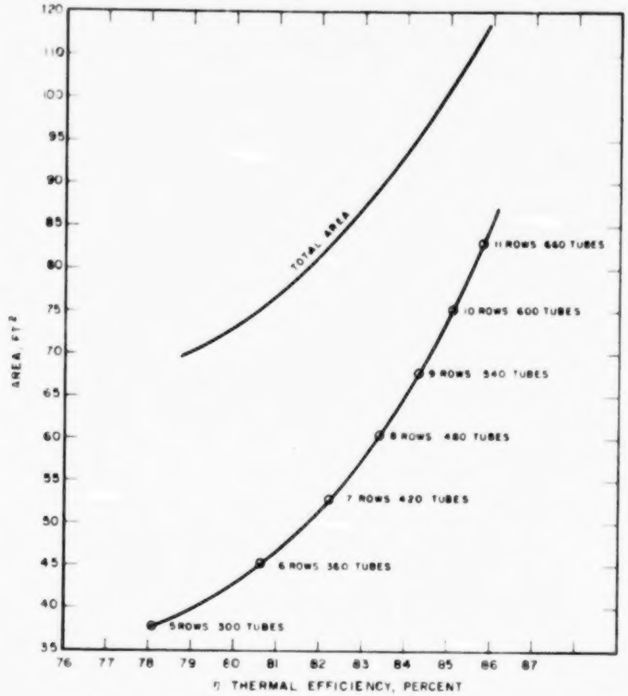

FIGURE 16. AEF-78 VAPOR GENERATOR EFFECT OF THERMAL EFFICIENCY UPON HEAT TRANSFER AREA REQUIRED

Since the design mass flow rate and not mass velocity is specified, make this substitution. Then Equation (24) becomes

$$\Delta p = \frac{w^2}{\sigma^3 A_f{}^3} \quad \frac{fA}{2 g_c \; 1} \qquad (25)$$

where

A_f is the heat exchanger frontal area

It may be clearly seen that both frontal area and contraction coefficient σ have a very strong effect upon the pressure drop.

For typical heat exchange configurations, the conductance variation with Reynolds modulus may be written in the form

$$\frac{h}{G} = K \, Re^{-m} \qquad (26)$$

where

h	is heat transfer conductance
K	is a constant dependent upon the configuration, but also combining some gas properties dependent upon the heat exchanger operating conditions
m	is approximately constant, and varies between 0.38 and 0.55 for must surfaces
Re	the Reynolds modulus, is $4\ r_h\ G/\mu$

Equation (26) in its expanded form, is

$$h = \left[K w^{(1\ -\ m)} \left(\frac{4\ r_h}{\mu} \right)^{(-m)} \right] \left(\frac{1}{A_f\ \sigma} \right)^{(1\ -\ m)} \tag{27}$$

Equation (27) indicates the manner in which the gas side conductance depends upon the gas flow rate, exchanger frontal area, and the matrix contraction coefficient.

From this relationship, the principal reason that the effectiveness (and efficiency) of a vapor generator rises at part load can be seen. The effectiveness is a function of the quantity NTU, which contains conductance in the numerator and flow rate in the denominator. The overall conductance is controlled by the gas side conductance in the usual vapor generator. If the flow rate is decreased, the gas side conductance decreases to a lesser extent, so the conductance-flow rate ratio (and the value of NTU) increases. Consequently, the heat exchange effectiveness rises.

The ratio of pressure drop to heat transfer conductance may be constructed from Equations (25) and (27)

$$\frac{\Delta P}{h} = \frac{w^{(1\ +\ m)}}{(\sigma A_f)^{(2\ +\ m)}} \ \frac{fA}{2 g_c\ \rho_1\ K} \left(\frac{4\ r_h}{\mu} \right)^{m} \tag{28}$$

Pressure drop rises with a decrease in free flow area much more rapidly than does the heat transfer conductance.

NOMENCLATURE

q	heat flux
C_p	specific heat at constant pressure
P_r	Prandtl number
μ	viscosity
k	thermal conductivity
ϵ	effectiveness
AU	overall thermal conductance
Z	distance along the tube
P	pressure
J	a function of quality and pressure
A, K	constants
NTU	number of transfer units
St	Stanton number
Re	Reynolds number
W	mass flow rate
x	an exponent which describes, in part, the dependence of Stanton number on Reynolds number, also quality
h	heat transfer coefficient, also enthalpy
C	capacitance rate
T	temperature

Preceding page blank

ΔP	pressure drop
G	total mass flow rate per unit free flow area, also steady state gain
v	specific volume
σ	ratio free flow/frontal area, or surface tension in lb/ft
f	fanning friction factor, or Darcy-Weisbach fraction factor
α	ratio gas side heat transfer area/volume, also void fraction
S	transverse spacing, center to center
D	spacing between tube rows, center to center
ϵp	effectiveness for one tube row
V_v	mean vapor velocity
R_v	volumetric flow ratio
ρ	density
C"C', m	empirically determined constants
L	matrix depth, also tube length
D_H	hydraulic diameter
No	overall surface effectiveness
g_c	gravitational mass-force-time-length conversion factor (4.17 x 10^8 ft/lbm/lb hr^2), or 32.2 ft lbm/lb sec^2
a	exponent describing dependence of Stanton number on Reynolds number
AF	frontal area
V	core volume
M	core weight, also a loss parameter defined by equation (20)
δ	fin thickness

ΔJ	a small perturbation in the quantity J
$\bar{\Theta}$	average surface heat flux for one channel of a parallel flow system, or its La Place transform
H	steady state change in coolant enthalpy as it flows through the channel
$A, B, C. D, E, \alpha, B$	parameters which depend on the unperturbed conditions in a parallel flow channel
z'	a weighted distance through the heated channel, defined by equation (11)
f_1	a function used to evaluate friction pressure drop in two phase flow, defined in equation (8) of Appendix VI.
$\bar{\rho}$	average static density
R_G	void fraction
λ	liquid-vapor volume flow rate ratio
g	acceleration due to gravity
A_f	flow area of heated channel
L_i	inlet channel length
A_{fi}	flow area of inlet channel
A_{fe}	flow area of exit channel
F	Darcy-Weisbach friction factor
K_i	entrance loss factor for heated channel
K_e	exit loss factor for heated channel
$\partial P_f/\partial z$	pressure gradient due to friction losses
B, B_2	defined in text
H_{fg}	latent heat of vaporization

b	tube radius
ϕ_{TBF}	two phase flow friction multiplier
I_1 through I_6	integrals used in evaluating hydrodynamic stability, defined in equations (25 through 30)
ωo	undamped natural frequency
η	damping factor
r, i,	functions tabulated in Reference (8)
h	enthalpy

Subscripts

sat	for saturated liquid
crit	critical (for dryout)
f	evaluated at the mean between bulk and wall temperature
G	gas phase
b	average bulk property
min	minimum capitance side
max	maximum capitance side
TPF	two phase flow
LO	computed assuming the entire flow is in the liquid phase
i	inlet, or at inlet to the row
e	exit
L	liquid phase
source	source
w	water

g	gas side
W	tube wall
m	mean value
h	hot side
c	cold side
v	vapor
LPF	computed assuming that only the liquid phase is flowing, that is, total flow rate is G(1-x)

REFERENCES

1. Duffy, T. E., Shekleton, J. R., LeCren, R. T., and Compton, W. A., "Low Emission Burner for Rankine Cycle Engines for Automobiles", Final Report RDR 1695, prepared by Solar Division of International Harvester for the Environmental Protection Agency, Office of Air Programs, Ann Arbor, Michigan, under Contract No. EHS 70-106 (1971).

2. Tong, L. S., *Boiling Heat Transfer and Two Phase Flow,* New York: John Wiley and Sons (1965).

3. Collier, J. G., and Pulling, D. J., "Instabilities in Two-Phase Flow", AERE-M 1105 (1963).

4. Quandt, E., "Analysis and Measurement of Flow Oscillations", *Chem. Engr. Prog. Symp. Ser.*, Vol. 57, No. 32, pp. 111-126 (1961).

5. Kays, W. M., and London, A. L., *Compact Heat Exchangers.* New York: McGraw-Hill (1958).

6. Bird, R. B., Stewart, W. C., and Lightfoot, E. N., *Transport Phenomena.* New York: John Wiley & Sons (1960).

7. Bennett, J. A. R., Collier, J. G., Pratt, H. R. C., and Thorton, J. D., "Heat Transfer to Two Phase Gas-Liquid Systems, Part I: Steam-Water Mixtures in the Liquid-Dispersed Region in an Annulus", *Trans. Inst. Chem. Engr.*, Vol. 39, pp. 113-126 (1961).

8. Martinelli, R. C. and Nelson, D. B., "Prediction of Pressure Drop During Forced Circulation Boiling of Water", *ASME Trans.* Vol. 70, pp. 695-702 (1948).

9. Bishop, A. A., Sandberg, R. O. and Tong, L. S., "Forced Convection Heat Transfer at High Pressure After the Critical Heat Flux", *ASME Preprint* 65-HT-31 (1965).

10. Tippets, F. E., "Analysis of the Critical Heat Flux Condition in High Pressure Boiling Water Flows", *Trans. ASME J. Heat Transfer,* Vol. 86C, pp. 23-28 (Feb. 1964).

Preceding page blank

11. Yamazaki, Y. and Shiba, M., "A Comparative Study on the Pressure Drop of Air-Water and Steam-Water Flows", Concurrent Gas Liquid Flow. Ed. by E. Rhodes, D. S. Scott, pp. 359-380, Plenum Press (1969).

12. Baker, O., "Simultaneous Flow of Oil and Gas", Oil and Gas J., Vol. 53, pp. 185-190 (1954).

13. Chemical Engineering (June 13, 1960).

14. Tong, L. S., Currin, H. B., and Thorp, A. G. II, "New Correlations Predict DNB Conditions", Nucleonics, Vol. 21, No. 5, pp. 43-47 (1963).

15. Peterson, J. R., "The Effect of Swirl Flow Upon the Performance of Monotube Steam Generators", SAE preprint 70016 for Automotive Engineering Congress in Detroit, Michigan (Jan. 12-16, 1970).

16. Kent's Mechanical Engineers Handbook, 12th Ed. New York: John Wiley & Sons (1958).

17. Kays, William and London, A. L., Compact Heat Exchangers, 2nd Edition, New York: McGraw-Hill Co. (1964).

18. Carslaw, H. S. and Jaeger, J. C., Conduction of Heat in Solids, Second Edition, Oxford (1959).